BioMed Research International

Helicase and Its Interacting Factors: Regulation Mechanism, Characterization, Structure, and Application for Drug Design

Guest Editors: Cheng-Yang Huang, Yoshito Abe, Huangen Ding, and I-Fang Chung

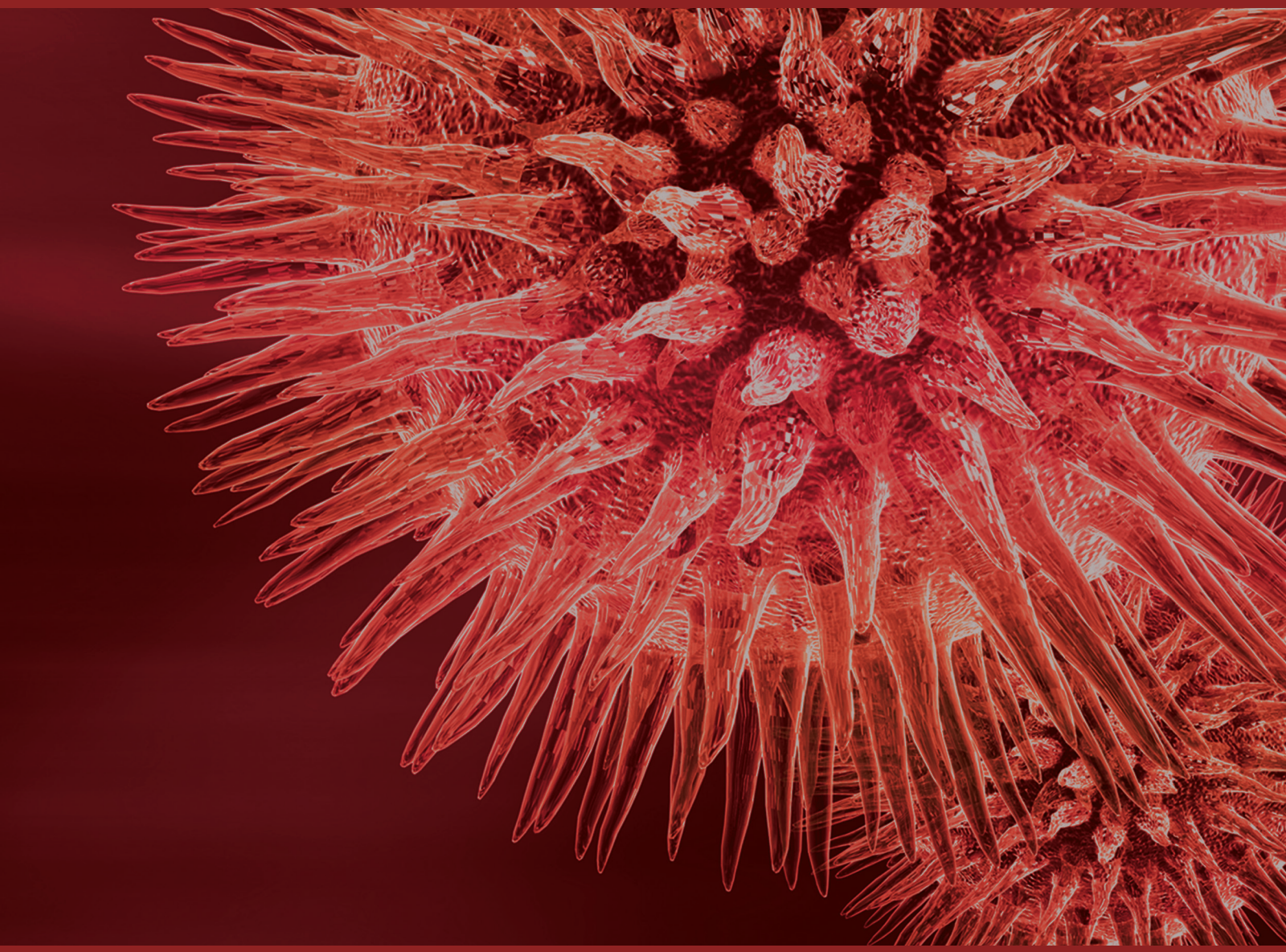

Helicase and Its Interacting Factors: Regulation Mechanism, Characterization, Structure, and Application for Drug Design

BioMed Research International

Helicase and Its Interacting Factors: Regulation Mechanism, Characterization, Structure, and Application for Drug Design

Guest Editors: Cheng-Yang Huang, Yoshito Abe, Huangen Ding, and I-Fang Chung

Contents

Hindawi Publishing Corporation
BioMed Research International
Volume 2015, Article ID 909047, 1 page
http://dx.doi.org/10.1155/2015/909047

Editorial

Helicase and Its Interacting Factors: Regulation Mechanism, Characterization, Structure, and Application for Drug Design

Cheng-Yang Huang,[1,2] Yoshito Abe,[3] Huangen Ding,[4] and I-Fang Chung[5]

[1]*School of Biomedical Sciences, Chung Shan Medical University, Taichung, Taiwan*
[2]*Department of Medical Research, Chung Shan Medical University Hospital, Taichung, Taiwan*
[3]*Department of Protein Structure, Function and Design, Kyushu University, Fukuoka, Japan*
[4]*Department of Biological Sciences, Louisiana State University, Baton Rouge, LA, USA*
[5]*Institute of Biomedical Informatics, National Yang-Ming University, Taipei, Taiwan*

Correspondence should be addressed to Cheng-Yang Huang; cyhuang@csmu.edu.tw

Received 11 December 2014; Accepted 11 December 2014

Helicases are motor proteins that separate nucleic acid duplexes and/or displace protein in reactions fueled by the binding and hydrolysis of nucleoside triphosphate (NTP). Because of their essential roles in all aspects of nucleic acid metabolism, helicases encoded by bacteria, viruses, and human cells are widely studied targets for new antiviral, antibiotic, and anticancer drugs. Recent evidence indicates that some accessory proteins can regulate their helicase and/or translocase activities. Knowledge of structure-activity relationships has led to the development of successful therapies, regulation modes, new DNA/protein interacting models, and novel inhibitors to deeply understand the acting mechanism of helicases and/or their interacting factor.

In this special issue, we presented original research papers and reviews on the topics of how DEAH/RHA helicases can be regulated by G-patch proteins (J. Robert-Paganin et al.), a possible role of the Mcm2-7 replicative helicase as a promising chemotherapeutic target for anticancer drug development (N. E. Simon and A. Schwacha), crystal structural analyses of *Deinococcus radiodurans* RecQ helicase (S.-C. Chen et al.) and a conserved hypothetical protein MJ0927 from *Methanocaldococcus jannaschii* (S.-C. Chen et al.), identification and characterization of human DNA helicase Rtel1 possessing a redox active iron-sulfur cluster (A. P. Landry and H. Ding), a role of the C-terminal domain of SSB in determination of the ssDNA binding site size (Y.-H. Huang and C.-Y. Huang), and the structural insight into the DNA-binding mode of the primosomal proteins PriA, PriB, and DnaT (Y.-H. Huang and C.-Y. Huang). We hope that the readers will find in this special issue accurate data, significant results, and updated reviews.

Cheng-Yang Huang
Yoshito Abe
Huangen Ding
I-Fang Chung

Hindawi Publishing Corporation
BioMed Research International
Volume 2015, Article ID 931857, 9 pages
http://dx.doi.org/10.1155/2015/931857

Review Article

Regulation of DEAH/RHA Helicases by G-Patch Proteins

Julien Robert-Paganin, Stéphane Réty, and Nicolas Leulliot

Laboratoire de Cristallographie et RMN Biologiques, UMR CNRS 8015, Faculté des Sciences Pharmaceutiques et Biologiques, Université Paris Descartes, Sorbonne Paris-Cité, 4 avenue de l'Observatoire, 75270 Paris Cedex 06, France

Correspondence should be addressed to Nicolas Leulliot; nicolas.leulliot@parisdescartes.fr

Received 20 June 2014; Revised 19 October 2014; Accepted 24 October 2014

Academic Editor: Huangen Ding

RNA helicases from the DEAH/RHA family are present in all the processes of RNA metabolism. The function of two helicases from this family, Prp2 and Prp43, is regulated by protein partners containing a G-patch domain. The G-patch is a glycine-rich domain discovered by sequence alignment, involved in protein-protein and protein-nucleic acid interaction. Although it has been shown to stimulate the helicase's enzymatic activities, the precise role of the G-patch domain remains unclear. The role of G-patch proteins in the regulation of Prp43 activity has been studied in the two biological processes in which it is involved: splicing and ribosome biogenesis. Depending on the pathway, the activity of Prp43 is modulated by different G-patch proteins. A particular feature of the structure of DEAH/RHA helicases revealed by the Prp43 structure is the OB-fold domain in C-terminal part. The OB-fold has been shown to be a platform responsible for the interaction with G-patch proteins and RNA. Though there is still no structural data on the G-patch domain, in the current model, the interaction between the helicase, the G-patch protein, and RNA leads to a cooperative binding of RNA and conformational changes of the helicase.

1. Introduction

Helicases have been historically defined as proteins able to unwind double-stranded (ds) nucleic acids in a nucleotide triphosphate- (NTP-) dependent manner [1, 2]. Sequence alignments revealed that overall sequence of helicases displays poor identity, but five superfamilies (SF) were defined from conserved motifs [3]. All these helicases possess RecA-like domains, so called because of the homology of this domain with *Escherichia coli* recombinase A [4, 5]. All the conserved motifs are located in the RecA-like domains and they constitute the structural and functional core of the helicase since it harbors NTP hydrolysis (Walker A and Walker B, Q motifs), nucleic acid binding, and helicase activities [6]. SF-1 and SF-2 helicases are monomeric but have tandem RecA-like domains, named RecA1 and RecA2, while SF-3, SF-4, SF-5, and SF-6 possess one RecA-like domain and are hexameric. In the case of SF-1 and SF-2, the two RecA-like domains are completed with ancillary regions in N-terminus and C-terminus or inserted in loops within the RecA-like domains. These regions modulate the activity or the specificity of the enzyme by autoinhibitory effects or by direct interaction with the nucleic acid and/or with a protein partner [7].

Helicases are often regulated by protein partners. In translation initiation, eIF4A is responsible for the unwinding of secondary structures during scanning of the 5′-UTR (5′-untranslated region). The activation and the recruitment of eIF4A need the interaction with eIF4B and eIF4G factors [8]. In ribosome biogenesis, the helicase Dbp8, involved in maturation of the small subunit, interacts with the nucleolar factor Esf2. *In vitro*, Esf2 can stimulate Dbp8 ATPase activity, suggesting that Esf2 also activates Dbp8 during ribosome biogenesis [9]. The RNA helicase activity of DEAH/RHA family helicases is also regulated by a special class of proteins that all contain G-patch domains (Table 1). The mechanisms of DEAH/RHA helicase activation by G-patch proteins are unclear and no structure of G-patch protein has been solved. In this review, we focus on the current knowledge about DEAH/RHA helicases regulation by G-patch proteins.

2. Functions of DEAH/RHA Helicases

The DEAH/RHA family (SF-2) is named after the sequence of the Walker B motif (Asp-Glu-Ala-His) and a member of the family, the RNA helicase A (RHA). The DEAH/RHA helicases

Table 1: Summary of biological functions of DEAH/RHA helicases activated by a G-patch protein. The different biological processes, in which Prp43/DHX15 and Prp2/DHX16 and their activators are implied, are listed. The yeast orthologs are listed in parenthesis.

DEAH/RHA	Functions	Protein partner
DHX15 (Prp43)	Splicing	**TFIP11 (Ntr1); RBM5**
	Ribosome biogenesis	**SQS1 (Pfa1); PINX1 (Gno1)**
	?	**GPATCH2**
	Immunity	**?**
DHX16 (Prp2)	Splicing	**(Spp2)**

Table 2: Human DEAH/RHA helicases with no known G-patch activator and biological processes in which they are implied. For each protein, the identified yeast ortholog is listed in parenthesis.

DEAH/RHA	Functions
DHX38 (Prp16)	Splicing
DHX8 (Prp22)	Splicing
DHX37 (Dhr1)	Ribosome biogenesis
DHX32 (Dhr2)	Ribosome biogenesis
DHX29 (YLR419w)	Translation initiation; immunity
DHX33	Transcription; immunity
DHX9	Genomic stability; immunity; RNA interference
DHX29	Translation initiation; immunity
DHX35	Splicing
DHX34	mRNA decay

are present in all essential processes of RNA metabolism such as transcription, translation, ribosome biogenesis, pre-mRNA splicing, or RNA sensing (Table 2). Members of the DEAH/RHA family are conserved across eukaryotes and contain the spliceosomal helicases Prp2, Prp16, Prp22, and Prp43 (resp., DHX16, DHX38, DHX8, and DHX15 in human) and of YLR419w (DHX29), Dhr1 (DHX37), and Dhr2 (DHX32). Other members of the family have no known homologues in yeast, such as DHX35, DHX9 (RNA helicase A), DHX57, DHX36, DHX30, DHX33, DHX40, and DHX34. Interestingly, many of these helicases are implicated in several different biological processes of RNA and/or DNA metabolism.

2.1. DEAH/RHA Helicases in Splicing. The implication of DEAH/RHA helicases in pre-mRNA splicing has been intensively studied in yeast *Saccharomyces cerevisiae* [10]. DEAH/RHA helicases reorganize the different ribonucleoprotein (RNP) complexes during the splicing reaction and their mode of action is highly regulated because they all act at a precise step of the catalytic cycle. In pre-mRNA splicing, four DEAH/RHA helicases have been characterized in yeast (Figure 1). Spliceosomal remodeling by Prp2/DHX16 is responsible for the removal or displacement of the Bud13, Cwc24, Cwc27, and SF3a/b factors from the spliceosome prior to the first catalytic step and also creates binding sites for the Yju1 and Cwc25 factors [11]. Prp16/DHX38 is implicated in rearrangements of the spliceosome after the first catalytic step necessary for the second catalytic step and includes an indirect contribution to Cwc25 recycling [12]. Prp22/DHX8 is responsible for the release of spliced mRNA [13, 14]. Prp43/DHX15 catalyzes the disassembly of the lariat-spliceosome, recycling the components of the spliceosome and allowing degradation of the lariat [15, 16].

Interestingly, DEAH/RHA helicases are also responsible for proofreading of spliced pre-mRNA. Prp16 can discard aberrant spliceosomes which are stalled at the first catalytic step and Prp22 discards aberrant spliceosomes that are stalled in the second catalytic step. In the two cases, aberrant spliceosomes are disassembled by Prp43, indicative of cooperation between DEAH/RHA helicases in spliceosome proofreading. Spliceosomal DEAH/RHA helicases have been proposed to function as molecular clocks: an aberrant spliceosome is slower in its catalytic steps and Prp16 or Prp22 remodels them before the catalytic reactions can take place. According to these results, spliceosome proofreading is driven by a kinetic competition between RNP remodeling activity of DEAH/RHA helicases and catalytic steps of the spliceosome [17, 18].

2.2. DEAH/RHA in Ribosome Biogenesis. Prp43 is remarkable because this helicase is required in two distinct pathways: splicing and ribosome biogenesis [19–21]. Prp43 is implicated in the biogenesis of the two ribosomal subunits and binds several sites on the pre-rRNA during the biogenesis. In budding yeast, a lack of Prp43 results in accumulation of pre-rRNA intermediates from both subunits [19–21], showing that Prp43 is one of the only factors implicated in the biogenesis of the two ribosomal subunits. Prp43 coprecipitates with RNA polymerase I, indicating that it associates with preribosomal particle on the nascent pre-rRNA [19–21]. CRAC experiments identified several binding sites of Prp43 on the pre-rRNA. One major site is located at the helix 44 of the 20S, close to the processing site D, supporting previous results implicating Prp43 in the regulation of D site cleavage by endonuclease Nob1 [22]. In these experiments, Prp43 also was cross-linked with several box C/D snoRNA binding sites such as helix 39/40. The fact that Prp43 immunoprecipitates with several snoRNA, that a Prp43 mutant impedes methylation of 27S by a C/D box snoRNA, and that depletion of Prp43 trapped snoRNAs in the preribosome supports the model in which Prp43 functions to remove snoRNA from pre-rRNA [19–21, 23].

2.3. DEAH/RHA in Translation Initiation. The role of DEAH/RHA helicases in translation initiation has mostly been investigated for the human homologue of YLR419w (DHX29) and DHX9. The DHX29 helicase is essential in translation initiation during the formation of the 43S complex, composed of the eIF2/GTP/Met-tRNAi^{Met} complex, initiation factors, and the ribosomal 40S subunit. DHX29 favors scanning of the mRNA by the 40S subunit in presence of stable secondary structures and mediates base-pairing between initiation codon and tRNAi^{Met} in order to form stable 48S complex [24].

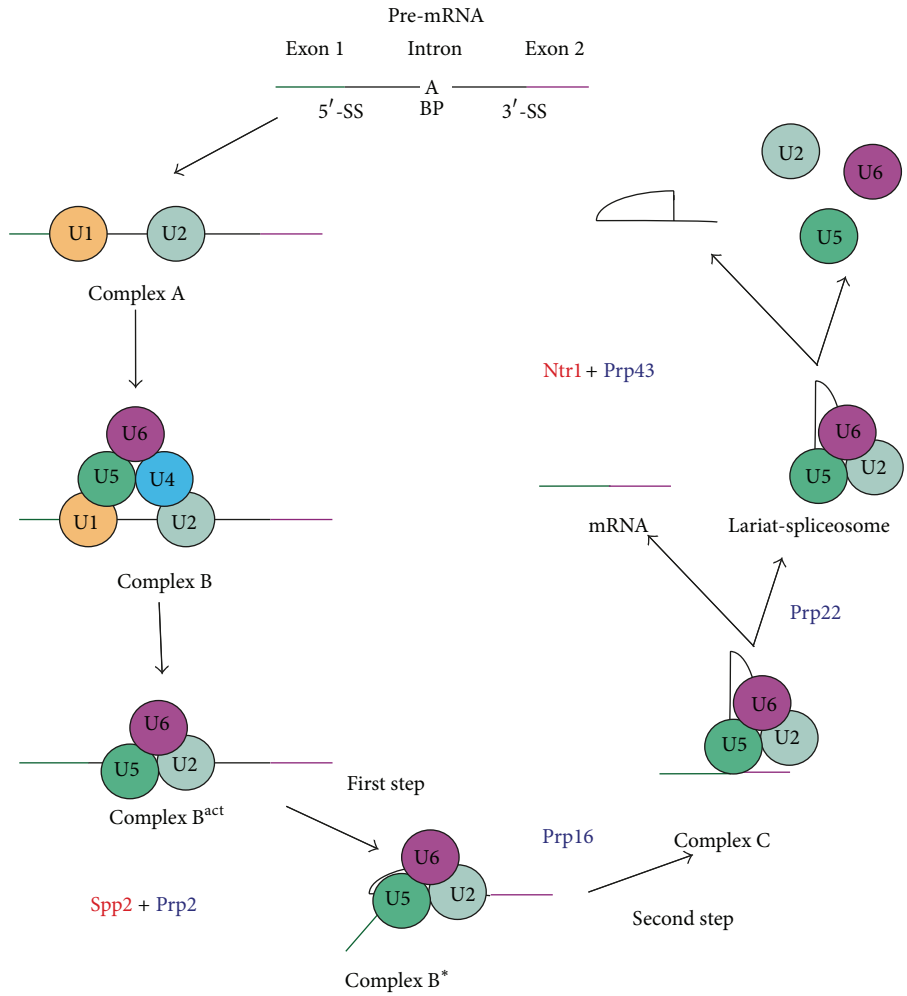

Figure 1: Schematic representation of the splicing cycle. Splicing is the removal of introns from pre-mRNA and ligation of exons in order to form the mature mRNA. The splicing cycle is a sequential set of reorganizations of the spliceosome, a complex composed of five snRNAs: U1, U2, U5, and U4/U6. U5 and U2/U6 constitute the catalytic core and catalyze the two nucleophilic attacks (catalytic steps). Four DEAH/RHA helicases (in black) and two known G-patch protein partners (in red) are involved in splicing. Prp2 is activated by Spp2 and acts prior to the first catalytic step. Prp16 acts between the two catalytic steps remodeling the spliceosome in order to permit the binding of essential factors for the second catalytic step. Prp2 is involved in the release of spliced mRNA from the lariat-spliceosome complex. Prp43 is activated by Ntr1 in the disassembly of the lariat-spliceosome complex. 5′-SS: 5′-splicing site, 3′-SS: 3′-splicing site, and BP: branch point.

The cryoEM structure of the 43S complex bound to DHX29 brought new insights into the mode of action of this helicase. The location of DHX29 on the structure suggests that the helicase does not directly contact mRNA but suggests that it remodels the 40S subunit structure, thereby favoring mRNA secondary structure unwinding in an indirect manner [25]. DHX9 is another DEAH/RHA helicase implied in translation initiation. This helicase stimulates translation of mRNA containing a PCE (posttranscriptional control element) but its mode of action and precise role remain elusive [26].

2.4. Other Roles of DEAH/RHA Helicases. A role of metazoan DEAH/RHA helicases in viral RNA sensing and immune responses has been elucidated more recently. DHX33 and DHX9 are able to sense viral RNA and to activate IPS-1 mediated signalization in order to stimulate the production of inflammatory cytokines in myeloid dendritic cells [27, 28]. The RNA-sensing activity of DHX29 has been demonstrated in human airway system cells [29]. It acts together with the RIG-I helicase, a well-characterised sensor of immunity, and interacts with viral RNA and activates the RIG-I-MAVS pathway by its CARD domains. The direct interaction between MAVS, DHX9, RIG-I, and nucleic acid triggers MAVS signaling pathway. Altogether these results indicate that DHX9 would act as a cosensor of RIG-I [29]. DHX15 has been related to viral infection related apoptosis and cytokines production. In this context, DHX15 senses viral RNA and interacts directly with MAVS in order to trigger signaling by the NF-κB pathway [30, 31].

In addition to their previously described functions, DHX9 and DHX33 have also been described in other processes. DHX9 was found to be essential for genomic stability. DHX9 is able to bind to intramolecular triplex DNA, hot-spots of mutations in human genome, and to prevent

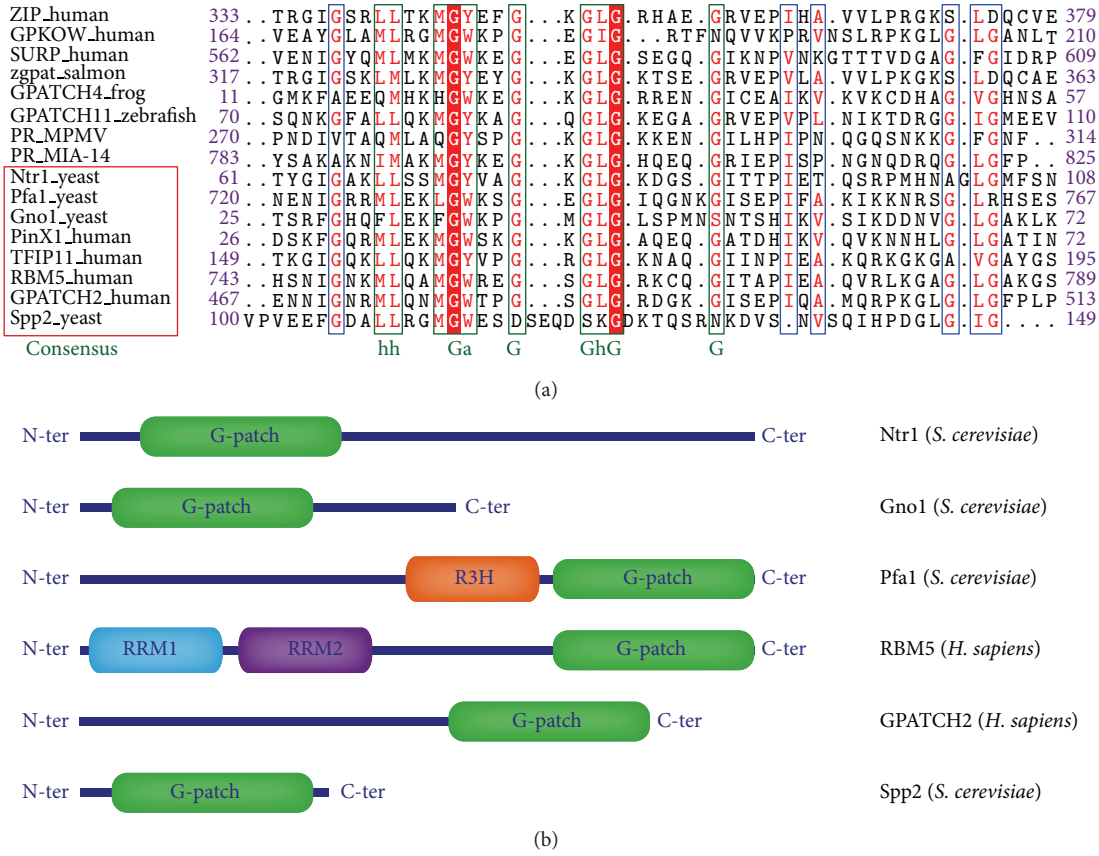

Figure 2: Sequence and organization of G-patch domains and G-patch protein partners. (a) Sequence alignments of G-patch domains from various G-patch proteins from different organisms. Sequences from G-patch protein partners of DEAH/RHA helicases from human and yeast are in the red box. The consensus sequence of G-patch is written in green: G is a glycine, a represents an aromatic residue, and h represents a hydrophobic residue. G-patch domain is a 50 AA glycine-rich domain with some residues invariably conserved like the aromatic residue after the first glycine. (b) Schematic representation of G-patch protein partners of DEAH/RHA helicases and their domains.

mutations and genomic instability, probably by acting on DNA structure [32]. The DHX33 helicase has been identified as a mediator of rRNA synthesis by promoting the access of RNA polymerase I to the rDNA loci. Its acts by remodeling rDNA structure and associating with the chromatin modulating protein UBF [33].

3. Regulation of DEAH-Box Activity by G-Patch Protein Partners

3.1. G-Patch Domain and G-Patch Proteins. The G-patch domain was identified by sequence alignment as a 45–50 amino acids conserved motif with a consensus *hhx*(3)G*a*x(2)G*x*G*h*G*x*(4)G where *a* is an aromatic residue, *h* is a hydrophobic residue, and *x* is a number of positions occupied by nonconserved residues (Figure 2(a)) [34]. According to secondary structure predictions, the G-patch is composed of two α-helices flanked by loops. In this first study, G-patch domains were found in eukaryotic proteins that contained RNA-binding domains such as SWAP, RRM, or R3H. This association with RNA-binding domains and the fact that G-patch domains were also found in proteins involved in splicing or transport of mRNA led to the assumption that these domains are involved in protein-RNA interactions.

In proteinases and reverse transcriptase (RT) from betaretroviruses, the G-patch domain was shown to be both protein-nucleic acid and protein-protein interaction domain. Retroviral proteinases from Mason-Pfizer virus (MPMV) and mouse intracisternal A-type particles endogenous retrovirus (MIA-14) contain a G-patch domain in its C-terminal domain. Electrophoretic mobility shift assay demonstrated that the G-patch domain of these proteinases is responsible for the association with single-stranded nucleic acids (DNA and RNA) without sequence specificity [35]. In addition, the G-patch of proteinase of MPMV is important for infectivity but this function does not seem to be linked with the protease activity. The G-patch associates with the reverse transcriptase suggesting that it can function as a protein-protein interaction module [36, 37]. This interaction increases RT activity possibly by maintaining a favorable conformation of the substrate RNA. The G-patch domain also potentially mediates the interaction of the MPMV proteinase with breast cancer-associated protein BCA3 [38].

The transcription repressor protein ZIP contains a G-patch and is also involved in both protein-nucleic acid and

protein-protein interactions. ZIP can repress the expression of the oncogene EGFR by the recruitment of the NuRD complex through its coiled-coil domain [39]. Interestingly, ZIP is expressed in another shorter isoform called sZIP that lacks the Zn finger, Tudor, and the first ten residues of the G-patch domains. This isoform is unable to bind DNA but interacts with the NuRD complex in competition with ZIP [40]. It is tempting to assume that the truncation of the G-patch domain coupled to the lack of Tudor and Zn finger domains is responsible for the loss of the interaction with DNA in ZIP. ZIP is able to dimerize and residues 361 to 430 are crucial for this dimerization. Interestingly, this region includes 18 residues of the G-patch domain [41].

G-patch domains are also found in several protein partners responsible for the activation of DEAH/RHA helicases. There are six known G-patch proteins interacting with DEAH/RHA helicases: RBM5, Ntr1/TFIP11, Gno1/PinX1, Spp2, Pfa1/Sqs1, and GPATCH2. Sequence alignments of G-patch domains and domains compositions of these proteins are represented in Figure 2(b). Alignments show that the aromatic residue after the first glycine is always conserved and is a tryptophan or a tyrosine. Glycine positions are well conserved except for the fifth glycine of Gno1 which is occupied by a serine. G-patch domain of Spp2 seems to be less conserved (Figure 2(a)). The G-patch is the only remarkable domain for GPATCH2, Spp2, Gno1, and Ntr1. However Pfa1 and RBM5 also display domains and motifs involved in RNA binding such as Zinc fingers, R3H, or RRMs (Figure 2(b)). As it was originally defined, the G-patch domain is associated with nucleic acids binding domains.

3.2. In Vivo Evidence of Regulation of DEAH-Box Helicases by G-Patch Proteins. The first activator of a DEAH/RHA helicase to be characterized is Spp2, a Prp2 regulator in splicing of pre-mRNA [42–45]. In budding yeast, Spp2 has been shown to interact with the spliceosome prior to the first catalytic step of splicing. Spp2 is required for efficient splicing and cell extracts depleted for Spp2 are blocked prior to the first catalytic step. Prp2 and Spp2 interact physically and the interaction is necessary for the activation of Prp2 function [42, 44].

The bifunctional Prp43 helicase is recruited and activated in splicing and ribosome biogenesis by different G-patch proteins. The function of Prp43 in splicing is mediated by the Ntr1 protein [46]. Ntr1 is a G-patch protein that interacts with the NineTeen related complex by the protein Ntr2 [47]. Splicing assays *in vitro* confirmed that Ntr1 was responsible for the activation of Prp43 in lariat-spliceosome disassembly [46]. Ntr1 forms a stable complex with Ntr2 and the Ntr1/Ntr2 complex associates with U5 by a direct interaction with Ntr2 [48]. Prp43 is recruited to the spliceosome by the Ntr1/Ntr2 complex, thereby targeting the helicase activity of Prp43 for spliceosome dissociation [47]. Interestingly, TFIP11, the human homolog of Ntr1, also possesses a G-patch domain and colocalizes with DHX15, the human homologue of Prp43 [49]. This interaction has been confirmed by isolation of postsplicing intron-lariat complexes where deletion of TFIP11 impairs spliceosome disassembly by DHX15 [50]. The G-patch protein RBM5 present only in metazoans has been shown to be a regulator of alternative splicing in apoptosis. Since RBM5 is able to activate helicase and ATPase activity of DHX15, it probably regulates splicing by activation of DHX15 [51].

The activity of Prp43 in ribosome biogenesis is stimulated by G-patch proteins Pfa1 and Gno1 (PinX1 in human) [19, 52]. Immunoprecipitation demonstrates that Prp43 associates with Pfa1 and pre-40S [19]. Other experiments have shown that Pfa1 is associated with the 90S, pre-40S, and pre-60S subunits [53]. Depletion experiments have demonstrated a genetic link between Pfa1 and Prp43 and the protein Ltv1 in ribosome biogenesis. Cells depleted for Ltv1 and lacking Pfa1 display an impairment of pre-rRNA processing. Complementation of these cells with Pfa1 and northern blot analysis of pre-rRNA show that Pfa1 plays a role in cleavages at sites A1 and A2 on 35S pre-rRNA and D cleavage site on 20S pre-RNA [53]. The stimulation of Prp43 function by Pfa1 in order to promote site D cleavage has been confirmed by the combination of *in vitro* and depletion experiments [22] and probably functions by promoting the release of snoRNA. No known homologues exist in humans for Pfa1, but G-patch proteins of unknown function that regulate DHX15 function, such as GPATCH2, may act as functional homologues in ribosome biogenesis [54].

Gno1 is important for pre-rRNA processing and maturation because deletion of this protein leads to accumulation of the 35S precursor [55]. Northern blot, immunoprecipitation, and pulse-chase analysis in ΔGno1 yeast strains show that Gno1 is recruited to the 90S and remains associated with the pre-60S and pre-40S. When Gno1 is deleted there is a severe accumulation of 20S and 27SB pre-rRNA in yeast. *In vitro* and *in vivo* data indicate that Gno1/PinX1 interacts with Prp43/DHX15 and probably triggers its function [52].

Interestingly, neither Pfa1 nor Gno1 is essential to the recruitment of Prp43 to the preribosome [19]. This is in contrast with G-patch proteins Spp2 and Ntr1 that are essential to the recruitment of Prp2 and Prp43 to the spliceosome. In ribosome biogenesis, the G-patch proteins only seem to activate Prp43 but do not recruit it. The fact that Prp43 is not specifically recruited to the preribosome can explain why several binding sites are detected by cross-link experiments [23]. The helicase could bind to several sites and need the interaction of Gno1 or Pfa1 in order to trigger its activity at specific sites.

Deletion of Gno1 reduces the accumulation of Pfa1 in pre-ribosomal particle, although deletion of Pfa1 does not affect Gno1 levels [53]. Despite this result, no direct interaction between Gno1 or its human homologue PinX1 and Pfa1 has been detected in pull-down assays [52, 53]. However, human PinX1 and TFIP11 were shown to interact by two-hybrid experiment and copurification from bacterial expression system [56]. A functional link between these activators is therefore still to be demonstrated.

3.3. Mechanism of Activation of DEAH/RHA Helicases by G-Patch Proteins. In order to characterize the specific role of the G-patch domain in regulation of helicase activity, functional studies have focused on the interaction between G-patch proteins and helicases and how this interaction modulates

helicase activity. The G-patch proteins are able to interact with Prp43 *in vitro* and to form a stable complex. The N-terminal domain (residues 1–120) of Ntr1 containing the G-patch is sufficient to interact with the Prp43 helicase and mutations in conserved residues of the G-patch domain disrupt the interaction [46]. In human cells, RBM5 is able to interact with DHX15 [51]. Similar results have been obtained with Pfa1 [53]; the Pfa1 C-terminal domain (574–767) containing the G-patch and the Pfa1 N-terminal domain (1–202) are able to form complex with Prp43. Therefore, Pfa1 possesses two distinct binding sites with Prp43 and only one of these sites contains the G-patch domain [53]. The interaction between Gno1 and Prp43 has been demonstrated by coimmunoprecipitation in yeast. Interestingly, Prp43 is also able to interact with its human homologue PinX1 and mutations of conserved residues in the G-patch domain of Gno1 or PinX1 reduce the interaction with Prp43. The interaction between Prp43/DHX15 and Gno1/PinX1 is conserved across the evolution and is mediated by the G-patch domain [52].

Prp43 displays only weak helicase activity *in vitro* on DNA/RNA substrates with a single-stranded RNA tail, and G-patch proteins are able to stimulate this helicase activity [57]. This activity is strongly stimulated by Ntr1 and especially by the N-terminal truncation (1–122) that contains the G-patch domain, while mutants of conserved residues of the G-patch domain cannot stimulate the helicase activity [46]. Pfa1 is also shown to activate helicase activity of Prp43 through its C-terminal domain (574–767) containing the G-patch [53]. In humans, RBM5 activates helicase activity of DHX15 and mutations in the G-patch domain [51]. According to these results, G-patch proteins are able to stimulate the weak helicase activity of Prp43 and the G-patch domain of these proteins mediates this activation.

The G-patch partners of Prp43 also stimulate Prp43 ATPase activity. In human, RBM5 and GPATCH2 are able to stimulate ATPase activity of DHX15 [51, 54]. The C-terminal domain of Pfa1 (574–767) is sufficient to stimulate ATPase activity of Prp43. Interestingly, Pfa1 can stimulate ATPase activity with and without RNA, but optimal stimulation occurs in presence of RNA [53]. Fusions of Prp43 with different fragments of Ntr1 show that the G-patch domain (51–110) is directly responsible for the activation of Prp43 helicase and ATPase activity [58]. Similar results have been obtained for Gno1/PinX1. PinX1 is able to stimulate ATPase activity of Prp43 and mutations in the G-patch domain impede the activation [52].

The structure of Prp43 has been solved by X-ray crystallography and this helicase contains six domains (Figure 3) including the two classical RecA-like domains and the OB-fold that is responsible for the interaction with RNA [59, 60]. Interestingly, Pfa1 fails to stimulate ATPase activity of the truncated version of Prp43 lacking the OB-fold domain. The Pfa1 C-terminal domain lacking the OB-fold domain does not interact with Prp43 [60]. Thus, the OB-fold domain of Prp43 seems to be a platform that mediates interaction with RNA and G-patch domain of its partners (Figure 4), probably by allosteric conformational rearrangements that would allow the enzyme to activate its ATPase activity.

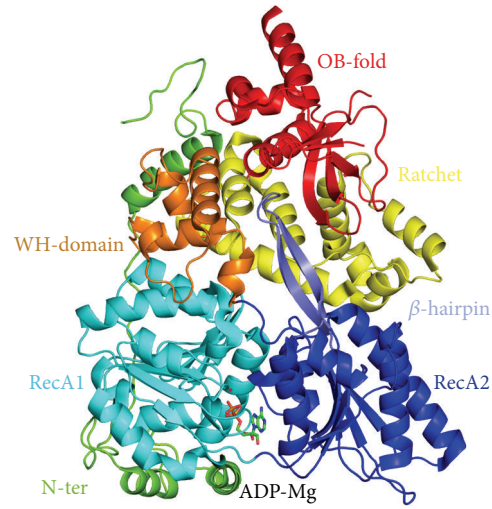

Figure 3: Structure of yeast Prp43 in complex with ADP (PDB code 2XAU). The protein contains six domains: the N-ter domain (green); the RecA1 and RecA2 domains which bind the nucleotide (cyan and dark blue, resp.); the WH domain (orange); the ratchet domain (yellow); and the OB-fold domain (red).

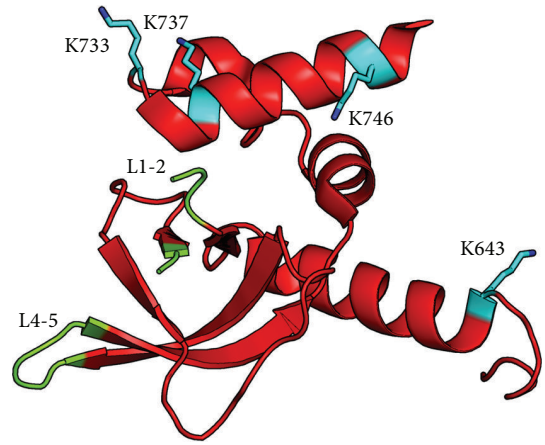

Figure 4: The OB-fold domain of Prp43 is implicated in the interaction of the helicase with Ntr1 and with RNA. The two loops L1-2 and L4-5 which have been involved in nucleic acid interaction [60] are colored in green. Residues that are involved in the interaction with Ntr1 according to cross-link experiments [58] are colored in cyan.

Recently, Ficner and coworkers have investigated the role of the G-patch of Ntr1 in the interaction with Prp43 and with RNA. By circular dichroism, the G-patch domain is seen unstructured in solution, but it could form secondary structure elements during the interaction with Prp43 or nucleic acid. Cross-linking coupled to mass spectrometry shows that the interaction is mediated by the C-terminal domains of Prp43 and the N-terminal domain of Ntr1, including a residue in the G-patch domain. Ntr1 and Prp43 both interact with RNA. Moreover, binding of Ntr1 to Prp43 promotes structural rearrangements of Prp43, especially in the OB-fold, supporting a model of cooperative binding to RNA by Prp43 and Ntr1 [58] (Figure 4).

In agreement with the *in vitro* activation of the ATPase and helicase activities, the G-patch of DEAH/RHA partners seems to be directly responsible for their activation *in vivo*. Mutations in the G-patch of Spp2 impede the action of Prp2 in the spliceosome. The OB-fold domain of Prp2 is able to interact with Spp2 and mutations in this domain impede this interaction. Mutation of a residue of the G-patch of Spp2 can restore the interaction of Spp2 with the mutant of Prp2, indicating that the G-patch of Spp2 is implicated in the interaction with the C-terminal domain of Prp2 [43]. Therefore, the OB-fold of Prp2 interacts with the G-patch domain of Spp2 and the G-patch of Spp2 activates Prp2 function *in vivo*. Pfa1 (201–767) is sufficient to diminish accumulation of 20S pre-rRNA [53]. Truncation of the G-patch domain of Pfa1 is unable to complement growth defect of cells lacking Pfa1 and Ltv1. In the case of Pfa1, the G-patch domain also seems to be responsible for the activation of Prp43 *in vivo*.

Conclusions and Perspectives. G-patch proteins are activators of DEAH/RHA helicases and the structural features of this activation are starting to be understood even if the overall mechanism remains elusive. Interestingly, not all the DEAH/RHA helicases are associated with a G-patch protein, and unidentified G-patch protein partners or additional G-patch proteins might be uncovered in metazoans. This possibility is supported by the fact that DHX15 is copurified with the ZIP-NuRD complex [39]. The lack of atomic structure of G-patch protein or DEAH/RHA helicase in complex with a G-patch protein is a limiting element to understand the precise structural features of the activation. These structures coupled to a better understanding of the activation of DEAH/RHA helicases could lead to an accurate model of this regulation. This model will be the key to understand how helicases can contribute to the fine regulation of essential processes in RNA metabolism. Comprehension of these mechanisms could help to understand how the interaction between G-patch protein and DEAH/RHA helicases can be implied in cancer as it has been demonstrated for DHX15 and GPATCH2 [54].

Conflict of Interests

The authors declare that there is no conflict of interests regarding the publication of this paper.

Acknowledgments

Work at UPD is supported by Paris Descartes University, CNRS, the RNPGenesis grant from Agence Nationale de la Recherche (ANR-11-JSV8-0004), the Institut Universitaire de France (Nicolas Leulliot), and the nanogears grant from Université Paris Sorbonne Idex. The authors thank Simon Lebaron for critical reading of the paper.

References

[1] M. Abdel-Monem and H. Hoffmann-Berling, "Enzymic unwinding of DNA. I. Purification and characterization of a DNA dependent ATPase from *Escherichia coli*," *European Journal of Biochemistry*, vol. 65, no. 2, pp. 431–440, 1976.

[2] M. Abdel Monem, H. Durwald, and H. Hoffmann Berling, "Enzymic unwinding of DNA. 2. Chain separation by an ATP dependent DNA unwinding enzyme," *European Journal of Biochemistry*, vol. 65, no. 2, pp. 441–449, 1976.

[3] A. E. Gorbalenya and E. V. Koonin, "Helicases: amino acid sequence comparisons and structure-function relationships," *Current Opinion in Structural Biology*, vol. 3, no. 3, pp. 419–429, 1993.

[4] R. M. Story, I. T. Weber, and T. A. Steitz, "The structure of the *E. coli recA* protein monomer and polymer," *Nature*, vol. 355, no. 6358, pp. 318–325, 1992.

[5] R. M. Story and T. A. Steitz, "Structure of the recA protein-ADP complex," *Nature*, vol. 355, no. 6358, pp. 374–376, 1992.

[6] M. R. Singleton, M. S. Dillingham, and D. B. Wigley, "Structure and mechanism of helicases and nucleic acid translocases," *Annual Review of Biochemistry*, vol. 76, pp. 23–50, 2007.

[7] M. E. Fairman-Williams, U.-P. Guenther, and E. Jankowsky, "SF1 and SF2 helicases: family matters," *Current Opinion in Structural Biology*, vol. 20, no. 3, pp. 313–324, 2010.

[8] A. Z. Andreou and D. Klostermeier, "EIF4B and eIF4G jointly stimulate eIF4A ATPase and unwinding activities by modulation of the eIF4A conformational cycle," *Journal of Molecular Biology*, vol. 426, no. 1, pp. 51–61, 2014.

[9] S. Granneman, C. Y. Lin, E. A. Champion, M. R. Nandineni, C. Zorca, and S. J. Baserga, "The nucleolar protein Esf2 interacts directly with the DExD/H box RNA helicase, Dbp8, to stimulate ATP hydrolysis," *Nucleic Acids Research*, vol. 34, no. 10, pp. 3189–3199, 2006.

[10] O. Cordin and J. D. Beggs, "RNA helicases in splicing," *RNA Biology*, vol. 10, no. 1, pp. 83–95, 2013.

[11] T. Ohrt, M. Prior, J. Dannenberg et al., "Prp2-mediated protein rearrangements at the catalytic core of the spliceosome as revealed by dcFCCS," *RNA*, vol. 18, no. 6, pp. 1244–1256, 2012.

[12] T. Ohrt, P. Odenwälder, J. Dannenberg et al., "Molecular dissection of step 2 catalysis of yeast pre-mRNA splicing investigated in a purified system," *RNA*, vol. 19, no. 7, pp. 902–915, 2013.

[13] B. Schwer, "A conformational rearrangement in the spliceosome sets the stage for Prp22-dependent mRNA release," *Molecular Cell*, vol. 30, no. 6, pp. 743–754, 2008.

[14] A. Aronova, D. Bacíková, L. B. Crotti, D. S. Horowitz, and B. Schwer, "Functional interactions between Prp8, Prp18, Slu7, and U5 snRNA during the second step of pre-mRNA splicing," *RNA*, vol. 13, no. 9, pp. 1437–1444, 2007.

[15] J. E. Arenas and J. N. Abelson, "Prp43: an RNA helicase-like factor involved in spliceosome dissassembly," *Proceedings of the National Academy of Sciences of the United States of America*, vol. 94, no. 22, pp. 11798–11802, 1997.

[16] J.-B. Fourmann, J. Schmitzová, H. Christian et al., "Dissection of the factor requirements for spliceosome disassembly and the elucidation of its dissociation products using a purified splicing system," *Genes and Development*, vol. 27, no. 4, pp. 413–428, 2013.

[17] P. Koodathingal, T. Novak, J. A. Piccirilli, and J. P. Staley, "The DEAH box ATPases Prp16 and Prp43 cooperate to proofread 5′ splice site cleavage during Pre-mRNA splicing," *Molecular Cell*, vol. 39, no. 3, pp. 385–395, 2010.

[18] R. M. Mayas, H. Maita, and J. P. Staley, "Exon ligation is proofread by the DExD/H-box ATPase Prp22p," *Nature Structural and Molecular Biology*, vol. 13, no. 6, pp. 482–490, 2006.

[19] S. Lebaron, C. Froment, M. Fromont-Racine et al., "The splicing ATPase Prp43p is a component of multiple preribosomal particles," *Molecular and Cellular Biology*, vol. 25, no. 21, pp. 9269–9282, 2005.

[20] D. J. Combs, R. J. Nagel, M. Ares Jr., and S. W. Stevens, "Prp43p is a DEAH-box spliceosome disassembly factor essential for ribosome biogenesis," *Molecular and Cellular Biology*, vol. 26, no. 2, pp. 523–534, 2006.

[21] N. B. Leeds, E. C. Small, S. L. Hiley, T. R. Hughes, and J. P. Staley, "The splicing factor Prp43p, a DEAH box ATPase, functions in ribosome biogenesis," *Molecular and Cellular Biology*, vol. 26, no. 2, pp. 513–522, 2006.

[22] B. Pertschy, C. Schneider, M. Gnädig, T. Schäfer, D. Tollervey, and E. Hurt, "RNA helicase Prp43 and its co-factor Pfa1 promote 20 to 18 S rRNA processing catalyzed by the endonuclease Nob1," *The Journal of Biological Chemistry*, vol. 284, no. 50, pp. 35079–35091, 2009.

[23] M. T. Bohnsack, R. Martin, S. Granneman, M. Ruprecht, E. Schleiff, and D. Tollervey, "Prp43 bound at different sites on the pre-rRNA performs distinct functions in ribosome synthesis," *Molecular Cell*, vol. 36, no. 4, pp. 583–592, 2009.

[24] V. P. Pisareva, A. V. Pisarev, A. A. Komar, C. U. T. Hellen, and T. V. Pestova, "Translation initiation on mammalian mRNAs with structured 5′UTRs requires DExH-box protein DHX29," *Cell*, vol. 135, no. 7, pp. 1237–1250, 2008.

[25] Y. Hashem, A. Des Georges, V. Dhote et al., "Structure of the mammalian ribosomal 43S preinitiation complex bound to the scanning factor DHX29," *Cell*, vol. 153, no. 5, pp. 1108–1119, 2013.

[26] A. Marintchev, "Roles of helicases in translation initiation: a mechanistic view," *Biochimica et Biophysica Acta: Gene Regulatory Mechanisms*, vol. 1829, no. 8, pp. 799–809, 2013.

[27] Y. Liu, N. Lu, B. Yuan et al., "The interaction between the helicase DHX33 and IPS-1 as a novel pathway to sense double-stranded RNA and RNA viruses in myeloid dendritic cells," *Cellular and Molecular Immunology*, vol. 11, no. 1, pp. 49–57, 2014.

[28] Z. Zhang, B. Yuan, N. Lu, V. Facchinetti, and Y. J. Liu, "DHX9 pairs with IPS-1 to sense double-stranded RNA in myeloid dendritic cells," *Journal of Immunology*, vol. 187, no. 9, pp. 4501–4508, 2011.

[29] N. Sugimoto, H. Mitoma, T. Kim, S. Hanabuchi, and Y.-J. Liu, "Helicase proteins DHX29 and RIG-I cosense cytosolic nucleic acids in the human airway system," *Proceedings of the National Academy of Sciences of the United States of America*, vol. 111, no. 21, pp. 7747–7752, 2014.

[30] K. Mosallanejad, Y. Sekine, S. Ishikura-Kinoshita et al., "The DEAH-Box RNA helicase DHX15 activates NF-κB and MAPK signaling downstream of MAVS during antiviral responses," *Science Signaling*, vol. 7, no. 323, article ra40, 2014.

[31] H. Lu, N. Lu, L. Weng, B. Yuan, Y. J. Liu, and Z. Zhang, "DHX15 senses double-stranded RNA in myeloid dendritic cells," *The Journal of Immunology*, vol. 193, no. 3, pp. 1364–1372, 2014.

[32] A. Jain, A. Bacolla, I. M. Del Mundo, J. Zhao, G. Wang, and K. M. Vasquez, "DHX9 helicase is involved in preventing genomic instability induced by alternatively structured DNA in human cells," *Nucleic Acids Research*, vol. 41, no. 22, pp. 10345–10357, 2013.

[33] Y. Zhang, J. T. Forys, A. P. Miceli, A. S. Gwinn, and J. D. Weber, "Identification of DHX33 as a mediator of rRNA synthesis and cell growth," *Molecular and Cellular Biology*, vol. 31, no. 23, pp. 4676–4691, 2011.

[34] L. Aravind and E. V. Koonin, "G-patch: A new conserved domain in eukaryotic RNA-processing proteins and type D retroviral polyproteins," *Trends in Biochemical Sciences*, vol. 24, no. 9, pp. 342–344, 1999.

[35] M. Svec, H. Bauerova, I. Pichova, J. Konvalinka, and K. Střížovsky, "Proteinases of betaretroviruses bind single-stranded nucleic acids through a novel interaction module, the G-patch," *FEBS Letters*, vol. 576, no. 1-2, pp. 271–276, 2004.

[36] H. Bauerova-Zabranska, J. Štokrová, K. Strísovský, E. Hunter, T. Ruml, and I. Pichová, "The RNA binding G-patch domain in retroviral protease is important for infectivity and D-type morphogenesis of Mason-Pfizer monkey virus," *Journal of Biological Chemistry*, vol. 280, no. 51, pp. 42106–42112, 2005.

[37] I. Krizova, R. Hadravova, J. Stokrova et al., "The G-patch domain of Mason-Pfizer monkey virus is a part of reverse transcriptase," *Journal of Virology*, vol. 86, no. 4, pp. 1988–1998, 2012.

[38] M. Rumlová, I. Křížová, R. Hadravová et al., "Breast carcinoma associated protein—a novel binding partner of Mason-Pfizer monkey virus protease," *The Journal of General Virology*, vol. 95, part 6, pp. 1383–1389, 2014.

[39] R. Li, H. Zhang, W. Yu et al., "ZIP: a novel transcription repressor, represses EGFR oncogene and suppresses breast carcinogenesis," *The EMBO Journal*, vol. 28, no. 18, pp. 2763–2776, 2009.

[40] W. Yu, R. Li, B. Gui, and Y. Shang, "sZIP, an alternative splice variant of ZIP, antagonizes transcription repression and growth inhibition by ZIP," *Journal of Biological Chemistry*, vol. 285, no. 19, pp. 14301–14307, 2010.

[41] B. Gui, X. Han, Y. Zhang et al., "Dimerization of ZIP promotes its transcriptional repressive function and biological activity," *The International Journal of Biochemistry & Cell Biology*, vol. 44, no. 6, pp. 886–895, 2012.

[42] J. Roy, K. Kim, J. R. Maddock, J. G. Anthony, and J. L. Woolford Jr., "The final stages of spliceosome maturation require Spp2p that can interact with the DEAH box protein Prp2p and promote step 1 of splicing," *RNA*, vol. 1, no. 4, pp. 375–390, 1995.

[43] E. J. Silverman, A. Maeda, J. Wei, P. Smith, J. D. Beggs, and R.-J. Lin, "Interaction between a G-patch protein and a spliceosomal DEXD/H-box ATPase that is critical for splicing," *Molecular and Cellular Biology*, vol. 24, no. 23, pp. 10101–10110, 2004.

[44] R. Krishnan, M. R. Blanco, M. L. Kahlscheuer, J. Abelson, C. Guthrie, and N. G. Walter, "Biased Brownian ratcheting leads to pre-mRNA remodeling and capture prior to first-step splicing," *Nature Structural and Molecular Biology*, vol. 20, no. 12, pp. 1450–1457, 2013.

[45] Z. Warkocki, P. Odenwälder, J. Schmitzová et al., "Reconstitution of both steps of Saccharomyces cerevisiae splicing with purified spliceosomal components," *Nature Structural and Molecular Biology*, vol. 16, no. 12, pp. 1237–1243, 2009.

[46] N. Tanaka, A. Aronova, and B. Schwer, "Ntr1 activates the Prp43 helicase to trigger release of lariat-intron from the spliceosome," *Genes and Development*, vol. 21, no. 18, pp. 2312–2325, 2007.

[47] R.-T. Tsai, C.-K. Tseng, P.-J. Lee et al., "Dynamic interactions of Ntr1-Ntr2 with Prp43 and with U5 govern the recruitment of Prp43 to mediate spliceosome disassembly," *Molecular and Cellular Biology*, vol. 27, no. 23, pp. 8027–8037, 2007.

[48] R.-T. Tsai, R.-H. Fu, F.-L. Yeh et al., "Spliceosome disassembly catalyzed by Prp43 and its associated components Ntr1 and Ntr2," *Genes and Development*, vol. 19, no. 24, pp. 2991–3003, 2005.

[49] X. Wen, S. Tannukit, and M. L. Paine, "TFIP11 interacts with mDEAH9, an RNA helicase involved in spliceosome disassembly," *International Journal of Molecular Sciences*, vol. 9, no. 11, pp. 2105–2113, 2008.

[50] R. Yoshimoto, N. Kataoka, K. Okawa, and M. Ohno, "Isolation and characterization of post-splicing lariat-intron complexes," *Nucleic Acids Research*, vol. 37, no. 3, pp. 891–902, 2009.

[51] Z. Niu, W. Jin, L. Zhang, and X. Li, "Tumor suppressor RBM5 directly interacts with the DExD/H-box protein DHX15 and stimulates its helicase activity," *FEBS Letters*, vol. 586, no. 7, pp. 977–983, 2012.

[52] Y. L. Chen, R. Capeyrou, O. Humbert et al., "The telomerase inhibitor Gno1p/PINX1 activates the helicase Prp43p during ribosome biogenesis," *Nucleic Acids Research*, vol. 42, no. 11, pp. 7330–7345, 2014.

[53] S. Lebaron, C. Papin, R. Capeyrou et al., "The ATPase and helicase activities of Prp43p are stimulated by the G-patch protein Pfa1p during yeast ribosome biogenesis," *The EMBO Journal*, vol. 28, no. 24, pp. 3808–3819, 2009.

[54] M. L. Lin, C. Fukukawa, J. H. Park et al., "Involvement of G-patch domain containing 2 overexpression in breast carcinogenesis," *Cancer Science*, vol. 100, no. 8, pp. 1443–1450, 2009.

[55] B. Guglielmi and M. Werner, "The yeast homolog of human PinX1 is involved in rRNA and small nucleolar RNA maturation, not in telomere elongation inhibition," *Journal of Biological Chemistry*, vol. 277, no. 38, pp. 35712–35719, 2002.

[56] G. Herrmann, S. Kais, J. Hoffbauer et al., "Conserved interactions of the splicing factor Ntr1/Spp382 with proteins involved in DNA double-strand break repair and telomere metabolism," *Nucleic Acids Research*, vol. 35, no. 7, pp. 2321–2332, 2007.

[57] N. Tanaka and B. Schwer, "Mutations in PRP43 that uncouple RNA-dependent NTPase activity and Pre-mRNA splicing function," *Biochemistry*, vol. 45, no. 20, pp. 6510–6521, 2006.

[58] H. Christian, R. V. Hofele, H. Urlaub, and R. Ficner, "Insights into the activation of the helicase Prp43 by biochemical studies and structural mass spectrometry," *Nucleic Acids Research*, vol. 42, no. 2, pp. 1162–1179, 2014.

[59] Y. He, G. R. Andersen, and K. H. Nielsen, "Structural basis for the function of DEAH helicases," *EMBO Reports*, vol. 11, no. 3, pp. 180–186, 2010.

[60] H. Walbott, S. Mouffok, R. Capeyrou et al., "Prp43p contains a processive helicase structural architecture with a specific regulatory domain," *EMBO Journal*, vol. 29, no. 13, pp. 2194–2204, 2010.

Hindawi Publishing Corporation
BioMed Research International
Volume 2014, Article ID 549719, 14 pages
http://dx.doi.org/10.1155/2014/549719

Review Article

The Mcm2-7 Replicative Helicase: A Promising Chemotherapeutic Target

Nicholas E. Simon and Anthony Schwacha

Department of Biological Sciences, University of Pittsburgh, Pittsburgh, PA 15260, USA

Correspondence should be addressed to Anthony Schwacha; schwacha@pitt.edu

Received 23 June 2014; Revised 8 August 2014; Accepted 10 August 2014; Published 28 August 2014

Academic Editor: Cheng-Yang Huang

Numerous eukaryotic replication factors have served as chemotherapeutic targets. One replication factor that has largely escaped drug development is the Mcm2-7 replicative helicase. This heterohexameric complex forms the licensing system that assembles the replication machinery at origins during initiation, as well as the catalytic core of the CMG (Cdc45-Mcm2-7-GINS) helicase that unwinds DNA during elongation. Emerging evidence suggests that Mcm2-7 is also part of the replication checkpoint, a quality control system that monitors and responds to DNA damage. As the only replication factor required for both licensing and DNA unwinding, Mcm2-7 is a major cellular regulatory target with likely cancer relevance. Mutations in at least one of the six *MCM* genes are particularly prevalent in squamous cell carcinomas of the lung, head and neck, and prostrate, and *MCM* mutations have been shown to cause cancer in mouse models. Moreover various cellular regulatory proteins, including the Rb tumor suppressor family members, bind Mcm2-7 and inhibit its activity. As a preliminary step toward drug development, several small molecule inhibitors that target Mcm2-7 have been recently discovered. Both its structural complexity and essential role at the interface between DNA replication and its regulation make Mcm2-7 a potential chemotherapeutic target.

1. Introduction

Misregulated DNA replication is a basic prerequisite for uncontrolled cellular proliferation, and the clinical targeting of eukaryotic replication factors has seen widespread use in cancer treatment. Small molecule inhibitors that predominantly target leading or lagging strand synthesis, such as topoisomerases [1], DNA polymerases [2], DNA ligase [3], proliferating cell nuclear antigen (PCNA) [4], ribonucleotide reductase [5], and telomerase [6], have been developed to clinically block uncontrolled cancer proliferation. Although proven chemotherapeutic agents, these compounds target both normal and malignant DNA replication and as such often exhibit deleterious side effects [7–10]. In contrast, few inhibitors have been developed that target replication initiation. As an essential factor that couples DNA replication to both cell cycle progression and checkpoint regulation (below), the Mcm2-7 complex offers a unique and intriguing alternative target for drug development.

Mcm2-7 forms the catalytic core of the helicase (CMG complex, below) that unwinds parental DNA to generate single-stranded templates for DNA polymerase (reviewed in [11]). Mcm2-7 was initially identified during a genetic screen for *S. cerevisiae* mutants that demonstrated defective plasmid segregation (minichromosome maintenance [12]). Subsequent work in yeast demonstrated that such *mcm* alleles cause a replication defect [13], and the corresponding proteins were later found to be components of "licensing factor," a biochemical activity isolated from *Xenopus* egg extracts that couples cell cycle progression to DNA replication [14]. However, due to the inherent enzymatic and regulatory complexity, the biochemical identification of Mcm2-7 as the replicative helicase took many years of work from multiple laboratories (reviewed in [11]).

Mcm2-7 is an unusually complex helicase. Unlike prokaryotic and viral hexameric helicases formed from six copies of an identical protein, Mcm2-7 consists of six different subunits (historically numbered from 2 → 7). Although each is distinct and essential [13, 15, 16], these subunits are all AAA+ ATPases and demonstrate partial sequence homology with one another [17]. As is common among AAA+ ATPases,

Mcm2-7 forms a toroidal complex with ATPase active sites at dimer interfaces formed from conserved motifs contributed by each adjoining subunit [18, 19] (Figure 1(a)). The six Mcm subunits demonstrate particularly high evolutionary conservation relative to other replication proteins; each subunit defines a gene family that is found in essentially all eukaryotes studied to date [20, 21]. Although most of the structural and mechanistic work to date has been performed on the Mcm2-7 complex from yeast and *Drosophila*, the strong evolutionary conservation of Mcm2-7 makes it likely that findings with lower eukaryotes will also apply to human DNA replication.

The structural complexity of Mcm2-7 appears to be related to its regulation. Both genetic and biochemical investigations demonstrate an unequal functional contribution among these six active sites for DNA unwinding [16, 19, 22–27] (Figure 1(b)). DNA unwinding appears to require only the Mcm4, 6, and 7 subunits, as this particular trimeric subassembly from a variety of different organisms is competent to unwind DNA *in vitro* [26, 28, 29]. Moreover, work from budding yeast has shown that a complex containing only the Mcm4 and 7 subunits is specifically capable of unwinding DNA [25], and biochemical analysis of the corresponding Mcm4/7 ATPase active site demonstrates that it is particularly important for both steady-state ATP hydrolysis and DNA unwinding activities of the Mcm2-7 hexamer [19, 23, 24]. In contrast, the Mcm2/5 ATPase active site serves to regulate the DNA unwinding activity through formation of a reversible discontinuity within the Mcm toroid structure (Mcm2/5 gate, Figure 1(b)): the gate-open conformation blocks helicase activity, whereas the gate-closed conformation is helicase-active [23, 30]. In general, regulation of the Mcm2/5 gate conformation may be the main function of the Mcm2, 3, and 5 subunits, as ablation of the Mcm2/5 ATPase site [22] as well as those flanking the gate (Mcm6/2 and Mcm5/3 [24]) biochemically reduce the ability of Mcm2-7 to alternate between the gate-open and gate-closed forms.

Accumulating evidence indicates that regulation of the Mcm2/5 gate conformation restricts DNA replication to S-phase and ensures that one and only one copy of the genome is replicated per cell cycle. This regulation is a two-step process that involves the Mcm2/5 gate; Mcm2-7 loads onto chromosomes during G1 but is activated for DNA unwinding only following passage into S-phase (Figure 1(c), legend [31]). During initiation in G1, Mcm2-7 origin loading requires several factors (e.g., Cdt1 and Cdc6) which together with the origin recognition complex (ORC) form the prereplication complex (pre-RC [32–35]). Mcm2-7 origin association does not occur passively; *in vitro*, Mcm ATP hydrolysis is required for pre-RC formation [36, 37]. At least one role of this ATP hydrolysis may be Mcm2/5 gate opening, as conditional forced dimerization of the Mcm2 and 5 subunits using Mcm alleles that contain rapamycin-mediated dimerization domains (to mimic the gate closed form) blocks Mcm2-7 DNA loading and cell cycle progression *in vivo* [38]. This effect is specific for the Mcm2 and 5 dimer interface, as forced dimerization between other neighboring subunits has no effect [38].

Structural evidence indicates that closure of the Mcm2/5 gate is required to activate DNA unwinding and elongation. Upon S-phase entry, several regulatory kinases (including the cyclin-dependent kinases (CDKs) and the Dbf4-dependent kinase (DDK)) activate Mcm2-7 by enabling the loading of the key accessary factors Cdc45 and GINS that in combination with Mcm2-7 form the CMG complex (Cdc45-Mcm2-7-GINS) [39–41]. Participation of both Cdc45 and GINS in the CMG complex greatly stimulates the *in vitro* DNA unwinding activity of Mcm2-7, and the *in vivo* formation of the CMG is presumably the main S-phase activation step of DNA replication [27]. Structural analysis of the CMG complex by transmission electron microscopy has determined the mechanism of Cdc45 and GINS activation; together these proteins bind across the Mcm2/5 gate and close the discontinuity [30]. Since Mcm loading and activation are mutually exclusive events (reviewed in [31]), the cell cycle regulation of DNA replication fundamentally centers on the loading and subsequent activation of Mcm2-7.

There is mounting evidence that Mcm2-7 is also a focus of regulation during elongation. The DNA replication checkpoint (DRC) monitors chromosome replication during S-phase; if damage is detected, it promotes genome stability by shutting down cell cycle progression and elongation until the problem is repaired (reviewed in [42]). In the event that the damage is not repaired, the pathway in metazoans eventually causes apoptosis and the elimination of potentially carcinogenic cells from the population [43]. Key to this checkpoint is the ATR sensor kinase and Chk1/2 effector kinases; all, if mutated, promote genome instability leading to cancer [44]. Although the mechanism is yet unclear, circumstantial evidence suggests that Mcm2-7 is regulated by the replication checkpoint. Mcm2-7 is directly phosphorylated during replication stress by ATR [45–48]. Moreover, Mcm2-7 physically associates with three conserved proteins that serve as mediator factors of the DRC (Claspin, Tipin, and Tof1 in metazoans, or Mrc1, Csm3, and Tof1 in budding yeast [49–52]), making it likely that this constitutive association with Mcm2-7 has regulatory significance.

Given the likely differential involvement of specific Mcm2-7 ATPase active sites in multiple aspects of DNA replication and its regulation, small molecule inhibitors could be profitably identified that selectively target these individual activities. Such inhibitors could prove useful for a variety of research as well as chemotherapy applications. Although various *in vitro* DNA replication systems have been established [53–56], dissecting-out the precise mechanistic roles of the various component proteins is difficult, an issue compounded by the fact that many replication factors are ATPases that are difficult to individually inactivate using available nonspecific ATPase inhibitors. Moreover, as various alterations in Mcm expression or function are linked to oncogenic DNA replication (e.g., [57]), Mcm2-7 is a promising drug target for the development of both general replication inhibitors that stem cellular proliferation, as well as potentially more sophisticated inhibitors that specifically target Mcm2-7 in tumor cells (discussed below).

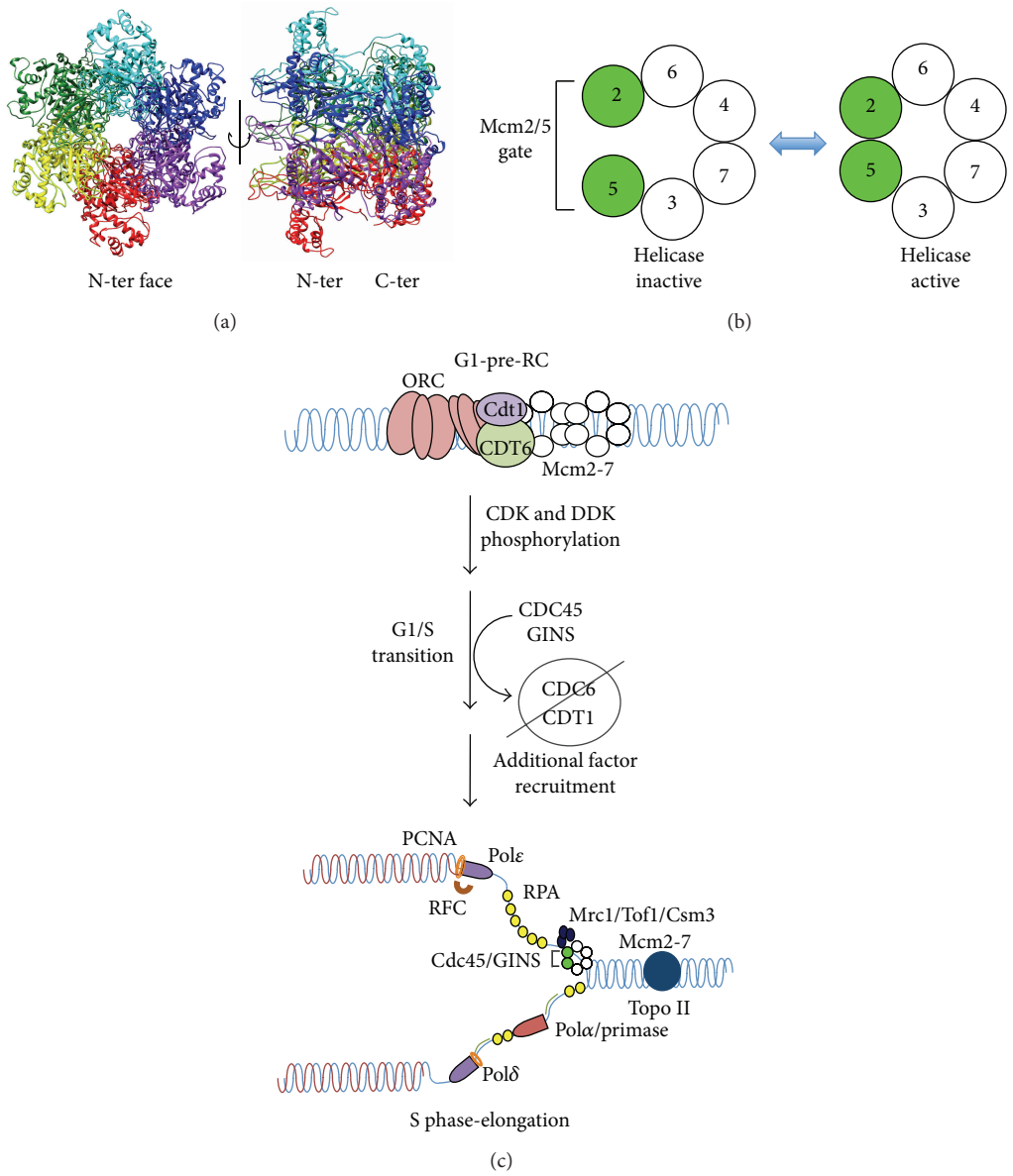

Figure 1: Mcm2-7 is a key regulatory component of cell cycle progression. (a) Homology model of the human Mcm2-7 complex. No high resolution structure yet exists for the eukaryotic Mcm2-7 complex. However, the archaea have homohexameric Mcm helicases, and a crystal structure of the *S. solfataricus* Mcm complex has been solved [58]. To generate a homology model, the human Mcm protein sequences were uploaded into the Phyre 2 server (http://www.sbg.bio.ic.ac.uk/phyre2/) that assigns secondary structure based upon alignment against homologous proteins with solved structures [59]. The resulting Mcm structure predictions were then threaded into an existing hexameric archaeal Mcm structure (PDB ID 2VL6) using PYMOL (http://www.pymol.org) and the previously determined arrangement of adjoining Mcm subunits [18, 19]. As shown, the Mcm2-7 complex generates a toroidal structure resembling the SV-40 large T antigen, a related AAA+ helicase [60]. (b) The Mcm complex is functionally asymmetric. Numerous lines of biochemical and structural evidence demonstrate that the six active sites formed by the six subunits *in trans* are functionally distinct (reviewed in [11]). The Mcm2/5 site has low ATP turnover, suggesting it is regulatory in nature and forms a reversible discontinuity that must be closed in order to activate helicase activity. (c) Mcm2-7 is the key component of S-phase activation (reviewed in [11, 31, 61]). In early G1 phase, Mcm hexamers are recruited to the origin recognition complex (ORC), and bound to origins of replication by the loading factors Cdc6 and Cdt1. The Mcm toroid is bound around dsDNA [35, 62], presumably requiring the ring to be opened at the Mcm 2/5 active site [38]. Along with ORC and Cdc6, head-to-head Mcm2-7 dimers remain in a biochemically inactive state as part of the prereplication complex until their irreversible activation by the regulatory kinases DDK (Dbf4 dependent kinase) and CDK (cyclin dependent kinase). CDC45 and GINS are targeted to the Mcm2-7 complex by the activity of additional recruitment factors such as Sld2, Sld3, and Dbp11, and the Mcm complex shifts from dsDNA bound state to a ssDNA bound state. DNA unwinding commences to provide a ssDNA template for the rest of the DNA replication machinery. Concurrently, Cdc6 and Cdt1 are removed from the nucleus to prevent reloading of the helicase and deleterious rereplication of the genome.

2. The Mcms and Cancer

Genomic instability, often caused by replication stress [65], is believed to be a necessary step in cancer development. As such, Mcm2-7 expression levels and activity need to be carefully balanced to preserve genome stability. Although yeast does not develop cancer *per se*, much of our knowledge of how Mcms affect genomic stability stem from studies of these organisms. In addition to the plasmid loss phenotype described earlier [12], Mcm mutations cause chromosome loss, DNA damage, and increased recombination in budding yeast [13, 66]. In *S. pombe*, Mcm mutants have been shown to accumulate DNA repair foci diagnostic of DNA double strand breaks (DSBs) [67]. Moreover, although the number of individual Mcm subunits in the nucleus considerably exceeds the number of replication origins [68, 69], as little as a twofold reduction in Mcm expression has been shown to cause genomic instability [68, 70]. In total, these defects have largely been interpreted as underreplication caused by reduced Mcm2-7 activity [71]. As both DNA replication and fundamental issues of genomic instability are highly conserved among eukaryotes, our knowledge of Mcm2-7 derived from simpler eukaryotes is likely directly relevant to cancer development in metazoan systems.

Consistent with their essential role in cellular proliferation, the Mcms have found common use as a cytological marker of cancer. Since Mcm protein is absent from chromatin in quiescent cells but abundant in active mitotic cells [72], many groups have studied the potential for using Mcm2-7 expression as an immunocytological marker for cellular proliferation [73–75]. Further studies validate the Mcm proteins (Mcm2 in particular) as excellent prognostic and diagnostic markers of human oral, colon, ovarian, and urothelial carcinomas that compare favorably with more traditional cytological markers such as PCNA and Ki-67 (reviewed in [76]).

Studies in both mice and human cells indicate that both *MCM* gene duplication and overexpression can contribute to cancer development (e.g., [77–79]). The recent high-throughput sequencing of various cancerous tissues indicates that the amplification of at least one of the *MCM* genes is relatively common. For example, in a study of 178 tumor genomes that had been corrected for somatic variations, 10% of lung squamous cell carcinomas contained amplifications in at least one *MCM* gene (http://www.cbioportal.org [80]). Moreover, direct reconstruction studies indicate that overexpression of individual Mcm subunits can stimulate cancer formation. Targeted overexpression of *MCM7* in epidermal tissue predisposed mice to form malignant tumors, as animals that overexpressed *MCM7* saw a decrease in the average time to develop tumors in response to carcinogens and an increase in the frequency and propensity of these tumors to form squamous cell carcinomas relative to wild type littermates [81].

Reductions in Mcm2-7 expression levels have also been linked to cancer. Systematic ablation of one of the two gene copies of either Mcm2, 3, 4, or 6, as well as combinations of these hemizygous alleles, have been studied in mice. In general, such mice show reduced MCM proteins levels, growth retardation, and reduced proliferation. Thus, as in budding yeast, MCM protein levels need to be critically managed in metazoans to ensure normal growth. Consistent with genomic instability studies in yeast [68, 70], an experimental reduction of Mcm2 expression in transgenic mice causes lymphomas [82, 83]. Such mice died in early adulthood from various cancers, and necropsy revealed a 100% penetrance of thymomas [83].

Moreover, *MCM* point mutations are common in tumors. For example, in a study of 178 tumor genomes that had been corrected for somatic variations, 12% of lung squamous cell carcinomas were found to contain point mutations in at least one of the six *MCM* genes (http://www.cbioportal.org [80]). Although several *MCM* point mutations have been shown to cause cancer, it is unclear if this is due to a general hypomorphic reduction in DNA replication potential, or a specific loss of Mcm regulation. For example, a specific viable *MCM* allele, $mcm4^{chaos3}$ ($mcm4^{F345I}$), was identified in a forward genetic screen for cancer-causing mouse alleles and results in spontaneous mammary tumors in 80% of mice [84, 85]. When this same allele was reconstructed into the yeast *MCM4* gene, the corresponding *S. cerevisiae* mutant demonstrated a classical plasmid loss phenotype, genomic instability, and reduced viability [84, 86]. In this case, the mcm^{chaos3} allele was shown to generate Mcm2-7 complexes with reduced physical stability, suggesting that the *chaos3* allele functions to nonspecifically reduce DNA replication potential [85]. In contrast, a second *mcm4* allele was identified as a spontaneous dominant mutation in a mouse colony that had acquired an early-onset leukemogenesis phenotype. The cancer phenotype was subsequently mapped to *MCM4*, and the relevant amino acid substitution ($mcm4^{D573H}$) was found to occur in the universally conserved Walker B ATPase motif. Unlike $mcm4^{chaos3}$, the mutant was not hypomorphic and failed to compliment a *MCM4* deletion in yeast complementation assays, suggesting that $mcm4^{D573H}$ is a dominant change of function allele that poisons normal Mcm2-7 helicase activity [87].

In total these mouse and tissue culture studies strongly imply that Mcm alterations can also drive human cancer. In normal human genomes, various single nucleotide polymorphisms in the *mcm* genes are commonly observed (http://www.ncbi.nlm.nih.gov/projects/SNP/). At least some of these polymorphisms may in themselves generate genomic instability in susceptible individuals, as at least some MCM polymorphisms cause genomic instability when assayed in budding yeast [88]. Intriguingly, among *mcm* cancer alleles listed in the cBioPortal (http://www.cbioportal.org), mutations that fall within the conserved ATPase motifs (Walker A and B, Sensor 1 and 2, and Arginine finger motif) commonly occur among all six Mcm genes. As such, some of these alleles may generate Mcm2-7 complexes with a specific biochemical defect in a particular step of DNA replication or its regulation rather than generating a generally hypomorphic situation.

Thus, the role of the Mcms in cancer development seems contradictory, as both underexpression (consistent with a tumor suppressor) and overexpression (consistent with an oncogene) are linked to cancer development. Although

a direct Mcm2-7-mediated biochemical defect in DNA replication cannot be ruled out in either case, the underlying causes behind these two conditions are likely to be very different, while underexpression likely reduces the level of Mcm2-7 complexes needed for normal DNA replication, while overexpression likely reflects inappropriate protein-protein interactions. Such interactions might serve to either titrate out factors that block abnormal proliferation (e.g., Rb, below), or upset a critical stoichiometric balance among Mcm subunits within the cell to increase nonproductive Mcm subassemblies at the expense of active hexamers. Alternatively, Mcm gene overexpression may lead to higher concentrations functional Mcm2-7 complexes per cell, resulting in a deleterious increase of origin activation and/or DNA unwinding. However, under either scenario, excess Mcm2-7 activity either directly or indirectly drives cellular proliferation. In total, these studies collectively provide strong evidence for a functional connection between the Mcm complex and cancer development, and modulating their activity may be an avenue for the development of novel therapeutics.

3. Various Tumor Suppressors and Regulatory Factors Bind Mcm2-7 and Inhibit Its Activity

Accumulating evidence suggests that during early cancer development, altered Mcm2-7 regulation resulting from oncogene expression leads to a particularly mutagenic form of DNA replication (oncogene-induced DNA replication stress [89–92]) that fuels genomic instability and proliferation. Evidence derived from the sequencing of tumor genomes suggests that such oncogenic replication stress occurs through alterations in Rb/E2F regulation and the control of G1/S phase progression, resulting in the production of DNA double-stranded breaks (DSBs), genomic instability and mutagenesis, and the subsequent loss of key regulators such as the p53 tumor suppressor (reviewed in [89, 90]).

The Rb (retinoblastoma) protein family members normally inhibit S-phase progression by binding to and subsequently inactivating members of the E2F family (reviewed in [93], Figure 2). The Rb family contains related factors with somewhat different properties; these include p105, p107, and p130 proteins [93]. In contrast the E2F proteins are transcriptional activators or repressors that directly control the transition into S-phase by modulating gene expression. Progression into S-phase depends upon CDK activity; Rb phosphorylation by CDK promotes E2F release and activates its transcription function. In turn, the CDKs themselves are inhibited by various regulatory proteins (e.g., CDK inhibitors (CKI)). Multiple CKIs exist in cells, and among others form the INK4 (e.g., $p16^{INK4a}$, $p15^{INK4b}$, $p18^{NK4c}$, and $p19^{INK4d}$) and KIP/CIP (e.g., $p27^{KIP1}$ and $p21^{CIP1}$) families [94, 95]. As such, both Rb and CKIs are inhibitors of cell cycle progression, and members of both families are commonly mutated in human tumors [96].

Although the details are yet unclear, altered replication origin firing may be the underlying cause behind oncogene-induced replication stress [65]. Work done in both yeast as well as metazoans suggests the existence of an optimal level of origin usage: both too few and too many firing origins lead to DSB formation (reviewed in [65]). As discussed above, the Mcms are the fundamental focus of both origin loading and activation, raising the strong likelihood that Mcm misregulation plays a role in oncogene-induced replication stress.

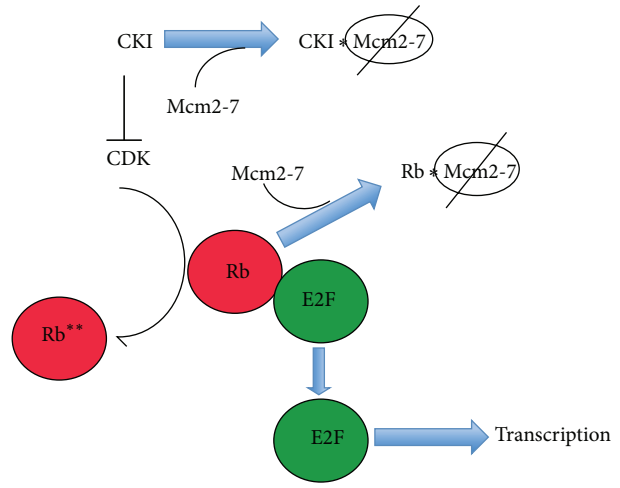

Figure 2: A simplified overview of the Rb/E2F pathway. In general, Rb binds to and inhibits E2F, resulting in the altered transcription of numerous S-phase relevant genes. During the G1/S part of the cell cycle, increased CDK activity leads to RB phosphorylation, which causes release and activation of E2F, and an induction of S-phase dependent gene expression. In turn, various inhibitors (CKI) modulate CDK activity. In addition to their well-established role in transcriptional regulation through E2F, both CKIs and Rb bind to and inactivate Mcm2-7; how this inhibition is reverded to facilitate subsequent DNA replication is currently unknown.

In support of this conjecture, both Rb and several CKIs have been shown to bind Mcm7 and inhibit Mcm2-7 activity (Table 1, Figure 2). A yeast two-hybrid screen aimed at identifying proteins that bind the N-terminal region of Rb showed that it forms a complex with the carboxy terminus of Mcm7. Immunoprecipitations with full length Rb (p105) and Mcm7 proteins recapitulated this interaction *in vitro* and also demonstrated that other Rb family members p107 and p130 also bind Mcm7 [97]. Furthermore, Rb and p130 inhibited DNA replication in a *Xenopus* DNA replication assay in an Mcm7-dependent manner [98], suggesting that physical interactions between Mcm7 and Rb have physiological significance.

Several CKIs have also been found to block Mcm2-7 function (Figure 2). The cyclin-D dependent kinase inhibitor $p16^{INK4a}$ has been shown to indirectly block Mcm origin loading by inhibiting the activities of Cdc6 and Cdt1 [101]. In contrast, the $p27^{kip1}$ factor, a CDK and DNA replication inhibitor (reviewed in [105]) has been shown to bind the AAA+ motor domain of Mcm7 [102]. This interaction appears physiologically relevant, as a truncated $p27^{kip1}$ protein capable of binding Mcm7 but lacking the ability to inhibit CDK was able to cause significant inhibition of DNA replication in an *in vitro* DNA replication system [102]. This

Table 1: Protein interactors and regulators of the Mcm2–7 complex.

Inhibitor	Phenotype	Subunits targeted	Reference
ING5	Binds Mcm2-7	Mcm2, 4, 6, & 7	[99]
NCOA4	Blocks origin firing, helicase activity	Mcm7	[100]
$p16^{INK4a}$	Blocks Mcm2-7 origin loading	Indirect (Cdc6, Cdt1)	[101]
$p27^{KIP1}$	Blocks *in vitro* replication	Mcm7	[102]
Prohibitin	Blocks *in vitro* replication	Mcm2 & 5	[103]
RAD17	Blocks checkpoint activation	Mcm7	[104]
Retinoblastoma protein/p130	Blocks *in vitro* replication	Mcm7	[97]

implies that the Mcm7/$p27^{kip1}$ interaction can regulate DNA replication independent of CDK inhibition.

In addition to factors directly involved in Rb/E2F regulation, other regulatory factors bind Mcm2-7 in an apparently functional manner. (1) Prohibitin, a scaffolding protein that, similar to Rb, had previously been shown to inhibit E2F transcription targets [106, 107], was found to physically interact primarily with Mcm2 and 5, perhaps functioning by interfering with the Mcm2/5 gate. Purified prohibitin also inhibited *in vitro* DNA replication, perhaps by inhibiting Mcm2-7 [103]. (2) The human Rad17 protein, which together with RFC 2-5 forms an alternative clamp loader that (along with the 911 complex) is required for ATR activation of the replication checkpoint cascade in metazoans [108], binds the C-terminus of Mcm7 [104]. Transfection of just the Mcm7-binding region of Rad17 into cell lines abolished UV-induced replication checkpoint activation, suggesting that this interaction is physiologically relevant [104]. (3) Recent work has demonstrated that the NCOA4 transcriptional coactivator also binds Mcm7 in a relevant manner to inhibit DNA replication by interacting with the CMG complex, blocking its helicase activity, and negatively regulating the activation of origins of replication [100]. (4) Finally, a variety of additional proteins have been shown to bind the C-terminus of Mcm7, but currently the physiological significance of the observed binding interactions is unknown or poorly understood. These include the ING5 tumor suppressor [99], ATRIP [45], and Cyclin D1 dependent kinase [109].

Although the mapping of specific interaction sites between Mcm7 and its various binding partners has not yet been performed at high resolution, available evidence suggests that these sites likely overlap conserved ATPase motifs. Rb binds a region of Mcm7 that is contained within a fragment encoding amino acids 583–719 of human Mcm7 [97], while Rad17 binding is contained within amino acids 521–620 [104]. Both putative interaction sites span the conserved Sensor 2 and Presensor 2 motifs of Mcm7 that together form part of the Mcm4/7 ATPase active site [11]. As this region spans essential active site motifs, it is evolutionary well conserved particularly among metazoans, and the binding of these regulatory factors to Mcm7 likely functions to block or alter ATP hydrolysis at the Mcm4/7 site.

Thus, the observed interactions between Mcm2-7 and the various regulatory factors may target key enzymatic activities, either DNA unwinding or regulation of the Mcm2/5 gate. The connection between Mcm2-7 and multiple members of the Rb/E2F signaling pathway appears to be direct and distinct from the role of this pathway in modulating gene expression. Finally, as most reported Mcm7 binding interactions target the Mcm7 C-terminus, competition among these factors for Mcm7 binding may be an important aspect of Mcm2-7 regulation.

4. Small Molecule Inhibitors and Potential Chemotherapeutic Agents of the Eukaryotic Replicative Helicase

Helicases are common enzymes. For example, *S. cerevisiae* contains 134 open reading frames (2% of its genome) that encode proteins containing helicase structural motifs [110]. Helicases in general have received recent drug-discovery attention, and small molecule inhibitors of viral helicases have been the focus of several high throughput screens (reviewed in [111]). Many viral helicases (e.g., SV40 large T antigen [112]) have multiple cellular functions in addition to bulk replication. This property increases the potency of such small molecule inhibitors, as more cellular systems are coordinately impacted, and the likelihood of acquiring drug resistance mutations is decreased. Mcm2-7 is similar in that it coordinates regulatory processes in addition to genome replication. Moreover, the heterohexameric organization of Mcm2-7 might prove particularly advantageous; it might be difficult for an organism to develop drug resistance if multiple Mcm ATPase active sites are targeted. However, in contrast to their prokaryotic and viral counterparts, no high throughput biochemical screens have been performed on the eukaryotic replicative helicase. The reason for this is largely practical: it is difficult to purify Mcm2-7 or the CMG complex in amounts large enough to perform these screens, and *in vitro* helicase activity has not been demonstrable for the whole complex until fairly recently [23, 113].

Given what is known about the biochemistry and genetics of Mcm2-7, one can broadly envision at least three different classes of small molecule inhibitors with potential chemotherapeutic utility. These include (1) enzymatic inhibitors (e.g., targeting the various ATPase active sites), (2) inhibitors that block physical or genetic interactions between Mcm subunits and other proteins, and (3) molecules that modulate Mcm expression levels.

Enzymatic inhibitors that block Mcm2-7's normal role in either DNA replication initiation or elongation are one obvious class. As mentioned in the Introduction, many types of inhibitors have been developed to block the function of specific replication factors as a means to block the cellular proliferation observed in cancer. Such inhibitors that target Mcm2-7 would potentially provide an additional useful weapon in this arsenal.

Two problems however exist with the identification of therapeutically useful biochemical inhibitors. First, as mentioned above, both the Mcm2-7 and CMG complexes are difficult to purify in sufficient quantity for extensive primary high-throughput screening. Although improved technology may ultimately solve this problem, cell-based screening approaches using engineered test organisms might be devised to identify Mcm inhibitors in a primary screen; such drug candidates could then be subsequently tested in appropriate secondary biochemical screens (e.g., [114]). Second, reduction of Mcm levels as little as twofold below endogenous levels has been shown to cause genomic instability, suggesting that a loss of Mcm activity is deleterious to healthy cells. However, it should be noted that many current chemotherapeutic agents induce genomic instability either as collateral damage (e.g., [115]), or to intentionally trigger apoptosis in sensitive (e.g., cancerous) cells (reviewed in [116]). Moreover, it should be noted that most of the genomic instability defects demonstrated by Mcm mutations are likely the results of elongation problems (e.g., replication fork collapse); potential Mcm inhibitors that block initiation (and hence formation of the replication fork) would likely block this form of genomic instability. In short, it may be possible to develop appropriate inhibitors for Mcm2-7 that balance chemotherapeutic utility with potential off-target genome instability effects.

Alternatively, targeted inhibitors that disrupt interaction between Mcm2-7 and other cellular proteins may be identified that specifically block abnormal DNA replication. Proteins that functionally interact within a cell often demonstrate a property termed synthetic lethality; mutations in either gene may individually support viability, but when combined caused lethality [117]. Thus, inhibitors of Mcm2-7 interacting proteins might be obtained that specifically target abnormal replication caused by Mcm mutants, while having little effect on cells with normal DNA replication. High throughput inhibitor screens that utilize synthetic lethality as a read-out have been developed (reviewed in [118]); the recent identification of PARP inhibitors that specifically target mutant BRAC1-containing cancer cells are an example of such a successful screening approach (reviewed in [119]).

Finally, chemotherapeutics might be identified to specifically tailor Mcm gene expression levels. Since Mcm-2-7 levels appears to be critically balanced to prevent genome instability, drugs that modulate Mcm2-7 gene expression could be profitably developed to either block cellular proliferation or potentially return it to normal levels. Alternatively, under conditions of replication stress (as is the case in cancer cells), specific reduction of Mcm protein levels sensitizes cells to other replication inhibitors [120], suggesting that combinational therapy with Mcm-specific inhibitors has the potential to increase the efficacy of existing treatments and their specificity for cancer cells. Although development of an inhibitor that specifically targets expression of very limited set of genes seems daunting, several recently discovered Mcm inhibitors show promise in this area (e.g., trichostatin A and widdrol).

To date, only a few compounds have been identified using low throughput or candidate approaches that directly target the complex's enzymatic activity and/or expression (Table 2).

(1) Heliquinomycin was originally identified as an inhibitor of *in vitro* replication in cell extract systems [126] and was later shown to biochemically inhibit the DNA unwinding properties of a specific Mcm subcomplex (Mcm467). This inhibition may be indirect, as it is believed that heliquinomycin blocks unwinding via an interaction with single-stranded DNA [121]. The drug may also have *in vivo* utility against Mcm2-7 as it has been shown to selectively decrease the proliferation of cancer cells overexpressing Mcm7 in tissue culture [122].

(2) A recent study has found that the fluoroquinolone ciprofloxacin and related compounds are able to selectively inhibit Mcm2-7 helicase activity at ~3–8-fold lower concentrations relative to other helicases [63]. Although the IC_{50} of this inhibition was relatively weak (~600 μM), cytotoxicity assays demonstrated that ciprofloxacin was able to inhibit both yeast and human cells at concentrations comparable to those that block *in vitro* helicase activity, consistent with the possibility that Mcm2-7 was also a cellular target of ciprofloxacin. This supposition was further supported by the finding that a known *Mcm* yeast mutant ($mcm4^{chaos3}$) demonstrated significant ciprofloxacin resistance in cellular culture.

(3) The classical histone deacetylase inhibitor trichostatin A (TSA) has been the subject considerable interest as an anticancer compound and has been demonstrated to be effective against a wide variety of cancers [127]. Recent evidence suggests that *MCM2* is a target of TSA. RT-PCR showed that *MCM2* gene expression is downregulated upon TSA treatment and that knockdown of Mcm2 induces cellular apoptosis in colon cancer cells. This downregulation of *MCM2* was dependent on TSA-mediated changes in the JNK signaling pathway [123].

(4) Widdrol, a naturally occurring aromatic compound derived from *Juniperus chinensis*, was observed to have antiproliferative activity against human colon adenocarcinoma HT29 cells [124]. Interestingly, this effect appeared to be due to a downregulation of *MCM* gene expression as a downstream consequence of DNA damage. The compound was later shown to cause DSBs which activate the DNA damage ATM/ATR mediated checkpoint, resulting in an upregulation of $p21^{CIP1}$ and a rapid decrease of MCM4 levels in HT29 cells, but not mouse fibroblasts [125]. Although the authors proposed that widdrol directly causes DNA damage, this DNA damage phenotype may occur through involvement of the Mcm complex, as both an *mcm* mutation in *S. pombe* has been shown to cause DSBs [67] and recently Mcm4 has been implicated in the DNA damage checkpoint [128].

Table 2: Small molecule inhibitors of Mcm2-7.

Inhibitor	Phenotype	Structure	IC_{50}	Subunits targeted	Reference
Ciprofloxacin	Blocks *in vitro* helicase activity, cellular growth	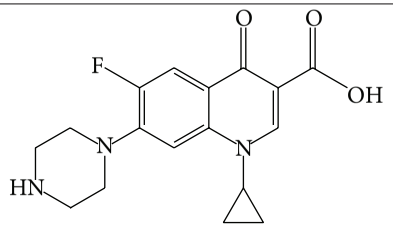	~600 μM (both for yeast/human cell cytotoxicity and for purified Mcm2-7 helicase activity)	Mcm2-7	[63]
Heliquinomycin	Blocks *in vitro* helicase activity, arrests growth of cancer cells	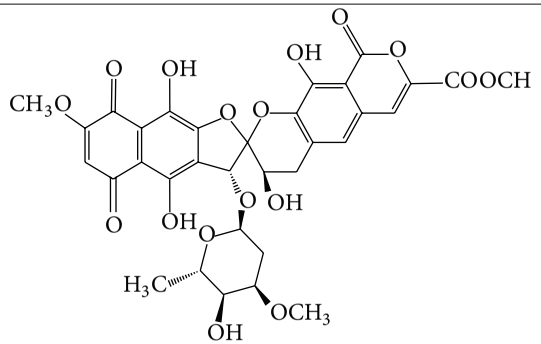	~3 μM (human Mcm467 helicase activity and cellular DNA synthesis)	Mcm467	[121, 122]
Trichostatin A	HDAC inhibitor, induces apoptosis	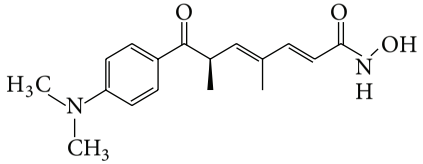	<1 μM (human cell cytotoxicity and Mcm2 protein levels)	Mcm2 protein levels	[123]
Widdrol	Growth inhibition, DNA damage, G1 arrest, downregulation of Mcms	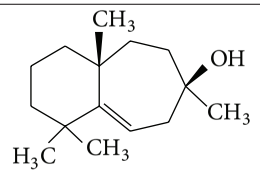	60–217 μM (human cell cytotoxicity and Mcm protein expression)	Mcm 2-7 Mcm4 (early) protein levels	[124, 125]

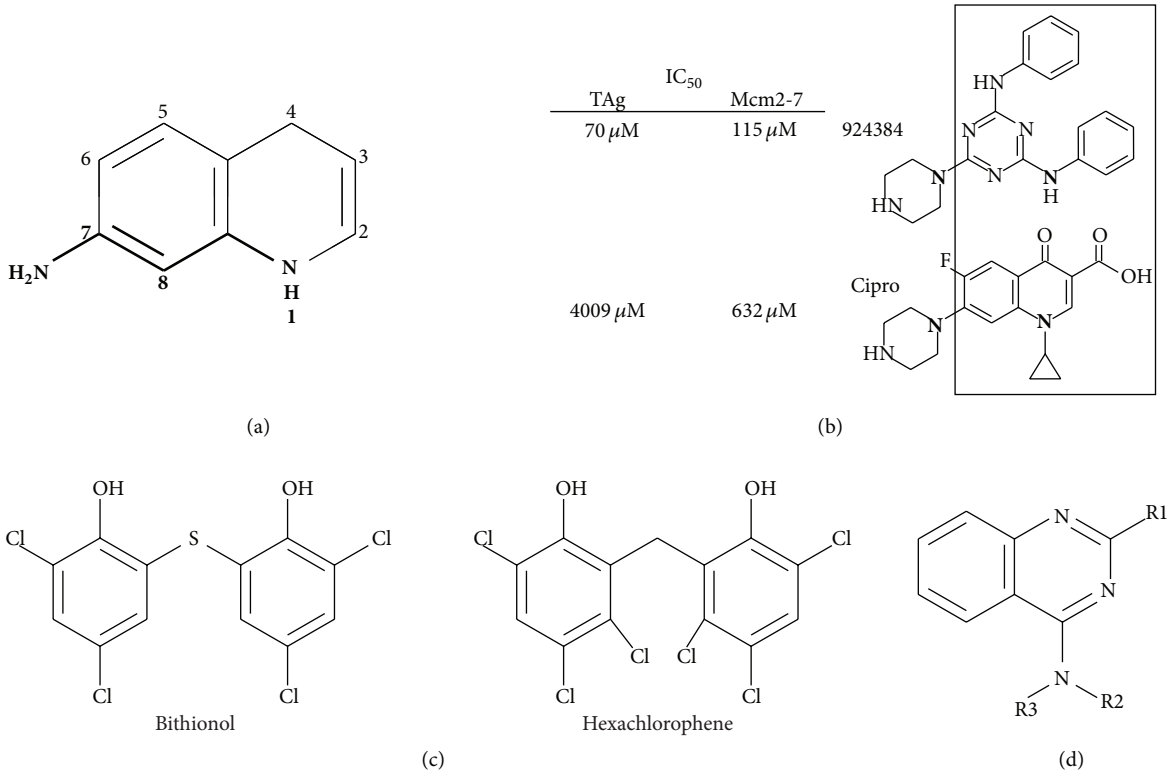

Figure 3: AAA+ inhibitors. (a) The basic quinolone structure and substitution numbering scheme are shown. From a previous study [63], most of the better Mcm2-7 inhibitors required both the nitrogen at position one and a nitrogen-containing substituent at position 7, with variation to the position 7 substituent often appearing to strongly module inhibitor activity. (b) Examination of inhibition of Mcm2-7 and SV-40 large T antigen comparing related fluoroquinolone and triazole inhibitors [63]. (c) SV-40 large T antigen inhibitors shown [64]. (d) Basic quinazoline structure shown; R-group substituents are discussed in the text.

5. Prospects for Mcm2-7 Chemotherapeutics

The development of Mcm2-7-specific small molecule inhibitors is at an early stage, and structure-activity relationship of these compounds is poorly understood. To date, the best information on potential molecular scaffolds for Mcm2-7 inhibitors comes from a study of Mcm2-7 fluoroquinolone inhibitors, as well as inhibitor studies targeting two related AAA+ ATPases—SV40 large T antigen and p97.

(1) Fluoroquinolones. To find better inhibitors than ciprofloxacin and elucidate the structural activity relationship between Mcm2-7 and fluoroquinolones, a library of ~150 additional compounds containing various fluoroquinolone substructures was tested biochemically for Mcm2-7-mediated DNA unwinding [63]. Although no inhibitors of greater specificity than ciprofloxacin were identified (i.e., increased ability to discriminate between SV-40 T antigen and Mcm2-7), inhibitors of greater potency were obtained, and common conserved features among them were evident. Particularly key appears to be the nature of a nitrogen-containing substituent arising from the quinolone 7 position, as well as the nitrogen present at the N1 position (Figure 3(a)). These structural features extend to various triazole compounds used in this study that also inhibit Mcm2-7 (e.g., 924384, Figure 3(b)). Since fluoroquinolones have a long history of use as antibiotics, development of Mcm2-7 fluoroquinolone-based inhibitors is attractive as much of the relevant pharmacology of this scaffold has been well-studied [129].

(2) Bisphenols. T antigen is a AAA+ ATPase and hexameric replicative helicase needed for SV-40 viral DNA replication (reviewed in [130]). A recent high-throughput screen for SV40 Large T antigen (TAg) inhibitors utilized the Spectrum Collection library of ~2200 FDA-approved bioactive compounds. This screen identified bisphenols as a novel compound class that inhibits both the ATPase activity of TAg *in vitro* and the ability of SV-40 to replicate *in vivo* [131]. Two particular molecules (bithionol and hexachlorophene, Figure 3(c)) were discovered with an IC_{50} for TAg ATPase activity in the single micromolar range. Further analysis determined that the critical structural components for TAg inhibition were flexibility at the linker between the phenol groups and the presence of small substituents at positions 2 and 4 of the phenols [131].

(3) Quinazolines. The p97/CDC48 ATPase is another toroidal eukaryotic hexameric AAA+ protein that in contrast to Mcm2-7 uses ATP-dependent conformation changes to unfold proteins (reviewed in [132]). Quinazoline derivatives have been shown to be effective p97 inhibitors [133]. Toward

development of better inhibitors, a structure-activity study tested an additional 200 quinazoline analogs for p97 inhibition, resulting in discovery of two new inhibitors (ML240 and ML241) that each had IC_{50}s for p97 ATP hydrolysis at submicromolar concentrations [134]. Their results indicate that substituent alterations at the R1 position greatly modulate p97 inhibition, a benzyl group at R2 is preferred, and substitution of the R3 hydrogen with anything larger blocks p97 inhibition (Figure 3(d)). Quinazoline derivatives may prove to be a generally useful inhibitor scaffold, as an independent study has found that a quinazoline-like compound (ciliobrevin) inhibits the ATPase activity of the AAA+ dynein motor protein [135].

6. Conclusions

Mcm2-7 is a structurally and functionally complex replication factor with a rich binding surface that directs multiple regulatory interactions of cancer significance, including those required for both Rb/E2F signaling as well as DNA replication. Given that all of these processes in isolation have been studied or used as therapeutic targets, Mcm2-7's involvement with all three suggests it is a promising target for blocking the proliferation of cancerous and precancerous cells. As Mcm2-7 contains six unique ATPase active sites and binds numerous regulatory proteins to a variety of different sites within the complex, inhibitors could be targeted to disrupt specific regulatory interactions. Although the ability to perform high throughput biochemical screens to identify Mcm2-7 inhibitors has limited utility due to the complexity of this system, recent developments using carefully engineered test organisms and whole cell assays, perhaps in conjunction with simpler and more genetically tractable model systems, suggest ways to conduct such targeted Mcm2-7 screens to identify novel inhibitors with therapeutic potential [114, 118, 136, 137].

Conflict of Interests

The authors declare that there is no conflict of interests regarding the publication of this paper.

Acknowledgments

The authors were funded by a NIH grant to Anthony Schwacha (RO1GM083985). The authors would like to thank S. Vijayraghavan for helpful comments on this paper.

References

[1] B. Pogorelčnik, A. Perdih, and T. Solmajer, "Recent developments of DNA poisons - human DNA topoisomerase IIα inhibitors—as anticancer agents," *Current Pharmaceutical Design*, vol. 19, no. 13, pp. 2474–2488, 2013.

[2] M. J. Keating, H. Kantarjian, M. Talpaz et al., "Fludarabine: a new agent with major activity against chronic lymphocytic leukemia," *Blood*, vol. 74, no. 1, pp. 19–25, 1989.

[3] D. K. Singh, S. Krishna, S. Chandra, M. Shameem, A. L. Deshmukh, and D. Banerjee, "Human DNA ligases: a comprehensive new look for cancer therapy," *Medicinal Research Reviews*, vol. 34, no. 3, pp. 567–595, 2014.

[4] Z. Tan, M. Wortman, K. L. Dillehay et al., "Small-molecule targeting of proliferating cell nuclear antigen chromatin association inhibits tumor cell growth," *Molecular Pharmacology*, vol. 81, no. 6, pp. 811–819, 2012.

[5] Y. Aye, M. Li, M. J. C. Long, and R. S. Weiss, "Ribonucleotide reductase and cancer: biological mechanisms and targeted therapies," *Oncogene*, 2014.

[6] B. Maji and S. Bhattacharya, "Advances in the molecular design of potential anticancer agents via targeting of human telomeric DNA," *Chemical Communications*, vol. 50, no. 49, pp. 6422–6438, 2014.

[7] V. R. Anderson and C. M. Perry, "Fludarabine: a review of its use in non-Hodgkin's lymphoma," *Drugs*, vol. 67, no. 11, pp. 1633–1655, 2007.

[8] H. G. Chun, B. R. Leyland-Jones, S. M. Caryk, and D. F. Hoth, "Central nervous system toxicity of fludarabine phosphate," *Cancer Treatment Reports*, vol. 70, no. 10, pp. 1225–1228, 1986.

[9] M. Mazevet, M. Moulin, A. Llach-Martinez et al., "Complications of chemotherapy, a basic science update," *La Presse Médicale*, vol. 42, no. 9, pp. e352–e361, 2013.

[10] Z. Livshits, R. B. Rao, and S. W. Smith, "An approach to chemotherapy-associated toxicity," *Emergency Medicine Clinics of North America*, vol. 32, no. 1, pp. 167–203, 2014.

[11] M. L. Bochman and A. Schwacha, "The Mcm complex: unwinding the mechanism of a replicative helicase," *Microbiology and Molecular Biology Reviews*, vol. 73, no. 4, pp. 652–683, 2009.

[12] G. T. Maine, P. Sinha, and B. W. Tye, "Mutants of S. cerevisiae defective in the maintenance of minichromosomes," *Genetics*, vol. 106, no. 3, pp. 365–385, 1984.

[13] K. M. Hennessy, A. Lee, E. Chen, and D. Botstein, "A group of interacting yeast DNA replication genes," *Genes and Development*, vol. 5, no. 6, pp. 958–969, 1991.

[14] P. Thömmes, Y. Kubota, H. Takisawa, and J. Julian Blow, "The RLF-M component of the replication licensing system forms complexes containing all six MCM/P1 polypeptides," *The EMBO Journal*, vol. 16, no. 11, pp. 3312–3319, 1997.

[15] K. Labib, J. A. Tercero, and J. F. X. Diffley, "Uninterrupted MCH2-7 function required for DNA replication fork progression," *Science*, vol. 288, no. 5471, pp. 1643–1647, 2000.

[16] A. Schwacha and S. P. Bell, "Interactions between two catalytically distinct MCM subgroups are essential for coordinated ATP hydrolysis and DNA replication," *Molecular Cell*, vol. 8, no. 5, pp. 1093–1104, 2001.

[17] E. V. Koonin, "A common set of conserved motifs in a vast variety of putative nucleic acid-dependent ATPases including MCM proteins involved in the initiation of eukaryotic DNA replication," *Nucleic Acids Research*, vol. 21, no. 11, pp. 2541–2547, 1993.

[18] M. J. Davey, C. Indiani, and M. O'Donnell, "Reconstitution of the Mcm2-7p heterohexamer, subunit arrangement, and ATP site architecture," *Journal of Biological Chemistry*, vol. 278, no. 7, pp. 4491–4499, 2003.

[19] M. L. Bochman, S. P. Bell, and A. Schwacha, "Subunit organization of Mcm2-7 and the unequal role of active sites in ATP hydrolysis and viability," *Molecular and Cellular Biology*, vol. 28, no. 19, pp. 5865–5873, 2008.

[20] L. M. Iyer and L. Aravind, "The evolutionary history of proteins involved in pre-replication complex assembly," in *DNA Replication and Human Disease*, M. L. DePamphilis, Ed., pp. 751–757,

Cold Spring Harbor Laboratory Press, Cold Spring Harbor, NY, USA, 2006.

[21] S. J. Aves, Y. Liu, and T. A. Richards, "Evolutionary diversification of eukaryotic DNA replication machinery," *Subcellular Biochemistry*, vol. 62, pp. 19–35, 2012.

[22] M. L. Bochman and A. Schwacha, "Differences in the single-stranded DNA binding activities of MCM2-7 and MCM467: MCM2 and MCM5 define a slow ATP-dependent step," *Journal of Biological Chemistry*, vol. 282, no. 46, pp. 33795–33804, 2007.

[23] M. L. Bochman and A. Schwacha, "The Mcm2-7 complex has in vitro helicase activity," *Molecular Cell*, vol. 31, no. 2, pp. 287–293, 2008.

[24] M. L. Bochman and A. Schwacha, "The Saccharomyces cerevisiae Mcm6/2 and Mcm5/3 ATPase active sites contribute to the function of the putative Mcm2-7 "gate"," *Nucleic Acids Research*, vol. 38, no. 18, Article ID gkq422, pp. 6078–6088, 2010.

[25] D. M. Kanter, I. Bruck, and D. L. Kaplan, "Mcm subunits can assemble into two different active unwinding complexes," *Journal of Biological Chemistry*, vol. 283, no. 45, pp. 31172–31182, 2008.

[26] Y. Ishimi, "A DNA helicase activity is associated with an MCM4, -6, and -7 protein complex," *Journal of Biological Chemistry*, vol. 272, no. 39, pp. 24508–24513, 1997.

[27] I. Ilves, T. Petojevic, J. J. Pesavento, and M. R. Botchan, "Activation of the MCM2-7 helicase by association with Cdc45 and GINS proteins," *Molecular Cell*, vol. 37, no. 2, pp. 247–258, 2010.

[28] J. Lee and J. Hurwitz, "Isolation and characterization of various complexes of the minichromosome maintenance proteins of Schizosaccharomyces pombe," *Journal of Biological Chemistry*, vol. 275, no. 25, pp. 18871–18878, 2000.

[29] D. L. Kaplan, M. J. Davey, and M. O'Donnell, "Mcm4,6,7 uses a "pump in ring" mechanism to unwind DNA by steric exclusion and actively translocate along a duplex.," *The Journal of biological chemistry*, vol. 278, no. 49, pp. 49171–49182, 2003.

[30] A. Costa, I. Ilves, N. Tamberg et al., "The structural basis for MCM2-7 helicase activation by GINS and Cdc45," *Nature Structural & Molecular Biology*, vol. 18, no. 4, pp. 471–477, 2011.

[31] S. P. Bell and A. Dutta, "DNA replication in eukaryotic cells," *Annual Review of Biochemistry*, vol. 71, pp. 333–374, 2002.

[32] O. M. Aparicio, D. M. Weinstein, and S. P. Bell, "Components and dynamics of DNA replication complexes in S. cerevisiae: redistribution of MCM proteins and Cdc45p during S phase," *Cell*, vol. 91, no. 1, pp. 59–69, 1997.

[33] T. Tanaka, D. Knapp, and N. Kim, "Loading of an Mcm protein onto DNA replication origins is regulated by Cdc6p and CDKs," *Cell*, vol. 90, no. 4, pp. 649–660, 1997.

[34] J. Sun, C. Evrin, S. A. Samel et al., "Cryo-EM structure of a helicase loading intermediate containing ORC-Cdc6-Cdt1-MCM2-7 bound to DNA," *Nature Structural and Molecular Biology*, vol. 20, no. 8, pp. 944–951, 2013.

[35] D. Remus, F. Beuron, G. Tolun, J. D. Griffith, E. P. Morris, and J. F. X. Diffley, "Concerted loading of Mcm2-7 double hexamers around DNA during DNA replication origin licensing," *Cell*, vol. 139, no. 4, pp. 719–730, 2009.

[36] G. Coster, J. Frigola, F. Beuron et al., "Origin licensing requires ATP binding and hydrolysis by the MCM replicative helicase," *Molecular Cell*, 2014.

[37] S. Kang, M. D. Warner, and S. P. Bell, "Multiple functions for Mcm2-7 ATPase motifs during replication initiation," *Molecular Cell*, 2014.

[38] S. A. Samel, A. Fernández-Cid, J. Sun et al., "A unique DNA entry gate serves for regulated loading of the eukaryotic replicative helicase MCM2-7 onto DNA," *Genes & Development*, vol. 28, no. 15, pp. 1653–1666, 2014.

[39] P. Zegerman and J. F. X. Diffley, "Phosphorylation of Sld2 and Sld3 by cyclin-dependent kinases promotes DNA replication in budding yeast," *Nature*, vol. 445, no. 7125, pp. 281–285, 2007.

[40] Y. Takayama, Y. Kamimura, M. Okawa, S. Muramatsu, A. Sugino, and H. Araki, "GINS, a novel multiprotein complex required for chromosomal DNA replication in budding yeast," *Genes and Development*, vol. 17, no. 9, pp. 1153–1165, 2003.

[41] S. Tanaka, T. Umemori, K. Hirai, S. Muramatsu, Y. Kamimura, and H. Araki, "CDK-dependent phosphorylation of Sld2 and Sld3 initiates DNA replication in budding yeast," *Nature*, vol. 445, no. 7125, pp. 328–332, 2007.

[42] D. Branzei and M. Foiani, "The Rad53 signal transduction pathway: replication fork stabilization, DNA repair, and adaptation," *Experimental Cell Research*, vol. 312, no. 14, pp. 2654–2659, 2006.

[43] Y. Cho and P. Liang, "S-phase-coupled apoptosis in tumor suppression," *Cellular and Molecular Life Sciences*, vol. 68, no. 11, pp. 1883–1896, 2011.

[44] N. Motoyama and K. Naka, "DNA damage tumor suppressor genes and genomic instability," *Current Opinion in Genetics and Development*, vol. 14, no. 1, pp. 11–16, 2004.

[45] D. Cortez, G. Glick, and S. J. Elledge, "Minichromosome maintenance proteins are direct targets of the ATM and ATR checkpoint kinases," *Proceedings of the National Academy of Sciences of the United States of America*, vol. 101, no. 27, pp. 10078–10083, 2004.

[46] Y. Ishimi, Y. Komamura-Kohno, H. Kwon, K. Yamada, and M. Nakanishi, "Identification of MCM4 as a target of the DNA replication block checkpoint system," *The Journal of Biological Chemistry*, vol. 278, no. 27, pp. 24644–24650, 2003.

[47] J. C. W. Randell, A. Fan, C. Chan et al., "Mec1 is one of multiple kinases that prime the Mcm2-7 helicase for phosphorylation by Cdc7," *Molecular Cell*, vol. 40, no. 3, pp. 353–363, 2010.

[48] H. Y. Yoo, A. Shevchenko, and W. G. Dunphy, "Mcm2 is a direct substrate of ATM and ATR during DNA damage and DNA replication checkpoint responses," *The Journal of Biological Chemistry*, vol. 279, no. 51, pp. 53353–53364, 2004.

[49] M. Bando, Y. Katou, M. Komata et al., "Csm3, Tof1, and Mrc1 form a heterotrimeric mediator complex that associates with DNA replication forks," *The Journal of Biological Chemistry*, vol. 284, no. 49, pp. 34355–34365, 2009.

[50] D. M. Chou and S. J. Elledge, "Tipin and Timeless form a mutually protective complex required for genotoxic stress resistance and checkpoint function," *Proceedings of the National Academy of Sciences of the United States of America*, vol. 103, no. 48, pp. 18143–18147, 2006.

[51] Y. Katou, Y. Kanoh, M. Bando et al., "S-phase checkpoint proteins Tof1 and Mrc1 form a stable replication-pausing complex," *Nature*, vol. 424, no. 6952, pp. 1078–1083, 2003.

[52] M. N. Nedelcheva, A. Roguev, L. B. Dolapchiev et al., "Uncoupling of unwinding from DNA synthesis implies regulation of MCM helicase by Tof1/Mrc1/Csm3 checkpoint complex," *Journal of Molecular Biology*, vol. 347, no. 3, pp. 509–521, 2005.

[53] J. P. J. Chong, P. Thömmes, A. Rowles, H. M. Mahbubani, and J. J. Blow, "Characterization of the Xenopus replication licensing system," *Methods in Enzymology*, vol. 283, pp. 549–564, 1997.

[54] T. Seki and J. F. X. Diffley, "Stepwise assembly of initiation proteins at budding yeast replication origins in vitro," *Proceedings of*

the National Academy of Sciences of the United States of America, vol. 97, no. 26, pp. 14115–14120, 2000.

[55] P. Pasero and S. M. Gasser, "In vitro DNA replication assays in yeast extracts," *Methods in Enzymology*, vol. 351, pp. 184–199, 2002.

[56] B. Stillman, R. D. Gerard, R. A. Guggenheimer, and Y. Gluzman, "T antigen and template requirements for SV40 DNA replication in vitro," *The EMBO Journal*, vol. 4, no. 11, pp. 2933–2939, 1985.

[57] J. Flach, S. T. Bakker, M. Mohrin et al., "Replication stress is a potent driver of functional decline in ageing haematopoietic stem cells," *Nature*, vol. 512, no. 7513, pp. 198–202, 2014.

[58] A. S. Brewster, G. Wang, X. Yu et al., "Crystal structure of a near-full-length archaeal MCM: functional insights for an AAA+ hexameric helicase," *Proceedings of the National Academy of Sciences of the United States of America*, vol. 105, no. 51, pp. 20191–20196, 2008.

[59] L. A. Kelley and M. J. E. Sternberg, "Protein structure prediction on the Web: a case study using the Phyre server.," *Nature protocols*, vol. 4, no. 3, pp. 363–371, 2009.

[60] D. Li, R. Zhao, W. Lilyestrom et al., "Structure of the replicative helicase of the oncoprotein SV40 large tumour antigen," *Nature*, vol. 423, no. 6939, pp. 512–518, 2003.

[61] A. Riera, S. Tognetti, and C. Speck, "Helicase loading: how to build a MCM2-7 double-hexamer," *Seminars in Cell and Developmental Biology*, vol. 30C, pp. 104–109, 2014.

[62] C. Evrin, P. Clarke, J. Zech et al., "A double-hexameric MCM2-7 complex is loaded onto origin DNA during licensing of eukaryotic DNA replication," *Proceedings of the National Academy of Sciences of the United States of America*, vol. 106, no. 48, pp. 20240–20245, 2009.

[63] N. Simon, M. L. Bochman, S. Seguin, J. L. Brodsky, W. L. Seibel, and A. Schwacha, "Ciprofloxacin is an inhibitor of the Mcm2-7 replicative helicase," *Bioscience Reports*, vol. 33, no. 5, article e00072, 2013.

[64] S. P. Seguin, C. W. Evans, M. Nebane-Akah et al., "High-throughput screening identifies a bisphenol inhibitor of SV40 large T antigen ATPase activity," *Journal of Biomolecular Screening*, vol. 17, no. 2, pp. 194–203, 2012.

[65] S. A. Hills and J. F. Diffley, "DNA replication and oncogene-induced replicative stress," *Current Biology*, vol. 24, no. 10, pp. R435–R444, 2014.

[66] S. I. Gibson, R. T. Surosky, and B.-. Tye, "The phenotype of the minichromosome maintenance mutant mcm3 is characteristic of mutants defective in DNA replication," *Molecular and Cellular Biology*, vol. 10, no. 11, pp. 5707–5720, 1990.

[67] J. M. Bailis, D. D. Luche, T. Hunter, and S. L. Forsburg, "Minichromosome maintenance proteins interact with checkpoint and recombination proteins to promote S-phase genome stability," *Molecular and Cellular Biology*, vol. 28, no. 5, pp. 1724–1738, 2008.

[68] M. Lei, Y. Kawasaki, and B. K. Tye, "Physical interactions among Mcm proteins and effects of Mcm dosage on DNA replication in Saccharomyces cerevisiae," *Molecular and Cellular Biology*, vol. 16, no. 9, pp. 5081–5090, 1996.

[69] A. M. Woodward, T. Göhler, M. G. Luciani et al., "Excess Mcm2-7 license dormant origins of replication that can be used under conditions of replicative stress," *Journal of Cell Biology*, vol. 173, no. 5, pp. 673–683, 2006.

[70] D. T. Liang, J. A. Hodson, and S. L. Forsburg, "Reduced dosage of a single fission yeast MCM protein causes genetic instability and S phase delay," *Journal of Cell Science*, vol. 112, no. 4, pp. 559–567, 1999.

[71] J. M. Bailis and S. L. Forsburg, "MCM proteins: DNA damage, mutagenesis and repair," *Current Opinion in Genetics and Development*, vol. 14, no. 1, pp. 17–21, 2004.

[72] M. A. Madine, M. Swietlik, C. Pelizon, P. Romanowski, A. D. Mills, and R. A. Laskey, "The roles of the MCM, ORC, and Cdc6 proteins in determining the replication competence of chromatin in quiescent cells," *Journal of Structural Biology*, vol. 129, no. 2-3, pp. 198–210, 2000.

[73] A. Freeman, L. S. Morris, A. D. Mills et al., "Minichromosome maintenance proteins as biological markers of dysplasia and malignancy," *Clinical Cancer Research*, vol. 5, no. 8, pp. 2121–2132, 1999.

[74] I. T. Todorov, B. A. Werness, H. Wang et al., "HsMCM2/BM28: a novel proliferation marker for human tumors and normal tissues," *Laboratory Investigation*, vol. 78, no. 1, pp. 73–78, 1998.

[75] K. Stoeber, T. D. Tlsty, L. Happerfield et al., "DNA replication licensing and human cell proliferation," *Journal of Cell Science*, vol. 114, part 11, pp. 2027–2041, 2001.

[76] C. Giaginis, S. Vgenopoulou, P. Vielh, and S. Theocharis, "MCM proteins as diagnostic and prognostic tumor markers in the clinical setting," *Histology and Histopathology*, vol. 25, no. 3, pp. 351–370, 2010.

[77] B. Ren, G. Yu, G. C. Tseng et al., "MCM7 amplification and overexpression are associated with prostate cancer progression," *Oncogene*, vol. 25, no. 7, pp. 1090–1098, 2006.

[78] L. Qian, Q. Luo, X. Zhao, and J. Huang, "Pathways enrichment analysis for differentially expressed genes in squamous lung cancer," *Pathology Oncology Research*, vol. 20, no. 1, pp. 197–202, 2014.

[79] C. Chuang, M. D. Wallace, C. Abratte, T. Southard, and J. C. Schimenti, "Incremental genetic perturbations to MCM2-7 expression and subcellular distribution reveal exquisite sensitivity of mice to DNA replication stress," *PLoS Genetics*, vol. 6, no. 9, Article ID e1001110, 2010.

[80] Cancer Genome Atlas Research Network, "Comprehensive genomic characterization of squamous cell lung cancers," *Nature*, vol. 489, no. 7417, pp. 519–525, 2012.

[81] K. A. Honeycutt, Z. Chen, M. I. Koster et al., "Deregulated minichromosomal maintenance protein MCM7 contributes to oncogene driven tumorigenesis," *Oncogene*, vol. 25, no. 29, pp. 4027–4032, 2006.

[82] D. Kunnev, M. E. Rusiniak, A. Kudla, A. Freeland, G. K. Cady, and S. C. Pruitt, "DNA damage response and tumorigenesis in Mcm2-deficient mice," *Oncogene*, vol. 29, no. 25, pp. 3630–3638, 2010.

[83] S. C. Pruitt, K. J. Bailey, and A. Freeland, "Reduced Mcm2 expression results in severe stem/progenitor cell deficiency and cancer," *Stem Cells*, vol. 25, no. 12, pp. 3121–3132, 2007.

[84] N. Shima, A. Alcaraz, I. Liachko et al., "A viable allele of Mcm4 causes chromosome instability and mammary adenocarcinomas in mice," *Nature Genetics*, vol. 39, no. 1, pp. 93–98, 2007.

[85] T. Kawabata, S. Luebben, S. Yamaguchi et al., "Stalled fork rescue via dormant replication origins in unchallenged S phase promotes proper chromosome segregation and tumor suppression," *Molecular Cell*, vol. 41, no. 5, pp. 543–553, 2011.

[86] X. C. Li and B. K. Tye, "Ploidy dictates repair pathway choice under DNA replication stress," *Genetics*, vol. 187, no. 4, pp. 1031–1040, 2011.

[87] B. N. Bagley, T. M. Keane, V. I. Maklakova et al., "A dominantly acting murine allele of Mcm4 causes chromosomal abnormalities and promotes tumorigenesis," *PLoS Genetics*, vol. 8, no. 11, Article ID e1003034, 2012.

[88] N. A. Steere, S. Yamaguchi, C. A. Andrews, I. Liachko, T. Nakamura, and N. Shima, "Functional screen of human MCM2-7 variant alleles for disease-causing potential," *Mutation Research*, vol. 666, no. 1-2, pp. 74–78, 2009.

[89] D. Hanahan and R. A. Weinberg, "The hallmarks of cancer," *Cell*, vol. 100, no. 1, pp. 57–70, 2000.

[90] S. Negrini, V. G. Gorgoulis, and T. D. Halazonetis, "Genomic instability—an evolving hallmark of cancer," *Nature Reviews Molecular Cell Biology*, vol. 11, no. 3, pp. 220–228, 2010.

[91] R. M. Jones, O. Mortusewicz, I. Afzal et al., "Increased replication initiation and conflicts with transcription underlie Cyclin E-induced replication stress," *Oncogene*, vol. 32, no. 32, pp. 3744–3753, 2013.

[92] J. Bartkova, Z. Hořejší, K. Koed et al., "DNA damage response as a candidate anti-cancer barrier in early human tumorigenesis," *Nature*, vol. 434, no. 7035, pp. 864–870, 2005.

[93] A. Sun, L. Bagella, S. Tutton, G. Romano, and A. Giordano, "From G0 to S phase: A view of the roles played by the retinoblastoma (Rb) family members in the Rb-E2F pathway," *Journal of Cellular Biochemistry*, vol. 102, no. 6, pp. 1400–1404, 2007.

[94] S. Ortega, M. Malumbres, and M. Barbacid, "Cyclin D-dependent kinases, INK4 inhibitors and cancer," *Biochimica et Biophysica Acta*, vol. 1602, no. 1, pp. 73–87, 2002.

[95] T. Fillies, M. Woltering, B. Brandt et al., "Cell cycle regulating proteins p21 and p27 in prognosis of oral squamous cell carcinomas," *Oncology Reports*, vol. 17, no. 2, pp. 355–359, 2007.

[96] M. Malumbres and M. Barbacid, "To cycle or not to cycle: a critical decision in cancer," *Nature Reviews Cancer*, vol. 1, no. 3, pp. 222–231, 2001.

[97] J. M. Sterner, S. Dew-Knight, C. Musahl, S. Kornbluth, and J. M. Horowitz, "Negative regulation of DNA replication by the retinoblastoma protein is mediated by its association with MCM7," *Molecular and Cellular Biology*, vol. 18, no. 5, pp. 2748–2757, 1998.

[98] M. Pacek and J. C. Walter, "A requirement for MCM7 and Cdc45 in chromosome unwinding during eukaryotic DNA replication," *The EMBO Journal*, vol. 23, no. 18, pp. 3667–3676, 2004.

[99] Y. Doyon, C. Cayrou, M. Ullah et al., "ING tumor suppressor proteins are critical regulators of chromatin acetylation required for genome expression and perpetuation," *Molecular Cell*, vol. 21, no. 1, pp. 51–64, 2006.

[100] R. Bellelli, M. D. Castellone, T. Guida et al., "NCOA4 transcriptional coactivator inhibits activation of DNA replication origins," *Molecular Cell*, vol. 55, no. 1, pp. 123–137, 2014.

[101] W. A. Braden, J. M. Lenihan, Z. Lan et al., "Distinct action of the retinoblastoma pathway on the DNA replication machinery defines specific roles for cyclin-dependent kinase complexes in prereplication complex assembly and S-phase progression," *Molecular and Cellular Biology*, vol. 26, no. 20, pp. 7667–7681, 2006.

[102] S. Nallamshetty, M. Crook, M. Boehm, T. Yoshimoto, M. Olive, and E. G. Nabel, "The cell cycle regulator p27Kip1 interacts with MCM7, a DNA replication licensing factor, to inhibit initiation of DNA replication," *FEBS Letters*, vol. 579, no. 29, pp. 6529–6536, 2005.

[103] W. Rizwani, M. Alexandrow, and S. Chellappan, "Prohibitin physically interacts with MCM proteins and inhibits mammalian DNA replication," *Cell Cycle*, vol. 8, no. 10, pp. 1621–1629, 2009.

[104] C. Tsao, C. Geisen, and R. T. Abraham, "Interaction between human MCM7 and Rad17 proteins is required for replication checkpoint signaling," *EMBO Journal*, vol. 23, no. 23, pp. 4660–4669, 2004.

[105] C. J. Sherr and J. M. Roberts, "CDK inhibitors: positive and negative regulators of G1-phase progression," *Genes & Development*, vol. 13, no. 12, pp. 1501–1512, 1999.

[106] S. Wang, N. Nath, M. Adlam, and S. Chellappan, "Prohibitin, a potential tumor suppressor, interacts with RB and regulates E2F function," *Oncogene*, vol. 18, no. 23, pp. 3501–3510, 1999.

[107] S. Wang, N. Nath, G. Fusaro, and S. Chellappan, "Rb and prohibitin target distinct regions of E2F1 for repression and respond to different upstream signals," *Molecular and Cellular Biology*, vol. 19, no. 11, pp. 7447–7460, 1999.

[108] L. A. Lindsey-Boltz, V. P. Bermudez, J. Hurwitz, and A. Sancar, "Purification and characterization of human DNA damage checkpoint Rad complexes," *Proceedings of the National Academy of Sciences of the United States of America*, vol. 98, no. 20, pp. 11236–11241, 2001.

[109] A. B. Gladden and J. A. Diehl, "The cyclin D1-dependent kinase associates with the pre-replication complex and modulates RB-MCM7 binding," *The Journal of Biological Chemistry*, vol. 278, no. 11, pp. 9754–9760, 2003.

[110] A. Shiratori, T. Shibata, M. Arisawa, F. Hanaoka, Y. Murakami, and T. Eki, "Systematic identification, classification, and characterization of the open reading frames which encode novel helicase-related proteins in *Saccharomyces cerevisiae* by gene disruption and Northern analysis," *Yeast*, vol. 15, no. 3, pp. 219–253, 1999.

[111] W. R. Shadrick, J. Ndjomou, R. Kolli, S. Mukherjee, A. M. Hanson, and D. N. Frick, "Discovering new medicines targeting helicases: challenges and recent progress," *Journal of Biomolecular Screening*, vol. 18, no. 7, pp. 761–781, 2013.

[112] D. T. Simmons, "SV40 large T antigen functions in DNA replication and transformation," *Advances in Virus Research*, vol. 55, pp. 75–134, 2000.

[113] S. E. Moyer, P. W. Lewis, and M. R. Botchan, "Isolation of the Cdc45/Mcm2-7/GINS (CMG) complex, a candidate for the eukaryotic DNA replication fork helicase," *Proceedings of the National Academy of Sciences of the United States of America*, vol. 103, no. 27, pp. 10236–10241, 2006.

[114] H. Luesch, T. Y. H. Wu, P. Ren, N. S. Gray, P. G. Schultz, and F. Supek, "A genome-wide overexpression screen in yeast for small-molecule target identification," *Chemistry and Biology*, vol. 12, no. 1, pp. 55–63, 2005.

[115] C. D. Glen and Y. E. Dubrova, "Exposure to anticancer drugs can result in transgenerational genomic instability in mice," *Proceedings of the National Academy of Sciences of the United States of America*, vol. 109, no. 8, pp. 2984–2988, 2012.

[116] D. Woods and J. J. Turchi, "Chemotherapy induced DNA damage response: convergence of drugs and pathways," *Cancer Biology and Therapy*, vol. 14, no. 5, pp. 379–389, 2013.

[117] L. Guarente, "Synthetic enhancement in gene interaction: a genetic tool come of age," *Trends in Genetics*, vol. 9, no. 10, pp. 362–366, 1993.

[118] D. A. Chan and A. J. Giaccia, "Harnessing synthetic lethal interactions in anticancer drug discovery," *Nature Reviews Drug Discovery*, vol. 10, no. 5, pp. 351–364, 2011.

[119] R. N. Eskander and K. S. Tewari, "PARP inhibition and synthetic lethality in ovarian cancer," *Expert Review of Clinical Pharmacology*, vol. 7, no. 5, pp. 613–622, 2014.

[120] A. Ibarra, E. Schwob, and J. Méndez, "Excess MCM proteins protect human cells from replicative stress by licensing backup origins of replication," *Proceedings of the National Academy of Sciences of the United States of America*, vol. 105, no. 26, pp. 8956–8961, 2008.

[121] Y. Ishimi, T. Sugiyama, R. Nakaya et al., "Effect of heliquinomycin on the activity of human minichromosome maintenance 4/6/7 helicase," *FEBS Journal*, vol. 276, no. 12, pp. 3382–3391, 2009.

[122] G. Toyokawa, K. Masuda, Y. Daigo et al., "Minichromosome Maintenance Protein 7 is a potential therapeutic target in human cancer and a novel prognostic marker of non-small cell lung cancer," *Molecular Cancer*, vol. 10, article 65, 2011.

[123] Y. Liu, G. He, Y. Wang, X. Guan, X. Pang, and B. Zhang, "MCM-2 is a therapeutic target of Trichostatin A in colon cancer cells," *Toxicology Letters*, vol. 221, no. 1, pp. 23–30, 2013.

[124] H. J. Kwon, Y. K. Hong, C. Park et al., "Widdrol induces cell cycle arrest, associated with MCM down-regulation, in human colon adenocarcinoma cells," *Cancer Letters*, vol. 290, no. 1, pp. 96–103, 2010.

[125] H. J. Yun, S. K. Hyun, J. H. Park, B. W. Kim, and H. J. Kwon, "Widdrol activates DNA damage checkpoint through the signaling Chk2-p53-Cdc25A-p21-MCM4 pathway in HT29 cells," *Molecular and Cellular Biochemistry*, vol. 363, no. 1-2, pp. 281–289, 2012.

[126] M. Chino, K. Nishikawa, M. Umekita et al., "Heliquinomycin, a new inhibitor of DNA helicase, produced by Streptomyces sp. MJ929-SF2. I. Taxonomy, production, isolation, physicochemical properties and biological activities," *Journal of Antibiotics*, vol. 49, no. 8, pp. 752–757, 1996.

[127] J. Chang, D. S. Varghese, M. C. Gillam et al., "Differential response of cancer cells to HDAC inhibitors trichostatin A and depsipeptide," *British Journal of Cancer*, vol. 106, no. 1, pp. 116–125, 2012.

[128] Y. J. Sheu, J. B. Kinney, A. Lengronne, P. Pasero, and B. Stillman, "Domain within the helicase subunit Mcm4 integrates multiple kinase signals to control DNA replication initiation and fork progression," *Proceedings of the National Academy of Sciences of the United States of America*, vol. 111, no. 18, pp. E1899–E1908, 2014.

[129] C. M. Oliphant and G. M. Green, "Quinolones: a comprehensive review," *The American Family Physician*, vol. 65, no. 3, pp. 455–464, 2002.

[130] P. An, M. T. S. Robles, and J. M. Pipas, "Large T antigens of polyomaviruses: amazing molecular machines," *Annual Review of Microbiology*, vol. 66, pp. 213–236, 2012.

[131] S. P. Seguin, A. W. Ireland, T. Gupta et al., "A screen for modulators of large T antigen's ATPase activity uncovers novel inhibitors of Simian Virus 40 and BK virus replication," *Antiviral Research*, vol. 96, no. 1, pp. 70–81, 2012.

[132] H. Meyer, M. Bug, and S. Bremer, "Emerging functions of the VCP/p97 AAA-ATPase in the ubiquitin system," *Nature Cell Biology*, vol. 14, no. 2, pp. 117–123, 2012.

[133] T. Chou, S. J. Brown, D. Minond et al., "Reversible inhibitor of p97, DBeQ, impairs both ubiquitin-dependent and autophagic protein clearance pathways," *Proceedings of the National Academy of Sciences of the United States of America*, vol. 108, no. 12, pp. 4834–4839, 2011.

[134] T. Chou, K. Li, K. J. Frankowski, F. J. Schoenen, and R. J. Deshaies, "Structure-activity relationship study reveals ML240 and ML241 as potent and selective inhibitors of p97 ATPase," *ChemMedChem*, vol. 8, no. 2, pp. 297–312, 2013.

[135] A. J. Firestone, J. S. Weinger, M. Maldonado et al., "Small-molecule inhibitors of the AAA+ ATPase motor cytoplasmic dynein," *Nature*, vol. 484, no. 7392, pp. 125–129, 2012.

[136] P. Y. Lum, C. D. Armour, S. B. Stepaniants et al., "Discovering modes of action for therapeutic compounds using a genome-wide screen of yeast heterozygotes," *Cell*, vol. 116, no. 1, pp. 121–137, 2004.

[137] G. Giaever, P. Flaherty, J. Kumm et al., "Chemogenomic profiling: identifying the functional interactions of small molecules in yeast," *Proceedings of the National Academy of Sciences of the United States of America*, vol. 101, no. 3, pp. 793–798, 2004.

Hindawi Publishing Corporation
BioMed Research International
Volume 2014, Article ID 171263, 8 pages
http://dx.doi.org/10.1155/2014/171263

Research Article

Crystal Structure of a Conserved Hypothetical Protein MJ0927 from *Methanocaldococcus jannaschii* Reveals a Novel Quaternary Assembly in the Nif3 Family

Sheng-Chia Chen,[1,2] Chi-Hung Huang,[1,2] Chia Shin Yang,[1,2] Shu-Min Kuan,[1] Ching-Ting Lin,[3] Shan-Ho Chou,[4] and Yeh Chen[1]

[1] *Department of Biotechnology, Hungkuang University, Taichung 433, Taiwan*
[2] *Taiwan Advance Biopharm (TABP), Inc., Xizhi City, New Taipei City 221, Taiwan*
[3] *School of Chinese Medicine, China Medical University, Taichung 40402, Taiwan*
[4] *Institute of Biochemistry and Agricultural Biotechnology Center, National Chung Hsing University, Taichung 40227, Taiwan*

Correspondence should be addressed to Yeh Chen; bluecrystalprotein@gmail.com

Received 30 May 2014; Revised 24 July 2014; Accepted 8 August 2014; Published 28 August 2014

Academic Editor: Cheng-Yang Huang

A Nif3 family protein of *Methanocaldococcus jannaschii*, MJ0927, is highly conserved from bacteria to humans. Although several structures of bacterial Nif3 proteins are known, no structure representing archaeal Nif3 has yet been reported. The crystal structure of *Methanocaldococcus jannaschii* MJ0927 was determined at 2.47 Å resolution to understand the structural differences between the bacterial and archaeal Nif3 proteins. Intriguingly, MJ0927 is found to adopt an unusual assembly comprising a trimer of dimers that forms a cage-like architecture. Electrophoretic mobility-shift assays indicate that MJ0927 binds to both single-stranded and double-stranded DNA. Structural analysis of MJ0927 reveals a positively charged region that can potentially explain its DNA-binding capability. Taken together, these data suggest that MJ0927 adopts a novel quartenary architecture that could play various DNA-binding roles in *Methanocaldococcus jannaschii*.

1. Introduction

Given that numerous genomes of diverse organisms have been sequenced to date, it is not surprising that the number of hypothetical proteins with unknown functions has also steadily increased. Structures of hypothetical proteins can provide hints for deciphering their functions [1]. Since Nif3-like protein is widely distributed from bacteria to higher eukaryotes, this conserved hypothetical protein has been identified as a target from which the protein function can be inferred based upon a structural perspective [2].

The name of the Nif3-like superfamily was originated from the yeast Nif3, which was identified as an NGG1p-interacting protein in a yeast two-hybrid screen [3]. Sequence analysis of all reported Nif3-like proteins indicated that only the N- and C-terminal regions of the Nif3 proteins are highly conserved during evolution [4]. Studies of several eukaryotic Nif3 homologs have indicated that NIF3 family proteins are involved in transcriptional regulation [5]. For example, Akiyama et al. have demonstrated that murine Nif3 can interact with Trip15/CSN2 to function as transcriptional repressors [5]. Yet, the biological functions of Nif3 proteins in both prokaryotes and archaea kingdoms remain obscure.

To date, the tertiary structures of several bacterial Nif3 proteins have been determined by X-ray crystallography including those of SP1609 from *Streptococcus pneumonia* (2FYW), YqfO from *Bacillus cereus* (2GX8) [6], YbgI from *Escherichia coli* (1NMP) [7], SA1388 from *Staphylococcus aureus* (2NYD) [8], and TTHA1606 from *Thermus thermophiles* HB8(2YYB) [9]. These structures have all been observed to adopt a similar α/β structure, forming a toroidal hexamer. In most Nif3 structures, two metal ions were also

Table 1: Data collection statistics for the MJ0927 crystal. Values in parentheses are for the highest resolution shell. Data of $C222_1$ form has been used in previous publication [10].

	Se-Met Nif3 ($P2_1$ form)			Nif3 ($C222_1$ form)
Data Collection				
Wavelength (Å)	Peak 0.9792	Edge 0.9793	Remote 0.9641	1.0000
Space group		$P2_1$		$C222_1$
Unit Cell (Å)		95.60, 77.21, 131.85 $\beta = 105.36$		81.21, 172.94, 147.42
Resolution range (Å)	30–2.8 (2.90–2.80)	30–2.7 (2.80–2.68)	30–2.75 (2.85–2.75)	30–2.47 (2.56–2.47)
Total observations	340792 (34238)	189181 (18903)	180913 (18198)	271300 (26582)
Unique reflections	45486 (4505)	51206 (5109)	48495 (4789)	37448 (3692)
Completeness (%)	99.8 (99.8)	99.7 (99.8)	99.7 (99.9)	99.3 (100)
$I/\sigma\langle I\rangle$	23.1 (4.4)	16.1 (2.8)	18.2 (2.8)	34.3 (4.6)
R_{merge} (%)	5.9 (33.3)	5.1 (33.6)	4.7 (33.3)	5.3 (46.5)
Refinement				
Resolution range (Å)		30–2.68 (2.73–2.68)		30–2.47 (2.53–2.47)
Reflections ($F > 0\sigma_F$)		51170 (2370)		37404 (2689)
R_{work} (%) for 90% data		18.8 (26.0)		18.1 (24.1)
R_{free} (%) for 10% data		25.7 (33.8)		23.6 (35.8)
RMS deviations				
Bond lengths (Å)		0.008		0.007
Bond angles (°)		1.13		1.08
Average B-factors (Å^2)				
Protein atoms		58.0		49.0
Water molecules		54.2		45.6
Model content				
Protein residues		1464		732
Waters		381		192

found to stably exist within the cavity of the hexameric toroid, although the functional roles of these metal ions are still unclear.

To understand the structural differences between archaeal and bacterial Nif3 proteins, MJ0927 was selected as a target for structure determination. The crystal structure of MJ0927 determined at 2.47 Å revealed that MJ0927 folds into two interlinked α/β domains. Six protomers of MJ0927 are found to form a novel hollow cage-like hexamer, in contrast to the toroid-shaped hexamers formed by other members of the Nif3 family. Additionally, we found that MJ0927 is a DNA-binding protein exhibiting the ability to bind to both single-stranded DNA (ssDNA) and double-stranded DNA (dsDNA). These data indicate that MJ0927 is a new member of the Nif3 family.

2. Materials and Methods

2.1. Cloning, Expression, and Purification. The gene cloning, protein expression, purification, crystallization, and diffraction for the native MJ0927 have been previously reported [10]. For expression of selenomethionyl (Se-Met) labeled MJ0927, the *E. coli* BL21(DE3) host cells were cultured in M9 medium supplemented with 40 μg mL^{-1} Se-Met at 37°C and induced by adding isopropyl β-D-thiogalactopyranoside to a final concentration of 0.5 mM when the cell density reached an OD_{600} of 0.6. Purification of selenomethionyl MJ0927 were performed using similar protocols as established for the native protein.

2.2. Crystallization, Data Collection, and Structure Determination. Purified selenomethionyl MJ0927 was concentrated to approximately 30 mg mL^{-1} for crystallization. Crystals were grown at 4°C using the sitting-drop vapor diffusion method by mixing 1 μL of protein solution with 1 μL of reservoir solution containing 5% PEG3350, 0.1 M sodium acetate, pH 5.0, 0.3 M sodium formate, 0.1 M ammonium sulfate, and 3% poly-γ-glutamic acid polymer (PGA-LM). Crystals were flash-cooled in the mother liquor supplemented with 25% glycerol as a cryoprotectant. X-ray diffraction data were collected using the BL13B1 beamline at the National Synchrotron Radiation Research Center (NSRRC) in Taiwan. A three-wavelength MAD data set was collected to solve the protein phases. Intensity data were scaled and reduced using the HKL-2000 program [11]. The Se-Met-labeled MJ0927 crystals were found to adopt space group $P2_1$. The MAD dataset was used for solving the structure and an *ab initio* model was built by using the Autosol and Autobuild Wizards

in the Phenix package [12], respectively. Twelve selenium sites were identified and the initial phases calculated from these sites were further improved by density modification. The resulting electron density map was readily interpretable and was used to build most of the MJ0927 structure, which was then refined by iterative manual model building in the Coot [13] and Phenix refinement module [14]. Finally, 244 residues out of a total of 249 amino acids could be clearly identified in the model of Se-Met MJ0927.

Crystals of native MJ0927 in the $C222_1$ space group were obtained using the reservoir solution containing 0.1 M $(NH_4)_2SO_4$, 0.3 M sodium formate, 0.1 M sodium acetate, 3% PGA-LM, and 20% MPD. The X-ray diffraction data of native MJ0927 were collected using the BL13C1 beamline at the NSRRC, Taiwan. The crystal structure was solved by the molecular replacement program Phaser [15] using the MJ0927 coordinates in $P2_1$ form as the template. Three molecules of MJ0927 are present in each asymmetric unit. Subsequent refinement of the coordinates and individual B factors were carried out in the Phenix refinement module. Noncrystallographic symmetry restraints were included only in the initial stages of refinement. The R values were refined to 18.1% and 23.6% for the R_{work} and R_{free}, respectively. The detailed crystallographic statistics were summarized in Table 1 [10]. Both coordinate sets have been deposited in the Protein Data Bank under the entries of 4IWG ($C222_1$ form) and 4IWM ($P2_1$ form).

2.3. Electrophoretic Mobility-Shift Assay (EMSA). Two types of DNA were used for the DNA-binding experiments: a single-stranded 37-bp oligonucleotide and a double-stranded 37-mer oligonucleotide (5′-ATGTGAATCAGTATGGTT-ACTATCTGCTGAAGGAAAT-3′ and 5′-ATTTCCTTC-AGCAGATAGTAACCATACTGATTCACAT-3′). These DNA were purchased from MDBio Inc. (Taiwan) and labeled by reaction with T4 polynucleotide kinase in the presence of [γ-^{32}P]ATP. The purified His-tag-free MJ0927 was incubated with 25 nM ssDNA or dsDNA for 60 min, in a 10 μL solution containing 50 mM Tris-HCl, pH 8.0, 100 mM NaCl, 5% glycerol, 100 μM bovine serum albumin, and 2 mM Tris(2-carboxyethyl)phosphine at 37°C. The samples were then loaded onto a native gel of 5% nondenaturing polyacrylamide in 0.5× TB buffer (45 mM Tris-HCl, pH 8.0, and 45 mM boric acid). The DNA and protein-DNA complexes were separated by electrophoresis. Gels were exposed to phosphor storage screens and analyzed on a phosphorimager (Typhoon 9200, GE Healthcare).

3. Results and Discussion

Two crystal forms of MJ0927 were obtained, one in the $P2_1$ and the other in the $C222_1$ space groups. The Se-Met labeled $P2_1$ crystal structure was solved at 2.8 Å resolution by using the multiwavelength anomalous diffraction (MAD) method. The refined structure was subsequently used as the template to solve the native $C222_1$ structure by a molecular replacement approach. The final model was refined to 2.47 Å resolution with good R_{work} and R_{free} values. Residues 6–249 of the polypeptide chain were well defined in the electron-density maps, excluding the 5 N-terminal end residues which were invisible. A ribbon representation of a single MJ0927 monomer is shown in Figure 1(a). The $P2_1$ crystal form contains six molecules in each asymmetric unit, forming a hexameric spheroid with a 32-symmetry (Figure 1(b)). The six independent molecules in the asymmetric unit superpose well with pairwise root-mean-square deviations (rmsd) ranging from 0.222 to 0.310 Å. The $C222_1$ crystal form contains a single copy of a trimer in each asymmetric unit. No significant structural differences of the individual molecules were observed between the $P2_1$ and $C222_1$ crystal forms.

Table 2: Interacting surfaces in MJ0927 and interactions at the interdimer interface.

Type of contacts	Monomer A Residue	Monomer D Residue
Salt bridges	Asp36	Lys87
	Asp96	Lys90
	Lys87	Asp36
	Lys90	Asp96
Hydrogen bonds	Arg79[O]	Asn29[ND2]
	Phe81[O]	Gly35[N]
	Ile78[O]	Ile78[N]
	Lys75[O]	Arg79[NH1]
	Gly27[O]	Arg79[NH1]
	Gly27[O]	Arg79[NH2]
	Leu32[O]	Asn80[ND2]
	Asn29[OD1]	Asn80[ND2]
	Gln33[O]	Phe81[N]
	Gly35[O]	Thr82[OG1]
	Asp96[OD1]	Tyr86[OH]
	Asp36[OD1]	Lys87[NZ]
	Asn29[ND2]	Arg79[O]
	Gly35[N]	Phe81[O]
	Ile78[N]	Ile78[O]
	Arg79[NH1]	Lys75[O]
	Arg79[NH1]	Gly27[O]
	Arg79[NH2]	Gly27[O]
	Asn80[ND2]	Asn29[OD1]
	Phe81[N]	Gln33[O]
	Tyr86[OH]	Asp96[OD1]

The overall structure of the MJ0927 monomer resembles a typical SCOP-classified NIF3-like fold [16] and is composed of 11 β-strands (β1–β11), nine α-helices (α1–α9), and one 3_{10}-helice. This protein appears to fold into two interlinked α/β Nif3 domains, each consisting of two α-helix layers sandwiching a single β-sheet (Figure 1(a)). The first domain (D1) contains a 5-stranded mixed β-sheet flanked by two α-helices and three α-helices on either side. The second domain (D2) is characterized by a central mixed β-sheet comprised of six β-strands with a pair of α-helices on both sides.

The MJ0927 hexamer can be described as two stacked trimers, consisting of monomers A-B-C and D-E-F, which are related by a two-fold symmetry (Figure 1(b)). The intratrimer

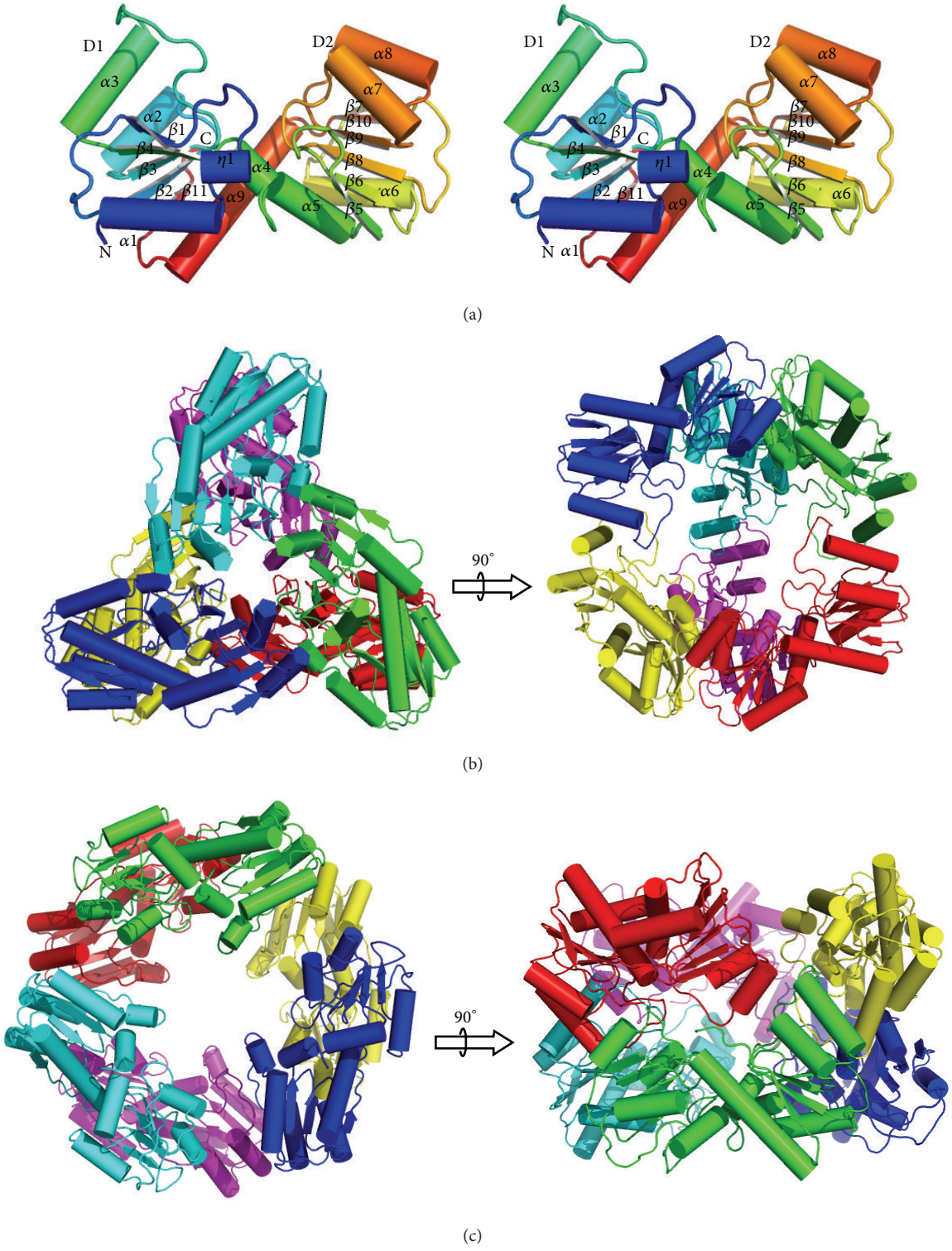

FIGURE 1: (a) Stereo view of MJ0927 monomer. The protein is rainbow-colored from blue at the N-terminus to red at the C-terminus. (b) The top and side views of the MJ0927 hexamer. The monomers A–F are colored in green, blue, cyan, red, yellow, and magenta, respectively. (c) The top and side views of the TTHA1606 hexamer. Each of the six monomers is in a different color.

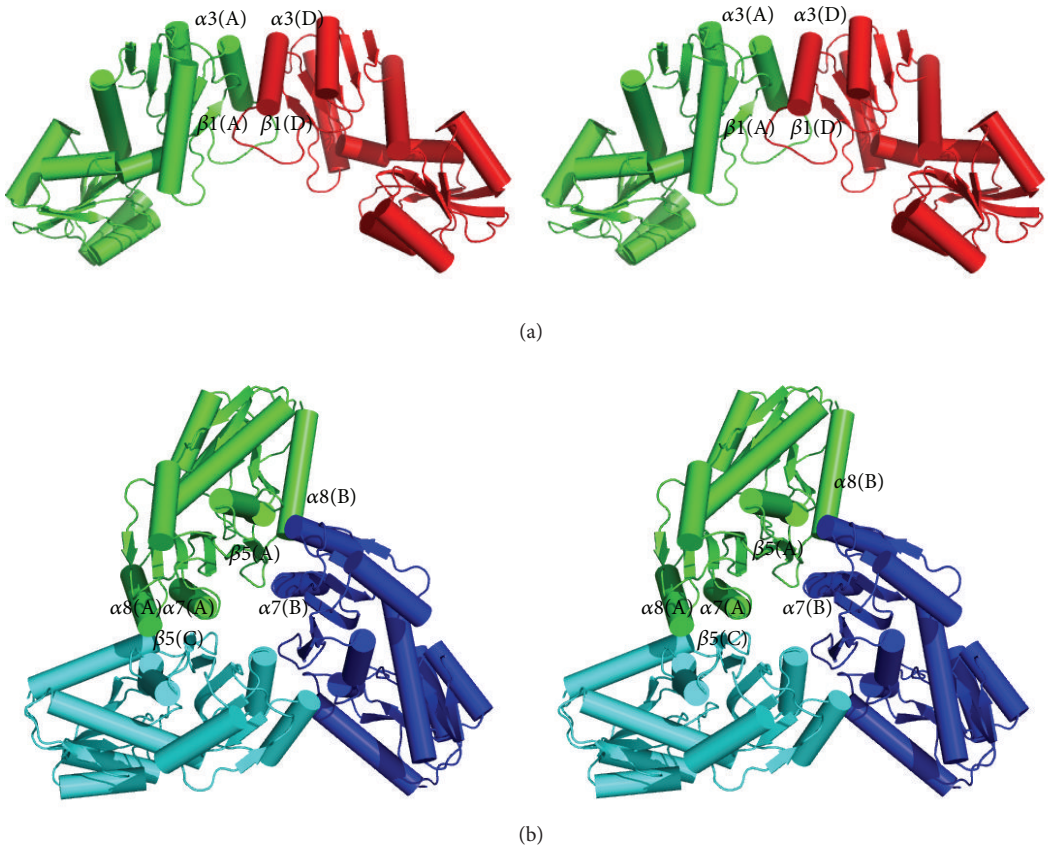

Figure 2: (a) Stereo view of the MJ0927 dimer. (b) A stereo top-view of the MJ0927 trimer along its 3-fold axis.

interface comprises two major regions, one consisting of a β-strand–helix interaction between β-strand β5 and helices α7 and α8 derived from one adjacent subunit, while the other is formed by helices α7 and α8, and β-strand β5 derived from another subunit (Figure 2(b)). The surface area of each subunit buried in the intratrimer interface is 1110 Å^2, representing ~9.1% of the surface area of each subunit. There are five direct hydrogen bonds and six salt bridges and extensive hydrophobic interactions between the monomers across the intratrimer interface (Table 3). Contacts between molecules A and D, B and E, or C and F occur through the interdimer interactions. The surface area of each subunit buried in the interdimer interface is 1207 Å^2, which constitutes ~10% of each subunit surface area. A total of 21 direct hydrogen bonds and four salt bridges are observed across the interdimer interface of each subunit (Table 2), with significant hydrophobic interactions formed by the helix α3, the β-strand β1, and the loop region $L\alpha_3\_\beta_3$ (Figure 2(a)). The hexamer is stabilized by a combination of interdimer and intratrimer interactions. These results are consistent with the previous gel filtration experiment showing that MJ0927 exists as a hexamer in solution [10].

Since MJ0927 is a thermophilic archaeal Nif3 protein, it is not surprising that the quaternary structure of MJ0927 differs from other bacterial Nif3 proteins with regard to the stabilizing structural elements, particularly the structural arrangement at the intratrimer interfaces. As seen in Figure 2(b), the intratrimer interfaces are tightly packed between the second domains of MJ0927 and the three subunits are arranged in a tail-to-tail manner. To date, trimer contacts in these solved bacterial Nif3 structures are only

Table 3: Interacting surfaces in MJ0927 and interactions at the intratrimer interface.

Type of contacts	Monomer A Residue	Monomer B Residue	Monomer C Residue
Salt bridges	Asp22	His204	
	Lys192	Glu191	
	Lys127	Asp194	
	Asp194		Lys127
	Glu191		Lys192
	His204		Asp22
Hydrogen bonds	Tyr188[OH]	Glu191[OE1]	
	Lys127[NZ]	Ala193[O]	
	Lys110[N]	Glu211[OE1]	
	Glu211[OE1]		Lys110[N]
	Glu191[OE1]		Tyr188[OH]

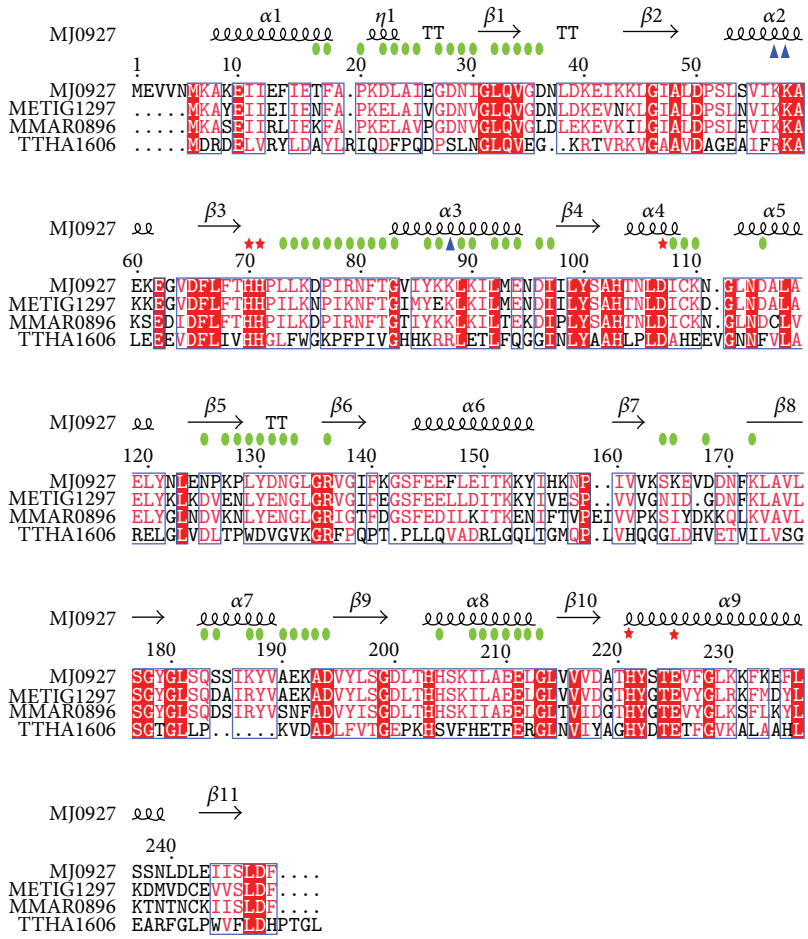

Figure 3: Sequence alignment of MJ0927with *Methanotorris igneus* METIG1297, *Methanococcus maripaludis* MMAR0896, and *Thermus thermophilus* HB8TTHA1606. The following NCBI gi accession numbers reference the sequences used for the alignment: MJ0927, 499172854; METIG1297, 503565355; MMAR0896, 501148655; TTHA1606, 499487006. Sequences are numbered according to MJ0927, and secondary structure elements are displayed above the alignment. Red asterisks indicate metal-binding residues. Blue triangles indicate residues predicted for DNA binding. Green circles indicate residues involved in hexamer formation. Residues that are completely conserved are highlighted in solid red boxes. Those with similarity of >70% are labeled in red. The alignment was generated with the ClustalW2 program [17] (http://www.ebi.ac.uk/Tools/msa/clustalw2/) and used as the input for the ESPript program [18], version 2.2 (http://espript.ibcp.fr/ESPript/cgi-bin/ESPript.cgi).

found in the SA1388 and YqfO [6, 8], which use PII-like domains that appear to cap the openings on either side of the central channel in the toroidal rings. Therefore, the trimer organization of MJ0927 is a unique structural feature that likely contributes to its increased structural stability and which has never been observed in other Nif3 proteins. In addition, a sequence alignment further revealed that the Nif3 members in the *Methanotorris*, *Methanocaldococcus*, and *Methanococcus* species likely exhibit similar hexameric spherical architectures, as residues involved in the hexamer formation are found to be highly conserved (Figure 3). Although the biological function of MJ0927 remains unclear, this sequence analysis suggests that the hexameric spherical structure and its overall shape are preserved during evolution and thus may have functional significance.

Additionally, sequence analysis revealed that the highly conserved metal-binding motifs are located in the cavity between the D1 and D2 domains, which consist of three histidines, one glutamate, and one aspartate (Figure 3). In the three bacterial Nif3 protein structures (YbgI, YqfO, and SA1388) [6–8], two divalent metal ions were found to occupy the metal-binding sites. However, no metal ion was observed in the metal-binding site of MJ0927 even though MJ0927 contains these conserved residues. The absence of endogenous metal ions in MJ0927 is similar to the structures reported for SP1609 and TTHA1606 [9], although the reason for this phenomenon is still unclear.

Since TTHA1606 has been shown to bind ssDNA [9], we are also interested to see if MJ0927 were capable of binding DNA. To assess the DNA-binding ability of MJ0927, purified proteins were incubated with ssDNA or dsDNA and the resulting complexes were separated by EMSA. Results of this analysis indicated that MJ0927 indeed is able to bind to

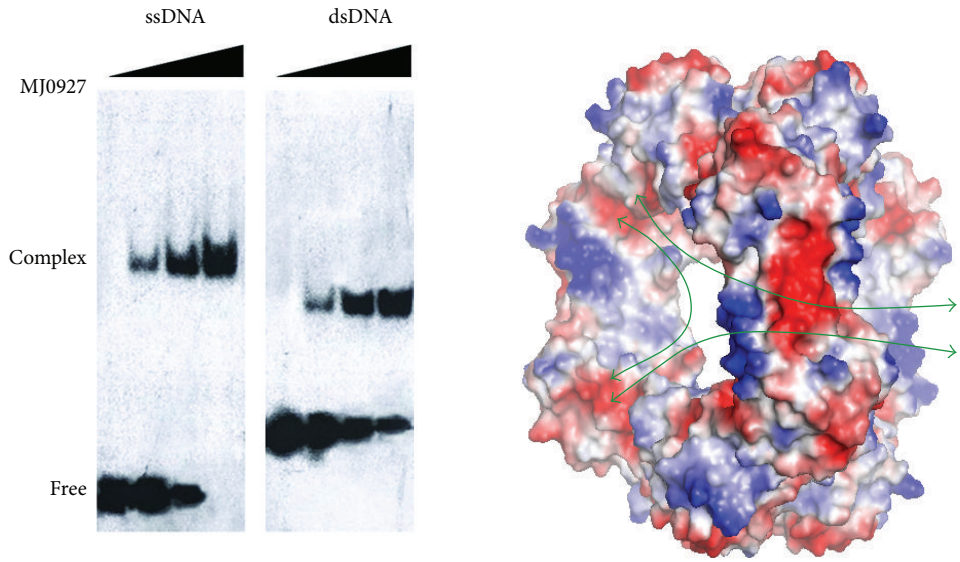

Figure 4: (a) EMSA analysis of MJ0927. 25 nM ssDNA was incubated with various amounts of MJ0927 at 0, 50, 250, and 500 μM in a 10-μL reaction mixture and 25 nM dsDNA was incubated with increasing amounts of MJ0927 at 0, 50, 100, and 200 μM. (b) Surface representations displaying the electrostatic potential of MJ0927. Electrostatic potential was calculated using the program APBS [19] implemented in PYMOL (The PyMOL Molecular Graphics System, Version 0.99rc6 Schrödinger, LLC.). Positive potential is shown in blue, neutral in white and negative potential in red. Green arrows indicate possible paths for DNA entry.

both ssDNA and dsDNA (Figure 4(a)). The dsDNA-binding property of MJ0927 was not observed in other Nif3 family proteins reported to date.

No Nif3-DNA complex structure has ever been reported yet. However, structural analyses of MJ0927 could provide some insights as to how the Nif3 protein binds to DNA. From the determined Nif3 structures reported to date, only those of MJ0927 and TTHA1606 were shown to bind ssDNA. Similar to TTHA1606, MJ0927 also possesses positively charged residues clustered on the helices α2 and α3 near the putative active site. Most of these residues share high sequence similarity between the MJ0927 and TTHA1606 Nif3 proteins, suggesting that the positively charged region may be involved in DNA binding (Figure 2(a)). Furthermore, the quaternary assembly of MJ0927 is significantly different to those previously solved bacterial Nif3 proteins. The bacterial Nif3s except for SA1388 and YqfO consist of three dimers forming toroidal ring quaternary structures, which possess an opened channel in the center of the hexamer (Figure 1(c)), whereas MJ0927 adopts an unusual assembly comprising a trimer of dimers that forms a cage-like architecture (Figure 1(b)). The architecture of MJ0927 leads to three large openings (Figure 4(b)). The diameter of the openings is approximately 33 Å, which is large enough to allow ssDNA or dsDNA entry. The sphere assembly of MJ0927 leads to larger openings than that of TTHA1606. Therefore, MJ0927 binds to both ssDNA and dsDNA, but TTHA1606 only binds to ssDNA.

4. Conclusions

MJ0927 is a member of the Nif3 family and is highly conserved among bacteria and humans. Here we describe the crystal structure of MJ0927, revealing an unusual hexameric assembly. Electrophoretic mobility-shift assays indicated that MJ0927 can bind to both ssDNA and dsDNA. The studies presented here clearly indicate that hexameric MJ0927 possesses ssDNA- and ds-DNA-binding properties and helps to further define its function. In a proposed follow-up study, we will try to determine the structure of MJ0927 in complex with DNA with the intent of identifying the DNA-binding residues of this protein to gain insight into its mechanism of action.

Conflict of Interests

The authors declare that there is no conflict of interests regarding the publication of this paper.

Authors' Contribution

Sheng-Chia Chen and Chi-Hung Huang contributed equally to this work.

Acknowledgments

The authors thank the National Synchrotron Radiation Research Center (NSRRC, Taiwan) for assistance during data collection. The authors are grateful to the staff of TCX-D900, Technology Commons, College of Life Science and Center for System Biology, NTU for help with the Art Robbins Instruments Phoenix protein crystallization robot. This work was supported by Grants from the National Science Council (NSC99-2313-B-241-001 and NSC100-2313-B-241-006 to Yeh

Chen) and by the Ministry of Education, Taiwan, ROC under the ATU plan.

References

[1] R. Xiao, S. Anderson, J. Aramini et al., "The high-throughput protein sample production platform of the Northeast Structural Genomics Consortium," *Journal of Structural Biology*, vol. 172, no. 1, pp. 21–33, 2010.

[2] M. Y. Galperin and E. V. Koonin, "'Conserved hypothetical' proteins: prioritization of targets for experimental study," *Nucleic Acids Research*, vol. 32, no. 18, pp. 5452–5463, 2004.

[3] J. A. Martens, J. Genereaux, A. Saleh, and C. J. Brandl, "Transcriptional activation by yeast PDR1p is inhibited by its association with NGG1p/ADA3p," *The Journal of Biological Chemistry*, vol. 271, no. 27, pp. 15884–15890, 1996.

[4] S. Tascou, T. W. Kang, R. Trappe, W. Engel, and P. Burfeind, "Identification and characterization of NIF3L1 BP1, a novel cytoplasmic interaction partner of the NIF3L1 protein," *Biochemical and Biophysical Research Communications*, vol. 309, no. 2, pp. 440–448, 2003.

[5] H. Akiyama, N. Fujisawa, Y. Tashiro, N. Takanabe, A. Sugiyama, and F. Tashiro, "The role of transcriptional corepressor Nif3l1 in early stage of neural differentiation via cooperation with Trip15/CSN2," *The Journal of Biological Chemistry*, vol. 278, no. 12, pp. 10752–10762, 2003.

[6] M. H. Godsey, G. Minasov, L. Shuvalova et al., "The 2.2 Å resolution crystal structure of *Bacillus cereus* Nif3-family protein YqfO reveals a conserved dimetal-binding motif and a regulatory domain," *Protein Science*, vol. 16, no. 7, pp. 1285–1293, 2007.

[7] J. E. Ladner, G. Obmolova, A. Teplyakov et al., "Crystal structure of Escherichia coli protein ybgI, a toroidal structure with a dinuclear metal site," *BMC Structural Biology*, vol. 3, article 1, 2003.

[8] K. S. Saikatendu, X. Zhang, L. Kinch, M. Leybourne, N. V. Grishin, and H. Zhang, "Structure of a conserved hypothetical protein SA1388 from *S. aureus* reveals a capped hexameric toroid with two PII domain lids and a dinuclear metal center," *BMC Structural Biology*, vol. 6, article 27, 2006.

[9] F. Tomoike, T. Wakamatsu, N. Nakagawa, S. Kuramitsu, and R. Masui, "Crystal structure of the conserved hypothetical protein TTHA1606 from Thermus thermophilus HB8," *Proteins: Structure, Function and Bioinformatics*, vol. 76, no. 1, pp. 244–248, 2009.

[10] S.-M. Kuan, H.-C. Chen, C.-H. Huang et al., "Crystallization and preliminary X-ray diffraction analysis of the Nif3-family protein MJ0927 from *Methanocaldococcus jannaschii*," *Acta Crystallographica F: Structural Biology and Crystallization Communications*, vol. 69, no. 1, pp. 80–82, 2013.

[11] Z. Otwinowski and W. Minor, "Processing of X-ray diffraction data collected in oscillation mode," *Methods in Enzymology A*, vol. 276, pp. 307–326, 1997.

[12] T. C. Terwilliger, P. D. Adams, R. J. Read et al., "Decision-making in structure solution using Bayesian estimates of map quality: the PHENIX AutoSol wizard," *Acta Crystallographica D: Biological Crystallography*, vol. 65, part 6, pp. 582–601, 2009.

[13] P. Emsley and K. Cowtan, "Coot: model-building tools for molecular graphics," *Acta Crystallographica Section D: Biological Crystallography*, vol. 60, no. 12, pp. 2126–2132, 2004.

[14] P. D. Adams, P. V. Afonine, G. Bunkóczi et al., "PHENIX: a comprehensive Python-based system for macromolecular structure solution," *Acta Crystallographica Section D: Biological Crystallography*, vol. 66, part 2, pp. 213–221, 2010.

[15] A. J. McCoy, R. W. Grosse-Kunstleve, P. D. Adams, M. D. Winn, L. C. Storoni, and R. J. Read, "Phaser crystallographic software," *Journal of Applied Crystallography*, vol. 40, no. 4, pp. 658–674, 2007.

[16] A. G. Murzin, S. E. Brenner, T. Hubbard, and C. Chothia, "SCOP: a structural classification of proteins database for the investigation of sequences and structures," *Journal of Molecular Biology*, vol. 247, no. 4, pp. 536–540, 1995.

[17] M. A. Larkin, G. Blackshields, N. P. Brown et al., "Clustal W and Clustal X version 2.0," *Bioinformatics*, vol. 23, no. 21, pp. 2947–2948, 2007.

[18] P. Gouet, X. Robert, and E. Courcelle, "ESPript/ENDscript: extracting and rendering sequence and 3D information from atomic structures of proteins," *Nucleic Acids Research*, vol. 31, no. 13, pp. 3320–3323, 2003.

[19] N. A. Baker, D. Sept, S. Joseph, M. J. Holst, and J. A. McCammon, "Electrostatics of nanosystems: application to microtubules and the ribosome," *Proceedings of the National Academy of Sciences of the United States of America*, vol. 98, no. 18, pp. 10037–10041, 2001.

Hindawi Publishing Corporation
BioMed Research International
Volume 2014, Article ID 342725, 8 pages
http://dx.doi.org/10.1155/2014/342725

Research Article

Crystal Structure of *Deinococcus radiodurans* RecQ Helicase Catalytic Core Domain: The Interdomain Flexibility

Sheng-Chia Chen,[1,2] Chi-Hung Huang,[1,2,3] Chia Shin Yang,[1,2] Tzong-Der Way,[4] Ming-Chung Chang,[5] and Yeh Chen[1]

[1] *Department of Biotechnology, Hungkuang University, Taichung 433, Taiwan*
[2] *Taiwan Advance Biopharm (TABP), Inc., Xizhi City, New Taipei City 221, Taiwan*
[3] *Institute of Biochemistry, National Chung-Hsing University, Taichung 40227, Taiwan*
[4] *Department of Biological Science and Technology, College of Life Sciences, China Medical University, Taichung 40402, Taiwan*
[5] *Department of Nutrition, Hungkuang University, Taichung 433, Taiwan*

Correspondence should be addressed to Ming-Chung Chang; mcchang@sunrise.hk.edu.tw
and Yeh Chen; bluecrystalprotein@gmail.com

Received 3 June 2014; Accepted 1 July 2014; Published 27 August 2014

Academic Editor: Cheng-Yang Huang

RecQ DNA helicases are key enzymes in the maintenance of genome integrity, and they have functions in DNA replication, recombination, and repair. In contrast to most RecQs, RecQ from *Deinococcus radiodurans* (DrRecQ) possesses an unusual domain architecture that is crucial for its remarkable ability to repair DNA. Here, we determined the crystal structures of the DrRecQ helicase catalytic core and its ADP-bound form, revealing interdomain flexibility in its first RecA-like and winged-helix (WH) domains. Additionally, the WH domain of DrRecQ is positioned in a different orientation from that of the *E. coli* RecQ (EcRecQ). These results suggest that the orientation of the protein during DNA-binding is significantly different when comparing DrRecQ and EcRecQ.

1. Introduction

RecQ helicases are a family of DNA strand-separating enzymes conserved from bacteria to humans that play a crucial role in the maintenance of genome stability [1]. Bacteria have only one RecQ homolog, whereas higher eukaryotic organisms express multiple homologs of RecQ enzymes. Five members of the RecQ family have been found in humans, namely, RECQ1, BLM, WRN, RECQ4, and RECQ5, and defects in three of the five RecQ family members are related to human disorders. Specifically, mutations in the human genes BLM, WRN, and RECQ4 cause Bloom's syndrome, Werner's syndrome, and Rothmund-Thomson syndrome, respectively. These mutations result in genomic instabilities and a predisposition to cancer [2, 3]

Most RecQ proteins share a helicase catalytic core and a C-terminal helicase-and-RNase-D-C-terminal (HRDC) domain. The minimal helicase catalytic core consists of two RecA-like domains, a Zn-binding domain (ZBD), and a winged-helix (WH) domain. Each individual domain has its own function and structure [4]. The helicase catalytic core is crucial for the ATPase and DNA-unwinding activities of these RecQ proteins. The HRDC domain is responsible for regulating DNA-binding affinity with a wide variety of DNA substrates [5]. To date, tertiary structures of the RecQ helicase catalytic core have been reported and determined by X-ray crystallography, including those of *E. coli* RecQ (PDB 1OYW) and human RecQ1 (hRecQ1) (PDB 2V1X) [4, 6]. These structures have been observed to adopt similar domain architectures, forming Y-shaped molecules. However, the hairpin structures and domain orientation of the WH domains, which are important for DNA binding and unwinding, are markedly distinct between the EcRecQ and the hRecQ1.

Deinococcus radiodurans is best known for extraordinary resistance to ionizing radiation, ultraviolet (UV) radiation,

and chemical mutagens. This bacterium can survive under conditions of 7000 kGy of ionizing radiation with only 10% cell death; a radiation dose of greater than 50 Gy is lethal to most organisms [7]. Over 100 double-strand breaks (DSBs) can be mended throughout its genome during a postirradiative incubation [2, 8]. Because of its remarkable ability to repair DNA damage, *D. radiodurans* can become an excellent model system for studying the mechanisms of DNA repair. In this bacterium, RecD is the only member that is identified in the RecBCD pathway, whereas all of the members associated with the RecFOR pathway have been found in the genome of *D. radiodurans*, suggesting that the RecFOR pathway is the main repair pathway of DNA damage in this organism [9].

D. radiodurans has a unique RecQ homolog with three HRDC domains (HRDC1, HRDC2, and HRDC3) at its C terminus. The function of DrRecQ has been characterized, confirming that the unusual domain arrangement of DrRecQ has the extraordinary ability to repair DNA damage in *D. radiodurans* [10]. HRDC1 and HRDC3 have also been structurally characterized [5, 11]. However, the structure of the helicase catalytic core remains undetermined. To better understand the structural and functional relationships of DrRecQ, we present crystal structures of the minimal helicase catalytic core from DrRecQ and its binary complex with ADP. Surprisingly, superposition of the apoenzyme against the binary complex reveals that the WH domain is positioned at a different orientation in these two structures, indicating the flexibility of the WH domain interdomain. Owing to the importance of the WH domain for DNA binding, its flexibility is likely involved in regulating DNA recognition. A comparison of DrRecQ and EcRecQ reveals that the domain orientation of the WH domain is significantly different between these two proteins, suggesting that the orientation of the DNA-binding motif is distinct between the DrRecQ and the EcRecQ.

Table 1: Data collection statistics for the DrRecQ crystals. Values in parentheses are for the highest resolution shell.

	DrRecQ	DrRecQ-ADP
Data Collection		
Wavelength (Å)	0.9762	0.9762
Space group	$P2_12_12_1$	$P2_12_12_1$
Unit Cell (Å)	85.79, 98.52, 152.88	84.75, 95.61, 183.83
Resolution range (Å)	30–2.8 (2.9-2.8)	30–2.9 (3.0-2.9)
Total observations	86816 (9033)	345728 (34587)
Unique reflections	31511 (3115)	33811 (3294)
Completeness (%)	96.3 (96.6)	99.9 (100.0)
$I/\sigma\langle I\rangle$	15.6 (2.9)	27.5 (3.8)
R_{merge} (%)	8.7 (54.3)	7.6 (67.8)
Refinement		
Resolution range (Å)	30–2.8 (2.9-2.8)	30-2.9 (3.0-2.9)
Reflections ($F > 0\,\sigma_F$)	31482 (3068)	33750 (3255)
R_{cryst} (%) for 95% data	21.3 (29.3)	22.2 (32.8)
R_{free} (%) for 5% data	28.5 (37.6)	29.5 (40.1)
RMS deviations		
Bond lengths (Å)	0.011	0.012
Bond angles (°)	1.58	1.78
Average *B*-factors ($Å^2$)		
protein atoms	56.8	71.3
Zinc ion	36.1	66.4
ADP		72.8
Number of nonhydrogen atoms		
Protein	7839	7943
Zinc	2	2
ADP		54

2. Materials and Methods

2.1. Cloning, Expression, Purification, Crystallization, and Data Collection of DrRecQ. The gene cloning, protein expression, and purification of DrRecQ have been previously reported [12]. DrRecQ was crystallized using the sitting-drop vapor diffusion method with a buffer containing 0.1 M HEPES (pH 7.7), 14% PEG 8 K, and 8% ethylene glycol. It formed orthorhombic crystals with the following cell dimensions: $a = 85.7$ Å, $b = 98.5$ Å, and $c = 152.8$ Å, with two molecules per asymmetric unit. All the DrRecQ crystals were cryoprotected with 25% glycerol added to the reservoir solution before flash cooling in a stream of nitrogen at 100 K. Crystals of DrRecQ diffracted at 2.8 Å at the National Synchrotron Radiation Research Center (NSRRC) BL13C1 in Taiwan. DrRecQ in complex with ADP was crystallized with a buffer containing 0.1 M imidazole (pH 7.2) and 16% PEG 20 K. The final crystals were orthorhombic with the following cell dimensions: $a = 84.7$ Å, $b = 95.6$ Å, and $c = 183.8$ Å, with two molecules per asymmetric unit. The crystal of the binary complex diffracted to a resolution of 2.9 Å at NSRRC BL13C1.

2.2. Structure Determination. The crystal structure of the helicase catalytic core of DrRecQ was solved using the molecular-replacement method and the Phaser program with the coordinates of EcRecQ derived from a search model [13]. The crystal structure of the DrRecQ-ADP complex was solved using the molecular replacement program Phaser and the structure of the apoform DrRecQ was derived from a search model. The structure was completed via multiple manual interactions in COOT [14]. Structure refinement was performed by using the Phenix program and refined with tight NCS restraints [15]. The quality of all models was assessed using the Molprobity program [16]. Stereochemical libraries were prepared using the Phenix program elBOW. The statistical analysis of the data collection and refinement is summarized in Table 1. The coordinates and structural factors of the DrRecQ and DrRecQ-ADP crystals have been deposited in Protein Data Bank with accession codes 4Q48 and 4Q47, respectively. The structural figures were prepared in the PyMOL program (The PyMOL Molecular Graphics System, Version 0.99rc6, Schrödinger, LLC.).

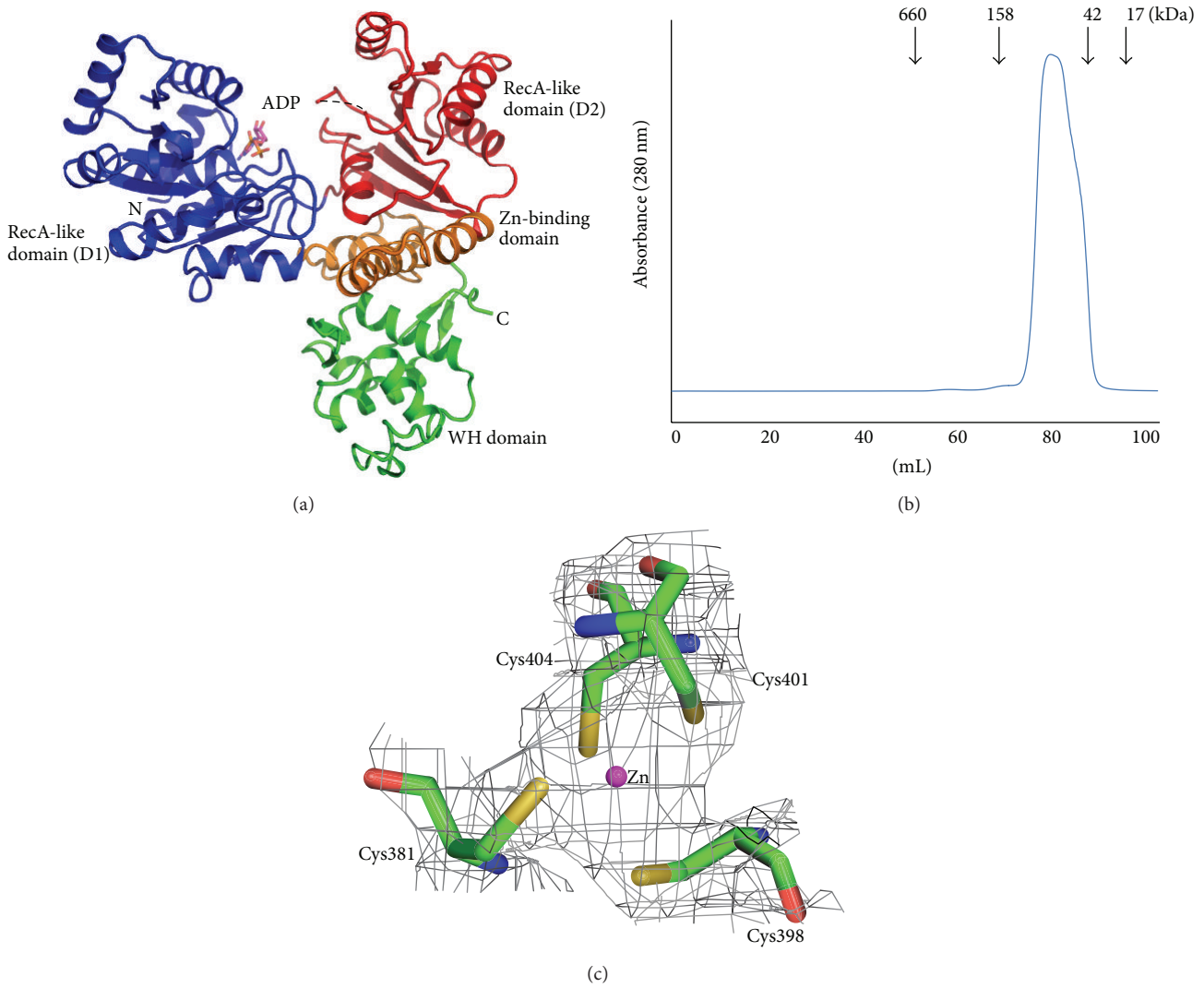

FIGURE 1: (a) Crystal structure of the *D. radiodurans* RecQ catalytic core. The two RecA-like domains, D1 and D2, are colored in blue and red, respectively. The zinc-binding domain is highlighted in orange and the WH domain in green. ADP (magenta) is depicted in stick representation. (b) The size exclusion chromatography profile of DrRecQ. (c) The zinc-binding site of DrRecQ. The four conserved cysteine residues are shown in stick and a zinc ion is colored in magenta. The $2F_o$-F_c electron density map contoured at the 2σ level is colored in gray.

3. Results and Discussion

3.1. Overall Structure. The crystal structure of the helicase catalytic core of RecQ from *D. radiodurans* was solved using the molecular-replacement method with the coordinates of EcRecQ from a search model and was refined at a resolution of 2.80 Å. The apoenzyme structure was subsequently used to solve the binary complex structure with ADP at resolution of 2.90 Å. In the binary complex structure, residues 5–517 of the polypeptide chain were well defined in the electron-density map; the exception was the 4 N-terminal end residues and residues 296–300, which were not visible. A ribbon representation of a monomer is shown in Figure 1(a). Both crystal forms contain two molecules in each asymmetric unit. Gel filtration analysis showed that the helicase catalytic core exists as a monomer in solution (Figure 1(b)). Thus, we consider the monomeric structure the biological unit.

The crystal structure reveals that the helicase catalytic core of DrRecQ is composed of four domains. The helicase catalytic core of DrRecQ contains four domains assembled in a trilobed or Y-shaped manner, with major clefts on its surface. The N-terminal part contains the common core structure of the RecQ helicase family, which consists of two canonical RecA-like domains, D1 (amino acids 1–207) and D2 (amino acids 208–341), that are each composed of a central β-sheet surrounded by α-helices. Highly conserved signature sequence motifs are located in a cleft at the interface of D1 and D2. These motifs are typically involved in the hydrolysis of ATP and nucleic acid binding. The following Zn-binding domain (amino acids 342–407) possesses a Zn-binding motif and two antiparallel helices. The electron density maps of the Zn-binding motif reveal that the zinc ion is tetrahedrally coordinated by the side chains of four conserved cysteine residues (Cys381, Cys398, Cys401, and Cys 404) (Figure 1(c)).

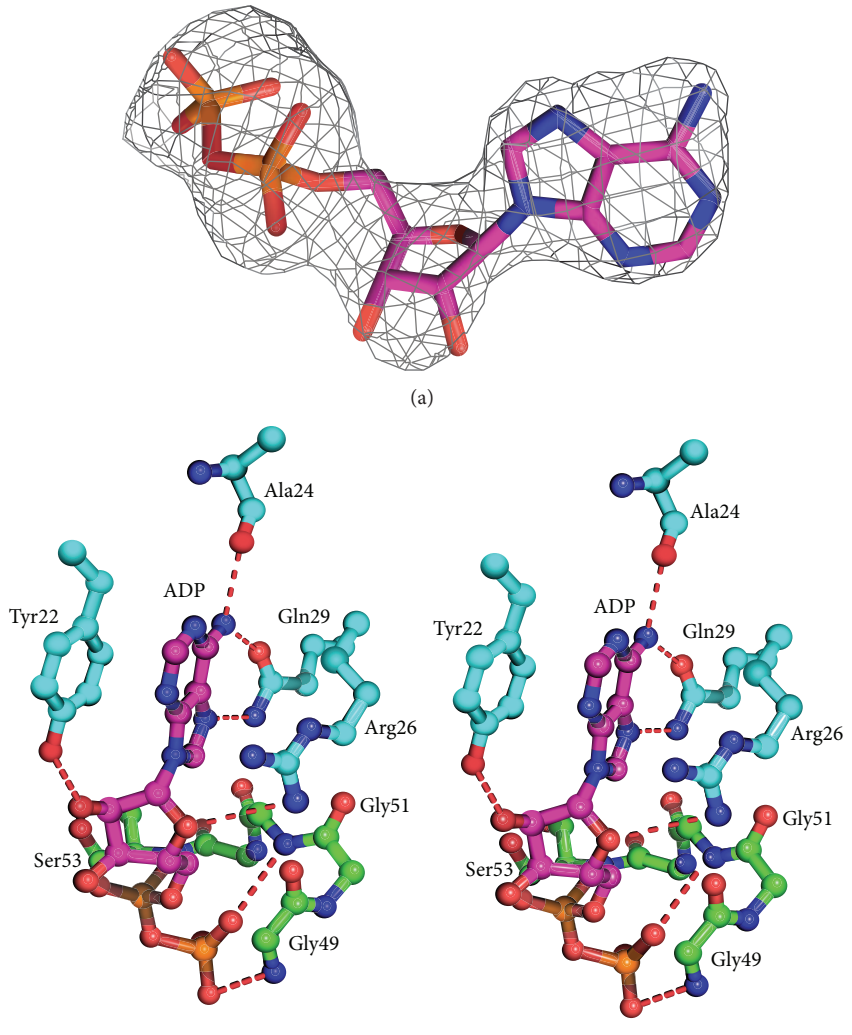

FIGURE 2: (a) The electron density for ADP from F_o-F_c map seen at 3σ. (b) Stereo view of the catalytic site in the DrRecQ catalytic core. The residues that interact with ADP in DrRecQ are shown as ball-and-stick models (magenta). Main chain and carbon are colored according to the conserved motifs: motif 0 (cyan) and motif I (green).

The zinc ion seems to be dispensable for the stabilization of the protein structure [4]. The C-terminal region adopts a WH fold (amino acids 407–517) and is structurally homologous to similar folds in WRN and RecQ1, even though they share very little sequence conservation. The WRN WH-DNA complex structure (PDB code 3AAF) showed that the WH domain directly participates in DNA binding and base pair separation [17]. Thus, the WH fold of DrRecQ was considered to be a DNA-binding domain for the recognition of different DNA substrates.

3.2. DrRecQ-ADP Interactions. The nucleotide-binding pock-et surrounded by conserved motifs is located at the D1 domain. Inspection of the electron density map revealed that electron density is strong in the pocket. Although we initially tried to model ATP into the experiment map, the γ-phosphate cannot fit well, suggesting that the ATP has been hydrolyzed to ADP during crystallization despite not adding a magnesium ion (Figure 2(a)). ADP is bound with extensive interactions with the protein (Figure 2(b)). The adenine moiety is sandwiched between Arg26 and Tyr22. The N6 and N7 atoms of the adenine ring are hydrogen-bonded to the side chain of Gln29, and the N6 atom is also situated within hydrogen-bonding distance of the main chain carbonyl oxygen atoms of Ala24. The ribosyl moiety is anchored via hydrogen bonds with the C-2 hydroxyl group of the side chain of Tyr22. The diphosphate is bound by backbone amides of motif I. ADP binding to the D1 domain causes slight alterations in motif I. The sequence alignment shows that motifs 0 (amino acids 16–29) and I (amino acids 45–53) are highly conserved in three RecQ proteins (Figure 3). All of the nucleotide-interacting residues of DrRecQ are conserved in EcRecQ and the ATPase-active conformation of DrRecQ is similar to those of other RecQ family members.

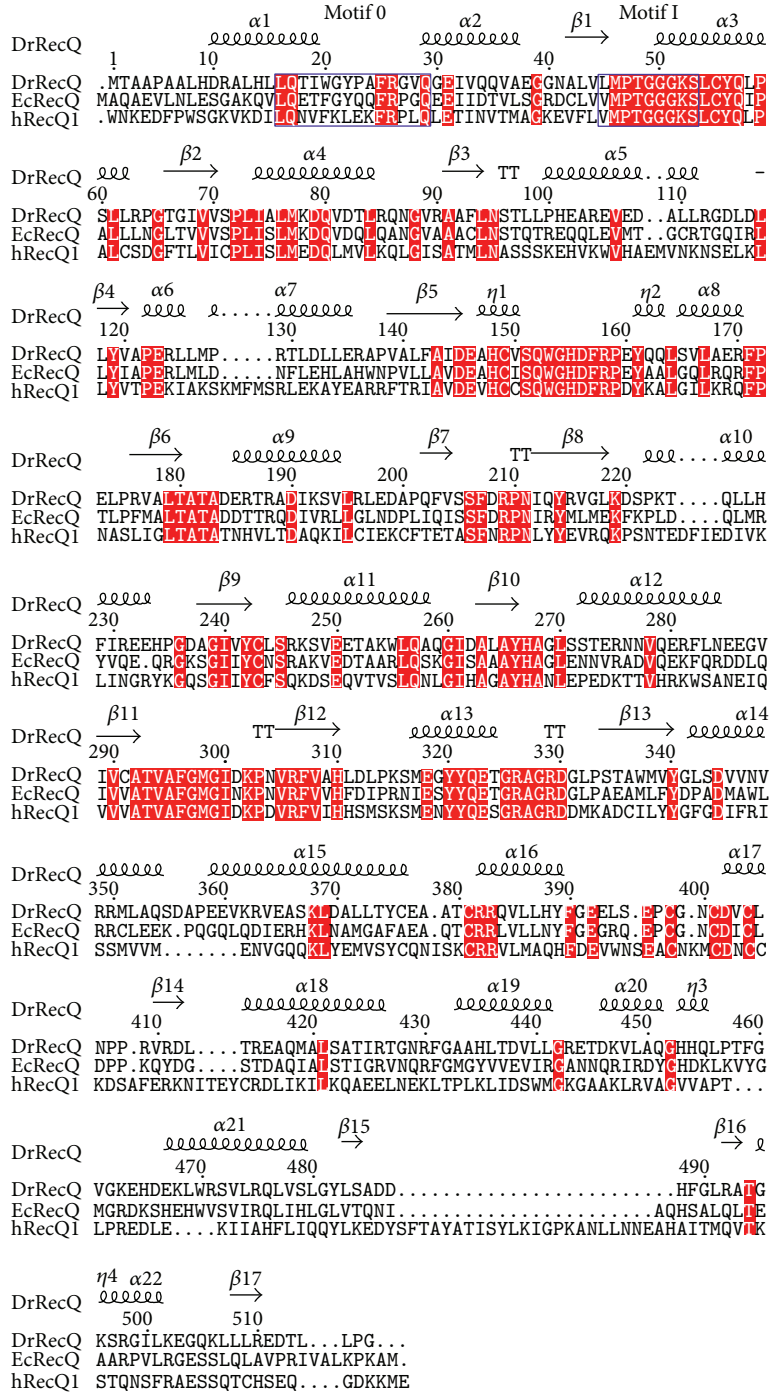

Figure 3: Sequence alignment of the catalytic core from various RecQ proteins. Conserved helicase motifs 0 and I are labeled and enclosed in blue boxes. The conserved residues are shaded in red.

3.3. Structural and Sequence Comparisons. Structural similarity searches with Dali revealed that DrRecQ is similar to other RecQ proteins [18]. The best hits include EcRecQ and hRecQ1. Most of the secondary structural elements in DrRecQ and EcRecQ are highly conserved. The percentages of sequence identity between DrRecQ with EcRecQ and hRecQ1 are 49% and 33%, respectively. The rmsd values of superimposition between DrRecQ with EcRecQ and hRecQ1 are 3.7 and 10.8 Å for 498 and 474 C_α, respectively. These data indicate that DrRecQ is more structurally similar to EcRecQ and more distant from hRecQ1. The domains of DrRecQ could individually superimpose well with both EcRecQ and hRecQ1, but the high rmsd value may be due to difference in the interdomain orientations between the structures. Comparison of the three structures demonstrates that there is conservation of domain architecture, specifically in the

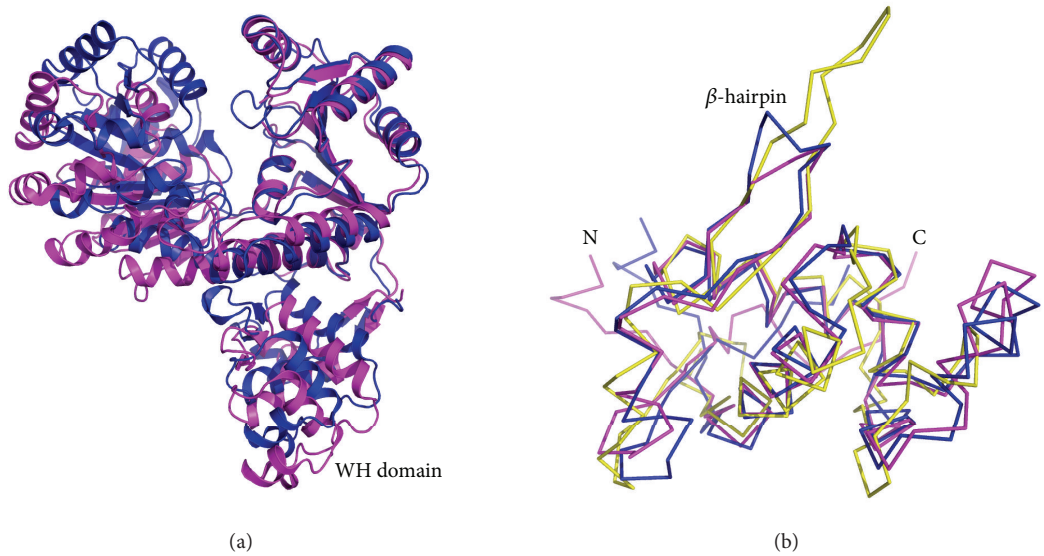

Figure 4: (a) Overlay of DrRecQ (magenta) and EcRecQ (blue). Structures were superposed using the RecA-like 2 domain as a reference. (b) Structure comparison of β-hairpins between RecQ members. The DrRecQ (magenta) is shown overlaid with human RecQ1 (yellow) and with *E. coli* RecQ (blue).

N-terminal portions of two RecA-like domains, the following Zn-binding domain and the C-terminal WH domain. A structural alignment was carried out for representing structures using the Pymol program with the resulting structural superimposition shown in Figure 4(a). These structures were superimposed using the D2 domain as reference, showing that the relative orientation of the WH domains is dramatically different. These results suggest that orientation of the DNA-binding motif is distinct when comparing DrRecQ and EcRecQ. Additionally, several studies have shown that the β-hairpin structures in the WH domains of the human RecQ members are necessary for DNA unwinding, while mutational analysis shows that H491 in the β-hairpin of EcRecQ is not required for helicase activity, suggesting a different mode of action between the bacterial and human RecQs [6]. A structural comparison of DrRecQ, hRecQ1, and EcRecQ reveals that the prominent β-hairpin of DrRecQ is shorter than hRecQ1 but resembles that of EcRecQ (Figure 4(b)). This may indicate that the functional role of β-hairpin of DrRecQ is similar to that of EcRecQ.

3.4. Interdomain Flexibility of DrRecQ. A structural overlay of the free and ADP-bound forms of DrRecQ reveals that the two structures differ in the relative positions and orientation of D1 and WH domains (Figure 5). A structural shift in the D1 and D2 domains indicates that a high degree of interdomain flexibility occurs. The motion may represent an interdomain motion required for interaction with DNA, though the detailed mechanism of DNA unwinding is still unclear. Moreover, the structural differences between the WH domains of the two forms are well demonstrated by the rigid-body movement between the Zn-binding and the WH domains. This relative domain orientation of DrRecQ was further analyzed using Chimera software [19]. The WH

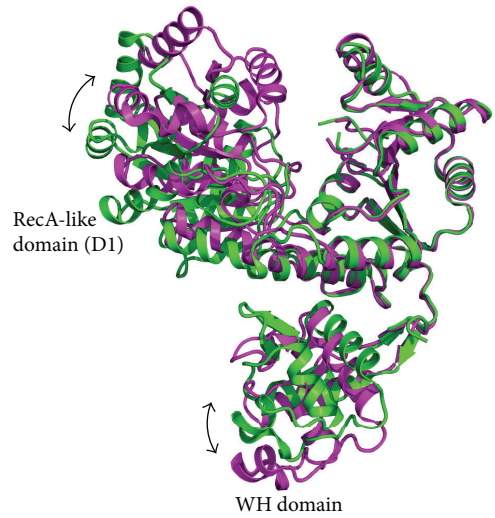

Figure 5: Interdomain flexibility of DrRecQ. The apoform is colored in magenta and the ADP-bound form in green. The structures are superimposed by using the RecA-like 2 domain as a reference.

domain rotates 24° toward the Zn-binding domain. Because the WH domain is not close to the nucleotide-binding pocket, differences in the orientation of the WH domain do not appear to be induced by ADP binding. This result is most likely due to DrRecQ crystallized in different conditions. The distinct domain orientation also indicates the interdomain flexibility of the WH domain. This motion generates a closed conformation in the binary complex structure and slightly enlarges the cleft between Zn-binding and WH domains in the apoform structure. To the best of our knowledge, the WH domain plays an important role in DNA binding and

unwinding, even though the bacterial RecQ-DNA complex structures that define how protein-DNA binding occurs are unavailable. The motion of the WH domain in DrRecQ may allow the WH domain to easily interact with different DNA substrates or to cope with HRDC domains as the DNA is unwinding, which seems to contribute to the remarkable ability of repairing DNA damage in this extremophilic organism. Moreover, the orientation of the DrRecQ WH domain is different than that observed in both EcRecQ and hRecQ1, which may reveal a functional difference in DNA binding and unwinding. The interdomain flexibility of the WH domain is most likely a unique structural feature of DrRecQ. In contrast, the orientation of the WH domain in EcRecQ is very similar in both the free and nucleotide-binding structures. In addition, Swan et al. recently solved the crystal structure of BLM [20], which observes the mobility of its WH domain when comparing structures of apo- and DNA-bound forms. On the basis of the structural analysis, they also suggest that multiple open conformations exist in the apoform of BLM. The attribute is also consistent with our structural analysis of DrRecQ. Collectively, these findings provide the first evidence of interdomain flexibility in DrRecQ and the structural basis for a model of the conformational change in the WH domain that is likely to regulate DNA-binding activity. Further studies are necessary to elucidate the possible roles of the interdomain flexibility of the WH domain in DrRecQ function.

4. Conclusion

In this study, we described crystal structures of the DrRecQ helicase catalytic core and its ADP-bound form. Structural comparison of the two structures found that rigid-body movement occurs in the WH domain, indicating that the WH domain displays interdomain flexibility in DrRecQ. The motion may be important for the remarkable DNA repair mechanism performed by DrRecQ. Because DrRecQ is essential for maintaining genome stability, these structures provide important clues for understanding the molecular mechanisms of DNA replication, recombination, and repair.

Conflict of Interests

The authors declare that there is no conflict of interests regarding the publication of this paper.

Authors' Contribution

Sheng-Chia Chen and Chi-Hung Huang contributed equally to this paper.

Acknowledgments

The authors thank the National Synchrotron Radiation Research Center (NSRRC, Taiwan) for assistance during data collection. They are grateful to the staff of TCX-D900, Technology Commons, College of Life Science and Center for System Biology, NTU, for help with the Art Robbins Instruments Phoenix protein crystallization robot. This work was supported by Grants from the National Science Council (NSC99-2313-B-241-001 and NSC100-2313-B-241-006 to Yeh Chen), and by the Ministry of Education, Taiwan, under the ATU plan.

References

[1] R. J. Monnat Jr., "Human RECQ helicases: roles in DNA metabolism, mutagenesis and cancer biology," *Seminars in Cancer Biology*, vol. 20, no. 5, pp. 329–339, 2010.

[2] J. A. Cobb and L. Bjergbaek, "RecQ helicases: lessons from model organisms," *Nucleic Acids Research*, vol. 34, no. 15, pp. 4106–4114, 2006.

[3] C. Z. Bachrati and I. D. Hickson, "RecQ helicases: suppressors of tumorigenesis and premature aging," *Biochemical Journal*, vol. 374, part 3, pp. 577–606, 2003.

[4] D. A. Bernstein, M. C. Zittel, and J. L. Keck, "High-resolution structure of the E.coli RecQ helicase catalytic core," *The EMBO Journal*, vol. 22, no. 19, pp. 4910–4921, 2003.

[5] S. Liu, W. Zhang, Z. Gao et al., "NMR structure of the N-terminal-most HRDC1 domain of RecQ helicase from Deinococcus radiodurans," *FEBS Letters*, vol. 587, no. 16, pp. 2635–2642, 2013.

[6] A. C. W. Pike, B. Shrestha, V. Popuri et al., "Structure of the human RECQ1 helicase reveals a putative strand-separation pin," *Proceedings of the National Academy of Sciences of the United States of America*, vol. 106, no. 4, pp. 1039–1044, 2009.

[7] K. Minton, "DNA repair in the extremely radioresistant bacterium Deinococcus radiodurans," *Molecular Microbiology*, vol. 13, no. 1, pp. 9–15, 1994.

[8] J. R. Battista, "Against all odds: the survival strategies of Deinococcus radiodurans," *Annual Review of Microbiology*, vol. 51, pp. 203–224, 1997.

[9] E. Bentchikou, P. Servant, G. Coste, and S. Sommer, "A major role of the RecFOR pathway in DNA double-strand-break repair through ESDSA in Deinococcus radiodurans," *PLoS Genetics*, vol. 6, no. 1, Article ID e1000774, 2010.

[10] L. Huang, X. Hua, H. Lu et al., "Three tandem HRDC domains have synergistic effect on the RecQ functions in Deinococcus radiodurans," *DNA Repair*, vol. 6, no. 2, pp. 167–176, 2007.

[11] M. P. Killoran and J. L. Keck, "Structure and function of the regulatory C-terminal HRDC domain from Deinococcus radiodurans RecQ," *Nucleic Acids Research*, vol. 36, no. 9, pp. 3139–3149, 2008.

[12] S.-C. Chen, C.-H. Huang, C.-S. Yang et al., "Expression, purification, crystallization and preliminary X-ray analysis of the RecQ helicase catalytic core from Deinococcus radiodurans," *Acta Crystallographica Section F: Structural Biology and Crystallization Communications*, vol. 68, no. 10, pp. 1234–1236, 2012.

[13] A. J. McCoy, R. W. Grosse-Kunstleve, P. D. Adams, M. D. Winn, L. C. Storoni, and R. J. Read, "Phaser crystallographic software," *Journal of Applied Crystallography*, vol. 40, no. 4, pp. 658–674, 2007.

[14] P. Emsley, B. Lohkamp, W. G. Scott, and K. Cowtan, "Features and development of Coot," *Acta Crystallographica Section D: Biological Crystallography*, vol. 66, no. 4, pp. 486–501, 2010.

[15] P. D. Adams, P. V. Afonine, G. Bunkóczi et al., "PHENIX: a comprehensive Python-based system for macromolecular structure solution," *Acta Crystallographica D: Biological Crystallography*, vol. 66, part 2, pp. 213–221, 2010.

[16] V. B. Chen, W. B. Arendall III, J. J. Headd et al., "MolProbity: all-atom structure validation for macromolecular crystallography," *Acta Crystallographica Section D: Biological Crystallography*, vol. 66, no. 1, pp. 12–21, 2010.

[17] K. Kitano, S.-Y. Kim, and T. Hakoshima, "Structural basis for DNA strand separation by the unconventional winged-helix domain of RecQ helicase WRN," *Structure*, vol. 18, no. 2, pp. 177–187, 2010.

[18] L. Holm and P. Rosenström, "Dali server: Conservation mapping in 3D," *Nucleic Acids Research*, vol. 38, no. 2, pp. W545–W549, 2010.

[19] E. F. Pettersen, T. D. Goddard, C. C. Huang et al., "UCSF Chimera—a visualization system for exploratory research and analysis," *Journal of Computational Chemistry*, vol. 25, no. 13, pp. 1605–1612, 2004.

[20] M. K. Swan, V. Legris, A. Tanner et al., "Structure of human Bloom's syndrome helicase in complex with ADP and duplex DNA," *Acta Crystallographica Section D*, vol. 70, part 5, pp. 1465–1475, 2014.

Hindawi Publishing Corporation
BioMed Research International
Volume 2014, Article ID 573936, 16 pages
http://dx.doi.org/10.1155/2014/573936

Research Article

C-Terminal Domain Swapping of SSB Changes the Size of the ssDNA Binding Site

Yen-Hua Huang[1] and Cheng-Yang Huang[1,2]

[1] *School of Biomedical Sciences, Chung Shan Medical University, No.110, Sec.1, Chien-Kuo N. Rd., Taichung City, Taiwan*
[2] *Department of Medical Research, Chung Shan Medical University Hospital, No.110, Sec.1, Chien-Kuo N. Rd., Taichung City, Taiwan*

Correspondence should be addressed to Cheng-Yang Huang; cyhuang@csmu.edu.tw

Received 26 May 2014; Accepted 9 July 2014; Published 4 August 2014

Academic Editor: Huangen Ding

Single-stranded DNA-binding protein (SSB) plays an important role in DNA metabolism, including DNA replication, repair, and recombination, and is therefore essential for cell survival. Bacterial SSB consists of an N-terminal ssDNA-binding/oligomerization domain and a flexible C-terminal protein-protein interaction domain. We characterized the ssDNA-binding properties of *Klebsiella pneumoniae* SSB (KpSSB), *Salmonella enterica* Serovar Typhimurium LT2 SSB (StSSB), *Pseudomonas aeruginosa* PAO1 SSB (PaSSB), and two chimeric KpSSB proteins, namely, KpSSBnStSSBc and KpSSBnPaSSBc. The C-terminal domain of StSSB or PaSSB was exchanged with that of KpSSB through protein chimeragenesis. By using the electrophoretic mobility shift assay, we characterized the stoichiometry of KpSSB, StSSB, PaSSB, KpSSBnStSSBc, and KpSSBnPaSSBc, complexed with a series of ssDNA homopolymers. The binding site sizes were determined to be 26 ± 2, 21 ± 2, 29 ± 2, 21 ± 2, and 29 ± 2 nucleotides (nt), respectively. Comparison of the binding site sizes of KpSSB, KpSSBnStSSBc, and KpSSBnPaSSBc showed that the C-terminal domain swapping of SSB changes the size of the binding site. Our observations suggest that not only the conserved N-terminal domain but also the C-terminal domain of SSB is an important determinant for ssDNA binding.

1. Introduction

Single-stranded DNA-binding protein (SSB) specifically binds to single-stranded DNA (ssDNA) and is known to have important functions in the DNA metabolic processes, such as DNA replication, repair, and recombination of both prokaryotes and eukaryotes [1–4]. During these reactions, SSB binds to and protects susceptible ssDNA from nucleolytic digestion and chemical attacks and also prevents secondary structure formation [5]. Many but not all bacterial and human mitochondrial SSBs are active as homotetramers [5–7], in which four oligonucleotide/oligosaccharide-binding folds (OB folds) form a DNA-binding domain [8–12]. However, SSB from the bacterial phylum Deinococcus-Thermus functions as a homodimer, in which each monomer contains two OB folds linked by a conserved spacer sequence [13–20]. SSB from *Sulfolobus solfataricus* is a monomer that includes one OB fold, which differentiates SSB from the bacterial form, and is likely to be a more ancestral "simple" SSB [21–25]. The DdrB protein from *Deinococcus radiodurans* is an alternative SSB and functions as a pentamer [26]. Recent studies found that a distinct SSB from hyperthermophilic Crenarchaea, termed ThermoDBP, has ssDNA-binding domains that are markedly different from the classical OB folds of bacterial SSB [27, 28].

Bacterial SSBs consist of two domains, namely, an N-terminal ssDNA-binding/oligomerization domain and a flexible C-terminal protein-protein interaction domain without a defined tertiary structure [3, 29]. Tyrosine phosphorylation of SSB increases binding to ssDNA by almost 200-fold in vitro [30, 31]. The N-terminal domain is separated from the highly conserved acidic tail of the last 10 C-terminal amino acid residues of SSB by a long proline- or glycine-rich hinge [3, 32]. SSB interacts with other auxiliary proteins that are essential for cell survival [33]. The C-terminal acidic tail of SSB, such as "DDDIPF," has been shown to bind to more than a dozen different proteins and the activity of some of these proteins is stimulated by their interactions with ssDNA-bound SSB [3].

The binding of SSB to ssDNA makes the glycine-rich region more easily accessible to other proteins such as proteases and DNA polymerase III [33, 34]. The C-terminus in SSB can also interact with the OB fold and regulate the ssDNA-binding activity of SSB itself [35, 36].

Studies on SSB from different organisms have grown rapidly during the past few years and knowledge on how SSBs interact with ssDNA has increased [22, 32, 37–46]. The most thoroughly studied SSB is that of *Escherichia coli* (EcSSB), which binds cooperatively to ssDNA [47]. The estimated binding site size of EcSSB is dependent on the salt concentration in fluorescence titrations with poly(dT) [47]. EcSSB mainly binds to 35- and 65-nucleotide- (nt) long ssDNA via the $(SSB)_{35}$- and $(SSB)_{65}$-binding modes, respectively. In the $(SSB)_{35}$-binding mode, two subunits of the EcSSB tetramer interact with ssDNA, whereas in the $(SSB)_{65}$-binding mode all four subunits participate in ssDNA binding. These different binding modes may be required during different stages of DNA metabolism for the in vivo function of SSB [48–50]. Although SSB binds to ssDNA via the highly conserved ssDNA-binding domain, the reason that the binding site sizes of SSBs from different organisms differ remains unclear. For example, differences are found among the binding site sizes of *Methanococcus jannaschii* SSB [51], the Gonococcal Genetic Island-encoded SSB from *Neisseria gonorrhoeae* [39], the thermostable *Thermotoga maritima* and *Thermotoga neapolitana* SSBs [32], and the psychrophilic bacterial SSBs [37]. In addition, the $(SSB)_{35}$- and $(SSB)_{65}$-binding modes are not found in some SSBs [32, 39, 42].

Previously, we have examined the electrophoretic mobility shift patterns of a His-tagged *Klebsiella pneumoniae* SSB (KpSSB) [40], a His-tagged *Salmonella enterica* serovar Typhimurium LT2 SSB (StSSB) [43], and a His-tagged *Pseudomonas aeruginosa* PAO1 SSB (PaSSB) [42] bound to different lengths of ssDNA. We also determined their corresponding binding site sizes, that is, 26, 22, and 29 nt per tetramer, respectively. The electrophoretic mobility shift assay (EMSA) is a well-established approach in studies of molecular biology [52], and the use of radioactive tracer in this assay allows visualization of the actual formation of the distinct protein-DNA complex(es)[53]. The expected result of EMSA is that when the length of the nucleotides is sufficient for the binding of two or more SSB molecules, the electrophoretic mobility of the higher SSB oligomer complex will be lower than that of the smaller SSB oligomer complex [52, 54]. Recent studies on SSB binding also reveal that determination of the ssDNA-binding site size by using EMSA is significantly consistent with that of the cocrystal structure of SSB with ssDNA [27].

KpSSB, StSSB, and PaSSB are similar proteins whose N-terminal ssDNA-binding domains are almost identical, except for different ssDNA-binding site sizes [40, 42, 43]. Thus, we should assess whether the glycine-rich hinge, which is not conserved among SSBs, is involved in the determination of the binding site size of SSB. In this study, we swapped the C-terminal domains of StSSB and PaSSB into that of KpSSB through protein chimeragenesis. Chimeras are proteins that contain segments from two or more different parent proteins and serve as valuable tools to understand enzyme mechanism and protein function [55]. The EMSA behavior (patterns) of the resultant chimeric proteins, namely, KpSSBnStSSBc and KpSSBnPaSSBc, was characterized and compared with untagged KpSSB, StSSB, and PaSSB (Figure 1). On the basis of the chimeragenesis results, the flexible C-terminal domain of SSB was found to be involved in determining the ssDNA-binding site sizes.

2. Materials and Methods

2.1. Materials. All restriction enzymes and DNA-modifying enzymes were purchased from New England Biolabs (Ipswich, MA, USA) unless explicitly stated otherwise. All chemicals were purchased from Sigma-Aldrich (St. Louis, MO, USA) unless explicitly stated otherwise. The *E. coli* strains TOP10F′ (Invitrogen, USA) and BL21(DE3)pLysS (Novagen, UK) were used for genetic construction and protein expression, respectively.

2.2. Construction of Plasmids for KpSSB, StSSB, and PaSSB Expression. The KpSSB [40], StSSB [43], and PaSSB [42] expression plasmids were constructed by the protocols described previously, with minor modification, to avoid having a His tag fused with the gene product. A fragment containing the coding sequence of KpSSB (*KPN04446*), StSSB (*STM4256*), and PaSSB (*PA4232*) (with the stop codon) was directly amplified by PCR by using the genomic DNA of *K. pneumoniae* subsp. *pneumoniae* MGH 78578, *S. enterica* serovar Typhimurium LT2, or *P. aeruginosa* PAO1 (Primers 1 to 6, resp.). During the process, NdeI and XhoI restriction sites were introduced at the 5′-end and the 3′-end of these genes, after which they were ligated into the pET21b vector (Novagen Inc., Madison, WI, USA) for protein expression in *E. coli* BL21. The expected gene product expressed by these plasmids does not contain any artificial residue, including a His tag. Primers used for construction of these plasmids are summarized in Table 1.

2.3. Construction of Plasmids for KpSSBnStSSBc and KpSSBnPaSSBc Expression through Protein Chimeragenesis. To investigate the effect of the C-terminal domain of SSB on the size of the ssDNA-binding site, the C-terminal domain of KpSSB was replaced by that of StSSB and PaSSB. pET21b-KpSSB (Primers 7 and 8), pET21b-StSSB (Primers 9 and 10), and pET21b-PaSSB (Primers 11 and 12) vectors were mutated to create a desired SacI site and to obtain the vectors for expression of the chimeric proteins KpSSBnStSSBc and KpSSBnPaSSBc. The D91E/Q92L-engineered pET21b-KpSSB vector, the D91E/Q92L-engineered pET21b-StSSB vector, and the G90E/Q91L-engineered pET21b-PaSSB vector were cut at NdeI and SacI sites. Subsequently, the KpSSBn, StSSBc-pET21b, and PaSSBc-pET21b fragments were purified. KpSSBn was ligated with StSSBc-pET21b and PaSSBc-pET21b fragments to generate the engineered pET21b-KpSSBnStSSBc and pET21b-KpSSBnPaSSBc vectors. To avoid artificial residues, positions 91 and 92 of the two plasmids were mutated back (Primers 13 to 16) to obtain pET21b-KpSSBnStSSBc and pET21b-KpSSBnPaSSBc vectors.

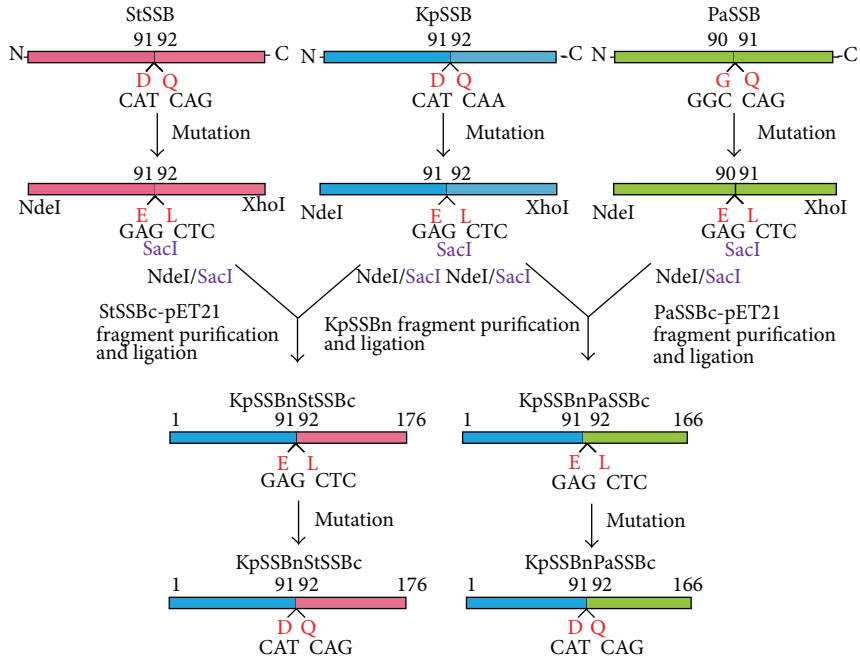

Figure 1: Construction of plasmids for expression of the chimeric KpSSBnStSSBc and KpSSBnPaSSBc proteins. To investigate the effect of the C-terminal domain of SSB on the size of the ssDNA-binding site, the C-terminal domain of KpSSB was replaced by that of StSSB and PaSSB. pET21b-KpSSB (Primers 7 and 8), pET21b-StSSB (Primers 9 and 10), and pET21b-PaSSB (Primers 11 and 12) vectors were mutated to create a desired SacI site and to obtain the vectors for expression of the chimeric proteins KpSSBnStSSBc and KpSSBnPaSSBc. The D91E/Q92L-engineered pET21b-KpSSB vector, the D91E/Q92L-engineered pET21b-StSSB vector, and the G90E/Q91L-engineered pET21b-PaSSB vector were cut at NdeI and SacI sites. Subsequently, the KpSSBn, StSSBc-pET21b, and PaSSBc-pET21b fragments were purified. KpSSBn was ligated with StSSBc-pET21b and PaSSBc-pET21b fragments to generate the engineered pET21b-KpSSBnStSSBc and pET21b-KpSSBnPaSSBc vectors. To avoid artificial residues, positions 91 and 92 of the two plasmids were mutated back (Primers 13 to 16) to obtain pET21b-KpSSBnStSSBc and pET21b-KpSSBnPaSSBc vectors. Thus, pET21b-KpSSBnStSSBc and pET21b-KpSSBnPaSSBc will express KpSSB1-91 fused StSSB92-176 and PaSSB91-165, respectively. Note that KpSSBnPaSSBc will have 166 amino acid residues.

Thus, pET21b-KpSSBnStSSBc and pET21b-KpSSBnPaSSBc will express KpSSB1-91 fused StSSB92-176 and PaSSB91-165, respectively. Note that KpSSBnPaSSBc will have 166 amino acid residues. Plasmids were verified by DNA sequencing. Underlined nucleotides indicate the designated site for mutation or the restriction site (Table 1).

2.4. Protein Expression and Purification. The recombinant SSBs were expressed using the protocol described previously [9, 40, 42, 43, 56–60]. Purification of these recombinant SSBs was carried out as described previously with the following modifications [61, 62]. Briefly, *E. coli* BL21(DE3) cells were individually transformed with the expression vector and grown to OD_{600} of 0.9 at 37°C in Luria-Bertani medium containing 250 μg/mL ampicillin with rapid shaking. Overexpression of the expression plasmids was induced by incubating with 1 mM isopropyl thiogalactoside (IPTG) for 3 h at 37°C. The cells overexpressing the protein were chilled on ice, harvested by centrifugation, resuspended in Buffer A (20 mM Tris-HCl, 5 mM imidazole, and 0.2 M ammonium sulfate, pH 7.9), and disrupted by sonication with ice cooling. The protein solution (50 mL) was precipitated from the supernatant of the cell lysate by incubation with 0.27 g/mL of ammonium sulfate for 30 min and centrifugation at 20000 g for 10 min. The pellets were washed twice with 2.0 mL of Buffer B (20 mM Tris-HCl, 5 mM imidazole, and 1.2 M ammonium sulfate, pH 7.9). After dialysis against Buffer C (20 mM Tris-HCl, 5 mM imidazole, 1 mM EDTA, and 100 mM NaCl, pH 7.9), the protein solution applied to the Q column (GE Healthcare Bio-Sciences, Piscataway, NJ, USA) was eluted with a linear NaCl gradient from 0.1 to 0.6 M with Buffer C using the AKTA-FPLC system (GE Healthcare Bio-Sciences, Piscataway, NJ, USA). The peak fractions with the ssDNA-binding activity were collected and dialyzed against Buffer D (20 mM potassium phosphate, 1 mM EDTA, and 100 mM NaCl, pH 7.0). The protein solution was then applied to the Heparin HP column (GE Healthcare Bio-Sciences, Piscataway, NJ, USA) and eluted with a linear NaCl gradient from 0.1 to 1.0 M with Buffer D. The peak fractions from this chromatographic step with the ssDNA-binding activity were collected and concentrated, and the purity of these SSBs was checked by Coomassie-stained SDS-PAGE (Mini-PROTEAN Tetra System, Bio-Rad, CA, USA; Figure 3).

2.5. Protein Concentration. The protein concentration of the solutions was determined by the Bio-Rad Protein Assay using bovine serum albumin as a standard (Bio-Rad, CA, USA). The Bio-Rad Protein Assay is a dye-binding assay in which a differential color change of a dye occurs in response to various concentrations of protein.

Table 1: Primers used for construction of plasmids.

Oligonucleotide	Primer
1 KpSSB-NdeI-N	GGGCATATGGCCAGCAGAGGCGTAAAC
2 KpSSB-XhoI-C	GGGCTCGAGTTAGAACGGGATGTCGTC
3 StSSB-NdeI-N	CTGAACATATGGCCAGCAGAGGCGTAA
4 StSSB-XhoI-C	TGGAACTCGAGTTAGAACGGAATGTCG
5 PaSSB-NdeI-N	TTGCTCATATGGCCCGTGGGGTTAACA
6 PaSSB-XhoI-C	TTGCACTCGAGTTAGAACGGAATGTCG
7 KpSSB(D91E/Q92L-SacI)-N	AAGTGGACCGAGCTCTCCGGTCAGGACA
8 KpSSB(D91E/Q92L-SacI)-C	GTCCTGACCGGAGAGCTCGGTCCACTT
9 StSSB(D91E/Q92L-SacI)-N	AAGTGGACCGAGCTCAGTGGCCAGGAA
10 StSSB(D91E/Q92L-SacI)-C	TTCCTGGCCACTGAGCTCGGTCCACTT
11 PaSSB(G90E/Q91L-SacI)-N	AAGTGGCAGGAGCTCGACGGTCAGGAT
12 PaSSB(G90E/Q91L-SacI)-C	ATCCTGACCGTCGAGCTCCTGCCACTT
13 KpSSBnStSSBc(E91D/L92Q)-N	AAGTGGACCGATCAGAGTGGCCAGGAA
14 KpSSBnStSSBc(E91D/L92Q)-C	TTCCTGGCCACTCTGATCGGTCCACTT
15 KpSSBnPaSSBc(E91D/L92Q)-N	AAGTGGACCGATCAGGACGGTCAGGAT
16 KpSSBnPaSSBc(E91D/L92Q)-C	ATCCTGACCGTCCTGATCGGTCCACTT

A fragment containing the coding sequence of KpSSB, StSSB, and PaSSB (with the stop codon) was cloned into the pET21b vector (using Primers 1–6). During the process, NdeI and XhoI restriction sites were introduced at the 5′-end and the 3′-end of these genes, after which they were ligated into the pET21b vector. To obtain the vectors for expression of the chimeric proteins KpSSBnStSSBc and KpSSBnPaSSBc, pET21b-KpSSB (Primers 7 and 8), pET21b-StSSB (Primers 9 and 10), and pET21b-PaSSB (Primers 11 and 12) vectors were mutated to create a desired SacI site. The D91E/Q92L-engineered pET21b-KpSSB vector, the D91E/Q92L-engineered pET21b-StSSB vector, and the G90E/Q91L-engineered pET21b-PaSSB vector were cut at NdeI and SacI sites. Subsequently, the KpSSBn, StSSBc-pET21b, and PaSSBc-pET21b fragments were purified. KpSSBn was ligated with StSSBc-pET21b and PaSSBc-pET21b fragments to generate the engineered pET21b-KpSSBnStSSBc and pET21b-KpSSBnPaSSBc vectors. To avoid artificial residues, positions 91 and 92 of the two plasmids were mutated back (Primers 13 to 16) to obtain pET21b-KpSSBnStSSBc and pET21b-KpSSBnPaSSBc vectors. Thus, pET21b-KpSSBnStSSBc and pET21b-KpSSBnPaSSBc will express KpSSB1-91 fused StSSB92-176 and PaSSB91-165, respectively. These plasmids were verified by DNA sequencing. Underlined nucleotides indicate the designated site for mutation or the restriction site.

2.6. Gel-Filtration Chromatography. Gel-filtration chromatography was carried out by the AKTA-FPLC system (GE Healthcare Bio-Sciences, Piscataway, NJ, USA). Briefly, purified protein (2 mg/mL) was applied to a Superdex 200 HR 10/30 column (GE Healthcare Bio-Sciences, Piscataway, NJ, USA) equilibrated with Buffer D. The column was operated at a flow rate of 0.5 mL/min, and 0.5 mL fractions were collected. The proteins were detected by measuring the absorbance at 280 nm. The column was calibrated with proteins of known molecular weight: thyroglobulin (670 kDa), γ-globulin (158 kDa), ovalbumin (44 kDa), and myoglobin (17 kDa). The K_{av} values for the standard proteins and the SSB variants were calculated from the equation: $K_{av} = (V_e - V_o)/(V_c - V_o)$, where V_o is column void volume, V_e is elution volume, and V_c is geometric column volume.

2.7. Electrophoretic Mobility Shift Assay (EMSA). EMSA [52] for these SSBs was carried out by the protocol described previously for DnaB [63], PriB [59, 64–66], DnaT [57, 67], and SSB proteins [40, 42, 43, 52]. Briefly, radiolabeling of various lengths of ssDNA oligonucleotides was carried out with [γ^{32}P]ATP (6000 Ci/mmol; PerkinElmer Life Sciences, Waltham, MA) and T4 polynucleotide kinase (Promega, Madison, WI, USA). The protein (0, 19, 37, 77, 155, 310, 630, 1250, 2500, and 5000 nM) was incubated for 30 min at 25°C with 1.7 nM DNA substrates (dT15–65) in a total volume of 10 μL in 20 mM Tris-HCl pH 8.0 and 100 mM NaCl. Aliquots (5 μL) were removed from each of the reaction solutions and added to 2 μL of gel-loading solution (0.25% bromophenol blue and 40% sucrose). The resulting samples were resolved on a native 8% polyacrylamide gel at 4°C in TBE buffer (89 mM Tris borate and 1 mM EDTA) for 1 h at 100 V and were visualized by autoradiography. Complexed and free DNA bands were scanned and quantified.

2.8. DNA-Binding Ability. The ssDNA-binding ability ($[\text{Protein}]_{50}$; $K_{d,\text{app}}$) for the protein was estimated from the protein concentration that binds 50% of the input ssDNA [52]. Each $[\text{Protein}]_{50}$ is calculated as the average of three measurements ± SD.

2.9. Bioinformatics. Sequence alignment of KpSSB, StSSB, and PaSSB was generated by CLUSTALW2 [68]. The structure of the C-terminal domain of these SSBs was modeled by $(\text{PS})^2$ (http://140.113.239.111/~ps2v2/docs.php/). The structures were visualized by using the program PyMol.

3. Results

3.1. Sequence Analysis. Based on the nucleotide sequence found, using a database search through the National Center for Biotechnology Information (NCBI), we predicted that KpSSB, StSSB, and PaSSB monomer proteins have lengths of 174, 176, and 165 amino acid residues, respectively. The size of the ssDNA-binding site of His-tagged KpSSB [40], StSSB

FIGURE 2: Multiple amino acid sequence alignment of SSB proteins. Sequence alignment of KpSSB, StSSB, and PaSSB was generated by CLUSTALW2. Identical amino acid residues are colored in red. Gly and Gln residues are shaded in cyan and gray. The N-terminal domains of these SSBs are significantly conserved.

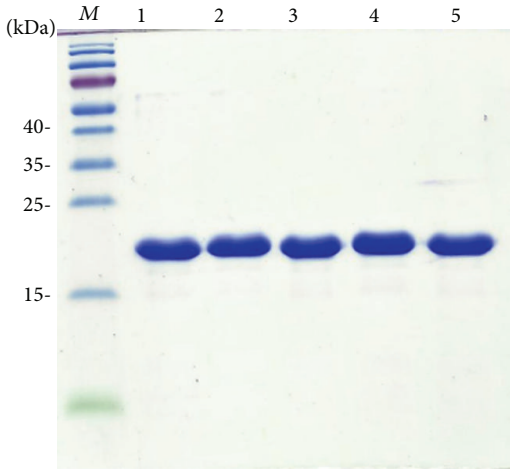

FIGURE 3: Protein purity. Coomassie Blue-stained SDS-PAGE (15%) of the purified KpSSB (lane 1), StSSB (lane 2), PaSSB (lane 3), KpSSBnStSSBc (lane 4), KpSSBnPaSSBc (lane 5), and molecular mass standards (*M*) are shown. The sizes of the standard proteins, from the top down, are as follows: 55, 40, 35, 25, 15, and 10 kDa. The purified SSBs migrated between the 25 and 15 kDa standards on the SDS-PAGE.

[43], and PaSSB [42] was determined to be 26 ± 1, 22 ± 1, and 29 ± 1 nt, respectively. The longer the length of the polypeptide chain, the smaller the size for ssDNA binding. Analysis of the primary structures of KpSSB, StSSB, and PaSSB by RPS-BLAST revealed the presence of a putative OB-fold domain that is common to all known SSBs. Figure 2 shows that the alignments of the amino acid sequences of KpSSB, StSSB, and PaSSB amino acid residues in their N-terminal domains are highly conserved (colored in red). In the *E. coli* SSB-ssDNA complex [11], four essential aromatic residues, namely, Trp40, Trp54, Phe60, and Trp88, participate in ssDNA binding via stacking interactions [11]. These residues are conserved in most SSB families, including KpSSB, StSSB, and PaSSB. The important motif in the C-terminal tail of *E. coli* SSB, DDDIPF residues, is also conserved in KpSSB, StSSB, and PaSSB. By contrast to those motifs, the residues found in the glycine-rich hinge of *E. coli* SSB are not conserved in KpSSB, StSSB, and PaSSB (Figure 2). Thus, the length and composition of the amino acid residues in the glycine-rich hinge may be responsible for the different ssDNA-binding site sizes of SSBs.

3.2. Expression and Purification of KpSSB, StSSB, and PaSSB. The N-terminal ssDNA-binding domain of SSB has been well-established to be highly conserved. However, SSBs possessing different ssDNA-binding site sizes have been reported. The reason that SSBs have similar ssDNA-binding domains but possess varying ssDNA-binding site sizes remains unclear. Although the ssDNA-binding site sizes of KpSSB, StSSB, and PaSSB have been reported, we reinvestigated the ssDNA-binding properties of KpSSB, StSSB, and PaSSB in the absence of a His tag to avoid the unknown effect of a His tag (hexahistidine) on the ssDNA binding of SSB.

3.3. KpSSB Bound to ssDNA. To investigate the length of nucleotides sufficient for the formation of the KpSSB-ssDNA complex and the ssDNA-binding ability of KpSSB, we studied the binding of KpSSB to dT20 (Figure 4(a)), dT25 (Figure 4(b)), dT35 (Figure 4(c)), dT45 (Figure 4(d)), dT50 (Figure 4(e)), dT55 (Figure 4(f)), and dT60 (Figure 4(g)) with different protein concentrations. As shown in Figure 4(a), no band shift was observed when KpSSB was incubated with dT20, indicating that KpSSB could not form a stable complex with this homopolymer. By contrast to dT20, longer dT homopolymers, which include dT25–50, produced a significant band shift (C, complex), that is, formation of a stable protein-DNA complex in solution. Furthermore, two different complexes for dT55 were formed by KpSSB (Figure 4(f)). At lower protein concentrations, KpSSB formed a single complex (C1) with dT55, similar to that observed with dT50 (Figure 4(e)). However, when the KpSSB concentration was increased, another slower migrating complex (C2) was observed.

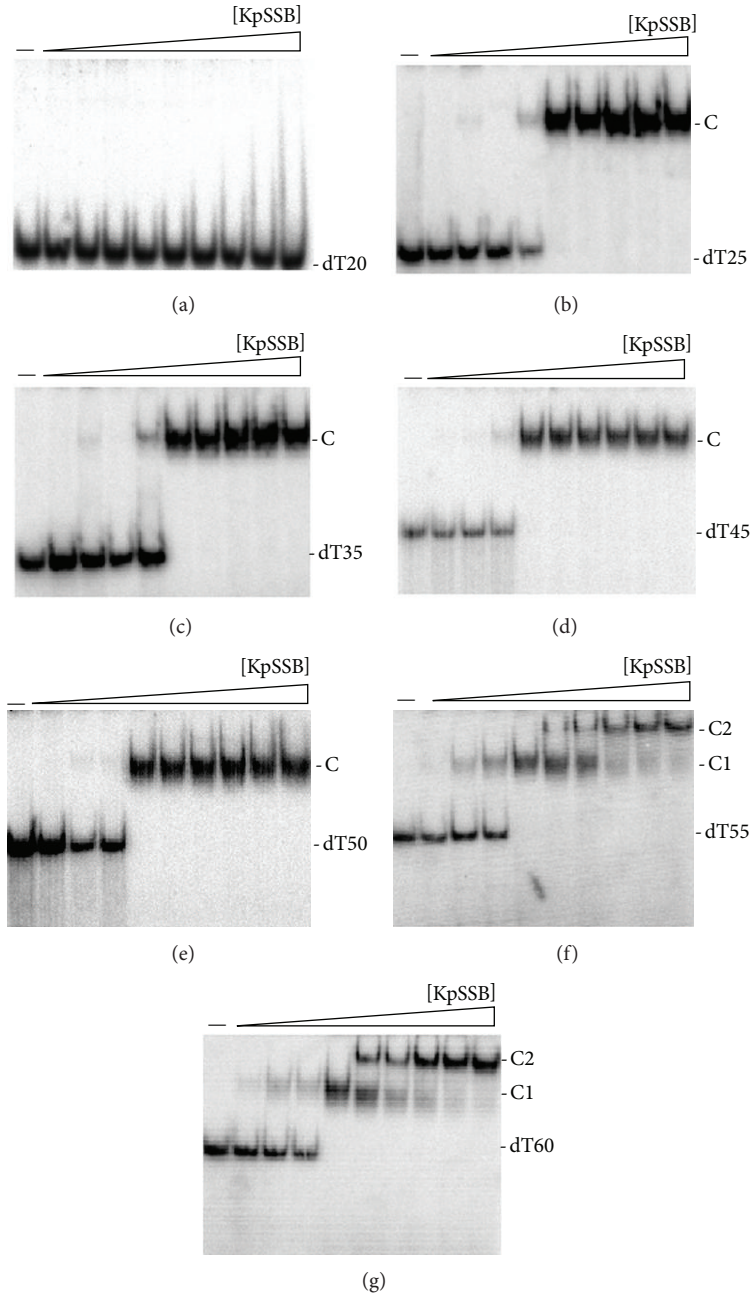

Figure 4: Binding of KpSSB to dT20–60. KpSSB (0, 19, 37, 77, 155, 310, 630, 1250, 2500, and 5000 nM) was incubated for 30 min at 25°C with 1.7 nM of (a) dT20, (b) dT25, (c) dT35, (d) dT45, (e) dT50, (f) dT55, or (g) dT60 in a total volume of 10 μL in 20 mM Tris-HCl pH 8.0 and 100 mM NaCl. Aliquots (5 μL) were removed from each reaction solution and added to 2 μL of gel-loading solution (0.25% bromophenol blue and 40% sucrose). The resulting samples were resolved on a native 8% polyacrylamide gel at 4°C in TBE buffer (89 mM Tris borate and 1 mM EDTA) for 1 h at 100 V and visualized by autoradiography. Complexed and free DNA bands were scanned and quantified.

Two different complexes of KpSSB were also observed to bind to dT60 (Figure 4(g)). The appearance of the second complex resulted from the increased KpSSB concentration, suggesting that two KpSSB proteins may be present per oligonucleotide. Although dT55 is only 5 nt longer than dT50 is, the presence of an extra 5 nt in dT55 compared with that of dT50 provides enough interaction space for the binding of two KpSSB proteins. Therefore, one KpSSB occupies 25 (50/2 = 25) nt to 27.5 (55/2 = 27.5) nt of the ssDNA. The EMSA results suggest that the length of an ssDNA (or the binding site size) [52] required for KpSSB binding is 26 ± 2 nt.

3.4. StSSB Bound to ssDNA. The binding of StSSB to dT15 (Figure 5(a)), dT20 (Figure 5(b)), dT30 (Figure 5(c)), dT40 (Figure 5(d)), dT45 (Figure 5(e)), and dT50 (Figure 5(f)) was

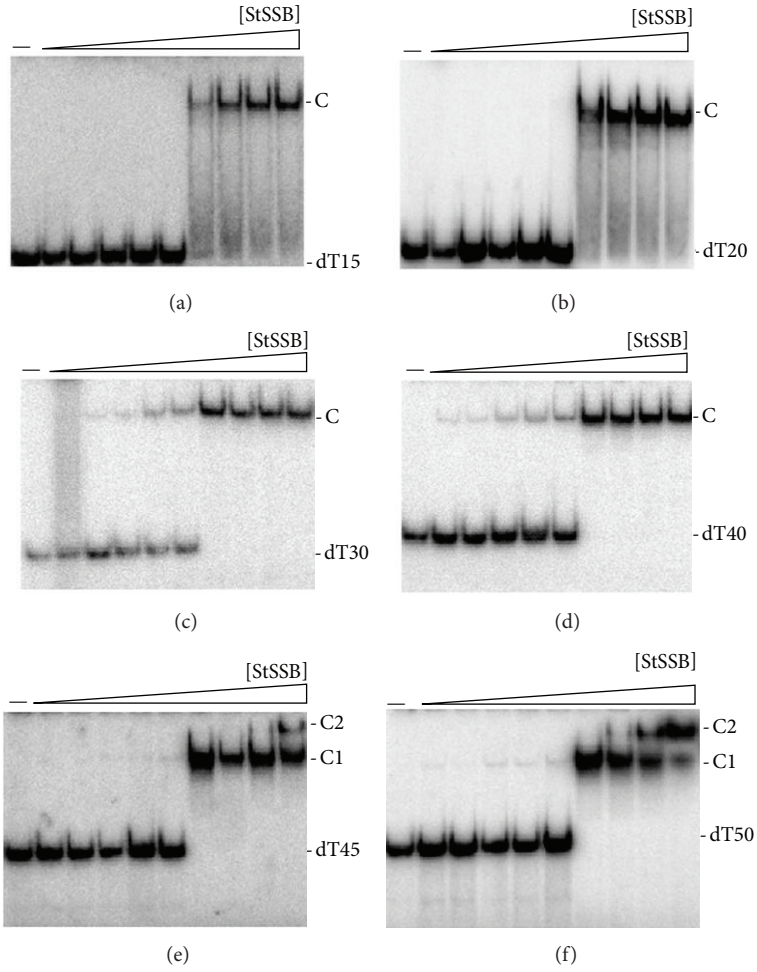

Figure 5: Binding of StSSB to dT15–50. StSSB (0, 19, 37, 77, 155, 310, 630, 1250, 2500, and 5000 nM) was incubated for 30 min at 25°C with 1.7 nM of (a) dT15, (b) dT20, (c) dT30, (d) dT40, (e) dT45, or (f) dT50 in a total volume of 10 μL in 20 mM Tris-HCl pH 8.0 and 100 mM NaCl. Aliquots (5 μL) were removed from each reaction solution and added to 2 μL of gel-loading solution (0.25% bromophenol blue and 40% sucrose). The resulting samples were resolved on a native 8% polyacrylamide gel at 4°C in TBE buffer (89 mM Tris borate and 1 mM EDTA) for 1 h at 100 V and visualized by autoradiography. Complexed and free DNA bands were scanned and quantified.

examined using EMSA. StSSB can bind and form a single complex with dT15 (Figure 5(a)) and dT20 (Figure 5(b)), but KpSSB cannot (Figure 4(a)). StSSB bound to dT15–40 and formed a single complex. For dT45 and dT50, two different complexes of StSSB appeared at high protein concentrations (Figures 5(e) and 5(f)). Therefore, one StSSB occupies 20 (40/2 = 20) nt to 22.5 (45/2 = 22.5) nt of the ssDNA. The EMSA results suggest that the length of an ssDNA (or the binding site size) [52] required for StSSB binding is 21 ± 2 nt.

3.5. PaSSB Bound to ssDNA. The binding of PaSSB to dT20 (Figure 6(a)), dT25 (Figure 6(b)), dT35 (Figure 6(c)), dT45 (Figure 6(d)), dT55 (Figure 6(e)), dT60 (Figure 6(f)), and dT65 (Figure 6(g)) was studied by EMSA. Unlike StSSB, no complex was observed when PaSSB was incubated with dT20. Some smears were observed, indicating that PaSSB interacts with dT20. However, the ssDNA may be too short to be fully wrapped by PaSSB. PaSSB could form a single complex with dT25–55 and form two distinct complexes with dT60 and dT65 (Figures 6(f) and 6(g)), respectively. Therefore, one PaSSB occupies 27.5 (55/2 = 27.5) nt to 30 (60/2 = 30) nt of the ssDNA. These results from EMSA suggest that the length of an ssDNA (or the binding site size) [52] required for PaSSB binding is 29 ± 2 nt. Although the SSBs, that is, KpSSB, StSSB, and PaSSB, have significantly similar ssDNA-binding domains, their binding site sizes are different and range from 19 (21 ± 2; StSSB) to 31 (29 ± 2; PaSSB) nt. The obtained EMSA results (Figures 4–6) also show that the binding site sizes of the untagged SSBs (KpSSB, StSSB, and PaSSB) were found to be almost identical to those of the His-tagged ones [40, 42, 43].

3.6. Design of the Chimeric KpSSB Proteins KpSSBnStSSBc and KpSSBnPaSSBc. The N-terminal ssDNA-binding domain of KpSSB, StSSB, and PaSSB is highly conserved (Figure 2), but their binding site sizes are different (Figures 4–6) and range from 19 nt to 31 nt. The C-terminal acidic tails, DDDIPF, are conserved (Figure 2), and these features led us to assess

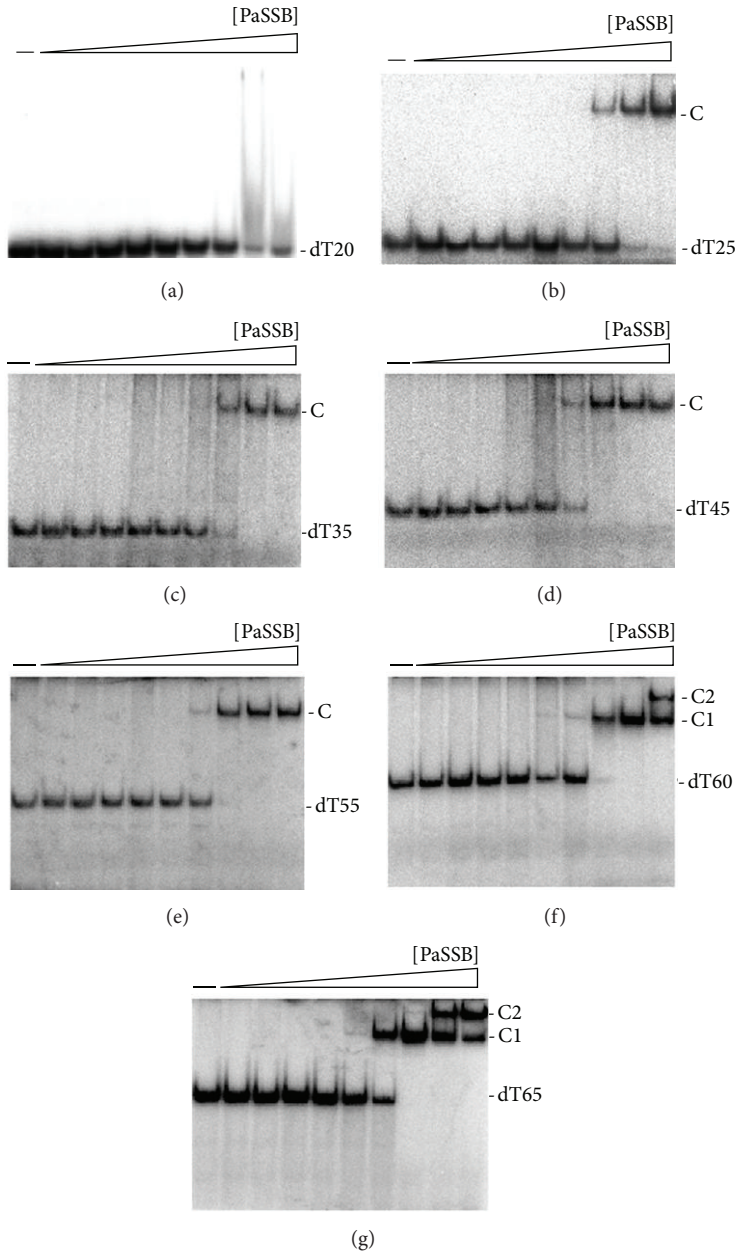

Figure 6: Binding of PaSSB to dT20–65. PaSSB (0, 19, 37, 77, 155, 310, 630, 1250, 2500, and 5000 nM) was incubated for 30 min at 25°C with 1.7 nM of (a) dT20, (b) dT25, (c) dT35, (d) dT45, (e) dT55, (f) dT60, or (g) dT65 in a total volume of 10 μL in 20 mM Tris-HCl pH 8.0 and 100 mM NaCl. Aliquots (5 μL) were removed from each reaction solution and added to 2 μL of gel-loading solution (0.25% bromophenol blue and 40% sucrose). The resulting samples were resolved on a native 8% polyacrylamide gel at 4°C in TBE buffer (89 mM Tris borate and 1 mM EDTA) for 1 h at 100 V and visualized by autoradiography. Complexed and free DNA bands were scanned and quantified.

whether the flexible glycine-rich hinge in the C-terminal domain, which is not conserved among SSBs, is involved in the determination of the binding site size of SSB. Thus, the C-terminal domains of StSSB and PaSSB were swapped with KpSSB through protein chimeragenesis.

3.7. KpSSBnStSSBc Bound to ssDNA. The binding of KpSSBnStSSBc to dT15 (Figure 7(a)), dT20 (Figure 7(b)), dT40 (Figure 7(c)), and dT45 (Figure 7(d)) was examined using EMSA. KpSSBnStSSBc exhibited significantly different ssDNA-binding properties from those of KpSSB. Unlike KpSSB (Figure 4), both KpSSBnStSSBc (Figure 8) and StSSB (Figure 5) can bind and form a single complex with dT15 and dT20. Similar to StSSB, KpSSBnStSSBc binds to dT15–40 and forms a single complex. For dT45, two different complexes of KpSSBnStSSBc appeared at high protein concentrations (Figure 8(d)); this EMSA feature was also similar to that of StSSB. One KpSSBnStSSBc occupies 20 (40/2 = 20) nt to 22.5 (45/2 = 22.5) nt of the ssDNA. These EMSA results suggest that the length of an ssDNA (or the binding site

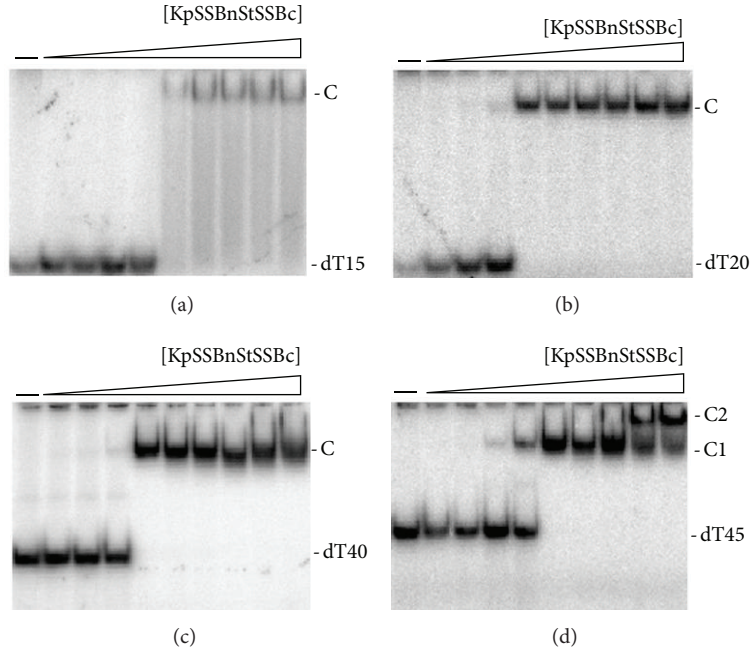

Figure 7: Binding of KpSSBnStSSBc to dT15–45. KpSSBnStSSBc (0, 19, 37, 77, 155, 310, 630, 1250, 2500, and 5000 nM) was incubated for 30 min at 25°C with 1.7 nM of (a) dT15, (b) dT20, (c) dT40, or (d) dT45 in a total volume of 10 μL in 20 mM Tris-HCl pH 8.0 and 100 mM NaCl. Aliquots (5 μL) were removed from each reaction solution and added to 2 μL of gel-loading solution (0.25% bromophenol blue and 40% sucrose). The resulting samples were resolved on a native 8% polyacrylamide gel at 4°C in TBE buffer (89 mM Tris borate and 1 mM EDTA) for 1 h at 100 V and visualized by autoradiography. Complexed and free DNA bands were scanned and quantified.

size) [52] required for KpSSBnStSSBc binding is 21 ± 2 nt, a value identical to that for StSSB (Figure 5). Swapping of the C-terminal domain of StSSB with KpSSB changes the size of the ssDNA-binding site from 26 nt to 21 nt.

3.8. KpSSBnPaSSBc Bound to ssDNA. The binding features of KpSSBnPaSSBc with dT20 (Figure 8(a)), dT25 (Figure 8(b)), dT40 (Figure 8(c)), dT55 (Figure 8(d)), and dT60 (Figure 8(e)) were studied by EMSA. Similar to the cases of KpSSB and PaSSB, no complex was observed when KpSSBnPaSSBc was incubated with dT20. However, KpSSBnPaSSBc still exhibited dramatically different ssDNA-binding properties from those of KpSSB. KpSSB can form two distinct complexes with dT55 (Figure 4(f)), but both KpSSBnPaSSBc (Figure 9) and PaSSB (Figure 6) cannot. One KpSSBnPaSSBc occupies 27.5 (55/2 = 27.5) nt to 30 (60/2 = 30) nt of the ssDNA. The above EMSA results suggest that the length of an ssDNA (or the binding site size) [52] required for KpSSBnPaSSBc binding is 29 ± 2 nt, a value identical to that of PaSSB. Swapping of the C-terminal domain of PaSSB to KpSSB changes the size of the ssDNA-binding site from 26 nt to 29 nt. Although these SSBs, namely, KpSSB, StSSB, PaSSB, KpSSBnStSSBc, and KpSSBnPaSSBc, have nearly identical ssDNA-binding domains, their binding site sizes are different (Table 2). Thus, the size of the ssDNA-binding site required for second SSB binding is likely to be dependent on the C-terminal domain of SSB.

3.9. Binding Constants of the SSB-ssDNA Complexes Determined from EMSA. To compare the ssDNA-binding abilities of KpSSB, StSSB, PaSSB, KpSSBnStSSBc, and KpSSBnPaSSBc, the midpoint values for input ssDNA binding, calculated from the titration curves of EMSA and referred to as $[\text{Protein}]_{50}$ (monomer), were quantified and are summarized in Table 2. Although the N-terminal ssDNA-binding domains of these SSB proteins are highly similar (Figure 2), their ssDNA-binding activities and binding site sizes are different (Table 2). $[\text{KpSSB}]_{50}$ values ranged from 100 nM to 220 nM; $[\text{StSSB}]_{50}$ values ranged from 420 nM to 650 nM; $[\text{PaSSB}]_{50}$ values ranged from 550 nM to 1700 nM; $[\text{KpSSBnStSSBc}]_{50}$ values ranged from 110 nM to 260 nM; and $[\text{KpSSBnPaSSBc}]_{50}$ values ranged from 220 nM to 390 nM. The ssDNA-binding ability is as follows, in the order of decreasing affinity: KpSSB > KpSSBnStSSBc > KpSSBnPaSSBc > StSSB > PaSSB. Results from the above analyses indicate that the exchange of the C-terminal domain in SSB significantly changed the ssDNA-binding ability and the DNA-binding behavior (complex number). The reason as to why swapping of the C-terminal domain can affect the ssDNA-binding activity of SSB remains unclear. The C-terminal domain of SSB is suggested to be involved in ssDNA binding. However, this relation is not evident in the results of the cocrystal structure.

3.10. Oligomeric State of KpSSBnStSSBc and KpSSBnPaSSBc in Solution. Gel-filtration chromatography was used to confirm

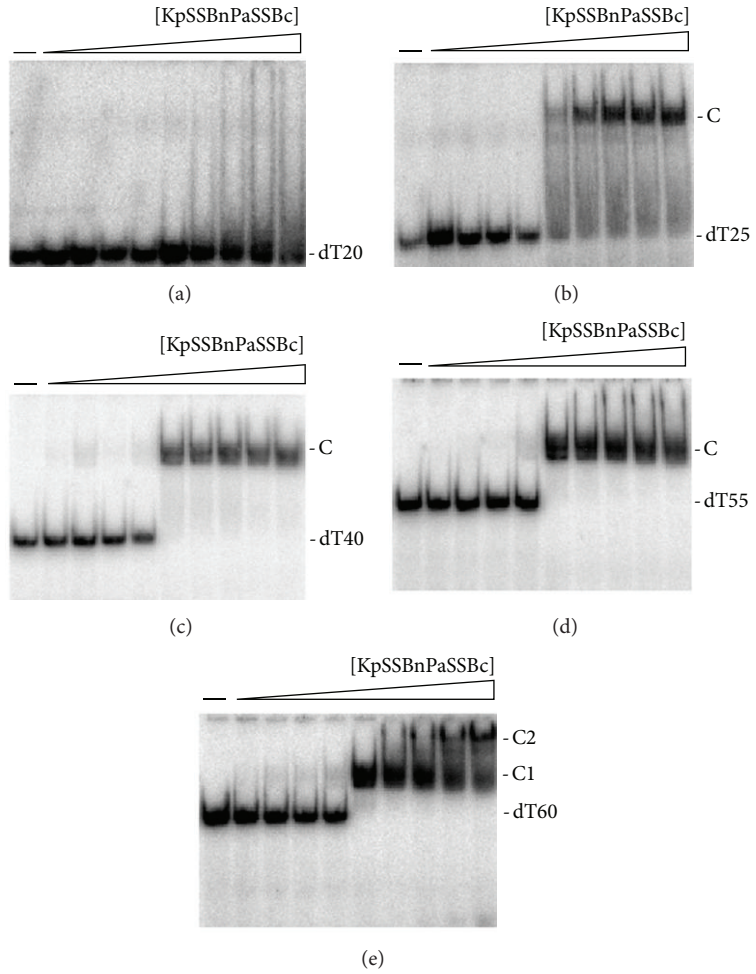

Figure 8: Binding of KpSSBnPaSSBc to dT20–60. KpSSBnPaSSBc (0, 19, 37, 77, 155, 310, 630, 1250, 2500, and 5000 nM) was incubated for 30 min at 25°C with 1.7 nM of (a) dT20, (b) dT25, (c) dT40, (d) dT55, or (e) dT60 in a total volume of 10 μL in 20 mM Tris-HCl pH 8.0 and 100 mM NaCl. Aliquots (5 μL) were removed from each reaction solution and added to 2 μL of gel-loading solution (0.25% bromophenol blue and 40% sucrose). The resulting samples were resolved on a native 8% polyacrylamide gel at 4°C in TBE buffer (89 mM Tris borate and 1 mM EDTA) for 1 h at 100 V and visualized by autoradiography. Complexed and free DNA bands were scanned and quantified.

that the oligomeric state of KpSSBnStSSBc and KpSSBnPaSSBc remains as tetramers after chimeragenesis. The analysis of purified KpSSBnStSSBc and KpSSBnPaSSBc (2 mg/mL) using a Superdex 200 HR 10/30 column revealed a single peak with elution volumes of 78.6 and 78.9 mL, respectively. Assuming that KpSSBnStSSBc and KpSSBnPaSSBc both have shapes and partial specific volumes similar to the standard proteins, the native molecular masses of KpSSBnStSSBc and KpSSBnPaSSBc were estimated to be 76641 and 74827 Da, as calculated from a standard linear regression equation, $K_{av} = -0.3684(\log Mw) + 2.2707$ (Figure 9). The native molecular masses for KpSSBnStSSBc and KpSSBnPaSSBc are approximately four times the mass of the monomer (~19 kDa). Therefore, KpSSBnStSSBc and KpSSBnPaSSBc under the above chromatographic conditions are stable tetramers in solution. Although the exchange of the C-terminal domain in SSB significantly changed the ssDNA-binding ability and DNA-binding behavior (complex number), protein chimeragenesis did not cause any change in the oligomeric state of SSB.

3.11. Summary of Gly, Gln, and Pro Number in SSBs. To analyze the C-terminal amino acid composition of SSBs, we further counted the number of Gly, Gln, and Pro residues in different SSB segments. SSB is abundant in Gly, Gln, and Pro (GQP) (Table 3). The GQP contents of KpSSB1–91, StSSB1–91, and PaSSB1–90 are similar. However, the Gly number of PaSSB116–165 is significantly lower than that of KpSSB116–174 and StSSB117–176; PaSSB116–165 contains only 1 Gly, but KpSSB116–174 and StSSB117–176 contain 11 and 12 Gly, respectively. In addition, we found different distribution patterns among KpSSB, StSSB, and PaSSB. Although they contain similar number of Gln (Q), the QQQ pattern is frequently found in PaSSB (Table 3).

3.12. Structural Modeling of SSBs. Given its disordered C-terminal domain, the crystal structure of the full-length SSB is lacking, even when SSB can be crystallized with DNA [69]. We attempted to model the structure by homology modeling using the bioinformatics program $(PS)^2$ to obtain an

Table 2: ssDNA binding properties of KpSSB, StSSB, PaSSB, KpSSBnStSSBc, and KpSSBnPaSSBc as analyzed by EMSA.

Protein	DNA	$[\text{Protein}]_{50}$ (nM)	Complex number
KpSSB	dT20	ND	0
	dT25	200 ± 20	1
	dT35	220 ± 30	1
	dT45	100 ± 10	1
	dT50	110 ± 20	1
	dT55	100 ± 20	2
	dT60	100 ± 10	2
StSSB	dT15	650 ± 120	1
	dT20	450 ± 80	1
	dT30	420 ± 60	1
	dT40	420 ± 80	1
	dT45	440 ± 60	2
	dT50	440 ± 50	2
PaSSB	dT20	ND	0
	dT25	1700 ± 250	1
	dT35	950 ± 180	1
	dT45	780 ± 160	1
	dT55	820 ± 90	1
	dT60	810 ± 110	2
	dT65	550 ± 70	2
KpSSBnStSSBc	dT15	260 ± 60	1
	dT20	110 ± 20	1
	dT40	120 ± 20	1
	dT45	160 ± 20	2
KpSSBnPaSSBc	dT20	ND	0
	dT25	390 ± 60	1
	dT40	220 ± 30	1
	dT55	230 ± 30	1
	dT60	230 ± 30	2

$[\text{Protein}]_{50}$ was calculated from the titration curves of EMSA by determining the concentration of the protein (μM) needed to achieve the midpoint value for input ssDNA binding. For some oligonucleotides, input ssDNA binding was the sum of the intensities from the two separate ssDNA-protein complexes. Errors are standard deviations determined by three independent titration experiments.

Table 3: Summary of Gly, Gln, and Pro number in SSB.

SSB segment	G	Q	P
KpSSB1–91	10	5	2
StSSB1–91	10	5	2
PaSSB1–90	11	6	2
KpSSB92–174	18	16	9
StSSB92–176	17	18	11
PaSSB91–165	5	15	11
KpSSB116–174	11	12	9
StSSB117–176	12	13	10
PaSSB116–165	1	12	11

in-depth understanding of the structure-function relationship of the C-terminal domains of these SSBs [70, 71].

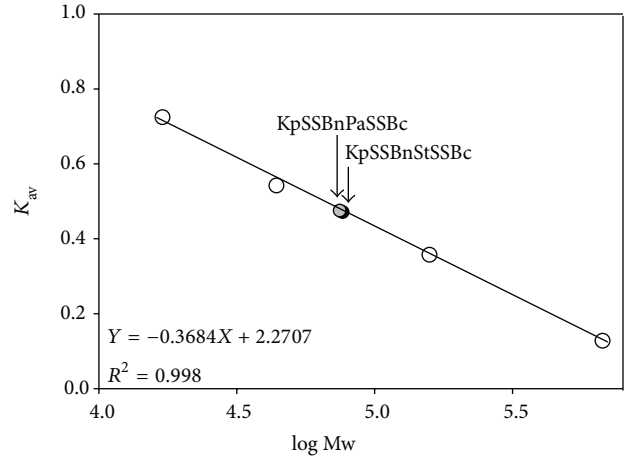

Figure 9: Gel-filtration chromatographic analyses of KpSSBnStSSBc and KpSSBnPaSSBc. Purified protein (2 mg/mL) was applied to a Superdex 200 HR 10/30 column (GE Healthcare Bio-Sciences, Piscataway, NJ, USA) equilibrated with Buffer D. The column was operated at a flow rate of 0.5 mL/min, and 0.5 mL fractions were collected. The proteins were detected by measuring the absorbance at 280 nm. The column was calibrated with proteins of known molecular weight: thyroglobulin (670 kDa), γ-globulin (158 kDa), ovalbumin (44 kDa), and myoglobin (17 kDa). The K_{av} values for the standard proteins and the SSB variants were calculated from the equation: $K_{av} = (V_e - V_o)/(V_c - V_o)$, where V_o is column void volume, V_e is elution volume, and V_c is geometric column volume.

$(\text{PS})^2$ (http://140.113.239.111/~ps2v2/docs.php/) is an automatic homology modeling server that combines both sequence and secondary structure information to detect the homologous proteins with remote similarity and the target-template alignment. After pasting the amino acid sequence to the website of $(\text{PS})^2$, only one hit (Protein Data Bank entry: 1QVC; EcSSB) for the C-terminal domains of KpSSB and StSSB was suggested. For the C-terminal domain of PaSSB, only one hit, that is, CstF-77 (Protein Data Bank entry: 2OOE; cleavage stimulation factor, CstF), but not EcSSB, was suggested as the template for modeling. Figure 10 shows that modeled structures of these SSB C-terminal domains are highly disordered but that of PaSSB is more ordered than that of other domains.

4. Discussion

In this study, we examined the sizes of the binding site of the untagged SSB and the chimeric SSB from the ubiquitous opportunistic pathogens *K. pneumoniae*, *S. enterica* serovar Typhimurium LT2, and *P. aeruginosa* PAO1. Many clinical strains of the abovementioned bacteria are highly resistant to antibiotics [72–75]. The development of clinically useful small-molecule antibiotics has been a seminal event in the field of infectious diseases [48]. Nucleic acid metabolism is one of the most basic biological functions and should be a prime target in antibiotic development [76–78]. Many bacterial SSBs form conserved protein interaction "hubs" that are essential to recruit many proteins involved in DNA

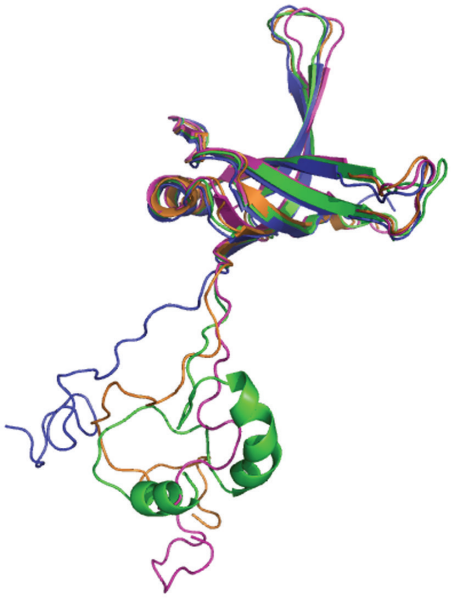

Figure 10: Structure modeling of SSB. The structures of KpSSB1–115, StSSB1–115, and PaSSB1–115 (the N-terminal domain of SSB) were modeled by SWISS-MODEL. The structures of KpSSB116–142, StSSB116–142, and PaSSB121–160 (the C-terminal domain of SSB) were modeled by $(PS)^2$. Other regions of SSBs could not be modeled by these two programs. The structures of the N-terminal domain and the C-terminal domain of these SSBs were manually linked (KpSSB1–142, blue; StSSB1–142, pink; PaSSB1–160, green) and superimposed with the crystal structure of EcSSB1–142 (orange) (PDB entry: 1QVC) for comparison. For clarity, only one subunit of the tetramer was shown for each SSB.

replication, recombination, and repair SSB/DNA nucleoprotein substrates [79]. Thus, SSBs may be promising targets in antibiotic development [80]. As a first step toward achieving this goal, we investigated why SSBs possess highly conserved N-terminal ssDNA-binding domain but exhibit varying binding site sizes. One significant clue is that their flexible hinges and the length at the C-terminus are different as revealed by sequence alignment (Figure 2).

The interactions of various SSBs with ssDNA have been analyzed using a variety of techniques such as tryptophan-fluorescence quenching [47], filter binding [81], EMSA [52, 82], analytical ultracentrifugation [83], electron microscopy [84], nuclease digestion [44], single-molecule fluorescence microscopy [48], and crystallographic analyses [11]. In this study, we have examined the electrophoretic mobility shift patterns of KpSSB, StSSB, PaSSB, KpSSBnStSSBc, and KpSSBnPaSSBc bound to different lengths of ssDNA and determined the corresponding binding site sizes to be 26, 21, 29, 22, and 29 nt per tetramer, respectively (Figures 4–8). PaSSB and KpSSBnPaSSBc have the largest sizes for ssDNA binding among the SSBs studied. We also identified His-tagged and untagged SSBs that have similar ssDNA-binding site sizes [40, 42, 43]. EMSA is a well-established approach in studies of molecular biology [52], and the use of radioactive tracer in this assay allows detection of the actual formation of the distinct protein-DNA complex(es) [53]. For example, DNase protection assay and footprinting assay using radioactive tracer can determine the specific DNA sequence complexed by a protein. In EMSA, when the length of the nucleotides is sufficient for the binding of two or more SSB molecules, the electrophoretic mobility of the higher SSB oligomer complex will be lower than that of the smaller SSB oligomer complex [52, 54]. In addition, results of the ssDNA-binding site size from EMSA and cocrystal structure of SSB were consistent [27]. Thus, throughout this paper, we determined the ssDNA-binding site sizes of SSB from the EMSA behavior.

Many SSBs bind to ssDNA with some degree of positive cooperativity. Cooperativity can result from direct protein-protein interactions between the nearest neighbors, such as the LAST motif in the T4 gene-32 protein [85] and the arginine-mediated interaction motif in *Thermus* SSB [86, 87]. Cooperativity can also result from the protein-induced distortion of adjacent DNA, as demonstrated in *Sulfolobus* SSB, PriB, and FOXK1a proteins [23, 60, 88]. In the cases of KpSSB, StSSB, and PaSSB (Figures 4–6), binding appeared to be nearly noncooperative for several DNAs because all DNA mainly shifts into the first complex (C1) before the appearance of the second complex (C2) when subjected to increasing protein concentrations. The length dependence of the $[SSB]_{50}$ values suggests that the amount of spacing is optimum for steric considerations (Table 2).

Because bacteria have varying genomic DNA sizes, their SSBs may need to evolve to have different binding site sizes for DNA metabolism. Results from protein chimeragenesis showed the C-terminal domain dependence of the binding site sizes of SSB (Figure 11). The experimental data showed that the binding site size of KpSSBnStSSBc was similar to that of StSSB and the size of the binding site of KpSSBnPaSSBc was similar to that of PaSSB. The reason for which the binding site size of SSB changed, followed by swapping of the C-terminal domain, remains unclear. Flexibility, number of glycine residues, and/or different QQQ patterns of the C-terminal domain of SSB (Figure 2 and Table 3) may be important factors for determining the ssDNA-binding site size. In fact, the C-terminal domain of PaSSB, that is, PaSSB116–165, has only 1 Gly residue, which is significantly less than that of KpSSB (11 Gly) and StSSB (12 Gly). Gly (and Pro) is an important component of the flexible region; a protein that contains low Gly content is predicted to have low flexibility. Unlike typical SSB [35, 69], PaSSB116–165 has a partial structure (Figure 10). Although KpSSB, StSSB, and PaSSB contain similar number of Gln (Q), the QQQ pattern is frequently found in PaSSB (Figure 2 and Table 3). PolyQ and repeated sequences GAGAG are commonly found in the structures of amyloids, silk fibers, and neurodegradation proteins [89–92]. Considering that the simple coil polyQ, the heptapeptide GNNQQNY, and the hexapeptide NNQQNY can cause protein aggregation and nucleation [93–95], the distribution of Gln in the C-terminal domain of a tetrameric SSB may also be an important determinant of the ssDNA-binding site size of SSB by some steric hindrances (Figure 11). However, the above speculation must be confirmed by further biochemical experiments.

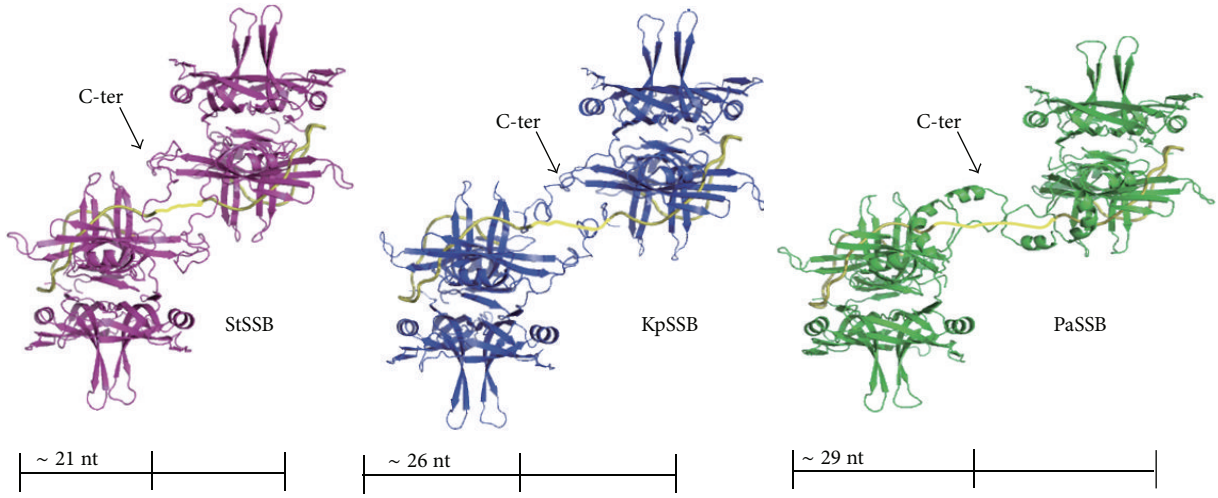

Figure 11: Possible models for explaining why SSBs are with different binding site sizes. Two modeled structures of KpSSB1–142 (blue), StSSB1–142 (pink), and PaSSB1–160 (green) complexed with ssDNA (gold) are shown. For clarity, only one C-terminal domain was shown for each SSB tetramer. By using the electrophoretic mobility shift assay and the protein chimeragenesis, we characterized that the binding site sizes of KpSSB, StSSB, PaSSB, KpSSBnStSSBc, and KpSSBnPaSSBc were 26, 21, 29, 21, and 29 nt per tetramer, respectively. KpSSB, StSSB, and PaSSB are similar proteins whose N-terminal ssDNA-binding domains are almost identical. Thus, the C-terminal domain of SSB may indirectly contribute to ssDNA binding and wrapping and affects the binding site size by the steric hindrance.

5. Conclusion

In this study, we characterized the ssDNA-binding properties of untagged SSBs from *K. pneumoniae*, *S. enterica* serovar Typhimurium LT2, and *P. aeruginosa* PAO1 and proposed a role of the C-terminal flexible domain for ssDNA binding from the protein chimeragenesis and EMSA results. The amino acid sequence of the N-terminal ssDNA-binding/oligomerization domain in these pathogenic SSBs is highly conserved, but their apparent binding site sizes are different. This finding indicates that the C-terminal protein-protein interaction domain may also indirectly contribute to ssDNA binding and wrapping.

Conflict of Interests

The authors declare that there is no conflict of interests regarding the publication of this paper.

Acknowledgment

This research was supported by a Grant from the National Science Council, Taiwan (NSC 102-2320-B-040-019 to Cheng-Yang Huang).

References

[1] R. Reyes-Lamothe, D. J. Sherratt, and M. C. Leake, "Stoichiometry and architecture of active DNA replication machinery in escherichia coli," *Science*, vol. 328, no. 5977, pp. 498–501, 2010.

[2] D. J. Richard, E. Bolderson, and K. K. Khanna, "Multiple human single-stranded DNA binding proteins function in genome maintenance: structural, biochemical and functional analysis," *Critical Reviews in Biochemistry and Molecular Biology*, vol. 44, no. 2-3, pp. 98–116, 2009.

[3] R. D. Shereda, A. G. Kozlov, T. M. Lohman, M. M. Cox, and J. L. Keck, "SSB as an organizer/mobilizer of genome maintenance complexes," *Critical Reviews in Biochemistry and Molecular Biology*, vol. 43, no. 5, pp. 289–318, 2008.

[4] D. J. Richard, E. Bolderson, L. Cubeddu et al., "Single-stranded DNA-binding protein hSSB1 is critical for genomic stability," *Nature*, vol. 453, no. 7195, pp. 677–681, 2008.

[5] R. R. Meyer and P. S. Laine, "The single-stranded DNA-binding protein of Escherichia coli," *Microbiological Reviews*, vol. 54, no. 4, pp. 342–380, 1990.

[6] C. Yang, U. Curth, C. Urbanke, and C. Kang, "Crystal structure of human mitochondrial single-stranded DNA binding protein at 2.4 Å resolution," *Nature Structural Biology*, vol. 4, no. 2, pp. 153–157, 1997.

[7] G. Webster, J. Genschel, U. Curth, C. Urbanke, C. Kang, and R. Hilgenfeld, "A common core for binding single-stranded DNA: structural comparison of the single-stranded DNA-binding proteins (SSB) from E. coli and human mitochondria," *FEBS Letters*, vol. 411, pp. 313–316, 1997.

[8] R. L. Flynn and L. Zou, "Oligonucleotide/oligosaccharide-binding fold proteins: a growing family of genome guardians," *Critical Reviews in Biochemistry and Molecular Biology*, vol. 45, no. 4, pp. 266–275, 2010.

[9] K. Chan, Y. Lee, C. Wang, H. Huang, and Y. Sun, "Single-Stranded DNA-Binding Protein Complex from Helicobacter pylori Suggests an ssDNA-Binding Surface," *Journal of Molecular Biology*, vol. 388, no. 3, pp. 508–519, 2009.

[10] D. L. Theobald, R. M. Mitton-Fry, and D. S. Wuttke, "Nucleic acid recognition by OB-fold proteins," *Annual Review of Biophysics and Biomolecular Structure*, vol. 32, pp. 115–133, 2003.

[11] S. Raghunathan, A. G. Kozlov, T. M. Lohman, and G. Waksman, "Structure of the DNA binding domain of *E. coli* SSB bound to

ssDNA," *Nature Structural Biology*, vol. 7, no. 8, pp. 648–652, 2000.

[12] A. G. Murzin, "OB(oligonucleotide/oligosaccharide binding)-fold: common structural and functional solution for non-homologous sequences," *EMBO Journal*, vol. 12, no. 3, pp. 861–867, 1993.

[13] N. P. George, K. V. Ngo, S. Chitteni-Pattu et al., "Structure and cellular dynamics of deinococcus radiodurans single-stranded DNA (ssDNA)-binding protein (SSB)-DNA complexes," *The Journal of Biological Chemistry*, vol. 287, no. 26, pp. 22123–22132, 2012.

[14] P. Filipkowski and J. Kur, "Identification and properties of the Deinococcus grandis and Deinococcus proteolyticus single-stranded DNA binding proteins (SSB)," *Acta Biochimica Polonica*, vol. 54, no. 1, pp. 79–87, 2007.

[15] P. Filipkowski, A. Duraj-Thatte, and J. Kur, "Identification, cloning, expression, and characterization of a highly thermostable single-stranded-DNA-binding protein (SSB) from *Deinococcus murrayi*," *Protein Expression and Purification*, vol. 53, no. 1, pp. 201–208, 2007.

[16] P. Filipkowski, M. Koziatek, and J. Kur, "A highly thermostable, homodimeric single-stranded DNA-binding protein from Deinococcus radiopugnans," *Extremophiles*, vol. 10, no. 6, pp. 607–614, 2006.

[17] P. Filipkowski, A. Duraj-Thatte, and J. Kur, "Novel thermostable single-stranded DNA-binding protein (SSB) from Deinococcus geothermalis," *Archives of Microbiology*, vol. 186, no. 2, pp. 129–137, 2006.

[18] G. Witte, C. Urbanke, and U. Curth, "Single-stranded DNA-binding protein of Deinococcus radiodurans: a biophysical characterization," *Nucleic Acids Research*, vol. 33, no. 5, pp. 1662–1670, 2005.

[19] D. A. Bernstein, J. M. Eggingtont, M. P. Killoran, A. M. Misic, M. M. Cox, and J. L. Keck, "Crystal structure of the Deinococcus radiodurans single-stranded DNA-binding protein suggests a mechanism for coping with DNA damage," *Proceedings of the National Academy of Sciences of the United States of America*, vol. 101, no. 23, pp. 8575–8580, 2004.

[20] S. Dabrowski, M. Olszewski, R. Piatek, A. Brillowska-Dabrowska, G. Konopa, and J. Kur, "Identification and characterization of single-stranded-DNA-binding proteins from Thermus thermophilus and Thermus aquaticus—new arrangement of binding domains," *Microbiology*, vol. 148, no. 10, pp. 3307–3315, 2002.

[21] R. Gamsjaeger, R. Kariawasam, C. Touma, A. H. Kwan, M. F. White, and L. Cubeddu, "Backbone and side-chain ^{1}H, ^{13}C and ^{15}N resonance assignments of the OB domain of the single stranded DNA binding protein from *Sulfolobus solfataricus* and chemical shift mapping of the DNA-binding interface," *Biomolecular NMR Assignments*, 2013.

[22] M. L. Rolfsmeier and C. A. Haseltine, "The single-stranded DNA binding protein of Sulfolobus solfataricus acts in the presynaptic step of homologous recombination," *Journal of Molecular Biology*, vol. 397, no. 1, pp. 31–45, 2010.

[23] I. D. Kerr, R. I. M. Wadsworth, L. Cubeddu, W. Blankenfeldt, J. H. Naismith, and M. F. White, "Insights into ssDNA recognition by the OB fold from a structural and thermodynamic study of Sulfolobus SSB protein," *EMBO Journal*, vol. 22, no. 11, pp. 2561–2570, 2003.

[24] C. A. Haseltine and S. C. Kowalczykowski, "A distinctive single-stranded DNA-binding protein from the Archaeon Sulfolobus solfataricus," *Molecular Microbiology*, vol. 43, no. 6, pp. 1505–1515, 2002.

[25] R. I. M. Wadsworth and M. F. White, "Identification and properties of the crenarchaeal single-stranded DNA binding protein from Sulfolobus solfataricus," *Nucleic Acids Research*, vol. 29, no. 4, pp. 914–920, 2001.

[26] S. Sugiman-Marangos and M. S. Junop, "The structure of DdrB from *Deinococcus*: a new fold for single-stranded DNA binding proteins," *Nucleic Acids Research*, vol. 38, no. 10, Article ID gkq036, pp. 3432–3440, 2010.

[27] H. Ghalei, H. V. Moeller, D. Eppers et al., "Entrapment of DNA in an intersubunit tunnel system of a single-stranded DNA-binding protein," *Nucleic Acids Research*, vol. 42, no. 10, pp. 6698–6708, 2014.

[28] S. Paytubi, S. A. McMahon, S. Graham et al., "Displacement of the canonical single-stranded DNA-binding protein in the thermoproteales," *Proceedings of the National Academy of Sciences of the United States of America*, vol. 109, no. 7, pp. E398–E405, 2012.

[29] T. H. Dickey, S. E. Altschuler, and D. S. Wuttke, "Single-stranded DNA-binding proteins: multiple domains for multiple functions," *Structure*, vol. 21, no. 7, pp. 1074–1084, 2013.

[30] D. Vujaklija and B. Macek, "Detecting posttranslational modifications of bacterial SSB proteins," *Methods in Molecular Biology*, vol. 922, pp. 205–218, 2012.

[31] I. Mijakovic, D. Petranovic, B. Macek et al., "Bacterial single-stranded DNA-binding proteins are phosphorylated on tyrosine," *Nucleic Acids Research*, vol. 34, no. 5, pp. 1588–1596, 2006.

[32] M. Olszewski, A. Grot, M. Wojciechowski, M. Nowak, M. Mickiewicz, and J. Kur, "Characterization of exceptionally thermostable single-stranded DNA-binding proteins from Thermotoga maritima and Thermotoga neapolitana," *BMC Microbiology*, vol. 10, article 260, 2010.

[33] U. Curth, J. Genschel, C. Urbanke, and J. Greipel, "In vitro and in vivo function of the C-terminus of Escherichia coil single-stranded DNA binding protein," *Nucleic Acids Research*, vol. 24, no. 14, pp. 2706–2711, 1996.

[34] G. Witte, C. Urbanke, and U. Curth, "DNA polymerase III chi subunit ties single-stranded DNA binding protein to the bacterial replication machinery," *Nucleic Acids Research*, vol. 31, pp. 4434–4440, 2003.

[35] D. Shishmarev, Y. Wang, C. E. Mason et al., "Otting, Intramolecular binding mode of the C-terminus of Escherichia coli single-stranded DNA binding protein determined by nuclear magnetic resonance spectroscopy," *Nucleic Acids Research*, vol. 42, pp. 2750–2757, 2014.

[36] A. G. Kozlov, M. M. Cox, and T. M. Lohman, "Regulation of single-stranded DNA binding by the C termini of Escherichia coli single-stranded DNA-binding (SSB) protein," *Journal of Biological Chemistry*, vol. 285, no. 22, pp. 17246–17252, 2010.

[37] M. Nowak, M. Olszewski, M. Spibida, and J. Kur, "Characterization of single-stranded DNA-binding proteins from the psychrophilic bacteria *Desulfotalea psychrophila, Flavobacterium psychrophilum, Psychrobacter arcticus, Psychrobacter cryohalolentis, Psychromonas ingrahamii, Psychroflexus torquis, and Photobacterium profundum*," *BMC Microbiology*, vol. 14, article 91, 2014.

[38] T. Paradzik, N. Ivic, Z. Filic et al., "Structure-function relationships of two paralogous single-stranded DNA-binding proteins from Streptomyces coelicolor: implication of SsbB in chromosome segregation during sporulation," *Nucleic Acids Research*, vol. 41, no. 6, pp. 3659–3672, 2013.

[39] S. Jain, M. Zweig, E. Peeters et al., "Characterization of the single stranded DNA binding protein SsbB encoded in the gonoccocal genetic island," *PLoS ONE*, vol. 7, no. 4, Article ID e35285, 2012.

[40] Y. H. Huang and C. Y. Huang, "Characterization of a single-stranded DNA-binding protein from Klebsiella pneumoniae: mutation at either Arg73 or Ser76 causes a less cooperative complex on DNA," *Genes to Cells*, vol. 17, no. 2, pp. 146–157, 2012.

[41] E. Antony, E. A. Weiland, S. Korolev, and T. M. Lohman, "Plasmodium falciparum SSB tetramer wraps single-stranded DNA with similar topology but opposite polarity to E. Coli SSB," *Journal of Molecular Biology*, vol. 420, no. 4-5, pp. 269–283, 2012.

[42] H. Jan, Y. L. Lee, and C. Y. Huang, "Characterization of a single-stranded DNA-binding protein from *pseudomonas aeruginosa* PAO1," *Protein Journal*, vol. 30, no. 1, pp. 20–26, 2011.

[43] Y.-H. Huang, Y.-L. Lee, and C.-Y. Huang, "Characterization of a single-stranded DNA binding protein from *Salmonella enterica* serovar typhimurium LT2," *Protein Journal*, vol. 30, no. 2, pp. 102–108, 2011.

[44] S. K. Bharti, K. Rex, P. Sreedhar, N. Krishnan, and U. Varshney, "Chimeras of *Escherichia coli* and *Mycobacterium tuberculosis* single-stranded DNA binding proteins: characterization and function in *Escherichia coli*," *PLoS ONE*, vol. 6, no. 12, Article ID e27216, 2011.

[45] M. T. Oliveira and L. S. Kaguni, "Functional roles of the N- and C-terminal regions of the human mitochondrial single-stranded DNA-binding protein," *PLoS ONE*, vol. 5, no. 10, Article ID e15379, 2010.

[46] A. G. Kozlov, J. M. Eggington, M. M. Cox, and T. M. Lohman, "Binding of the dimeric Deinococcus radiodurans single-stranded DNA binding protein to single-stranded DNA," *Biochemistry*, vol. 49, no. 38, pp. 8266–8275, 2010.

[47] T. M. Lohman and M. E. Ferrari, "Escherichia coli single-stranded DNA-binding protein: multiple DNA-binding modes and cooperatives," *Annual Review of Biochemistry*, vol. 63, pp. 527–570, 1994.

[48] R. Zhou, A. G. Kozlov, R. Roy et al., "SSB functions as a sliding platform that migrates on DNA via reptation," *Cell*, vol. 146, pp. 222–232, 2011.

[49] R. Roy, A. G. Kozlov, T. M. Lohman, and T. Ha, "SSB protein diffusion on single-stranded DNA stimulates RecA filament formation," *Nature*, vol. 461, pp. 1092–1097, 2009.

[50] R. Roy, A. G. Kozlov, T. M. Lohman, and T. Ha, "Dynamic structural rearrangements between DNA binding modes of E. coli SSB protein," *Journal of Molecular Biology*, vol. 369, no. 5, pp. 1244–1257, 2007.

[51] T. J. Kelly, P. Simancek, and G. S. Brush, "Identification and characterization of a single-stranded DNA-binding protein from the archaeon Methanococcus jannaschii," *Proceedings of the National Academy of Sciences of the United States of America*, vol. 95, no. 25, pp. 14634–14639, 1998.

[52] C. Y. Huang, *Determination of the Binding Site-Size of the Protein-DNA Complex by Use of the Electrophoretic Mobility Shift Assay*, InTech Press, Rijeka, Croatia, 2012.

[53] A. Kornberg, "Ten commandments of enzymology, amended," *Trends in Biochemical Sciences*, vol. 28, no. 10, pp. 515–517, 2003.

[54] W. Zhang, X. Lü, and J. Shen, "EMSA and single-molecule force spectroscopy study of interactions between bacillus subtilis single-stranded DNA-binding protein and single-stranded DNA," *Langmuir*, vol. 27, no. 24, pp. 15008–15015, 2011.

[55] M. Ostermeier and S. J. Benkovic, "Evolution of protein function by domain swapping," *Advances in Protein Chemistry*, vol. 55, pp. 29–77, 2000.

[56] W. F. Peng and C. Y. Huang, "Allantoinase and dihydroorotase binding and inhibition by flavonols and the substrates of cyclic amidohydrolases," *Biochimie*, vol. 101, pp. 113–122, 2014.

[57] Y. H. Huang, M. J. Lin, and C. Y. Huang, "DnaT is a single-stranded DNA binding protein," *Genes to Cells*, vol. 18, no. 11, pp. 1007–1019, 2013.

[58] Y. Y. Ho, Y. H. Huang, and C. Y. Huang, "Chemical rescue of the post-translationally carboxylated lysine mutant of allantoinase and dihydroorotase by metal ions and short-chain carboxylic acids," *Amino Acids*, vol. 44, no. 4, pp. 1181–1191, 2013.

[59] Y. H. Huang, Y. Lo, W. Huang, and C. Y. Huang, "Crystal structure and DNA-binding mode of Klebsiella pneumoniae primosomal PriB protein," *Genes to Cells*, vol. 17, no. 10, pp. 837–849, 2012.

[60] C. Y. Huang, C. Y. Hsu, Y. Sun, H. Wu, and C. Hsiao, "Complexed crystal structure of replication restart primosome protein PriB reveals a novel single-stranded DNA-binding mode," *Nucleic Acids Research*, vol. 34, no. 14, pp. 3878–3886, 2006.

[61] T. Kinebuchi, H. Shindo, H. Nagai, N. Shimamoto, and M. Shimizu, "Functional domains of Escherichia coli single-stranded DNA binding protein as assessed by analyses of the deletion mutants," *Biochemistry*, vol. 36, no. 22, pp. 6732–6738, 1997.

[62] N. Shimamoto, N. Ikushima, H. Utiyama, H. Tachibana, and K. Horie, "Specific and cooperative binding of *E. coli* single-stranded DNA binding protein to mRNA," *Nucleic Acids Research*, vol. 15, no. 13, pp. 5241–5250, 1987.

[63] H. Lin and C. Y. Huang, "Characterization of flavonol inhibition of DnaB helicase: Real-time monitoring, structural modeling, and proposed mechanism," *Journal of Biomedicine and Biotechnology*, vol. 2012, Article ID 735368, 2012.

[64] Y. H. Huang, H. H. Lin, and C. Y. Huang, "A single residue determines the cooperative binding property of a primosomal DNA replication protein, PriB, to single-stranded DNA," *Bioscience, Biotechnology and Biochemistry*, vol. 76, no. 6, pp. 1110–1115, 2012.

[65] H. C. Hsieh and C. Y. Huang, "Identification of a novel protein, PriB, in *Klebsiella pneumoniae*," *Biochemical and Biophysical Research Communications*, vol. 404, no. 1, pp. 546–551, 2011.

[66] J. H. Liu, T. W. Chang, C. Y. Huang et al., "Crystal structure of PriB, a primosomal DNA replication protein of *Escherichia coli*," *The Journal of Biological Chemistry*, vol. 279, no. 48, pp. 50465–50471, 2004.

[67] Y. H. Huang and C. Y. Huang, "The N-terminal domain of DnaT, a primosomal DNA replication protein, is crucial for PriB binding and self-trimerization," *Biochemical and Biophysical Research Communications*, vol. 442, pp. 147–152, 2013.

[68] M. A. Larkin, G. Blackshields, N. P. Brown et al., "Clustal W and Clustal X version 2.0," *Bioinformatics*, vol. 23, no. 21, pp. 2947–2948, 2007.

[69] S. N. Savvides, S. Raghunathan, K. Fütterer, A. G. Kozlov, T. M. Lohman, and G. Waksman, "The C-terminal domain of full-length *E. coli* SSB is disordered even when bound to DNA," *Protein Science*, vol. 13, no. 7, pp. 1942–1947, 2004.

[70] C.-C. Chen, J.-K. Hwang, and J.-M. Yang, "(PS)2-v2: template-based protein structure prediction server," *BMC Bioinformatics*, vol. 10, article 366, 2009.

[71] C. Chen, J. Hwang, and J. Yang, "(PS)2: protein structure prediction server," *Nucleic Acids Research*, vol. 34, pp. W152–W157, 2006.

[72] K. Bush and J. F. Fisher, "Epidemiological expansion, structural studies, and clinical challenges of new β-lactamases from gram-negative bacteria," *Annual Review of Microbiology*, vol. 65, pp. 455–478, 2011.

[73] K. K. Kumarasamy, M. A. Toleman, T. R. Walsh et al., "Emergence of a new antibiotic resistance mechanism in India, Pakistan, and the UK: a molecular, biological, and epidemiological study," *The Lancet Infectious Diseases*, vol. 10, no. 9, pp. 597–602, 2010.

[74] K. Bush and M. J. MacIelag, "New β-lactam antibiotics and β-lactamase inhibitors," *Expert Opinion on Therapeutic Patents*, vol. 20, no. 10, pp. 1277–1293, 2010.

[75] K. Bush, "Alarming β-lactamase-mediated resistance in multidrug-resistant *Enterobacteriaceae*," *Current Opinion in Microbiology*, vol. 13, no. 5, pp. 558–564, 2010.

[76] A. Srivastava, M. Talaue, S. Liu et al., "New target for inhibition of bacterial RNA polymerase: "switch region"," *Current Opinion in Microbiology*, vol. 14, no. 5, pp. 532–543, 2011.

[77] K. Chono, K. Katsumata, T. Kontani et al., "ASP2151, a novel helicase-primase inhibitor, possesses antiviral activity against varicella-zoster virus and herpes simplex virus types 1 and 2," *Journal of Antimicrobial Chemotherapy*, vol. 65, no. 8, pp. 1733–1741, 2010.

[78] M. T. Black and K. Coleman, "New inhibitors of bacterial topoisomerase GyrA/ParC subunits," *Current Opinion in Investigational Drugs*, vol. 10, no. 8, pp. 804–810, 2009.

[79] A. H. Marceau, D. A. Bernstein, B. W. Walsh, W. Shapiro, L. A. Simmons, and J. L. Keck, "Protein interactions in genome maintenance as novel antibacterial targets," *PLoS ONE*, vol. 8, no. 3, Article ID e58765, 2013.

[80] D. Lu, D. A. Bernstein, K. A. Satyshur, and J. L. Keck, "Small-molecule tools for dissecting the roles of SSB/protein interactions in genome maintenance," *Proceedings of the National Academy of Sciences of the United States of America*, vol. 107, no. 2, pp. 633–638, 2010.

[81] I. Wong and T. M. Lohman, "A double-filter method for nitrocellulose-filter binding: application to protein-nucleic acid interactions," *Proceedings of the National Academy of Sciences of the United States of America*, vol. 90, no. 12, pp. 5428–5432, 1993.

[82] M. Mitas, J. Y. Chock, and M. Christy, "The binding-site sizes of Escherichia coli single-stranded-DNA-binding protein and mammalian replication protein A are 65 and $\geq$ 54 nucleotides respectively," *Biochemical Journal*, vol. 324, no. 3, pp. 957–961, 1997.

[83] C. Urbanke, G. Witte, and U. Curth, "Sedimentation velocity method in the analytical ultracentrifuge for the study of protein-protein interactions," *Methods in Molecular Biology*, vol. 305, pp. 101–114, 2005.

[84] S. Chrysogelos and J. Griffith, "Escherichia coli single-strand binding protein organizes single-stranded DNA in nucleosome-like units," *Proceedings of the National Academy of Sciences of the United States of America*, vol. 79, no. 19, pp. 5803–5807, 1982.

[85] J. R. Casas-Finet, K. R. Fischer, and R. L. Karpel, "Structural basis for the nucleic acid binding cooperativity of bacteriophage T4 gene 32 protein: the (Lys/Arg)3(Ser/Thr)2 (LAST) motif," *Proceedings of the National Academy of Sciences of the United States of America*, vol. 89, pp. 1050–1054, 1992.

[86] G. Witte, R. Fedorov, and U. Curth, "Biophysical analysis of *Thermus aquaticus* single-stranded DNA binding protein," *Biophysical Journal*, vol. 94, no. 6, pp. 2269–2279, 2008.

[87] R. Fedorov, G. Witte, C. Urbanke, D. J. Manstein, and U. Curth, "3D structure of Thermus aquaticus single-stranded DNA-binding protein gives insight into the functioning of SSB proteins," *Nucleic Acids Research*, vol. 34, no. 22, pp. 6708–6717, 2006.

[88] K. L. Tsai, C. Y. Huang, C. H. Chang, Y. J. Sun, W. J. Chuang, and C. D. Hsiao, "Crystal structure of the human FOXK1a-DNA complex and its implications on the diverse binding specificity of winged helix/forkhead proteins," *Journal of Biological Chemistry*, vol. 281, no. 25, pp. 17400–17409, 2006.

[89] A. H. Mao, N. Lyle, and R. V. Pappu, "Describing sequence-ensemble relationships for intrinsically disordered proteins," *Biochemical Journal*, vol. 449, no. 2, pp. 307–318, 2013.

[90] R. Wetzel, "Physical chemistry of polyglutamine: Intriguing tales of a monotonous sequence," *Journal of Molecular Biology*, vol. 421, no. 4-5, pp. 466–490, 2012.

[91] H. T. Orr, "Polyglutamine neurodegeneration: expanded glutamines enhance native functions," *Current Opinion in Genetics and Development*, vol. 22, no. 3, pp. 251–255, 2012.

[92] M. Figiel, W. J. Szlachcic, P. M. Switonski, A. Gabka, and W. J. Krzyzosiak, "Mouse models of polyglutamine diseases: review and data table. Part I," *Molecular Neurobiology*, vol. 46, no. 2, pp. 393–429, 2012.

[93] J. Nasica-Labouze and N. Mousseau, "Kinetics of amyloid aggregation: a study of the GNNQQNY prion sequence," *PLoS Computational Biology*, vol. 8, no. 11, Article ID e1002782, 2012.

[94] J. Nasica-Labouze, M. Meli, P. Derreumaux, G. Colombo, and N. Mousseau, "A multiscale approach to characterize the early aggregation steps of the amyloid-forming peptide gnnqqny from the yeast prion sup-35," *PLoS Computational Biology*, vol. 7, no. 5, Article ID e1002051, 2011.

[95] J. R. Lewandowski, P. C. A. van der Wel, M. Rigney, N. Grigorieff, and R. G. Griffin, "Structural complexity of a composite amyloid fibril," *Journal of the American Chemical Society*, vol. 133, no. 37, pp. 14686–14698, 2011.

Hindawi Publishing Corporation
BioMed Research International
Volume 2014, Article ID 285791, 8 pages
http://dx.doi.org/10.1155/2014/285791

Research Article

The N-Terminal Domain of Human DNA Helicase Rtel1 Contains a Redox Active Iron-Sulfur Cluster

Aaron P. Landry and Huangen Ding

Department of Biological Sciences, Louisiana State University, 202 Life Sciences Building, Baton Rouge, LA 70803, USA

Correspondence should be addressed to Huangen Ding; hding@lsu.edu

Received 9 June 2014; Accepted 8 July 2014; Published 24 July 2014

Academic Editor: Cheng-Yang Huang

Human telomere length regulator Rtel1 is a superfamily II DNA helicase and is essential for maintaining proper length of telomeres in chromosomes. Here we report that the N-terminal domain of human Rtel1 (RtelN) expressed in *Escherichia coli* cells produces a protein that contains a redox active iron-sulfur cluster with the redox midpoint potential of −248 ± 10 mV (pH 8.0). The iron-sulfur cluster in RtelN is sensitive to hydrogen peroxide and nitric oxide, indicating that reactive oxygen/nitrogen species may modulate the DNA helicase activity of Rtel1 via modification of its iron-sulfur cluster. Purified RtelN retains a weak binding affinity for the single-stranded (ss) and double-stranded (ds) DNA *in vitro*. However, modification of the iron-sulfur cluster by hydrogen peroxide or nitric oxide does not significantly affect the DNA binding activity of RtelN, suggesting that the iron-sulfur cluster is not directly involved in the DNA interaction in the N-terminal domain of Rtel1.

1. Introduction

In vertebrates, telomeres are the protective structures at the end of chromosomes and are composed of a repetitive TTAGGG sequence and associated proteins that form a core structure known as the Shelterin complex [1, 2]. Telomeres become shorter with each round of DNA replication and are compensated for by telomerase [3]. In addition to telomerase, the telomere length is regulated by other genetic [4] and epigenetic [5] factors. Among them, telomere length regulator 1 (Rtel1) has an essential role in maintaining proper length of telomeres [4, 6]. Deletion of Rtel1 in mice is embryonic lethal with increased incidence of chromosomal abnormalities and telomere loss [4]. In humans, Rtel1 is highly expressed in several types of tumor tissues [7] and specific mutations in Rtel1 have been attributed to dyskeratosis congenita and Hoyeraal-Hreidarsson syndrome [8, 9].

Human Rtel1 is a superfamily II DNA helicase [10] and is homologous to other human DNA helicases XPD (Xeroderma pigmentosum factor D) [11], FancJ (Fanconi's anaemia complementation group J)/BACH1 (for BRCA1-associated C-terminal helicase) [12, 13], and ChlR1 (a protein required for normal mitotic progression) [14]. However, unlike other DNA helicases, Rtel1 preferentially disrupts the D-loop of the T-loop structure formed at the end of telomeres [15] and may act as an antirecombinase to prevent formation of D-loop [6, 16]. In the absence of Rtel1, the T-loop structure could be erroneously resolved as a substrate for homologous recombination [16], leading to telomere deficiency. On the other hand, excessive activity of Rtel1 would be detrimental as increased Rtel1 helicase activity would disengage the T-loop structure, leading to telomere deprotection and genomic instability [16]. Thus, the helicase activity of Rtel1 must be tightly regulated to maintain proper length of telomeres in chromosomes [6].

The sequence alignment analyses revealed that the N-terminal domain of human Rtel1 contains a conserved region for hosting a putative iron-sulfur cluster via four cysteine residues (Figure 1) [17]. It has previously been reported that the DNA helicase Rad3 from yeast [18], XPD homologues from archaea [19–22], DNA-damage-inducible DNA helicase DinG from *Escherichia coli* [23], and AddAB-type helicase-nuclease from *Bacillus subtilis* [24] contain a [4Fe-4S] cluster essential for the helicase activity. However, the existence of

```
Rad3   108   LTSRKNLCLHPEVSKERKGTVVDEKCRRMTNGQAKRKLEEDpeA   NVELCEYHENLYNIE   VEDYLPKGVFSFEKL
XPD    109   LSSRKNLCIHPEVTPLRFGKDVDGKCHSLTASYVRAQYQHD--T   SLPHCRFYEEFDAHG   REVPLPAGIYNLDDL
Rtel1  162   LGSREQLCIHPEVKKQESNHLQIHLCRKKVASR-----------   ---SCHFYNNVEEKS   LEQELASPILDIEDL
FancJ  276   LSSRDHTCVHPEVVG---NFNRNEKCMELLDGKNGK--------  ---SCYFYHGVHKIS[5]QTFQGMCKAWDIEEL
Chl1   260   LGSRQNLCVNEDVKSLGSVQLINDRCVDMQRSRHEKKKGAEEEK[7]KQAACPFYNHEQMGL   LRDEALAEVKDMEQL

RAD3   182   LKYCEEKTLCPYFIVRRMISLCNIIIYSYHYLLDPKIAERVSNEVSKDSIVIFDEAHN
XPD    181   KALGRRQGWCPYFLARYSILHANVVVYSYHYLLDPKIADLVSKELARKAVVVFDEAHN
Rtel1  222   VKSGSKHRVCPYYLSRNLKQQADIIFMPYNYLLDAKSRRAHNIDL-KGTVVIFDEAHN
FancJ  341   VSLGKKLKACPYYTARELIQDADIIFCPYNYLLDAQIRESMDLNL-KEQVVILDEAHN
Chl1   341   LALGKEARACPYYGSRLAIPAAQLVVLPYQMLLHAATRQAAGIRL-QDQVVIIDEAHN
```

Figure 1: Alignment of the N-terminal domain of some human DNA helicases. Sequence alignment of yeast DNA helicase Rad3 and human DNA helicase XPD, Rtel1, FancJ, and Chl1 was generated by cobalt (NCBI). Four conserved cysteine residues proposed for hosting an iron-sulfur cluster in these DNA helicases are highlighted in yellow.

the iron-sulfur cluster in any human DNA helicases has not been experimentally demonstrated. Here, we report that expression of the N-terminal domain (residues 1–312) of human Rtel1 (RtelN) in *E. coli* cells produces a protein that contains a redox active iron-sulfur cluster with redox midpoint potential (E_{m7}) of -248 ± 10 mV (pH 8.0). Purified RtelN retains a weak binding activity for the single-stranded (ss) and double-stranded (ds) DNA, and disruption of the iron-sulfur cluster by hydrogen peroxide or nitric oxide does not affect the DNA binding activity of RtelN, suggesting that iron-sulfur cluster in the N-terminal domain may not be directly involved in the DNA interaction in Rtel1.

2. Materials and Methods

2.1. Protein Preparation. The DNA fragment encoding the N-terminal domain (residues 1–312) (RtelN) of human regulator of telomere length 1 (Rtel1) was synthesized for expression in *E. coli* cells (Genescript co.). The gene was subcloned into an expression plasmid pET28b$^+$ which was introduced into *E. coli* BL21 cells. The *E. coli* cells hosting the expression plasmid were grown in LB media to an $OD_{600\,nm}$ of ~0.6 before isopropyl β-D-1-thiogalactopyranoside (200 μM) was added to induce the protein expression for three hours. The cells were harvested and passed through French press once. Recombinant RtelN in pellets was solubilized by adding urea (6 M), and the protein was purified using a nickel-agarose column attached to a FPLC system (GE Biosciences), followed by passing through a HiTrap desalting column. The molecular weight of RtelN was confirmed by the MALDI mass spectrometer (Chemistry Department, LSU). The concentration of purified RtelN was measured from the absorption peak at 280 nm using an extinction coefficient of 25.5 mM^{-1} cm^{-1}. The total iron content in purified RtelN sample was determined using an iron indicator FerroZine [25]. The total acid-labile sulfide content was determined according to Siegel's method [26]. The single-stranded DNA binding protein SSB [27] was prepared as described previously [28].

2.2. The DNA Binding Activity Assay of RtelN. The DNA binding activity assay was carried out using a fluorescence labeled 40 mer (5′-F*-AATTGC-GATCTAGCTCGCCAGU-AG-CGACCTTATCTGATGA-3′). For single-stranded (ss) DNA binding assay, the 40 mer (0.5 μM) was incubated with increasing concentrations of protein in buffer containing Tris (20 mM, pH 8.0), NaCl (50 mM), β-mercaptoethanol (1 mM), $MgCl_2$ (1 mM), and bovine serum albumin (0.5 mg/mL). For double-strand (ds) DNA binding assay, the fluorescence labeled 40 mer was annealed to a complementary ssDNA in an annealing buffer containing Tris (50 mM, pH 8.0), NaCl (50 mM), and $MgCl_2$ (10 mM). Prepared dsDNA labeled with fluorescence was incubated with increasing concentrations of protein in buffer as described above. After incubation at room temperature for 15 min, samples were loaded on to a 0.6% agarose gel in TAE buffer. The agarose gel was run at 10 V per cm for 30 min at room temperature and photographed in a KODAK Gel Logic 200 Imaging System.

2.3. Redox Titration of the RtelN Iron-Sulfur Cluster. A specially-designed cuvette was used for redox titration experiments as described by Leslie Dutton [29]. Briefly, purified RtelN (20 μM) dissolved in buffer containing Tris (50 mM, pH 8.0) and NaCl (500 mM) was incubated with a redox mediator safranin O (1 μM) in a sealed cuvette and equilibrated with pure argon gas for 45 minutes at room temperature. The redox potential was adjusted by adding a small amount of freshly prepared sodium dithionite using a gas-tight 10-μL Hamilton micro-syringe (Hamilton Co., Reno, NV). The redox potential was monitored with a redox microelectrode (Microelectrodes Inc., Bedford, NH) which was calibrated using a standard ZoBell solution (E_h = +238 mV) containing potassium ferricyanide (5 mM) and potassium ferrocyanide (5 mM) in buffer containing Tris (20 mM, pH 8.0) and NaCl (500 mM). The redox titration data were fitted to the Nernst equation with $n = 1$ using KaleidaGraph (Synergy Software co.).

2.4. Hydrogen Peroxide and Nitric Oxide Treatments of RtelN. For hydrogen peroxide (H_2O_2) treatments, purified RtelN was incubated with different concentrations of H_2O_2 at room temperature for 30 min, followed by repurification of the protein from the incubation solutions. For nitric oxide (NO) treatments, purified RtelN dissolved in a sealed

vial was purged with pure argon gas for 15 min, followed by incubation with the NO-releasing reagent diethylamine NONOate (Cayman Chemicals co.) at 37°C for 10 min. RtelN was repurified after the NO treatment. Modification of the iron-sulfur cluster in RtelN by H_2O_2 or NO was quantified by the UV-visible absorption spectrometer.

2.5. The Circular Dichroism (CD) and Electron Paramagnetic Resonance (EPR) Measurements. The circular dichroism (CD) spectra were recorded on a Jasco J-815 CD spectrometer (AgCenter Biotechnology Laboratories, LSU) at room temperature. The composition of secondary structures was obtained using the CDNN program [30]. The electron paramagnetic resonance (EPR) spectra were recorded at X-band on a Bruker ESR-300 spectrometer equipped with an Oxford Instruments 910 continuous flow cryostat. EPR conditions were as follows: microwave frequency, 9.45 GHz; microwave power, 10 mW; modulation frequency, 100 kHz; modulation amplitude, 2 mT; sample temperature, 10 K; receive gain, 1×10^5.

3. Results

3.1. The N-Terminal Domain of Human Rtel1 Hosts an Iron-Sulfur Cluster. When the N-terminal domain of human Rtel1 (RtelN) was expressed in *E. coli* cells, the cell pellets had a dark-red color (Figure 2(a) insert). Recombinant RtelN was purified from the *E. coli* cells as described in the Materials and Methods. The UV-visible absorption measurements showed that purified RtelN had an absorption peak at 415 nm (Figure 2(a)), similar to that of *S. acidocaldarius* XPD [4Fe-4S] cluster [22] and *E. coli* DinG [4Fe-4S] cluster [23]. Purified RtelN was further subjected to the Circular dichroism (CD) measurements. As shown in Figure 2(b), purified RtelN adopted an ordered structure with about 25% alpha-helix, 32% beta-sheet, 20% beta turns, and 22% random coil. The iron and sulfide content analyses revealed that purified RtelN contained 0.83 ± 0.13 iron and 0.75 ± 0.16 acid-labile sulfide per protein.

The low iron and sulfide contents in purified RtelN could be due to the protein purification process under denaturation conditions. To fully reconstitute the iron-sulfur clusters in RtelN, renatured protein was reconstituted with excess iron and sulfide as described previously [23]. After reconstitution, the iron and sulfide contents in RtelN were increased to 3.5 ± 0.3 iron and 3.2 ± 0.5 sulfide per RtelN, respectively, indicating that each RtelN monomer may bind a [4Fe-4S] cluster.

3.2. The Iron-Sulfur Cluster in RtelN Is Redox Active. When freshly prepared sodium dithionite was added to the solution containing RtelN, the absorption peak at 415 nm of the RtelN iron-sulfur cluster was completely eliminated (Figure 3(a)). The absorption peak at 415 nm was restored when the reduced RtelN iron-sulfur cluster was reoxidized by oxygen (data not shown), suggesting that the RtelN iron-sulfur cluster can be reversibly reduced. This notion was further confirmed by the electron paramagnetic resonance (EPR) measurements: while purified RtelN was EPR silent, addition of sodium dithionite to purified RtelN produced an EPR spectrum with g_x = 1.918, g_y = 1.994, and g_z = 2.050 (Figure 3(b)), a spectrum similar to that of the reduced *E. coli* DNA helicase DinG [4Fe-4S] cluster [23].

Redox titration experiments were carried out to determine the redox midpoint potential (E_m) of the RtelN iron-sulfur cluster. The amplitude of the absorption peak at 415 nm of RtelN was plotted as a function of redox potentials in the solution (Figure 3(c)). The data from three sets of experiments were fitted to a Nernst equation (n = 1) with an E_{m8} of −248 ± 10 mV, which is about 140 mV higher than that of the *E. coli* DinG [4Fe-4S] cluster [23].

3.3. Purified RtelN Has a Weak DNA Binding Activity. The N-terminal domain of the archaeal DNA helicase XPD comprises part of the catalytic center [20]. To test whether the N-terminal domain of Rtel1 also contributes to the catalytic site, we examined the DNA binding activity of purified RtelN. As shown in Figure 4(a), purified RtelN formed a protein-DNA complex with the single-stranded (ss) DNA. FhuF, an iron-sulfur protein with a similar molecular weight as RtelN but with no known DNA binding activity [31], failed to bind any ssDNA, indicating that the ssDNA binding in RtelN is specific. Nevertheless, compared with the single-stranded DNA binding protein SSB [27], the binding affinity of RtelN for ssDNA was at least 10-fold-weaker. In parallel, we also determined the double-stranded (ds) DNA binding activity of RtelN under the same experimental conditions. Figure 4(b) shows that RtelN could also bind dsDNA with the similar binding affinity as for ssDNA. In contrast, both FhuF and SSB did not bind any dsDNA as expected. Thus, purified RtelN has a binding activity for both ssDNA and dsDNA *in vitro*.

3.4. The Iron-Sulfur Cluster Is Not Required for the DNA Binding Activity of RtelN. Ironically, iron-sulfur clusters in proteins are often sensitive to reactive oxygen species [32] and nitrogen species [33, 34]. To test if the iron-sulfur clusters in RtelN can be modified by reactive oxygen species, we incubated RtelN with hydrogen peroxide at room temperature. Figure 5(a) shows that addition of increasing amounts of hydrogen peroxide removed the absorption peak at 415 nm of purified RtelN, indicating that the iron-sulfur cluster in RtelN are disrupted by hydrogen peroxide. Purified RtelN was also incubated with the nitric oxide-releasing reagent NONOate in solution. Again, the absorption peak at 415 nm of the RtelN iron-sulfur cluster was largely abolished as the concentration of nitric oxide was increased (Figure 5(b)). Thus, the iron-sulfur cluster in RtelN is sensitive to both hydrogen peroxide and nitric oxide.

We then examined the DNA binding activity of RtelN after the protein was treated with hydrogen peroxide and nitric oxide. Figure 5(c) shows that the DNA binding activity of RtelN remained almost the same when the iron-sulfur cluster was modified by hydrogen peroxide or nitric oxide, suggesting that iron-sulfur cluster is not required for the DNA binding activity of RtelN.

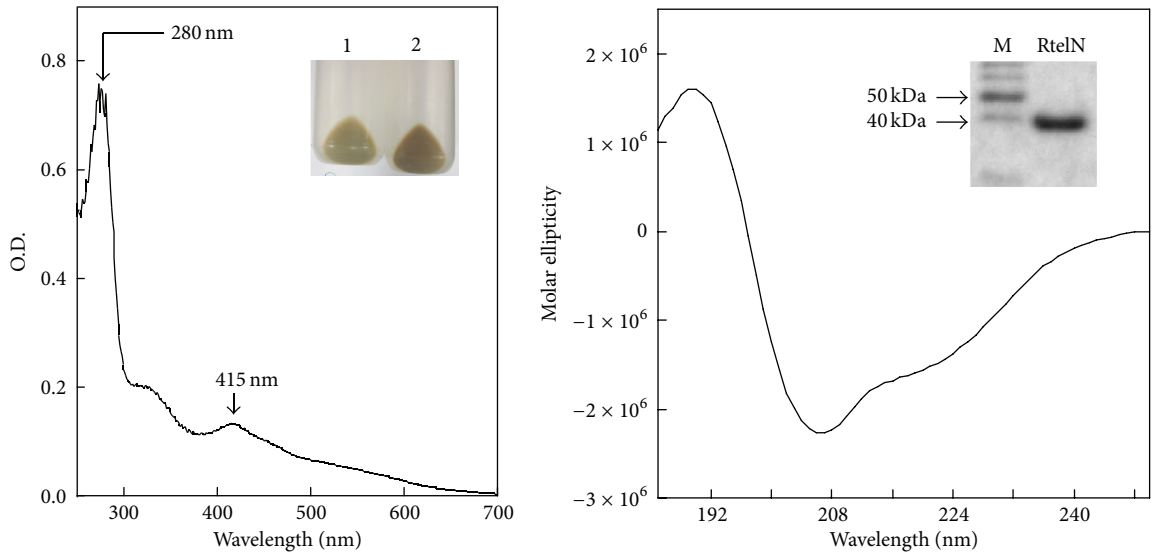

Figure 2: N-terminal domain of Rtel1 (RtelN) contains an iron-sulfur cluster. (a) UV-visible absorption spectrum of purified RtelN. Purified RtelN (30 μM) was dissolved in buffer containing Tris (20 mM, pH 8.0) and NaCl (500 mM). The absorption peak at 415 nm indicates an iron-sulfur cluster in RtelN. Inset is a photograph of cell pellets after induction with (sample 2) or without (sample 1) IPTG (200 μM). (b) Circular dichroism (CD) spectrum of purified RtelN. Purified RtelN (6.75 μM) was dissolved in potassium phosphate buffer (10 mM, pH 8.0). The spectrum was an average of three scans. Insert is a photograph of the SDS-PAGE gel of purified RtelN. Left lane, molecular marker (M); right lane, purified RtelN.

4. Discussion

Recent studies have identified a new set of iron-sulfur cluster-containing enzymes that are involved in DNA processing in bacteria and eukaryotic cells [17]. Among these enzymes are a group of DNA helicases that require an intact iron-sulfur cluster for the DNA helicase activity [11, 35]. For example, it has been shown that the DNA helicase Rad3 from yeast and XPD homologues from archaea contain a [4Fe-4S] cluster essential for the enzyme activity [19–22]. In human XPD, mutations in the N-terminal domain that hosts a putative iron-sulfur cluster have been associated with several genetic diseases including xeroderma pigmentosum [20]. Interestingly, in addition to XPD, humans have at least three other DNA helicases: FancJ (Fanconi's anaemia complementation group J)/BACH1 (for BRCA1-associated C-terminal helicase) [12, 13], ChlR1 (a protein required for normal mitotic progression) [14], and Rtel1 of telomere length regulation [4, 6] that contain a putative iron-sulfur cluster binding site in the N-terminal domain (Figure 1). However, the existence of the [4Fe-4S] clusters in any of these human DNA helicases has not been experimentally demonstrated. Here we find that the N-terminal domain of human Rtel1 (RtelN) expressed in *E. coli* cells contains a redox active [4Fe-4S] cluster and that the iron-sulfur cluster in purified RtelN is highly sensitive to hydrogen peroxide and nitric oxide. The results suggest that human Rtel1, like XPD from archaea [19–22], likely contains a [4Fe-4S] cluster.

Despite the findings of the iron-sulfur clusters in these DNA helicases, specific function of the [4Fe-4S] clusters in the DNA helicases remains largely elusive [17]. In previous studies, we reported that oxidation of the reduced iron-sulfur cluster in *E. coli* DNA helicase DinG reversibly switches on the enzyme activity, and proposed that iron-sulfur cluster may regulate the helicase activity in response to redox signals [23]. Here, we have tested the idea further in the human DNA helicase Rtel1. While attempts to purify a full-length human Rtel1 from *E. coli* cells were not successful, we were able to prepare the soluble N-terminal domain (residues 1–312) of human Rtel1 (RtelN). The results demonstrated that RtelN contains a redox active iron-sulfur cluster with a redox midpoint potential of -248 ± 10 mV (pH 8.0) (Figure 3). The redox potential in cytosol and nucleus of mammalian cells has been reported to be around -325 mV (pH 7.0) [36]. However, when cells are under oxidative stress or during apoptosis and differentiation, the intracellular redox potential could increase to as high as +200 mV [37]. Assuming the redox midpoint potential of the iron-sulfur cluster in Rtel1 is similar to that in RtelN, we would expect that the iron-sulfur cluster in Rtel1 is in reduced state in cells under normal physiological conditions. Under oxidative stress or during apoptosis and differentiation [37], the iron-sulfur cluster in Rtel1 would be fully oxidized. We envision that oxidation of the reduced iron-sulfur cluster in Rtel1, like that in the *E. coli* DinG [23], may change the DNA helicase activity of the protein in response to redox signals. Thus, fluctuation of intracellular redox potential may result in change of the Rtel1's DNA helicase activity by changing the redox state of the iron-sulfur cluster. While the iron-sulfur cluster appears to be dispensable for the DNA binding activity of purified RtelN

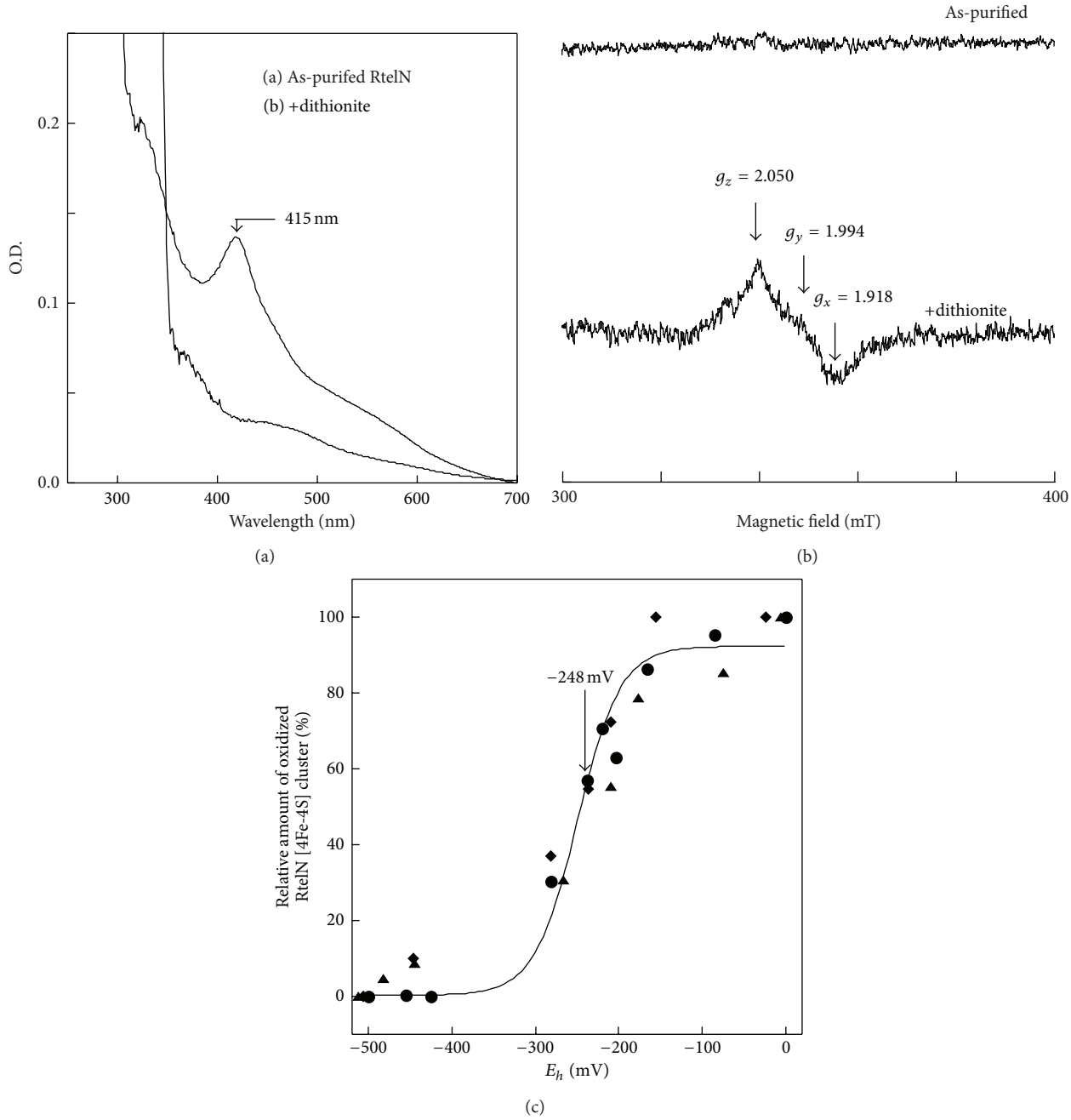

Figure 3: Redox titration of the RtelN iron-sulfur cluster. (a) UV-visible spectra of purified RtelN. Purified RtelN (40 μM) (spectrum 1) was reduced with freshly prepared sodium dithionite (2 mM) (spectrum 2). (b) EPR spectra of purified RtelN. RtelN (90 μM) (spectrum 1) was reduced with freshly prepared sodium dithionite (2 mM) (spectrum 2). (c) Redox titration of purified RtelN. The amplitudes of the absorbance peak at 415 nm were normalized to 0 and 100% for the fully reduced and oxidized RtelN iron-sulfur cluster in solution, respectively. The solid line drawn through three sets of data points represents the best fit to a Nernst equation ($n = 1$) with $E_m = -248 \pm 10$ mV.

(Figure 5), the iron-sulfur cluster could have an important role in other steps of the reaction catalyzed by Rtel1.

The telomere length of chromosomes has been linked to intracellular oxidative stress in human cells [38]. The finding that the RtelN iron-sulfur cluster is sensitive to hydrogen peroxide and nitric oxide (Figure 5) may provide a rational explanation for the association between the telomere length of chromosomes and oxidative stress in cells. Since the iron-sulfur cluster is essential for the DNA helicase activity of XPD from yeast and archaea [19–22], disruption of iron-sulfur clusters in protein would likely change the helicase activity of Rtel1 in human cells. If the iron-sulfur cluster in Rtel1 is as sensitive to hydrogen peroxide or nitric oxide as that in RtelN, the DNA helicase activity of Rtel1 could be modulated

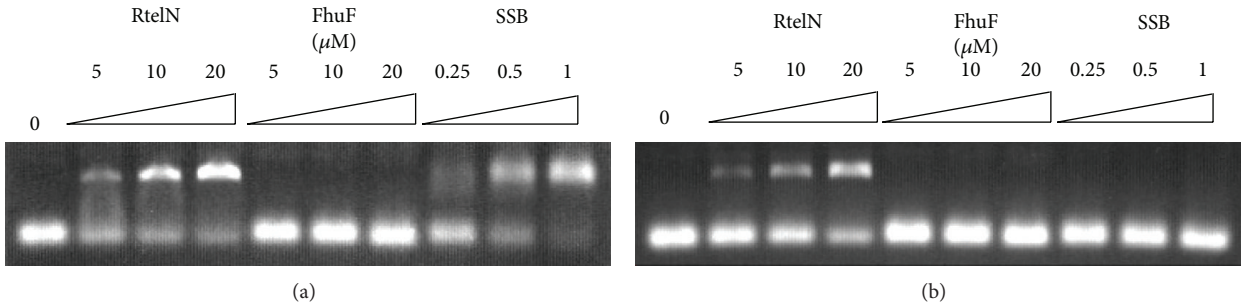

FIGURE 4: DNA binding activity of purified RtelN. (a) ssDNA binding activity of RtelN. A fluorescence-labeled ssDNA (0.5 μM) was incubated with the indicated amount of protein. FhuF is an iron-sulfur protein that has no DNA binding activity. SSB is *E. coli* ssDNA binding protein. The DNA-protein complex and free DNA probe were resolved on a 0.6% agarose gel. (b) dsDNA binding activity of RtelN. A fluorescence-labeled dsDNA (0.5 μM) was incubated with the indicated amount of protein. The DNA-protein complex and free DNA probe were resolved on a 0.6% agarose gel. The results are representatives of three independent experiments.

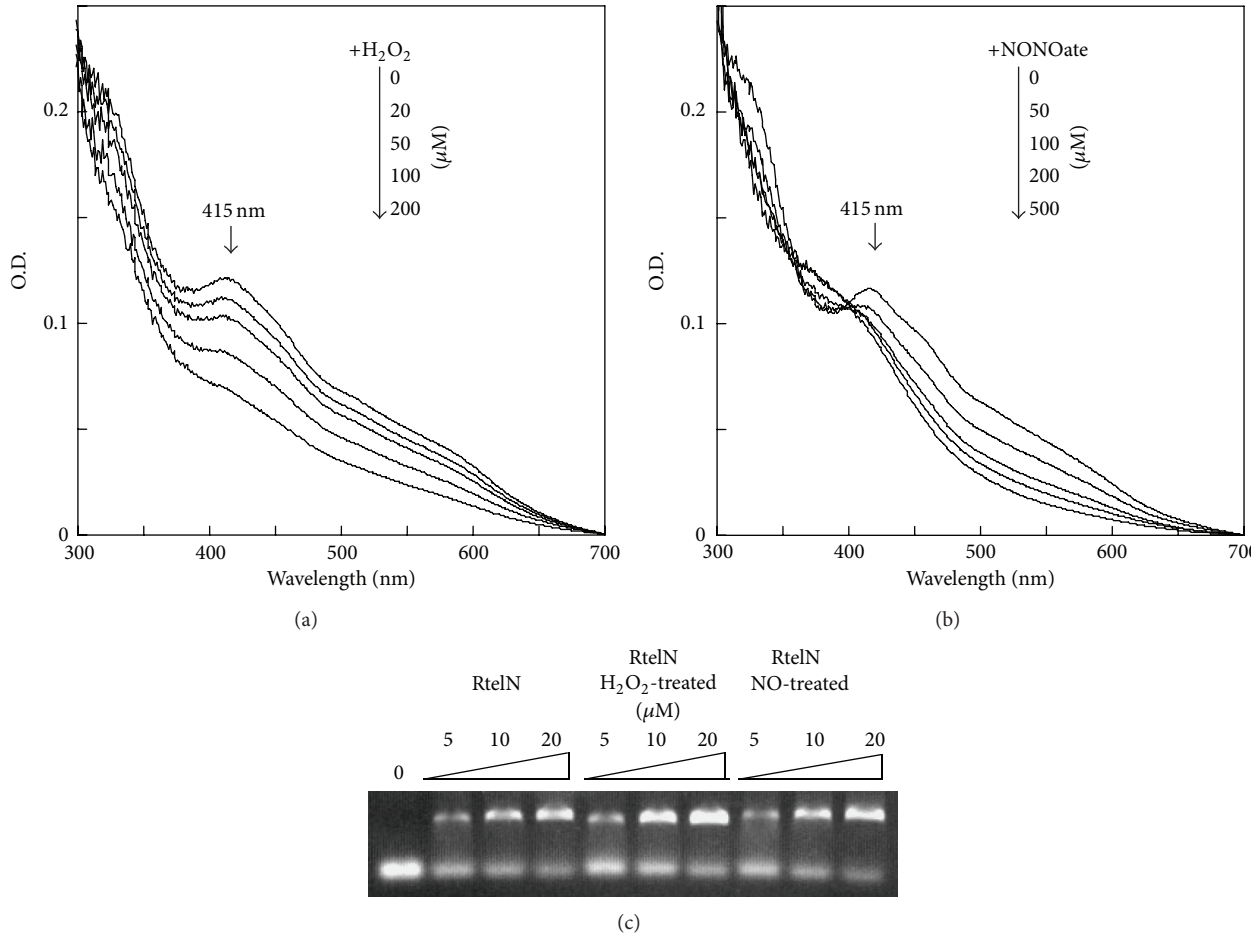

FIGURE 5: DNA binding activity of RtelN with modified iron-sulfur cluster. (a) Effect of H_2O_2 on the RtelN iron-sulfur cluster. RtelN (20 μM) was incubated with the indicated concentrations of H_2O_2 (0 to 200 μM) at room temperature for 30 min. The UV-visible spectra were taken after incubation. (b) Effect of NO on the RtelN iron-sulfur cluster. RtelN (20 μM) was incubated with the indicated concentrations of the NO releasing reagent diethylamine NONOate (0 to 500 μM) at 37°C for 10 min. The UV-visible spectra were taken after incubation. (c) ssDNA binding activity of RtelN after the iron-sulfur cluster was modified. Untreated RtelN and RtelN treated with 200 μM H_2O_2 or 500 μM NONOate were incubated with the fluorescence-labeled ssDNA (0.5 μM). The DNA-protein complex and free DNA probe were resolved on a 0.6% agarose gel. The results are representative of three independent experiments.

by intracellular reactive oxygen/nitrogen species. Therefore, modification of the iron-sulfur cluster in Rtel1 by reactive oxygen/nitrogen species could at least in part contribute to the telomere length of chromosomes in cells [38]. Evidently, additional experiments are required to illustrate the regulatory role of the iron-sulfur cluster in the human Rtel1 and other DNA helicases.

Abbreviations

EPR: Electron paramagnetic resonance
E_m: Midpoint redox potential
Rtel1: Human telomere length regulator
RtelN: The N-terminal domain of Rtel1
ssDNA: Single-stranded DNA
dsDNA: Double-stranded DNA.

Conflict of Interests

The authors declare that there is no conflict of interests regarding the publication of this paper.

Acknowledgment

This work was supported in part by the National Cancer Institute of the National Institute of Health Grant CA107494, the American Heart Association Grant 13GRNT16890014 (to HD), and the Louisiana Board of Regents Graduate Scholarship (to APL).

References

[1] T. de Lange, "How telomeres solve the end-protection problem," *Science*, vol. 326, no. 5955, pp. 948–952, 2009.

[2] A. Sfeir, S. T. Kosiyatrakul, D. Hockemeyer et al., "Mammalian telomeres resemble fragile sites and require TRF1 for efficient replication," *Cell*, vol. 138, no. 1, pp. 90–103, 2009.

[3] E. H. Blackburn, "Switching and signaling at the telomere," *Cell*, vol. 106, no. 6, pp. 661–673, 2001.

[4] H. Ding, M. Schertzer, X. Wu et al., "Regulation of murine telomere length by Rtel: an essential gene encoding a helicase-like protein," *Cell*, vol. 117, no. 7, pp. 873–886, 2004.

[5] Y. Jeffrey Chiang, R. T. Calado, K. S. Hathcock, P. M. Lansdorp, N. S. Young, and R. J. Hodes, "Telomere length is inherited with resetting of the telomere set-point," *Proceedings of the National Academy of Sciences of the United States of America*, vol. 107, no. 22, pp. 10148–10153, 2010.

[6] E. Uringa, J. L. Youds, K. Lisaingo, P. M. Lansdorp, and S. J. Boulton, "RTEL1: an essential helicase for telomere maintenance and the regulation of homologous recombination," *Nucleic Acids Research*, vol. 39, no. 5, pp. 1647–1655, 2011.

[7] C. Bai, B. Connolly, M. L. Metzker et al., "Overexpression of M68/DcR3 in human gastrointestinal tract tumors independent of gene amplification and its location in a four-gene cluster," *Proceedings of the National Academy of Sciences of the United States of America*, vol. 97, no. 3, pp. 1230–1235, 2000.

[8] A. J. Walne, T. Vulliamy, M. Kirwan, V. Plagnol, and I. Dokal, "Constitutional mutations in RTEL1 cause severe dyskeratosis congenita," *The American Journal of Human Genetics*, vol. 92, no. 3, pp. 448–453, 2013.

[9] B. J. Ballew, M. Yeager, K. Jacobs et al., "Germline mutations of regulator of telomere elongation helicase 1, RTEL1, in Dyskeratosis congenita," *Human Genetics*, vol. 132, no. 4, pp. 473–480, 2013.

[10] M. E. Fairman-Williams, U. P. Guenther, and E. Jankowsky, "SF1 and SF2 helicases: family matters," *Current Opinion in Structural Biology*, vol. 20, no. 3, pp. 313–324, 2010.

[11] M. F. White, "Structure, function and evolution of the XPD family of iron-sulfur-containing $5' \rightarrow 3'$ DNA helicases," *Biochemical Society Transactions*, vol. 37, no. 3, pp. 547–551, 2009.

[12] S. B. Cantor and S. Guillemette, "Hereditary breast cancer and the BRCA1-associated FANCJ/BACH1/BRIP1," *Future Oncology*, vol. 7, no. 2, pp. 253–261, 2011.

[13] J. A. Sommers, N. Rawtani, R. Gupta et al., "FANCJ uses its motor ATPase to destabilize protein-DNA complexes, unwind triplexes, and inhibit RAD51 strand exchange," *The Journal of Biological Chemistry*, vol. 284, no. 12, pp. 7505–7517, 2009.

[14] Y. Wu, J. A. Sommers, I. Khan, J. P. de Winter, and R. M. Brosh Jr., "Biochemical characterization of Warsaw breakage syndrome helicase," *Journal of Biological Chemistry*, vol. 287, no. 2, pp. 1007–1021, 2012.

[15] J. L. Youds, D. G. Mets, M. J. McIlwraith et al., "RTEL-1 enforces meiotic crossover interference and homeostasis," *Science*, vol. 327, no. 5970, pp. 1254–1258, 2010.

[16] L. J. Barber, J. L. Youds, J. D. Ward et al., "RTEL1 maintains genomic stability by suppressing homologous recombination," *Cell*, vol. 135, no. 2, pp. 261–271, 2008.

[17] M. F. White and M. S. Dillingham, "Iron-sulphur clusters in nucleic acid processing enzymes," *Current Opinion in Structural Biology*, vol. 22, no. 1, pp. 94–100, 2012.

[18] R. A. Pugh, M. Honda, H. Leesley et al., "The iron-containing domain is essential in Rad3 helicases for coupling of ATP hydrolysis to DNA translocation and for targeting the helicase to the single-stranded DNA-double-stranded DNA junction," *The Journal of Biological Chemistry*, vol. 283, no. 3, pp. 1732–1743, 2008.

[19] H. Liu, J. Rudolf, K. A. Johnson et al., "Structure of the DNA Repair Helicase XPD," *Cell*, vol. 133, no. 5, pp. 801–812, 2008.

[20] L. Fan, J. O. Fuss, Q. J. Cheng et al., "XPD helicase structures and activities: insights into the cancer and aging phenotypes from XPD mutations," *Cell*, vol. 133, no. 5, pp. 789–800, 2008.

[21] S. C. Wolski, J. Kuper, P. Hänzelmann et al., "Crystal structure of the FeS cluster-containing nucleotide excision repair helicase XPD," *PLoS Biology*, vol. 6, article e149, no. 6, 2008.

[22] J. Rudolf, V. Makrantoni, W. J. Ingledew, M. J. R. Stark, and M. F. White, "The DNA repair helicases XPD and FancJ have essential iron-sulfur domains," *Molecular Cell*, vol. 23, no. 6, pp. 801–808, 2006.

[23] B. Ren, X. Duan, and H. Ding, "Redox control of the DNA damage-inducible protein DinG helicase activity via its iron-sulfur cluster," *Journal of Biological Chemistry*, vol. 284, no. 8, pp. 4829–4835, 2009.

[24] J. T. P. Yeeles, R. Cammack, and M. S. Dillingham, "An iron-sulfur cluster is essential for the binding of broken DNA by AddAB-type helicase-nucleases," *The Journal of Biological Chemistry*, vol. 284, no. 12, pp. 7746–7755, 2009.

[25] R. E. Cowart, F. L. Singleton, and J. S. Hind, "A comparison of bathophenanthrolinedisulfonic acid and ferrozine as chelators of iron(II) in reduction reactions," *Analytical Biochemistry*, vol. 211, no. 1, pp. 151–155, 1993.

[26] L. M. Siegel, "A direct microdetermination for sulfide," *Analytical Biochemistry*, vol. 11, no. 1, pp. 126–132, 1965.

[27] R. D. Shereda, A. G. Kozlov, T. M. Lohman, M. M. Cox, and J. L. Keck, "SSB as an organizer/mobilizer of genome maintenance complexes," *Critical Reviews in Biochemistry and Molecular Biology*, vol. 43, no. 5, pp. 289–318, 2008.

[28] Z. Cheng, A. Caillet, B. Ren, and H. Ding, "Stimulation of Escherichia coli DNA damage inducible DNA helicase DinG by the single-stranded DNA binding protein SSB," *FEBS Letters*, vol. 586, no. 21, pp. 3825–3830, 2012.

[29] P. Leslie Dutton, "Redox potentiometry: determination of midpoint potentials of oxidation-reduction components of biological electron-transfer systems," *Methods in Enzymology*, vol. 54, pp. 411–435, 1978.

[30] G. Böhm, R. Muhr, and R. Jaenicke, "Quantitative analysis of protein far UV circular dichroism spectra by neural networks," *Protein Engineering*, vol. 5, no. 3, pp. 191–195, 1992.

[31] K. Müller, B. F. Matzanke, V. Schünemann, A. X. Trautwein, and K. Hantke, "FhuF, an iron-regulated protein of Escherichia coli with a new type of [2Fe-2S] center," *European Journal of Biochemistry*, vol. 258, no. 3, pp. 1001–1008, 1998.

[32] S. Jang and J. A. Imlay, "Micromolar intracellular hydrogen peroxide disrupts metabolism by damaging iron-sulfur enzymes," *The Journal of Biological Chemistry*, vol. 282, no. 2, pp. 929–937, 2007.

[33] A. P. Landry, X. Duan, H. Huang, and H. Ding, "Iron-sulfur proteins are the major source of protein-bound dinitrosyl iron complexes formed in Escherichia coli cells under nitric oxide stress," *Free Radical Biology and Medicine*, vol. 50, no. 11, pp. 1582–1590, 2011.

[34] D. R. Hyduke, L. R. Jarboe, L. M. Tran, K. J. Y. Chou, and J. C. Liao, "Integrated network analysis identifies nitric oxide response networks and dihydroxyacid dehydratase as a crucial target in Escherichia coli," *Proceedings of the National Academy of Sciences of the United States of America*, vol. 104, no. 20, pp. 8484–8489, 2007.

[35] Y. Wu and R. M. Brosh Jr., "DNA helicase and helicase-nuclease enzymes with a conserved iron-sulfur cluster," *Nucleic Acids Research*, vol. 40, no. 10, pp. 4247–4260, 2012.

[36] C. T. Dooley, T. M. Dore, G. T. Hanson, W. C. Jackson, S. J. Remington, and R. Y. Tsien, "Imaging dynamic redox changes in mammalian cells with green fluorescent protein indicators," *Journal of Biological Chemistry*, vol. 279, no. 21, pp. 22284–22293, 2004.

[37] J. M. Hansen, Y. M. Go, and D. P. Jones, "Nuclear and mitochondrial compartmentation of oxidative stress and redox signaling," *Annual Review of Pharmacology and Toxicology*, vol. 46, pp. 215–234, 2006.

[38] J. M. J. Houben, H. J. J. Moonen, F. J. van Schooten, and G. J. Hageman, "Telomere length assessment: biomarker of chronic oxidative stress?" *Free Radical Biology and Medicine*, vol. 44, no. 3, pp. 235–246, 2008.

Hindawi Publishing Corporation
BioMed Research International
Volume 2014, Article ID 195162, 14 pages
http://dx.doi.org/10.1155/2014/195162

Review Article

Structural Insight into the DNA-Binding Mode of the Primosomal Proteins PriA, PriB, and DnaT

Yen-Hua Huang[1] and Cheng-Yang Huang[1,2]

[1] *School of Biomedical Sciences, Chung Shan Medical University, No. 110, Section 1, Chien-Kuo N. Road, Taichung City 40201, Taiwan*
[2] *Department of Medical Research, Chung Shan Medical University Hospital, No. 110 Section 1, Chien-Kuo N. Road, Taichung City 40201, Taiwan*

Correspondence should be addressed to Cheng-Yang Huang; cyhuang@csmu.edu.tw

Received 18 April 2014; Revised 20 June 2014; Accepted 1 July 2014; Published 21 July 2014

Academic Editor: Yoshito Abe

Replication restart primosome is a complex dynamic system that is essential for bacterial survival. This system uses various proteins to reinitiate chromosomal DNA replication to maintain genetic integrity after DNA damage. The replication restart primosome in *Escherichia coli* is composed of PriA helicase, PriB, PriC, DnaT, DnaC, DnaB helicase, and DnaG primase. The assembly of the protein complexes within the forked DNA responsible for reloading the replicative DnaB helicase anywhere on the chromosome for genome duplication requires the coordination of transient biomolecular interactions. Over the last decade, investigations on the structure and mechanism of these nucleoproteins have provided considerable insight into primosome assembly. In this review, we summarize and discuss our current knowledge and recent advances on the DNA-binding mode of the primosomal proteins PriA, PriB, and DnaT.

1. Introduction

Genome integrity should be maintained from generation to generation to ensure proper cell function and survival [1–3]. In bacteria, some exogenous and endogenous sources of DNA damage can inactivate a large proportion of replication forks [4, 5]. When DNA is damaged, the replication machinery, originally initiated at *oriC*, can be arrested and disassembled anywhere along the DNA, leading to replication failure [5, 6]. To reload DnaB helicase for *oriC*-independent DNA replication, collapsed DNA replication forks must be reactivated by the replication restart primosome [7, 8]. Primosome is the protein complex responsible for the conversion of single-stranded circular DNA to the replicative-form DNA in the replication cycle of ϕX174 phage [9, 10]. After DNA repair, the replication restart primosome [11–13], a formidable enzymatic machine, can translocate along the single-stranded DNA-binding protein (SSB), unwind the duplex DNA, and prime the Okazaki fragments required for the progression of replication forks [14]. In *Escherichia coli*, the replication restart primosome is composed of PriA helicase, PriB, PriC, DnaB helicase, DnaC, DnaT, and DnaG primase [3]. To date, two DnaB helicase-recruiting pathways are known: PriA-PriB-DnaT-DnaC-dependent and PriC-DnaC-dependent systems; the former system uses fork structures without gaps in the leading strand, whereas the latter system preferentially uses fork structures with large gaps (>5 nucleotides) in the leading strand [3]. As shown in Figure 1, PriA can bind directly and assemble a primosome on the template without gaps in the leading strand, and PriC initiates the assembly of a primosome on a fork containing gaps in the leading strand.

A hand-off mechanism for PriA-directed primosome assembly [15] has been proposed (Figure 2), whereby (i) PriA recognizes and binds to a replication fork; (ii) PriB joins PriA to form a PriA-PriB-DNA ternary complex; (iii) DnaT participates in this nucleocomplex to form a triprotein complex, in which PriB is released from ssDNA due to recruitment of DnaT; (iv) the PriA-PriB-DnaT-DNA quaternary complex

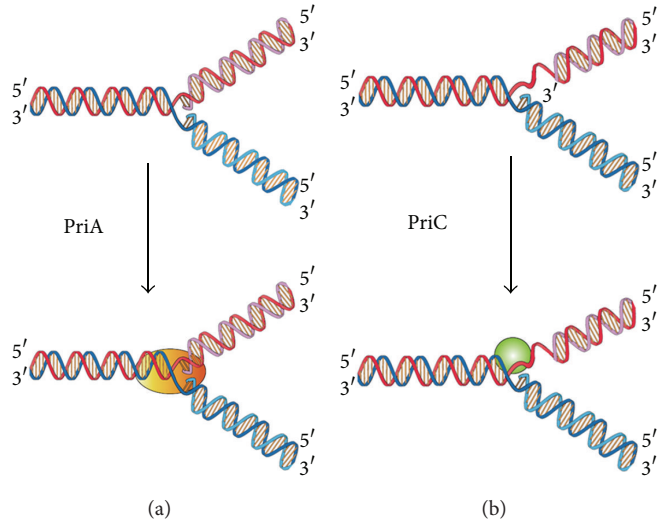

Figure 1: Two DnaB helicase-recruiting pathways for DNA replication restart at the stalled replication fork in vitro. The PriA-directed pathway (i.e., PriA-PriB-DnaT-DnaC-dependent reaction) preferentially uses fork structures without gaps in the leading strand, whereas the PriC-directed pathway (i.e., PriC-DnaC-dependent system) preferentially uses fork structures containing large gaps (>5 nucleotides) in the leading strand.

loads the DnaB/C complex; (v) DnaB is loaded on the lagging strand template. Genetic analyses suggest that these primosomal proteins are essential replication proteins for bacterial cell growth [12, 16–21]. These proteins are required for reinitiating chromosomal DNA replication in bacteria; thus, blocking their activities would be detrimental to bacterial survival [22, 23]. Several primosomal proteins, such as PriA, PriB, PriC, and DnaT, are not found in humans; thus, these proteins may be potential targets in developing antibiotics for the six antibiotic-resistant pathogens (*Enterococcus faecium*, *Staphylococcus aureus*, *Klebsiella pneumoniae*, *Acinetobacter baumannii*, *Pseudomonas aeruginosa*, and *Enterobacter* sp.) [24, 25]. The recently discovered inhibitor CGS 15943 targets *Neisseria gonorrhoeae* PriA helicase with an IC_{50} of 114 ± 24 μM [26].

Over the past 10 years, considerable progress has been made in the structural mechanisms of the replication restart primosome assembly. The structural information is a prerequisite for formulating any model of the assembly mechanism of the primosome (Table 1). In the following sections, we summarize and discuss our current knowledge and recent advances on the DNA-binding mode of the primosomal proteins PriA, PriB, and DnaT.

2. Structural Insights into the DNA-Binding Mode

2.1. PriA Helicase. PriA functions as a scaffold that recruits other primosomal proteins. It was originally discovered as an essential factor for the conversion of single-stranded circular DNA to the replicative-form DNA of ϕX174 single-stranded phage in vitro [27]. The *priA* mutant of *E. coli* exhibits complex phenotypes that include reduced viability, chronic induction of SOS response, rich media sensitivity, decreased homologous recombination, sensitivity to UV irradiation, defective double-stranded break repair, and both induced and constitutive stable DNA replication [6, 12, 28–30]. The native PriA is a monomer with a molecular mass of ~82 kDa. The tertiary structure of the monomer contains two functional domains, namely, the helicase domain (HD), which encompasses ~540 amino acid residues from the C-terminus, and the DNA-binding domain, which comprises ~181 amino acid residues from the N-terminus [31–33]. PriA is a DEXH-type helicase that unwinds DNA with a 3′ to 5′ polarity [34]. Fuelled by the binding and hydrolysis of ATP, PriA moves along the nucleic acid filaments with other primosomal proteins and separates double-stranded DNA into their complementary single strands [35]. PriA preferentially binds to a D-loop-like structure by recognizing a bend at the three-way branched DNA structures and duplex DNA with a protruding 3′ single strand [32, 36, 37]. PriA interacts with SSB [38], PriB [15, 39, 40], and DnaT [15]. PriA can unwind the nascent lagging strand DNA to create a suitable binding site to help PriC load the DnaB helicase onto stalled replication forks where a gap exists in the nascent leading strand [41, 42]. The crystal structures of the N-terminal 105 amino acid residue segment of *E. coli* PriA (EcPriA) in complex with different deoxydinucleotides show a feasible interaction model for the base-non-selective recognition of the 3′-terminus of DNA between the nucleobase and the DNA-binding sites of EcPriA [43].

Figure 3(a) shows that the alignment consensus of 150 sequenced PriA homologs by ConSurf [44] reveals the degree of variability at each position along the primary sequence. The highly variable amino acid residues are colored teal, whereas the highly conserved are colored burgundy. A consensus sequence was established by determining the most commonly found amino acid residue at each position relative to the primary sequence of *K. pneumoniae* PriA (KpPriA).

Table 1: List of the structures of the primosomal proteins available in Protein Data Bank.

	PDB ID	X-ray	NMR	Length
PriA	2D7E	The N-terminal domain of *Escherichia coli* PriA		105
	2DwN	The N-terminal domain of *Escherichia coli* PriA bound to AG		105
	2D7G	The N-terminal domain of *Escherichia coli* PriA bound to AA		105
	2D7H	The N-terminal domain of *Escherichia coli* PriA bound to CCC		105
	2Dwl	The N-terminal domain of *Escherichia coli* PriA bound to AC		105
	2Dwm	The N-terminal domain of *Escherichia coli* PriA bound to AT		105
	4NL4	*Klebsiella pneumoniae* PriA bound to ADP		731
	4NL8	*Klebsiella pneumoniae* PriA bound to SSB C-terminal tail peptide		731
PriB	2CCZ	*Escherichia coli* PriB bound to ssDNA (15 mer)		104
	1V1Q	*Escherichia coli* PriB		104
	1WOC	*Escherichia coli* PriB		100
	1TXY	*Escherichia coli* PriB		100
	2PNH	*Escherichia coli* PriB E39A		100
	4APV	*Klebsiella pneumoniae* PriB		102
	3K8A	*Neisseria gonorrhoeae* PriB		100
	4FDB	*Ralstonia solanacearum* PriB		99
	3EN2	*Ralstonia solanacearum* PriB		95
	3FHW	*Bordetella parapertussis* PriB		102
	3KLW	*Bordetella pertussis* PriB		98
	4GS3	The N-terminal domain of *Thermoanaerobacter tengcongensis* PriB		104
DnaT		None		
DnaB	4ESV	*Geobacillus stearothermophilus* DnaB bound to DNA (14 mer)		441
	2R6E	*Geobacillus stearothermophilus* DnaB		441
	2R6D	*Geobacillus stearothermophilus* DnaB		441
	2R6A	*Geobacillus stearothermophilus* DnaB bound to DnaG		441
	2R6C	*Geobacillus stearothermophilus* DnaB bound to DnaG		441
	4M4W	*Geobacillus stearothermophilus* DnaB bound to DnaG and DnaI		454
	2R5U	The N-terminal domain of *Mycobacterium tuberculosis* DnaB		167
	2Q6T	*Thermus aquaticus* DnaB		440
	3GXV	The N-terminal domain of *Helicobacter pylori* DnaB		121
	4A1F	The C-terminal domain of *Helicobacter pylori* DnaB		323
	4NMN	*Aquifex aeolicus* DnaB bound to ADP		434
	2VYF	*Geobacillus kaustophilus* DnaC		441
	2VYE	*Geobacillus kaustophilus* DnaC bound to ssDNA (9 mer)		441
	1B79	The N-terminal domain of *Escherichia coli* DnaB		128
	1JWE		The N-terminal domain of *Escherichia coli* DnaB	114
DnaC	3EC2	*Aquifex aeolicus* DnaC 42–221		180
	3ECC	*Aquifex aeolicus* DnaC bound to ADP	The N-terminal domain of *Bacillus subtilis* DnaI	185
	2W58	*Geobacillus kaustophilus* DnaI		199
	4M4W	*Geobacillus stearothermophilus* DnaB bound to DnaG and DnaI		278

Table 1: Continued.

	PDB ID	X-ray	NMR	Length
	2QGZ	*Streptococcus pyogenes* DnaI		308
	2K7R			106
DnaG	3B39	*Escherichia coli* DnaG 109–427 bound to ssDNA (15 mer)		321
	1DD9	*Escherichia coli* DnaG 115–428		338
	1DDE	*Escherichia coli* DnaG 115–428		338
	1T3W	The C-terminal domain of *Escherichia coli* DnaG		148
	2HAJ		*Escherichia coli* DnaG 447–581	135
	4E2K	*Staphylococcus aureus* DnaG 108–428		321
	4EDG	*Staphylococcus aureus* DnaG 108–428 bound to ATP		321
	4EDK	*Staphylococcus aureus* DnaG 108–428 bound to GTP		319
	4EDT	*Staphylococcus aureus* DnaG 108–428 bound to ppGpp		321
	4EDV	*Staphylococcus aureus* DnaG 108–428 bound to ppGpp		321
	4EE1	*Staphylococcus aureus* DnaG 108–428 bound to CTP		321
	4EDR	*Staphylococcus aureus* DnaG 108–428 bound to UTP		321
	2LZN		*Staphylococcus aureus* DnaG 462-605	143
	1Z8S		*Bacillus stearothermophilus* DnaG 452–597	146
	4EHS	The C-terminal domain of *Helicobacter pylori* DnaG 438–559		122
	4M4W	*Geobacillus stearothermophilus* DnaB bound to DnaI and DnaG		143
	2R6A	*Geobacillus stearothermophilus* DnaB bound to DnaG		143
	2R6C	*Geobacillus stearothermophilus* DnaB bound to DnaG		143
	2AU3	*Aquifex aeolicus* DnaG 1–403		403
PriC	2RT6		The N-terminal domain of *Escherichia coli* PriC	98

Length and amino acid residues.

The amino acid sequences of KpPriA and EcPriA share 88% identity [45]. The N-terminal 19–219 amino acid residues in PriA are not highly conserved. The crystal structure of KpPriA has been recently determined [45]. KpPriA has six subdomains (Figure 3(b)), namely, a 3′ DNA-binding domain (3′BD; orange), a winged-helix domain (WH; green), two lobes of the helicase core (colored hot pink and blue, resp.), a Cys-rich region (CRR; dark blue), and a C-terminal domain (CTD; red). The 3′BD and WH comprise the N-terminal DNA-binding domain (DBD), and the other four subdomains (two lobes of the helicase core, CRR, and CTD) comprise the HD. Asp17, located in the 3′BD of EcPriA, is crucial for the 3′ base-non-selective recognition of DNA [43], and Arg697, located in the CTD of KpPriA, is crucial for the C-terminal tail of SSB (SSB-Ct) binding and induction of structural changes in the SSB-DNA complex [45]; both are significantly invariable. Many biochemical and genetic studies have been performed on the DNA-binding mode of PriA [7, 8], but the structural basis for the full length PriA-DNA complex is still lacking.

To elucidate the structural mechanism of DNA binding and unwinding by PriA, Bhattacharyya et al. [45] compared the structure of the full length KpPriA with those of other DNA helicases of superfamily II, namely, RecQ1 (Protein Data Bank entry: 2WWY) [46, 47] and Hel308 (Protein Data Bank entry: 2P6R) [48]. The structures of these helicases have been solved in complex with substrate DNA. RecQ1 and Hel308 bind to single-stranded DNA tailed duplex and unwind via the DNA unwinding wedge element, a prominent β-hairpin for strand separation [47, 49]. PriA also shares sequence similarity with other helicases, such as PcrA (Protein Data Bank entry: 3PJR) [50], a DNA helicase of superfamily I, and RecG (Protein Data Bank entry: 1GM5) [51], a DNA helicase of superfamily II. The structures of

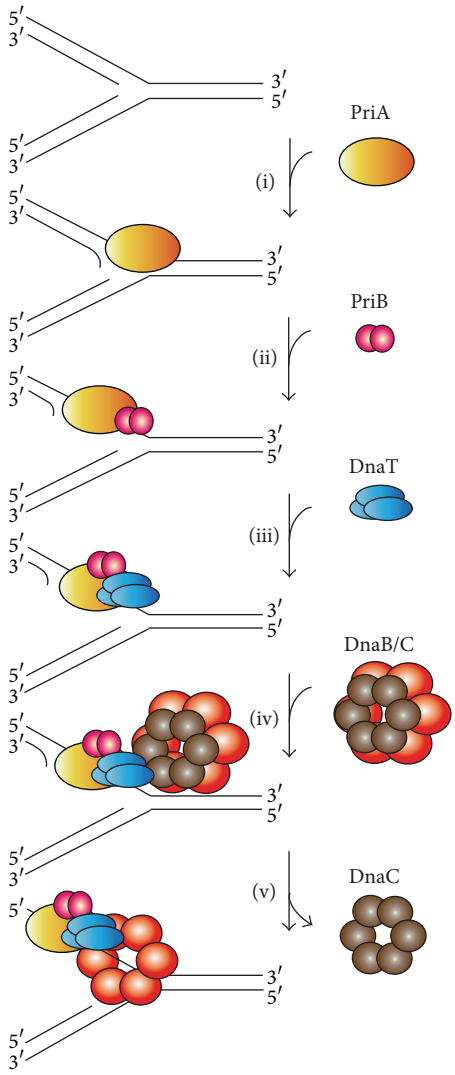

FIGURE 2: A hand-off mechanism for the replication restart primosome assembly. The proposed assembly mechanism is as follows. (i) PriA recognizes and binds to a replication fork, (ii) PriB joins PriA to form a PriA-PriB-DNA ternary complex, (iii) DnaT participates in this nucleocomplex to form a triprotein complex, in which PriB is released from ssDNA due to recruitment of DnaT, (iv) the PriA-PriB-DnaT-DNA quaternary complex loads the DnaB/C complex, and (v) DnaB is loaded on the lagging strand template.

these helicases bound to DNA, along with KpPriA, are shown in Figure 3(c) for comparison. According to the crystal structures of the helicase-DNA complex, the two lobes of the helicase core of KpPriA (colored hot pink and blue, resp.) are aligned and manually superimpose the location of the dsDNA from the complex structure with KpPriA structure. These modeled structures of KpPriA show that the DNA-binding modes and thus the DNA-unwinding modes are different. Considering the known ssDNA-binding site at DBD and the putative wedge element in KpPriA located at CRR, KpPriA may use the Hel308-based model to bind DNA. The DNA-binding mode, fork DNA recognition site(s), and the helicase translocation using either the inchworm stepping or Brownian motor mechanism [52] must be further confirmed by additional biophysical and structural studies.

2.2. PriB Protein. PriB is a basic accessory protein in PriA-directed DNA replication restart primosome [11, 13]. It was originally discovered as an essential factor for the conversion of single-stranded circular DNA to the replicative-form DNA of ϕX174 single-stranded phage in vitro. In contrast to the ϕX174 model, *del(priB)302* mutant has almost wild-type phenotypes [53], suggesting that PriB is not absolutely required for bacterial DNA replication. PriB was formerly known as the "n protein" because it can be inactivated by treatment with *N*-ethylmaleimide [54]. In a PriA-PriB-DnaT-dependent reaction, PriB is the second protein to be assembled in the protein-DNA complex. It stabilizes the binding of PriA to DNA hairpin [35, 55] and then stimulates PriA helicase activity [40, 56]. The PriA stimulation by PriB correlates with the ability of PriB to form a stable PriA-PriB-DNA complex [40]. PriB also facilitates the association of DnaT with PriA [57]. More than one PriA-PriB complex is possibly involved in the initiation of primosome formation, and the effect of PriB on the PriA-DNA association is dependent on the DNA structure [58]. PriB interacts with PriA [15, 39], DnaT [15, 59, 60], SSB [54, 61], and itself [61, 62] and does not interact with DnaA, DnaB, DnaC, or DnaG [61]. The mechanisms of DnaC-DnaB complex loading by PriA-PriB-DnaT complex at the forks and then DnaB-DnaG complex formation remain unclear.

PriB is a homodimer with polypeptide chains of 104 amino acid residues [63–65] (Figure 4(a)). Each PriB monomer has an oligonucleotide/oligosaccharide-binding (OB) fold structure [66–69] with three flexible β-hairpin loops: L_{12} (residues 20–24), L_{23} (residues 37–44), and L_{45} (residues 81–88) (Figure 4(b)). PriB can bind to ssDNA [15, 39, 40, 54, 56, 62–65, 70–73], ssRNA [65], double-stranded DNA [56, 70], and circular ϕX viral DNA [73]. Although PriB is a dimer, it has only one DNA-binding site [73], which is located in loop L_{45} centrally within the dimer, and this site occupies a total site size of 12 ± 1 nucleotides [72]. The N-terminal 1–49 amino acid residue region of PriB is crucial for dimerization, whereas the C-terminal 50–104 amino acid residue region is crucial for ssDNA binding [71]. PriB shares structural similarity with the N-terminal DNA-binding domain of the *E. coli* SSB (EcSSB) [63–65, 74, 75]. Sequence comparisons and operon organization analyses also show that PriB evolves from the duplication of the SSB gene [76], but they differ in their ssDNA-binding properties and strategies [70, 73]. For example, EcSSB possesses three conserved aromatic residues (Trp40, Trp54, and Phe60) in the L_{45} loop of the OB fold. These residues serve important functions in ssDNA binding. Two of these residues (Trp40 and Phe60 in EcSSB) are replaced with nonconserved amino acids in the PriB family. In contrast to the EcSSB-DNA complex, the L_{23} loop from each subunit of PriB makes a close contact with the β-barrel core. The longer and extended L_{23} loops in EcSSB greatly increase the interactions between EcSSB and ssDNA [73, 75].

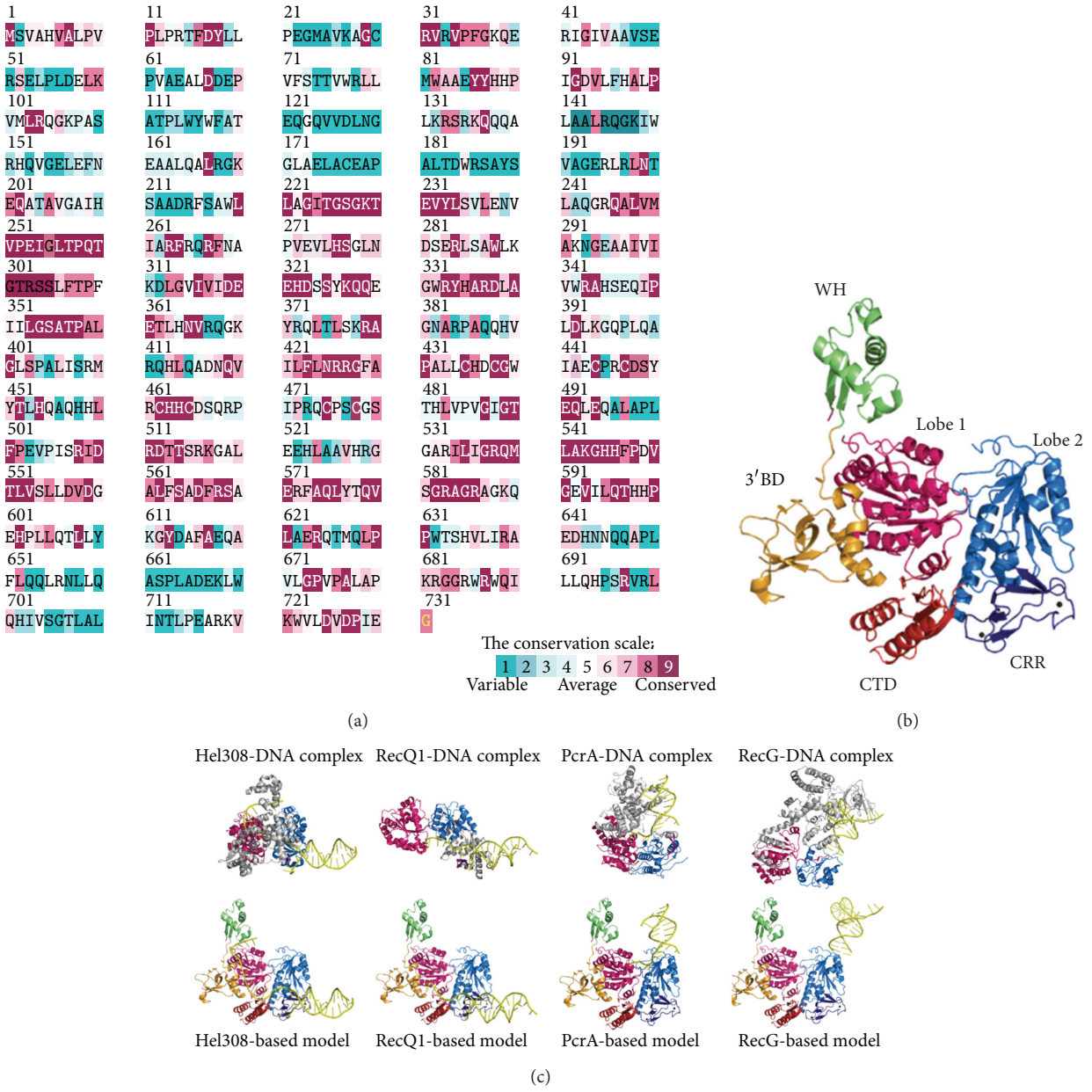

Figure 3: (a) Amino acid sequence alignment of KpPriA. An alignment consensus of 150 sequenced PriA homologs by the program ConSurf reveals the degree of variability at each position along the primary sequence. Highly variable amino acids are colored teal, whereas those highly conserved are colored burgundy. A consensus sequence was established by determining the most commonly found amino acid residue at each position relative to the primary sequence of KpPriA. The N-terminal 19–219 amino acid residues in PriA are not highly conserved. Asp17, located in the 3′BD of EcPriA, is crucial for the 3′ base-non-selective recognition of DNA, and Arg697, located in the CTD of KpPriA, is crucial for the SSB-Ct binding and induction of structural changes in the SSB-DNA complex; both are significantly invariable. (b) Crystal structure of KpPriA. KpPriA has six subdomains (Protein Data Bank entry: 4NL4), namely, a 3′ DNA-binding domain (3′BD; orange), a winged-helix domain (WH; green), two lobes of the helicase core (colored hot pink and blue, resp.), a Cys-rich region (CRR; dark blue), and a C-terminal domain (CTD; red). 3′BD and WH comprise the N-terminal DNA-binding domain (DBD), and the other four subdomains (two lobes of the helicase core, CRR, and CTD) comprise the helicase domain (HD). (c) Putative DNA-binding mode of KpPriA. The DNA-binding models of KpPriA are directly constructed by manually superimposing the KpPriA with DNA-bound crystal structure of Hel308 (Protein Data Bank entry: 2P6R), RecQ1 (Protein Data Bank entry: 2WWY), PcrA (Protein Data Bank entry: 3PJR), and RecG (Protein Data Bank entry: 1GM5). Considering the known ssDNA-binding site at DBD and the putative wedge element in KpPriA located at CRR, KpPriA may use the Hel308-based model to bind DNA. The β-hairpin, an important motif for DNA strand separation by helicase, is colored in magenta.

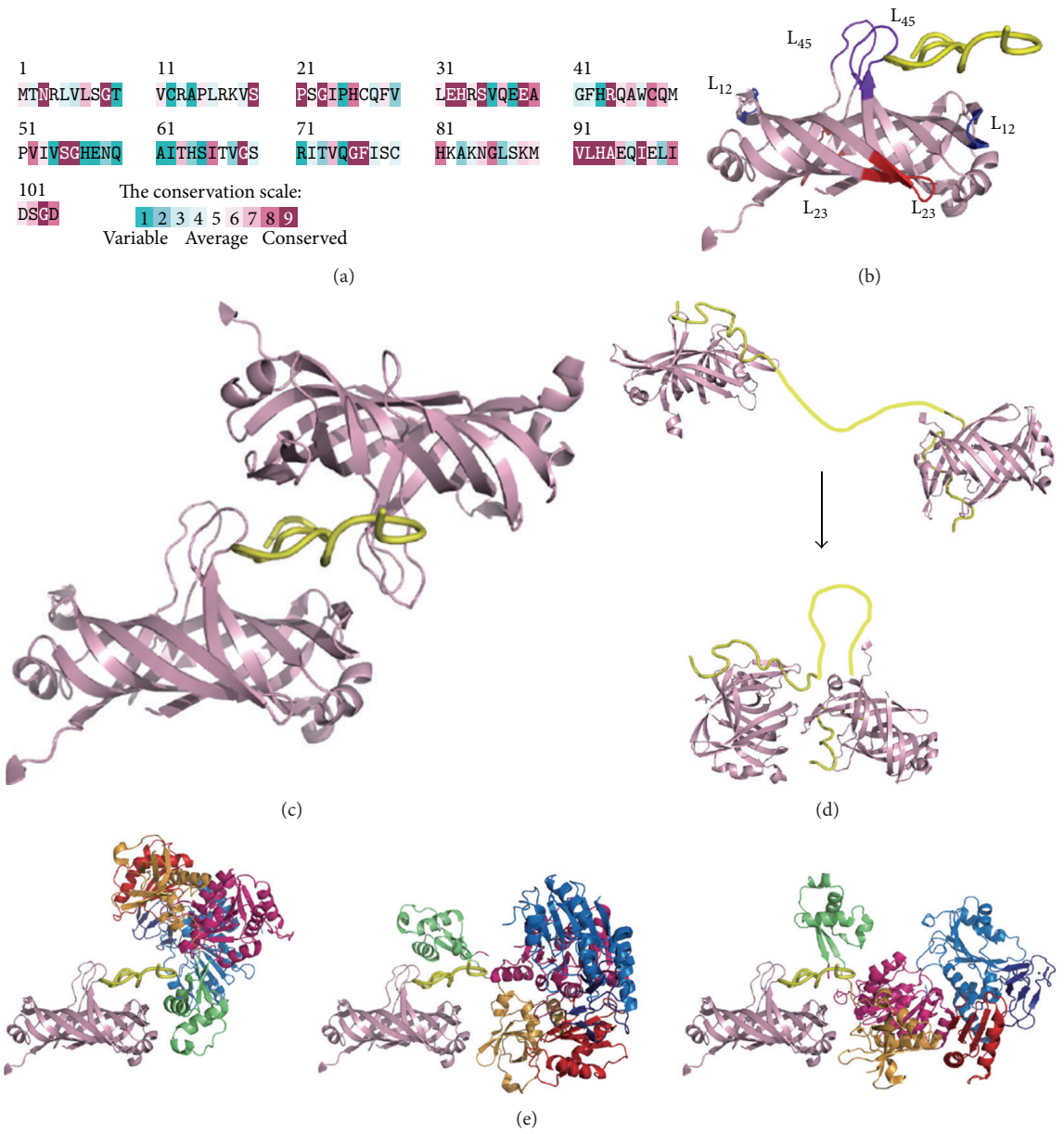

FIGURE 4: (a) Amino acid sequence alignment of EcPriB. An alignment consensus of 111 sequenced PriB homologs by the program ConSurf reveals the degree of variability at each position along the primary sequence. In general, the overall amino acid sequences among PriB proteins are not highly conserved, including many residues found important for ssDNA binding by EcPriB, such as Phe42, Trp47, Lys82, Lys84, and Lys89. (b) EcPriB is a homodimer with polypeptide chains of 104 amino acid residues. Each PriB monomer has an OB-fold structure with three flexible β-hairpin loops: L_{12} (residues 20–24; colored in blue), L_{23} (residues 37–44; colored in red), and L_{45} (residues 81–88; colored in purple blue). The ssDNA in the complex is shown in gold. (c) Crystal structure of EcPriB in complex with DNA. The complex structure of EcPriB (Protein Data Bank entry: 2CCZ) shows that a single dT15 ssDNA periodically interacts with two OB folds from two symmetrically related EcPriB dimers in the crystal and that the DNA is sandwiched by PriB dimers via their L_{45} loops. (d) Possible working model of interaction between two PriB proteins on ssDNA. PriB proteins cooperatively bind to ssDNA in two steps: two PriB proteins independently interact with ssDNA and then interact with each other through His64 on the ssDNA. The ssDNA in the complex is shown in gold. The region in ssDNA that does not directly interact with PriB, proposed in this two-step binding model, is colored in yellow. (e) Proposed models for PriA-DNA-PriB structure. These models are based on these observations: (1) two PriB dimers are complexed with a single dT15; (2) PriA has a highly electropositive ssDNA-binding region in DBD, and the basic DBD in PriA may be involved in complex with PriB; (3) DBD of PriA alone in solution forms a dimer and not a monomer as the full-length PriA.

Figure 4(a) shows the alignment consensus of 111 sequenced PriB homologs by ConSurf [44]. The alignment indicates that the overall amino acid sequences among PriB proteins are not highly conserved; only 21 amino acid residues are significantly conserved: Asn3, Gly9, Ser20, Pro21, Gly23, Glu32, His33, Ser35, Glu39, Arg44, Ser55, Gly56, Gly69, Gly76, Phe77, Val91, Leu92, His93, Ala94, Ile97, and Gly103. Many residues important for ssDNA binding by *E. coli* PriB (EcPriB), such as Phe42 [64], Trp47 [64, 73], Lys82 [64, 73], Lys84 [73], and Lys89 [73], are not conserved. PriB may be a nonessential facilitating factor in DNA replication restart [53], and many prokaryotic genomes do not contain a recognizable homolog of *priB* [39]. Hence, we speculate that these residues among PriB proteins for binding ssDNA do not need to be precisely conserved.

We previously described the crystal structure of EcPriB in complex with ssDNA dT15 (Protein Data Bank entry: 2CCZ) [73]. A single dT15 ssDNA periodically interacts with two OB folds from two symmetrically related EcPriB dimers in the crystal, sandwiched by PriB dimers via their L_{45} loops (Figure 4(c)). Although the precise function of more than one PriB self-assembled on DNA to form a high-density nucleoprotein complex is still unclear, PriB binds DNA with strong cooperativity [70, 72, 73] in two steps (Figure 4(d)): two PriB proteins independently interact with ssDNA in primary binding mode, and then the proteins interact with each other through His64 on the ssDNA [77]. Whether the resultant ssDNA bound by more than one PriB forms a unique structure suitable for further assembly process for the primosome is not clearly known. The complex structure [73] and the thermodynamic analysis [72] indicate that the PriB dimer behaves like a protein with half-site reactivity, where only one monomer of the PriB dimer can engage in interactions with the DNA and the partner protein. The importance of the binding site on PriB for ssDNA to overlap the binding sites for PriA and DnaT needs to be investigated [15]. Each preprimosome may contain two PriB dimers [60]; whether or not this cocrystal structure, in which two PriB dimers are complexed with a single dT15 ssDNA, is an artificial or an actual binding mode for ssDNA by PriB also remains unclear. PriA may have a function similar to a monomer of the symmetrical PriB dimer in the crystal to stabilize the partially disordered ssDNA because the cooperation between PriB and PriA may be necessary to form a stable PriA-DNA-PriB complex. That is, the PriB-ssDNA-PriB complex (Figure 4(c)) may mimic the structure of the PriA-ssDNA-PriB complex (Figure 4(e)). We proposed three binding ways by use of the crystal structures of PriA and PriB. EcPriA has a highly electropositive ssDNA-binding region (amino acid residues 1–198) containing 8 Lys and 14 Arg residues in DBD; thus, the basic DBD in EcPriA may be involved in complex with EcPriB [73]. The DBD of EcPriA alone in solution forms a dimer and not a monomer as EcPriA [31], suggesting that another unknown stabilization factor is needed. The DBD of PriA and one of the monomers of PriB may bind to ssDNA cooperatively to decrease the dissociation rate of PriA from the DNA during helix unwinding [73]. The crystal structure of PriA in complex with PriB and DNA is necessary to elucidate the assembly mechanism of the replication restart primosome.

More than a mere ssDNA-binding protein, PriB can bind both ssDNA and dsDNA with comparable affinity [70]. SSB can also bind dsDNA but with far less affinity than ssDNA [78]. According to the crystal structures of some dimeric proteins complexed with dsDNA found in the Protein Data Bank, PriB binds dsDNA in three possible ways (Figure 5). First, PriB may bind to dsDNA via the replication terminator protein- (RTP-) binding mode (Protein Data Bank entry: 1F4K) [79]. RTP, a dimeric WH protein [80, 81], uses two recognition helices to bind the major grooves of dsDNA. The PriB dimer also has two helices but does not contain any aromatic or positively charged residues as RTP. Thus, PriB binds to dsDNA via the RTP-binding mode that can be ruled out. Second, PriB may bind to dsDNA via the HU-binding mode (Protein Data Bank entry: 1P51) [82, 83]. HU is a dimeric nucleoid-associated protein that mainly uses two β sheets to bind dsDNA. Third, PriB may bind dsDNA in a manner similar to binding ssDNA. The structure-based mutational analysis indicates that the residues in PriB crucial for ssDNA binding are also crucial for dsDNA binding [70]. These residues responsible for ssDNA and dsDNA binding are almost overlapped; thus, PriB may use a similar approach to bind to the phosphate backbone of ssDNA and dsDNA through several positively charged residues. This phenomenon may be the reason for the comparable binding affinities of PriB to ssDNA and dsDNA. We speculate that, during evolution [76], the conserved aromatic and other residues in the L_{45} loop of the OB fold in SSB are changed into nonconserved and positively charged residues in PriB to more precisely fit the requirement for assembly of the replication restart primosome at the stalled DNA forks.

2.3. DnaT Protein. DnaT is an essential protein in the assembly of the PriA-directed DNA replication restart primosome [6, 11–13, 15, 55, 57]. It provides a specific recognition site for loading the replicative DnaB helicase during the promosome assembly [15, 42]. DnaT, formerly known as the "protein i" [84–86], was originally discovered as a critical factor for the conversion of single-stranded circular DNA to the replicative-form DNA of ϕX174 single-stranded phage [9] and pBR322 plasmid replication, but not for R1 plasmid replication [87]. Genetic analysis for *E. coli* DnaT suggests that a replication protein is essential for bacterial cell growth because the colony size, cell morphology, inability to properly partition nucleoids, UV sensitivity, and basal SOS expression of the *dnaT822* mutant are similar to those of *priA2::kan* mutants [18]. DnaT is required for *E. coli* growth at elevated pressure [88] and for the lytic cycle of Mu growth [89]. DnaT is a homotrimer of ~22 kDa subunits [86, 90], but it also exists in solution as a monomer-trimer equilibrium system [91]. In a PriA-PriB-DnaT-dependent reaction, DnaT is the third protein to be assembled in the protein-DNA complex (Figure 2). The association of DnaT with PriA is facilitated by PriB [57]. Although the function of DnaT in the recruitment of DnaB helicase has been proposed, the fundamental function of DnaT for the replication restart primosome assembly is not widely known.

We have recently identified and characterized that DnaT is a ssDNA-binding protein [90]. Based on the alignment

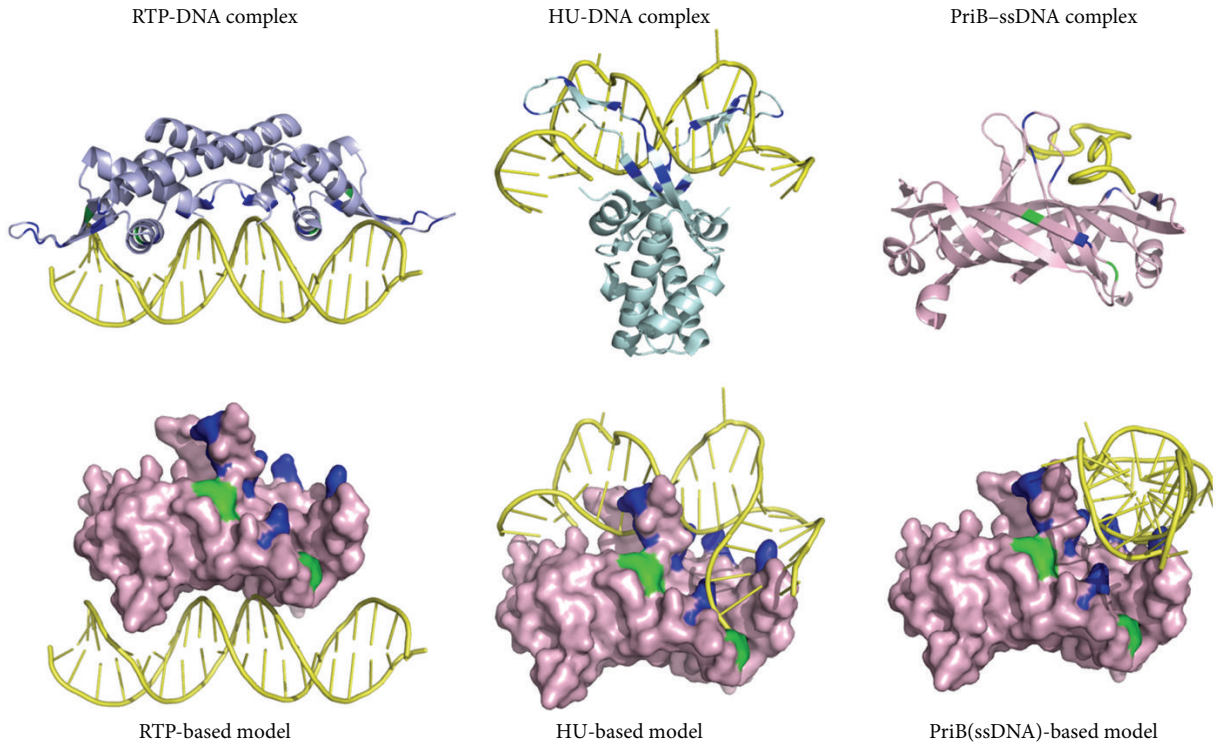

Figure 5: Putative dsDNA-binding mode of PriB. The DNA-binding models of PriB are directly constructed by manually superimposing the PriB dimer with DNA-bound crystal structure of RTP (Protein Data Bank entry: 1F4K), HU (Protein Data Bank entry: 1P51), and B-form dsDNA. The hydrophobic (green) and basic residues (blue) of RTP, Lys14, Arg16, Lys51, Arg59, Lys71, Lys74, Lys76, Lys77, Lys81, Lys91, Tyr58, and Tyr88, located on the dsDNA-binding surface, are indicated. The basic residues Arg53, Arg55, Lys56, Arg58, Arg61, Lys64, Lys68, and Arg75 of HU located on the dsDNA-binding surface are also indicated. Considering the known dsDNA-binding sites in PriB, PriB may use the HU-based model to bind dsDNA. Alternatively, PriB may use a similar approach to bind ssDNA and dsDNA because the residues responsible for ssDNA and dsDNA binding are almost overlapped.

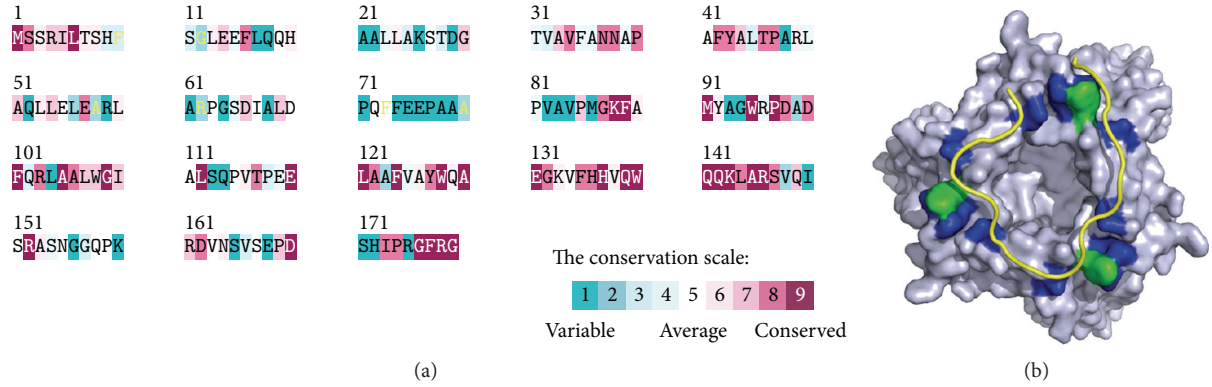

Figure 6: (a) Amino acid sequence alignment of KpDnaT. An alignment consensus of 29 sequenced DnaT homologs by the program ConSurf reveals the degree of variability at each position along the primary sequence. In general, the amino acid residues in the C-terminal region of KpDnaT are highly conserved. (b) Modeled structure of KpDnaT. The structure of KpDnaT is modeled by the bioinformatic program $(PS)^2$ and then manually built using threefold symmetry with a 25 mer ssDNA (gold). The highly conserved hydrophobic (green) and basic residues (blue) of KpDnaT, His136, His137, Trp140, Lys143, Arg146, and Arg151 located on the potential ssDNA-binding surface are indicated.

consensus of 29 sequenced DnaT homologs by ConSurf [44], we found that the amino acid residues in the C-terminal region of *K. pneumoniae* DnaT (KpDnaT) are highly conserved (Figure 6(a)) and that KpDnaT contains 10 Arg, 5 Lys, and 18 aromatic amino acid residues (11 Phe, 4 Trp, and 3 Tyr). We attempted to assess whether or not KpDnaT, especially at the C-terminal region, has ssDNA-binding activity because the aromatic stacking and electropositive interactions serve important functions in ssDNA binding by proteins [73, 75, 92–94]. KpDnaT can form distinct complexes with ssDNA of

different lengths, and the size of the binding site is 26 ± 2 nucleotides for a trimeric KpDnaT [90]. Although DnaT is not an OB-fold protein predicted from sequence analysis and structure modeling, the activity for ssDNA binding by DnaT, assayed in the same manner, is even higher than that of PriB, an OB-fold protein [90]. The two-domain structure for DnaT is characterized by the involvement of the N-terminal domain (amino acid residues 1–83) in PriB binding and the C-terminal domain (amino acid residues 84–179) in ssDNA binding [59].

To date, little is known about the ssDNA-binding mode of non-OB-fold proteins, particularly trimeric proteins. No protein with amino acid sequence similar to DnaT is found in the structure databank. Thus, homology modeling for the DnaT structure by several homology-based programs is not successful, including the use of SWISS-MODEL (http://swissmodel.expasy.org/) [95]. To obtain an indepth understanding of the structure-function relationship of KpDnaT, its 3D structure has been modeled by the bioinformatic program $(PS)^2$ [96, 97]. $(PS)^2$ (http://140.113.239.111/~ps2v2/docs.php) is an automatic homology modeling server that combines both sequence and secondary structure information to detect the homologous proteins with remote similarity and target-template alignment [96, 97]. The modeled structure of KpDnaT, manually built using threefold symmetry with a hit of alpha-aminotransferase from *Pyrococcus horikoshii* (Protein Data Bank entry: 1GD9) suggested from $(PS)^2$, is a ring-shaped trimer (Figure 6(b)) [59, 90]. Based on the structural model of KpDnaT, we suggested that the positively charged (blue) and aromatic residues (green) located in the C-terminus of DnaT are involved in ssDNA binding: H136, H137, W140, K143, R146, and R151 (Figure 6(b)). These residues in DnaT are significantly conserved among the 29 sequenced DnaT proteins (Figure 6(a)). F73 and F74 are also potential binding sites for ssDNA, but they are not completely conserved in DnaT family. The ring-like structure of KpDnaT is slightly similar to that of the hexameric (comprised of three dimers) DnaC helicase from *Geobacillus kaustophilus*, a DnaB-like helicase [92]. DnaT may bind to DnaB with a stoichiometry of 1 : 2, one DnaT monomer to a DnaB dimer. However, the DnaT structure is only a modeled structure, and these speculations, including the putative DNA and DnaB-binding modes of DnaT, must be further confirmed by additional biophysical studies.

3. Perspectives

Most DNA helicases of superfamily I and superfamily II are almost nonhexameric and have poor dsDNA unwinding activities when acting alone in vitro [98]. Some helicases might function as ssDNA translocases rather than helicases, and self-assembly and/or interactions with accessory proteins are required to activate helicase activity [98]. Several monomeric ssDNA translocases of superfamily I can potentially displace proteins that are bound to ssDNA by translocating along the ssDNA and be activated by self-assembly, removal of an autoinhibitory domain, or direct interactions with an accessory protein(s) [38, 40, 99–101]. For PriA, the self-assembly and removal of an autoinhibitory domain for higher helicase activity have not been reported. However, poor helicase activity for PriA, which can be significantly stimulated by PriB [40] and SSB [38], is found. Based on the structure of KpPriA bound to an SSB C-terminal peptide (Trp-Met-Asp-Phe-Asp-Asp-Asp-Ile-Pro-Phe) and the study of a single-molecule FRET (smFRET), Bhattacharyya et al. [45] proposed a pushing mechanism, which is similar to that for the RecA recombinase [102], for PriA-mediated replication restart. For SSB-bound DNA replication forks, PriA translocase activity may push SSB along the lagging-strand template to expose additional ssDNA for PriB and DnaT binding and that will ultimately serve as a binding site for DnaB [45]. This model provides structural insight into the molecular mechanism for initiating replication restart primosome assembly. The interaction of PriB with PriA is weak, and the stimulation of PriA by PriB via an interaction with ssDNA is not DNA structure-specific [40]. Thus, the targeting of stalled forks and recombination intermediates during replication restart likely correlates with PriA alone. More structural studies for these primosomal proteins are still necessary to elucidate the interaction between PriB and DnaT, as well as the release from the replication restart system. Several studies have raised new interesting questions as to whether or not PriA, PriB, and DnaT are always synchronically expressed for physiological needs and whether or not PriB and DnaT have additional functions for other systems. PriA and DnaT are required for *E. coli* growth at elevated pressure [88]; however, why PriB is not necessary to be synchronically expressed has yet to be determined. Many prokaryotic genomes do not contain a recognizable homolog of *priB* and *dnaT* (e.g., *P. aeruginosa*; Table 2). Thus, further operon and gene regulation analyses for PriB and DnaT expression, not limited to replication restart, should be also investigated in combination with the biochemical and structural investigations.

Table 2: Examples for some different PriA-directed primosome systems.

	PriA size (amino acid residues)	Partner proteins found in NCBI
Escherichia coli and *Klebsiella pneumoniae*	731	PriB, PriC, DnaT, DnaC, DnaB helicase, and DnaG
Staphylococcus aureus	802	DnaD, DnaB, DnaI, DnaC helicase, and DnaG
Pseudomonas aeruginosa	739	Only DnaB helicase and DnaG are found

PriA is conserved in bacteria, but its primosomal partners are not.

Conflict of Interests

The authors declare that there is no conflict of interests regarding the publication of this paper.

Acknowledgments

The authors would like to thank three anonymous reviewers and the editor for their comments. This research was supported by a grant from the National Science Council, Taiwan (NSC 102-2320-B-040-019 to C.Y. Huang).

References

[1] G. Smeenk and H. van Attikum, "The chromatin response to DNA breaks: leaving a mark on genome integrity," *Annual Review of Biochemistry*, vol. 82, pp. 55–80, 2013.

[2] S. Panier and D. Durocher, "Push back to respond better: regulatory inhibition of the DNA double-strand break response," *Nature Reviews Molecular Cell Biology*, vol. 14, pp. 661–672, 2013.

[3] R. C. Heller and K. J. Marians, "Replisome assembly and the direct restart of stalled replication forks," *Nature Reviews Molecular Cell Biology*, vol. 7, no. 12, pp. 932–943, 2006.

[4] R. L. Maher, A. M. Branagan, and S. W. Morrical, "Coordination of DNA replication and recombination activities in the maintenance of genome stability," *Journal of Cellular Biochemistry*, vol. 112, no. 10, pp. 2672–2682, 2011.

[5] P. McGlynn and R. G. Lloyd, "Recombinational repair and restart of damaged replication forks," *Nature Reviews Molecular Cell Biology*, vol. 3, no. 11, pp. 859–870, 2002.

[6] M. M. Cox, M. F. Goodman, K. N. Kreuzer, D. J. Sherratt, S. J. Sandler, and K. J. Marians, "The importance of repairing stalled replication forks," *Nature*, vol. 404, no. 6773, pp. 37–41, 2000.

[7] H. Masai, T. Tanaka, and D. Kohda, "Stalled replication forks: making ends meet for recognition and stabilization," *BioEssays*, vol. 32, no. 8, pp. 687–697, 2010.

[8] C. B. Gabbai and K. J. Marians, "Recruitment to stalled replication forks of the PriA DNA helicase and replisome-loading activities is essential for survival," *DNA Repair*, vol. 9, no. 3, pp. 202–209, 2010.

[9] K. J. Marians, "Prokaryotic DNA replication," *Annual Review of Biochemistry*, vol. 61, pp. 673–719, 1992.

[10] R. Schekman, A. Weiner, and A. Kornberg, "Multienzyme systems of DNA replication: proteins required for chromosome replication are resolved with the aid of a simple viral DNA template," *Science*, vol. 186, no. 4168, pp. 987–993, 1974.

[11] S. J. Sandler and K. J. Marians, "Role of PriA in replication fork reactivation in Escherichia coli," *Journal of Bacteriology*, vol. 182, no. 1, pp. 9–13, 2000.

[12] S. J. Sandler, "Multiple genetic pathways for restarting DNA replication forks in *Escherichia coli* K-12," *Genetics*, vol. 155, no. 2, pp. 487–497, 2000.

[13] K. J. Marians, "PriA-directed replication fork restart in *Escherichia coli*," *Trends in Biochemical Sciences*, vol. 25, no. 4, pp. 185–189, 2000.

[14] S. S. Patel, M. Pandey, and D. Nandakumar, "Dynamic coupling between the motors of DNA replication: hexameric helicase, DNA polymerase, and primase," *Current Opinion in Chemical Biology*, vol. 15, no. 5, pp. 595–605, 2011.

[15] M. Lopper, R. Boonsombat, S. J. Sandler, and J. L. Keck, "A hand-off mechanism for primosome assembly in replication restart," *Molecular Cell*, vol. 26, no. 6, pp. 781–793, 2007.

[16] R. Boonsombat, S. Yeh, A. Milne, and S. J. Sandler, "A novel dnaC mutation that suppresses priB rep mutant phenotypes in Escherichia coli K-12," *Molecular Microbiology*, vol. 60, no. 4, pp. 973–983, 2006.

[17] S. J. Sandler, "Requirements for replication restart proteins during constitutive stable DNA replication in Escherichia coli K-12," *Genetics*, vol. 169, no. 4, pp. 1799–1806, 2005.

[18] J. D. McCool, C. C. Ford, and S. J. Sandler, "A dnaT mutant with phenotypes similar to those of a priA2::kan mutant in Escherichia coli K-12," *Genetics*, vol. 167, no. 2, pp. 569–578, 2004.

[19] T. Hinds and S. J. Sandler, "Allele specific synthetic lethality between priC and dnaAts alleles at the permissive temperature of 30∘C in *E. coli* K-12," *BMC Microbiology*, vol. 4, article 47, 2004.

[20] S. J. Sandler, J. D. McCool, T. T. Do, and R. U. Johansen, "PriA mutations that affect PriA-PriC function during replication restart," *Molecular Microbiology*, vol. 41, no. 3, pp. 697–704, 2001.

[21] J. Liu, L. Xu, S. J. Sandler, and K. J. Marians, "Replication fork assembly at recombination intermediates is required for bacterial growth," *Proceedings of the National Academy of Sciences of the United States of America*, vol. 96, no. 7, pp. 3552–3555, 1999.

[22] A. H. Marceau, D. A. Bernstein, B. W. Walsh, W. Shapiro, L. A. Simmons, and J. L. Keck, "Protein interactions in genome maintenance as novel antibacterial targets," *PLoS ONE*, vol. 8, no. 3, Article ID e58765, 2013.

[23] D. Lu, D. A. Bernstein, K. A. Satyshur, and J. L. Keck, "Small-molecule tools for dissecting the roles of SSB/protein interactions in genome maintenance," *Proceedings of the National Academy of Sciences of the United States of America*, vol. 107, no. 2, pp. 633–638, 2010.

[24] K. Bush, "Alarming β-lactamase-mediated resistance in multidrug-resistant *Enterobacteriaceae*," *Current Opinion in Microbiology*, vol. 13, no. 5, pp. 558–564, 2010.

[25] H. W. Boucher, G. H. Talbot, J. S. Bradley et al., "Bad bugs, no drugs: no ESKAPE! An update from the Infectious Diseases Society of America," *Clinical Infectious Diseases*, vol. 48, no. 1, pp. 1–12, 2009.

[26] B. Sunchu, L. Berg, H. E. Ward, and M. E. Lopper, "Identification of a small molecule PriA helicase inhibitor," *Biochemistry*, vol. 51, no. 51, pp. 10137–10146, 2012.

[27] K. Arai and A. Kornberg, "Unique primed start of phage phi X174 DNA replication and mobility of the primosome in a direction opposite chain synthesis," *Proceedings of the National Academy of Sciences of the United States of America*, vol. 78, no. 1, pp. 69–73, 1981.

[28] H. Masai, T. Asai, Y. Kubota, K. Arai, and T. Kogoma, "Escherichia coli PriA protein is essential for inducible and constitutive stable DNA replication," *EMBO Journal*, vol. 13, no. 22, pp. 5338–5345, 1994.

[29] P. Nurse, K. H. Zavitz, and K. J. Marians, "Inactivation of the Escherichia coli PriA DNA replication protein induces the SOS response," *Journal of Bacteriology*, vol. 173, no. 21, pp. 6686–6693, 1991.

[30] A. Kornberg, "Replication deficiencies in priA mutants of Escherichia coli lacking the primosomal replication n' protein," *Proceedings of the National Academy of Sciences of the United States of America*, vol. 88, no. 8, pp. 3029–3032, 1991.

[31] M. R. Szymanski, P. J. Bujalowski, M. J. Jezewska, A. M. Gmyrek, and W. Bujalowski, "The N-terminal domain of the *Escherichia coli* pria helicase contains both the DNA- and nucleotide-binding sites. Energetics of domain-DNA interactions and allosteric effect of the nucleotide cofactors," *Biochemistry*, vol. 50, no. 43, pp. 9167–9183, 2011.

[32] H. Chen, S. H. North, and H. Nakai, "Properties of the PriA helicase domain and its role in binding PriA to specific DNA structures," *Journal of Biological Chemistry*, vol. 279, no. 37, pp. 38503–38512, 2004.

[33] T. Tanaka, T. Mizukoshi, C. Taniyama, D. Kohda, K. Arai, and H. Masai, "DNA binding of PriA protein requires cooperation of the N-terminal D-loop/arrested-fork binding and C-terminal helicase domains," *Journal of Biological Chemistry*, vol. 277, no. 41, pp. 38062–38071, 2002.

[34] C. A. Ouzounis and B. J. Blencowe, "Bacterial DNA replication initiation factor priA is related to proteins belonging to the "DEAD-box" family," *Nucleic Acids Research*, vol. 19, no. 24, article 6953, 1991.

[35] J. Y. Ng and K. J. Marians, "The ordered assembly of the phiX174-type primosome. I. Isolation and identification of intermediate protein-DNA complexes," *Journal of Biological Chemistry*, vol. 271, no. 26, pp. 15642–15648, 1996.

[36] P. Nurse, J. Liu, and K. J. Marians, "Two modes of PriA binding to DNA," *Journal of Biological Chemistry*, vol. 274, no. 35, pp. 25026–25032, 1999.

[37] P. McGlynn, A. A. Al-Deib, J. Liu, K. J. Marians, and R. G. Lloyd, "The DNA replication protein PriA and the recombination protein RecG bind D-loops," *Journal of Molecular Biology*, vol. 270, no. 2, pp. 212–221, 1997.

[38] C. J. Cadman and P. McGlynn, "PriA helicase and SSB interact physically and functionally," *Nucleic Acids Research*, vol. 32, no. 21, pp. 6378–6387, 2004.

[39] J. Dong, N. P. George, K. L. Duckett, M. A. P. DeBeer, and M. E. Lopper, "The crystal structure of *Neisseria gonorrhoeae* PriB reveals mechanistic differences among bacterial DNA replication restart pathways," *Nucleic Acids Research*, vol. 38, no. 2, Article ID gkp1031, pp. 499–509, 2009.

[40] C. J. Cadman, M. Lopper, P. B. Moon, J. L. Keck, and P. McGlynn, "PriB stimulates PriA helicase via an interaction with single-stranded DNA," *The Journal of Biological Chemistry*, vol. 280, no. 48, pp. 39693–39700, 2005.

[41] R. C. Heller and K. J. Marians, "Unwinding of the nascent lagging strand by Rep and PriA enables the direct restart of stalled replication forks," *Journal of Biological Chemistry*, vol. 280, no. 40, pp. 34143–34151, 2005.

[42] R. C. Heller and K. J. Marians, "The disposition of nascent strands at stalled replication forks dictates the pathway of replisome loading during restart," *Molecular Cell*, vol. 17, no. 5, pp. 733–743, 2005.

[43] K. Sasaki, T. Ose, N. Okamoto et al., "Structural basis of the 3′-end recognition of a leading strand in stalled replication forks by PriA," *EMBO Journal*, vol. 26, no. 10, pp. 2584–2593, 2007.

[44] M. Landau, I. Mayrose, Y. Rosenberg et al., "ConSurf 2005: the projection of evolutionary conservation scores of residues on protein structures," *Nucleic Acids Research*, vol. 33, no. 2, pp. W299–W302, 2005.

[45] B. Bhattacharyya, N. P. George, T. M. Thurmes et al., "Structural mechanisms of PriA-mediated DNA replication restart," *Proceedings of the National Academy of Sciences of the United States of America*, vol. 111, no. 4, pp. 1373–1378, 2014.

[46] A. Vindigni, F. Marino, and O. Gileadi, "Probing the structural basis of RecQ helicase function," *Biophysical Chemistry*, vol. 149, no. 3, pp. 67–77, 2010.

[47] A. C. W. Pike, B. Shrestha, V. Popuri et al., "Structure of the human RECQ1 helicase reveals a putative strand-separation pin," *Proceedings of the National Academy of Sciences of the United States of America*, vol. 106, no. 4, pp. 1039–1044, 2009.

[48] K. Büttner, S. Nehring, and K. Hopfner, "Structural basis for DNA duplex separation by a superfamily-2 helicase," *Nature Structural and Molecular Biology*, vol. 14, no. 7, pp. 647–652, 2007.

[49] B. Lucic, Y. Zhang, O. King et al., "A prominent β-hairpin structure in the winged-helix domain of RECQ1 is required for DNA unwinding and oligomer formation," *Nucleic Acids Research*, vol. 39, no. 5, pp. 1703–1717, 2011.

[50] S. S. Velankar, P. Soultanas, M. S. Dillingham, H. S. Subramanya, and D. B. Wigley, "Crystal structures of complexes of PcrA DNA helicase with a DNA substrate indicate an inchworm mechanism," *Cell*, vol. 97, no. 1, pp. 75–84, 1999.

[51] M. R. Singleton, S. Scaife, and D. B. Wigley, "Structural analysis of DNA replication fork reversal by RecG," *Cell*, vol. 107, no. 1, pp. 79–89, 2001.

[52] S. S. Patel and I. Donmez, "Mechanisms of helicases," *Journal of Biological Chemistry*, vol. 281, no. 27, pp. 18265–18268, 2006.

[53] S. J. Sandler, K. J. Marians, K. H. Zavitz, J. Coutu, M. A. Parent, and A. J. Clark, "dnaC mutations suppress defects in DNA replication- and recombination-associated functions in priB and priC double mutants in Escherichia coli K-12," *Molecular Microbiology*, vol. 34, no. 1, pp. 91–101, 1999.

[54] R. L. Low, J. Shlomai, and A. Kornberg, "Protein n, a primosomal DNA replication protein of *Escherichia coli*: purification and characterization," *Journal of Biological Chemistry*, vol. 257, no. 11, pp. 6242–6250, 1982.

[55] G. C. Allen Jr. and A. Kornberg, "Assembly of the primosome of DNA replication in Escherichia coli," *Journal of Biological Chemistry*, vol. 268, no. 26, pp. 19204–19209, 1993.

[56] C. Feng, B. Sunchu, M. E. Greenwood, and M. E. Lopper, "A bacterial PriB with weak single-stranded DNA binding activity can stimulate the DNA unwinding activity of its cognate PriA helicase," *BMC Microbiology*, vol. 11, article 189, 2011.

[57] J. Liu, P. Nurse, and K. J. Marians, "The ordered assembly of the φX174-type primosome. III. PriB facilitates complex formation between PriA and DnaT," *Journal of Biological Chemistry*, vol. 271, no. 26, pp. 15656–15661, 1996.

[58] M. R. Szymanski, M. J. Jezewska, and W. Bujalowski, "Binding of two PriA-PriB complexes to the primosome assembly site initiates primosome formation," *Journal of Molecular Biology*, vol. 411, no. 1, pp. 123–142, 2011.

[59] Y. H. Huang and C. Y. Huang, "The N-terminal domain of DnaT, a primosomal DNA replication protein, is crucial for PriB binding and self-trimerization," *Biochemical and Biophysical Research Communications*, vol. 442, pp. 147–152, 2013.

[60] J. Y. Ng and K. J. Marians, "The ordered assembly of the φX174-type primosome. II. Preservation of primosome composition from assembly through replication," *The Journal of Biological Chemistry*, vol. 271, no. 26, pp. 15649–15655, 1996.

[61] Y. H. Huang, M. J. Lin, and C. Y. Huang, "Yeast two-hybrid analysis of PriB-interacting proteins in replication restart primosome: a proposed PriB-SSB interaction model," *The Protein Journal*, vol. 32, no. 6, pp. 477–483, 2013.

[62] Y. H. Huang, H. H. Lin, and C. Y. Huang, "A single residue determines the cooperative binding property of a primosomal DNA replication protein, PriB, to single-stranded DNA," *Bioscience, Biotechnology and Biochemistry*, vol. 76, no. 6, pp. 1110–1115, 2012.

[63] S. Shioi, T. Ose, K. Maenaka et al., "Crystal structure of a biologically functional form of PriB from *Escherichia coli* reveals a potential single-stranded DNA-binding site," *Biochemical and*

Biophysical Research Communications, vol. 326, no. 4, pp. 766–776, 2005.

[64] M. Lopper, J. M. Holton, and J. L. Keck, "Crystal structure of PriB, a component of the *Escherichia coli* replication restart primosome," *Structure*, vol. 12, no. 11, pp. 1967–1975, 2004.

[65] J. H. Liu, T. W. Chang, C. Y. Huang et al., "Crystal structure of PriB, a primosomal DNA replication protein of *Escherichia coli*," *The Journal of Biological Chemistry*, vol. 279, no. 48, pp. 50465–50471, 2004.

[66] M. P. Horvath, "Structural anatomy of telomere OB proteins," *Critical Reviews in Biochemistry and Molecular Biology*, vol. 46, no. 5, pp. 409–435, 2011.

[67] R. L. Flynn and L. Zou, "Oligonucleotide/oligosaccharide-binding fold proteins: a growing family of genome guardians," *Critical Reviews in Biochemistry and Molecular Biology*, vol. 45, no. 4, pp. 266–275, 2010.

[68] I. D. Kerr, R. I. M. Wadsworth, L. Cubeddu, W. Blankenfeldt, J. H. Naismith, and M. F. White, "Insights into ssDNA recognition by the OB fold from a structural and thermodynamic study of *Sulfolobus*SSB protein," *The EMBO Journal*, vol. 22, no. 11, pp. 2561–2570, 2003.

[69] A. G. Murzin, "OB(oligonucleotide/oligosaccharide binding)-fold: common structural and functional solution for non-homologous sequences," *The EMBO Journal*, vol. 12, no. 3, pp. 861–867, 1993.

[70] Y. H. Huang, Y. H. Lo, W. Huang, and C. Y. Huang, "Crystal structure and DNA-binding mode of Klebsiella pneumoniae primosomal PriB protein," *Genes to Cells*, vol. 17, no. 10, pp. 837–849, 2012.

[71] H. C. Hsieh and C. Y. Huang, "Identification of a novel protein, PriB, in *Klebsiella pneumoniae*," *Biochemical and Biophysical Research Communications*, vol. 404, no. 1, pp. 546–551, 2011.

[72] M. R. Szymanski, M. J. Jezewska, and W. Bujalowski, "Interactions of the Escherichia coli Primosomal PriB Protein with the Single-stranded DNA. Stoichiometries, Intrinsic Affinities, Cooperativities, and Base Specificities," *Journal of Molecular Biology*, vol. 398, no. 1, pp. 8–25, 2010.

[73] C. Y. Huang, C. H. Hsu, Y. J. Sun, H. N. Wu, and C. D. Hsiao, "Complexed crystal structure of replication restart primosome protein PriB reveals a novel single-stranded DNA-binding mode," *Nucleic Acids Research*, vol. 34, no. 14, pp. 3878–3886, 2006.

[74] K. W. Chan, Y. J. Lee, C. H. Wang, H. Huang, and Y. J. Sun, "Single-stranded DNA-binding protein complex from *Helicobacter pylori* suggests an ssDNA-binding surface," *Journal of Molecular Biology*, vol. 388, no. 3, pp. 508–519, 2009.

[75] S. Raghunathan, A. G. Kozlov, T. M. Lohman, and G. Waksman, "Structure of the DNA binding domain of *E. coli* SSB bound to ssDNA," *Nature Structural Biology*, vol. 7, no. 8, pp. 648–652, 2000.

[76] V. A. Ponomarev, K. S. Makarova, L. Aravind, and E. V. Koonin, "Gene duplication with displacement and rearrangement: origin of the bacterial replication protein PriB from the single-stranded DNA-binding protein Ssb," *Journal of Molecular Microbiology and Biotechnology*, vol. 5, no. 4, pp. 225–229, 2003.

[77] S. Fujiyama, Y. Abe, T. Takenawa et al., "Involvement of histidine in complex formation of PriB and single-stranded DNA," *Biochimica et Biophysica Acta*, vol. 184, pp. 299–307, 2014.

[78] R. R. Meyer and P. S. Laine, "The single-stranded DNA-binding protein of Escherichia coli," *Microbiological Reviews*, vol. 54, no. 4, pp. 342–380, 1990.

[79] J. A. Wilce, J. P. Vivian, A. F. Hastings et al., "Structure of the RTP-DNA complex and the mechanism of polar replication fork arrest," *Nature Structural Biology*, vol. 8, no. 3, pp. 206–210, 2001.

[80] K. L. Tsai, Y. J. Sun, C. Y. Huang, J. Y. Yang, M. C. Hung, and C. D. Hsiao, "Crystal structure of the human FOXO3a-DBD/DNA complex suggests the effects of post-translational modification," *Nucleic Acids Research*, vol. 35, no. 20, pp. 6984–6994, 2007.

[81] K. L. Tsai, C. Y. Huang, C. H. Chang, Y. J. Sun, W. J. Chuang, and C. D. Hsiao, "Crystal structure of the human FOXK1a-DNA complex and its implications on the diverse binding specificity of winged helix/forkhead proteins," *Journal of Biological Chemistry*, vol. 281, no. 25, pp. 17400–17409, 2006.

[82] D. Kamashev, A. Balandina, A. K. Mazur, P. B. Arimondo, and J. Rouviere-Yaniv, "HU binds and folds single-stranded DNA," *Nucleic Acids Research*, vol. 36, no. 3, pp. 1026–1036, 2008.

[83] K. K. Swinger, K. M. Lemberg, Y. Zhang, and P. A. Rice, "Flexible DNA bending in HU-DNA cocrystal structures," *The EMBO Journal*, vol. 22, no. 14, pp. 3749–3760, 2003.

[84] H. Masai and K. Arai, "Initiation of lagging-strand synthesis for pBR322 plasmid DNA replication in vitro is dependent on primosomal protein i encoded by dnaT," *The Journal of Biological Chemistry*, vol. 263, no. 29, pp. 15016–15023, 1988.

[85] H. Masai, M. W. Bond, and K. Arai, "Cloning of the Escherichia coli gene for primosomal protein i: the relationship to dnaT, essential for chromosomal DNA replication," *Proceedings of the National Academy of Sciences of the United States of America*, vol. 83, no. 5, pp. 1256–1260, 1986.

[86] K. Arai, R. McMacken, S. Yasuda, and A. Kornberg, "Purification and properties of Escherichia coli protein i, a prepriming protein in ØX174 DNA replication," *The Journal of Biological Chemistry*, vol. 256, no. 10, pp. 5281–5286, 1981.

[87] H. Masai and K. Arai, "Escherichia coli dnaT gene function is required for pBR322 plasmid replication but not for R1 plasmid replication," *Journal of Bacteriology*, vol. 171, no. 6, pp. 2975–2980, 1989.

[88] S. L. Black, A. Dawson, F. B. Ward, and R. J. Allen, "Genes required for growth at high hydrostatic pressure in *Escherichia coli* K-12 identified by genome-wide screening," *PLoS One*, vol. 8, Article ID e73995, 2013.

[89] S. Jang, S. J. Sandler, and R. M. Harshey, "Mu insertions are repaired by the double-strand break repair pathway of *Escherichia coli*," *PLoS Genetics*, vol. 8, no. 4, Article ID e1002642, 2012.

[90] Y. H. Huang, M. J. Lin, and C. Y. Huang, "DnaT is a single-stranded DNA binding protein," *Genes Cells*, vol. 18, pp. 1007–1019, 2013.

[91] M. R. Szymanski, M. J. Jezewska, and W. Bujalowski, "The *Escherichia coli* primosomal dnat protein exists in solution as a monomer-trimer equilibrium system," *Biochemistry*, vol. 52, no. 11, pp. 1845–1857, 2013.

[92] Y. H. Lo, K. L. Tsai, Y. J. Sun, W. T. Chen, C. Y. Huang, and C. D. Hsiao, "The crystal structure of a replicative hexameric helicase DnaC and its complex with single-stranded DNA," *Nucleic Acids Research*, vol. 37, no. 3, pp. 804–814, 2009.

[93] D. L. Theobald, R. M. Mitton-Fry, and D. S. Wuttke, "Nucleic acid recognition by OB-fold proteins," *Annual Review of Biophysics and Biomolecular Structure*, vol. 32, pp. 115–133, 2003.

[94] C. Yang, U. Curth, C. Urbanke, and C. H. Kang, "Crystal structure of human mitochondrial single-stranded DNA binding protein at 2.4 A resolution," *Nature Structural Biology*, vol. 4, no. 2, pp. 153–157, 1997.

[95] K. Arnold, L. Bordoli, J. Kopp, and T. Schwede, "The SWISS-MODEL workspace: a web-based environment for protein structure homology modelling," *Bioinformatics*, vol. 22, no. 2, pp. 195–201, 2006.

[96] C.-C. Chen, J.-K. Hwang, and J.-M. Yang, "$(PS)^2$-v2: template-based protein structure prediction server," *BMC Bioinformatics*, vol. 10, article 366, 2009.

[97] C. C. Chen, J. K. Hwang, and J. M. Yang, "(PS)2: protein structure prediction server," *Nucleic Acids Research*, vol. 34, pp. W152–W157, 2006.

[98] T. M. Lohman, E. J. Tomko, and C. G. Wu, "Non-hexameric DNA helicases and translocases: mechanisms and regulation," *Nature Reviews Molecular Cell Biology*, vol. 9, no. 5, pp. 391–401, 2008.

[99] W. Zhang, M. S. Dillingham, C. D. Thomas, S. Allen, C. J. Roberts, and P. Soultanas, "Directional loading and stimulation of PcrA helicase by the replication initiator protein RepD," *Journal of Molecular Biology*, vol. 371, no. 2, pp. 336–348, 2007.

[100] R. D. Shereda, D. A. Bernstein, and J. L. Keck, "A central role for SSB in Escherichia coli RecQ DNA helicase function," *Journal of Biological Chemistry*, vol. 282, no. 26, pp. 19247–19258, 2007.

[101] S. W. Matson and A. B. Robertson, "The UvrD helicase and its modulation by the mismatch repair protein MutL," *Nucleic Acids Research*, vol. 34, no. 15, pp. 4089–4097, 2006.

[102] R. Roy, A. G. Kozlov, T. M. Lohman, and T. Ha, "SSB protein diffusion on single-stranded DNA stimulates RecA filament formation," *Nature*, vol. 461, pp. 1092–1097, 2009.